ELECTRONIC SPECTROSCOPY OF VARIOUS MOLECULAR SYSTEMS BY LOW-ENERGY, VARIABLE-ANGLE, ELECTRON IMPACT

Thesis by

Robert Paul Frueholz

In Partial Fulfillment of the Requirements

for the Degree of

Doctor of Philosophy

California Institute of Technology

Pasadena, California

1978

(submitted May 16, 1978)

This Thesis is dedicated to my parents, Alberta and Rudolf.

Acknowledgments

Many people have assisted me in the studies reported in this thesis and I am very happy to acknowledge their help. I am grateful to Professor Aron Kuppermann for his continuing interest in these experiments. It was through his activities that we obtained the loan of the instrument with which most of the studies reported here were conducted. Finally, his demands for complete thoroughness in our studies, though sometimes momentarily annoying, have consistently improved the quality of our results.

I have enjoyed interacting with members of the Kuppermann research group on both scientific and social levels. Oren A. Mosher and Wayne M. P. Flicker introduced me to electron scattering. I am grateful to Oren for instilling in me a particular sense of intellectual pride in our electron scattering studies. Wayne provided me with valuable insights on thesis preparation. Working with both Wayne and Oren on several publications has been valuable to me and enjoyable. I have worked with Ronald Rianda for nearly four years on both electron scattering and laser multiphoton experiments. Ron has proved himself to be a valuable colleague many times. In addition to coauthoring several papers with him, I have been amazed by his insights into Third World politics and pleased by his expert docking techniques.

R. H. (Bob the Bopper) Reiner always proved to be a source of sound scientific advice. His continuing interest in the origins of modern popular music supplied much amusement. In my first three years at Caltech, Jon Burke's assistance with our electron scattering

data handling was invaluable. Jon's consistent knowledge about the Meleagris gallopavo was always fascinating. Mark Keil and Tom Slankas, the Beamer's, were always available to give technical advice or spend a few minutes discussing our vicissitudinous lives in the subbasement. Finally, I have enjoyed working with Jeff Sell the last four years both in the research group and T.A.-ing together.

I am very grateful to Sandor Trajmar of the Jet Propulsion Laboratory for consenting to loan to us the electron impact spectrometer with which most of the studies reported here were performed. In addition he was a ready source of advice concerning the instrument.

The Caltech Chemistry Department instrument shop has been invaluable during the last five years. Virtually every member has made a significant contribution to our research effort. Mr. W. W. Schuelke, as supervisor has been a constant source of valuable suggestions and ideas. Instrument makers, Mr. Guy Duremberg and Mr. Tony Stark have done an incomparable job in constructing the EIS III spectrometer. They have always been willing to explain how construction was progressing. Mr. Bill Schuelke and Mr. Delmer Dill have also contributed to the construction of the EIS III instrument. Mr. Rich Ehrich, design engineer and draftsman, has made an excellent set of technical drawings for the EIS III instrument. He has successfully translated our initial ideas and requirements into an operational instrument. My interactions with these gentlemen have always been enjoyable.

I also wish to thank the Department of Energy for financial support. I am very grateful to my parents for tolerating me at home

for the last five years. They have been a source of emotional support as well as adding to my financial stability.

Abstract

The technique of low-energy, variable-angle, electron impact spectroscopy has been used to study the electronic spectroscopy of several groups of molecules. In each of the molecules, spin-forbidden and spin-allowed transitions have been investigated as well as excitations lying above the first ionization potential. Studies were performed at incident electron beam energies between 25 eV and 75 eV, at scattering angles ranging from 0° to 80°. The excitation energy region studied was from 0 eV to energies greater than 15 eV. Molecules investigated were selected because of their inherent spectroscopic interest; elucidation of their spectra would aid in explaining photochemical processes in which they are involved; and in some cases the molecules were of an energy-related nature.

Ketene (H_2CCO) is a molecule of particular photochemical interest. Transitions were observed in its spectra at energies of 3.7 eV, 5.3 eV and 5.86 eV. They are assigned, respectively, to an $n \rightarrow \pi^*$, $\tilde{X}\,{}^1A_1 \rightarrow {}^1A_2$ transition, a $\pi \rightarrow \pi^*$, $\tilde{X}\,{}^1A_1 \rightarrow {}^3A_1$ transition and an $n \rightarrow 3s$, singlet → singlet, Rydberg transition. Both 1,3,5-cycloheptatriene and 1,3,5,7-cyclooctatetraene are also of photochemical interest. They have both been found to be efficient dye laser quenchers and their low-lying triplet states are of importance in these quenching mechanisms. Three singlet → triplet transitions were located in 1,3,5,7-cyclooctatetraene's spectrum with maxima at 3.05 eV, 4.05 eV, and 4.84 eV. The spin-allowed transitions are also discussed. In the spectrum of 1,3,5-cycloheptatriene two triplet states were located at

3.05 eV and 3.95 eV.

Electron-impact spectra of benzene and eleven fluorine substituted derivatives were obtained. Each molecule shows an absorption maximum at about 3.9 eV corresponding to a singlet → triplet, $\pi \rightarrow \pi^*$, transition. In benzene, fluorobenzene, o-difluorobenzene, m-difluorobenzene, and 1,3,5-trifluorobenzene, an additional singlet → triplet transition was detected at about 5.7 eV. Three singlet → singlet transitions analogous to the 4.90 eV, 6.20 eV, and 6.95 eV benzene excitations are seen in each of the fluorine-substituted molecules. The more highly substituted compounds exhibit an additional singlet → singlet transition which is most clearly observed in the hexafluorobenzene spectrum at 5.32 eV.

The electronic spectroscopy of conjugated cis-1,3-dienyl systems has been investigated by obtaining the spectra of 1,3-cyclopentadiene, 1,3-cyclohexadiene, and 1,3-cycloheptadiene. In each molecule a single low-lying triplet state was detected with maximum intensity at 3.10 eV, 2.94 eV, and 2.99 eV, respectively. The singlet-state spectra were also investigated and discussed in terms of interacting ethylenic units. The spectrum of 1,3-cyclopentadiene was compared to those of the heterocycles, furan (C_4H_4O), thiophene (C_4H_4S) and pyrrole (C_4H_4NH). 1,3-Cyclopentadiene's spectrum is best discussed in terms of a cis-1,3-dienyl system.

The electron-impact spectra of cyclohexene and norbornene were obtained along with those of the non-conjugated dienes, 1,4-cyclohexadiene and norbornadiene. In cyclohexene and norbornene a single

singlet → triplet excitation was observed at 4.24 eV and 4.10 eV, respectively. Transitions corresponding to $\pi \rightarrow \pi^*$ singlet excited states and $\pi \rightarrow 3s$ Rydberg states were also observed. The spectra of norbornadiene and 1,4-cyclohexadiene are discussed in terms of ethylenic units interacting via through-bond and through-space effects. The lowest feature in the norbornadiene spectrum appears to be due to the superposition of two singlet → triplet transitions with approximate locations at 3.4 eV and 3.9 eV. In the spectrum of 1,4-cyclohexadiene, the lowest feature is also believed to result from two singlet → triplet transitions; however, the transitions overlap so heavily that individual locations could not be determined.

Finally, in two appendices the electronic spectroscopy of nitric oxide and UF_6 and WF_6 are discussed. Weak structure in the NO spectrum occurring between 5.22 eV and 5.60 eV has been assigned as vibronic bands belonging to the $X^2\Pi \rightarrow a^4\Pi$ transition. Structure with an apparent Franck-Condon envelope extending from 5.70 eV to approximately 7 eV with intensity maxima at 6.29 eV was assigned to the $X^2\Pi \rightarrow b^4\Sigma^-$ transition. The UF_6 and WF_6 spectra were discussed in terms of recent calculations and by drawing parallels between the two spectra.

TABLE OF CONTENTS

Table of Contents (continued) Page

1. INTRODUCTION

The studies reported here concern the elastic and inelastic scattering of electrons from molecular targets. The inelastic collision results in the excitation of the target molecule from its ground state to higher electronic states. A much broader range of excited electronic states is readily accessible via low-energy electron scattering than is easily accessible using optical techniques.[1]

The experimental method used most often when employing electron scattering to study excited electronic states makes use of the electron "energy-loss spectrum". This technique, which was used exclusively in our studies, consists of focusing an energy selected beam of electrons into a target chamber containing the sample gas. The target gas is maintained at low enough pressure to insure that a given electron undergoes only a single collision. After the scattering process the electrons are energy analyzed at a fixed angle to determine the amount of energy transferred to the molecule. A graph of the intensity of the scattered electrons versus energy-loss, at a fixed incident electron kinetic energy (impact energy, E_0) and scattering angle (θ), constitutes an energy-loss spectrum. This spectrum is the electron-impact equivalent of an optical absorption spectrum, and the two types of spectra may be directly compared.

The more traditional techniques of optical spectroscopy supply various types of information which may be used in assigning electronic transitions, thereby yielding knowledge about the excited states of a given molecule. First, transition energies may be accurately deter-

mined, although several different instruments will be needed to investigate the entire excitation energy region over which electronic transitions might be expected (from about 1 eV to 15 eV). At excitation energies above about 12 eV (1050 Å) where the LiF cut-off occurs this becomes quite difficult. In addition to excitation energies, optical experiments can often be performed with sufficient resolution to allow the study of vibrational and in some cases even rotational structure. This can provide valuable and possibly definitive information when determining the symmetry of an excited state.[2]

Finally, the relative absorption intensities of transitions can be of assistance when attempting an assignment. In optical studies[3] a typical $\pi \rightarrow \pi^*$, spin and symmetry allowed (i.e., electric dipole allowed) transition will have an oscillator strength, f, of approximately 1, while a spin allowed but symmetry forbidden excitation will have an f number generally ranging from 1×10^{-1} to 1×10^{-4}. For spin forbidden excitations, symmetry-allowed transitions will have oscillator strengths ranging from 1×10^{-4} to 1×10^{-8}, while a spin-forbidden transition which is also symmetry forbidden will have an f number less than 1×10^{-8}. The intensities of the spin-forbidden transitions are so low that their detection is often difficult if not impossible using optical techniques.

Electron impact spectroscopy also supplies similar information concerning the nature of the excited states of molecules. Excitation energies are readily obtained from energy-loss spectra. A significant advantage over optical studies is that the entire range of electronic excitation energies may be investigated using a single instrument.

Transitions occurring at 20 eV energy-loss are as easily studied as those occurring at 2 eV. However, the obtainable resolution in electron scattering experiments, particularly at excitation energies below 10 eV, is usually significantly poorer than that in an equivalent optical study. Fairly good resolution in electron scattering studies is about 30 meV (~ 250 cm^{-1}).[4] This is several orders of magnitude lower than in optical experiments. It should be noted, though, that for higher-lying excited electronic states vibrational structure is often lacking because of uncertainty broadening due to the extremely short life times of these states.[5]

The relative intensities of various types of transitions in electron scattering experiments is significantly different from those in optical studies. The principal difference is that the $\Delta S = 0$ selection rule of optical spectroscopy[3] is relaxed in electron impact. Spin-forbidden transitions which, as was previously indicated, are very weak in optical spectroscopy, typically are 0.02 to 0.5 times as intense as optically allowed excitations, at scattering angles greater than 40° and impact energies in the range 60 eV to 20 eV.[1] In some cases, helium for example, the most intense feature in the energy-loss spectrum corresponds to a spin-forbidden transition.[6] This relative intensity increase for spin-forbidden transitions represents an enhancement of between three to eight orders of magnitude when compared to optical spectra.

The mechanism which relaxes the $\Delta S = 0$ selection rule is known as the "exchange" excitation. First discussed by Oppenheimer[7] in 1928, the incident electron is interchanged with a molecular electron.

While the exchange process must still conserve the overall spin of the incident electron-target molecule system, the molecule may undergo a net spin change of unity while the scattered electron will have the opposite spin as compared to the incident electron.

The intensities of spin-allowed but electric dipole-forbidden transitions are also enhanced relative to optically allowed excitations in electron scattering. Typically these transitions are from 0.05 to 0.25 times as intense as optically allowed excitations. In electron scattering, spin-allowed transitions proceed primarily via a direct mechanism in which the incident electron interacts with the target through coulombic forces. These coulomb interactions are believed to distort or polarize the molecular charge distribution and effectively alter the molecular symmetry allowing enhancement of dipole forbidden transitions.

Electron scattering experiments also provide information for which there is no optical analog. In many cases the nature of the transition may be determined by studying the electron impact spectrum at different scattering angles and impact energies. The experimentally determined differential cross section (DCS) $\frac{d\sigma_n}{d\Omega}(E_0, \theta, \varphi)$, supplies information about angular and energy dependence of the scattering process. The quantity $d\sigma_n(E_0, \theta, \varphi)$ equals the number of electrons which excited molecules to the n^{th} state, and then scattered into an element of solid angle $d\Omega = \sin\theta \, d\theta \, d\varphi$, per unit time divided by the flux density of incoming electrons. The angle θ is the spherical polar colatitude angle measured with respect to the incident beam direction and the angle ϕ is the azimuthal angle about this direction. The DCS

has units of area per unit solid angle per target molecule. If the target molecules are randomly oriented, as is the case for all experiments reported here, the DCS is independent of ϕ.

The following characteristics have been observed for the differential cross section when associated with various types of transitions.[1] Excitations fully allowed with respect to both spin and electric dipole selection rules display sharply forward peaked DCS's, which decrease by about 2 orders of magnitude as the scattering angle increases from 10° to 80°. The DCS is most intense at 0° scattering angle because the excitation occurs via long-range coulombic forces. Spin allowed but symmetry forbidden transitions are also forward peaked but often less so than symmetry allowed transitions. Spin forbidden transitions display a distinctly different angular behavior. Their DCS's are generally constant within a factor of 2 or 3 over the angular range 10° to 80°. This behavior is the result of the exchange mechanism for excitation in which the outgoing electron "forgets" the direction the incident electron came from and thus the DCS is relatively isotropic.

The previous discussion indicates that both optical and electron impact forms of spectroscopy supply information useful in studying the excited states of molecules. Each technique has its own strengths and weaknesses. Rather than considering one method superior to the other they should be considered as complementary procedures. Spectroscopic study of a molecular system should not be considered complete until both optical and electron scattering techniques have been applied.

The author has been actively involved in the study of the electronic spectroscopy of numerous molecular systems using the electron

scattering technique. In section 4 the results of these studies are discussed in detail. The molecules studied were 1,3,5,7-cyclo-octatetraene, fluorinated benzenes, ketene, 1,3,5-cycloheptatriene, 1,3-cyclic dienes, and unsaturated bridged and unbridged six-member rings. Some of these compounds were studied in collaboration with Dr. W. M. Flicker, Dr. O. A. Mosher, and Mr. R. Rianda. In addition to these molecules the author in association with Mr. Rianda has investigated the electronic spectroscopy of UF_6 and WF_6 and nitric oxide; descriptions of these studies are included as appendices. Also a series of cyanide-containing molecules including hydrogen cyanide, cyanogen and various straight-chain nitriles, along with nitrogen dioxide, nitrous oxide, and dichlorodifluoromethane were investigated. The spectra of these molecules will be described in detail in the thesis of Mr. Rianda.

The remainder of this thesis is divided as follows: section 2 provides a discussion of theoretical techniques used to study electron-molecule scattering; section 3 is a brief description of the experimental apparatus along with information concerning the final stages of construction of a new electron impact spectrometer. Finally, section 5 consists of a short summary of the research conducted.

References

1. (a) A. Kuppermann, J. K. Rice, and S. Trajmar, J. Phys. Chem. 72, 3894 (1968); (b) S. Trajmar, J. K. Rice, and A. Kuppermann, Adv. Chem. Phys. 18, 15 (1970).
2. G. Herzberg, Electronic Spectra of Polyatomic Molecules (D. Van Nostrand, Inc., 1966).
3. S. P. McGlynn, T. Azumi, and M. Kinoshita, Molecular Spectroscopy of the Triplet State (Prentice-Hall, Inc., New Jersey, 1969), pp. 10-30.
4. W. M. Flicker, Ph.D. Thesis, California Institute of Technology, pp. 248-289 (1969).
5. J. P. Byrne and I. G. Ross, Aust. J. Chem. 24, 1107 (1971).
6. J. K. Rice, Ph.D. Thesis, California Institute of Technology, pp. 248-289 (1969).
7. J. R. Oppenheimer, Phys. Rev. 32, 361 (1928).

2. ELECTRON-MOLECULE SCATTERING THEORY

2.1 Introduction

A rigorous discussion of electron-atom and electron-molecule scattering processes proceeds directly from the time-independent Schrödinger equation. While systems of differential equations describing these processes are readily obtained, their solutions are extremely complicated. Only for very simple atomic and molecular systems have accurate elastic and inelastic differential cross sections (DCS's) been obtained. Most calculations involve making approximations of one form or another to reduce the mathematics to some level of tractability.

In this chapter the rigorous equations will be derived. Most of the emphasis, however, will be on the approximation techniques. It is important to understand what approximations are made and what is their physical basis. This chapter is not meant to be a comprehensive review of electron scattering theory but rather to introduce the reader to some of the more important areas of this theory and also to allow him to approach the literature with enough information to begin a detailed study of any particular method.

2.2 Scattering Theory Based on Eigenfunction Expansions

We wish to consider the scattering of a incident electron with momentum $\hbar K_0$ off a target molecule in state ϕ_0 with energy E_0. After the interaction the molecule is left in state ϕ_n with energy E_n

while the scattered electron has momentum $\hbar K_n$. Since the Hamiltonian for this process is taken to be time independent the total energy, E, is a constant and $E = \frac{\hbar^2 K_n^2}{2m} + E_0 = \frac{\hbar^2 K_n^2}{2m} + E_n$.

The time-independent Schrödinger equation for the scattering process may be written as

$$H\Psi = E\Psi , \tag{2.1}$$

where H is the total Hamiltonian describing the electron-molecule system, Ψ is the time independent wavefunction and E is the total energy of the system, which consists of a free electron and a molecule with N-1 electrons and N′ nuclei.

Writing the Hamiltonian explicitly yields

$$H = -\frac{\hbar^2}{2m}\sum_{i=1}^{N}\nabla^2_{\underset{\sim}{r}_i} - \hbar^2\sum_{i=1}^{N'}\frac{\nabla^2_{\underset{\sim}{R}_i}}{2M_i} - e^2\sum_{i=1}^{N}\sum_{j=1}^{N'}\frac{Z_j}{|\underset{\sim}{r}_i - \underset{\sim}{R}_j|} +$$

$$+ e^2\sum_{i=1}^{N}\sum_{\substack{j=1\\ i>j}}^{N}\frac{1}{|\underset{\sim}{r}_i - \underset{\sim}{r}_j|} + e^2\sum_{i=1}^{N'}\sum_{\substack{j=1\\ i>j}}^{N'}\frac{1}{|\underset{\sim}{R}_i - \underset{\sim}{R}_j|} \tag{2.2}$$

where m and M_i are the mass of the electron and the mass of the i^{th} nucleus, $\underset{\sim}{r}_i$ and $\underset{\sim}{R}_j$ are the positions of the i^{th} electron and j^{th} nucleus, and Z_j is the charge of the j^{th} nucleus. The terms on the right of Eq. 2.2 correspond to the electrons' kinetic energies, the nuclear kinetic energies, the electron-nuclei attractive potential energy, and the repulsive potential energies of electron-electron and nucleus-nucleus interactions.

The standard method for solving Eq. 2.1 involves expanding Ψ in terms of eigenstates of the molecule, ϕ_n, which are antisymmetrized functions of the space and spin coordinates of the N-1 molecule electrons.

$$\Psi(\underset{\sim}{r}_1,\ldots,\underset{\sim}{r}_N,\underset{\sim}{R}_1,\ldots,\underset{\sim}{R}_{N'}) = \sum_n{}' (1 - P_{op})[F_n(\underset{\sim}{r}_1)\,\phi_n(\underset{\sim}{r}_1,\ldots,\underset{\sim}{r}_N,\underset{\sim}{R}_N,\ldots,\underset{\sim}{R}_{N'})]. \quad (2.3)$$

In Eq. 2.3, the expansion coefficients are functions, $F_n(\underset{\sim}{r}_\ell)$, which depend on the space and spin coordinates of only the ℓ^{th} electron. P_{op}, defined as $\sum_{\ell=2}^{N} P_{1\ell}$, is a permutation operator which interchanges each electron, in turn, with the "first" electron. This permutation antisymmetrizes the entire wavefunction so that the Pauli Exclusion Principle is satisfied. The prime on the summation symbol indicates that the sum is over bound and continuum states of the target.

The expression for Ψ is substituted into the Schrödinger equation. Use is made of the fact that ϕ_n satisfies Eq. 2.4,

$$\left(-\frac{\hbar^2}{2m}\sum_{i=2}^{N}\nabla^2_{\underset{\sim}{r}_i} - e^2\sum_{i=2}^{N}\sum_{j=1}^{N'}\frac{Z_j}{|\underset{\sim}{r}_i - \underset{\sim}{R}_j|} + e^2\sum_{i=1}^{N}\sum_{\substack{j=1\\ i>j}}^{N}\frac{1}{|\underset{\sim}{r}_i - \underset{\sim}{r}_j|}\right)$$

$$\times\,\phi_m(\underset{\sim}{r}_2,\ldots,\underset{\sim}{r}_N) = \epsilon_m\,\phi_m(\underset{\sim}{r}_2,\ldots,\underset{\sim}{r}_N)\ , \quad (2.4)$$

also that the ϕ_n are taken to be orthonormal. Finally multiplication of the equation by $\phi^*_m(\underset{\sim}{r}_2,\ldots,\underset{\sim}{r}_N)$ and integration over the electronic coordinates $\underset{\sim}{r}_2,\ldots,\underset{\sim}{r}_N$ yields Eq. 2.5.[1]

$$(\nabla_1^2 + K_m^2)\, F_m(\underset{\sim}{r}_1) = \sum_n{}' \frac{2m}{\hbar^2} \langle \phi_m | V_{1\text{-mol}} | \phi_n \rangle F_n(\underset{\sim}{r}_1)$$

$$+ (N - 1) \sum_n{}' \langle \phi_m(\underset{\sim}{r}_2, \ldots, \underset{\sim}{r}_N) | \phi_n(\underset{\sim}{r}_1, \underset{\sim}{r}_3, \ldots, \underset{\sim}{r}_N) \times$$

$$\times (\nabla_2^2 + k_n^2 - \frac{2m}{\hbar^2} V_{2\text{-mol}})\, F_n(\underset{\sim}{r}_2) \rangle \,. \tag{2.5}$$

In this equation $V_{i\text{-mol}}$ is defined by the expression

$$V_{i\text{-mol}} \equiv e^2 \sum_{\substack{k=1 \\ (i \neq k)}}^{N} \frac{1}{r_{ik}} - e^2 \sum_{j=1}^{N'} \frac{Z_j}{|\underset{\sim}{r}_i - \underset{\sim}{R}_j|} \,. \tag{2.6}$$

Equation 2.5 is one of an infinite set of coupled integro-differential equations.

Not only must $F_m(\underset{\sim}{r})$ satisfy (2.5) but it must also possess the appropriate asymptotic behavior. Far from the interaction region, if the scattering is elastic, $F_0(\underset{\sim}{r})$ must be the superposition of a plane wave and a scattered spherical wave, while for inelastic scattering only a scattered spherical wave is present. These requirements are summarized in the asymptotic boundary condition

$$F_n(\underset{\sim}{r}) \underset{r \to \infty}{\sim} (e^{i\underset{\sim}{K} \cdot \underset{\sim}{r}}\, \delta_{on} + f_{on} \frac{e^{iK_n r}}{r})\, s_n \,, \tag{2.7}$$

where s_n is a single electron spin function. The quantity f_{on} can be related to the DCS for scattering, $^2 \frac{d\sigma_{on}}{d\Omega}(K_o, \theta, \varphi)$.

$$\frac{d\sigma_{on}}{d\Omega}(K_o,\theta,\phi) = \frac{K_n}{K_o}\left|f_{on}(K_o,\theta,\varphi)\right|^2 \quad , \tag{2.8}$$

while integration of the DCS over 4π steradians yields the integral cross section, $Q_{on}(K_o)$.

$$Q_{on}(K_o) = \int_0^{2\pi} d\phi \int_0^{\pi} \frac{d\sigma_{on}(K_o,\theta,\varphi)}{d\Omega} \sin\theta \, d\theta \quad . \tag{2.9}$$

A "partial wave" expansion is often incorporated into equation 2.3. This is particularly true for studies of electron-atom scattering.[3-8] In this case $F(\underset{\sim}{r})$ becomes

$$F_m(\underset{\sim}{r}) = \sum_{\ell=0}^{\infty} \sum_{m'=-\ell}^{\ell} \frac{f_{m\ell m'}(r)}{r} Y_{\ell m'}(\theta,\varphi) \, . \tag{2.10}$$

Now a given $f_{n\ell m'}(r)$ must satisfy the equation

$$\left(\frac{d^2}{dr_1^2} + K_m^2 - \frac{\ell(\ell+1)\hbar^2}{r_1^2}\right) f_{m\ell m'}(r_1) = \int r_1 Y^*_{\ell m'}(\theta,\varphi) \times (\text{r.h.s. Eq. 2.5}) \, d\tau_1 . \tag{2.11}$$

$f_{m\ell m'}(r)$ must also satisfy an asymptotic boundary condition

$$f_{m\ell m'}(r) \underset{r\to\infty}{\sim} A_{m\ell m'} \sin(K_n r - \ell\pi/2 + \delta_{m\ell m'}) \, , \tag{2.12}$$

where $\delta_{m\ell m'}$ is the partial-wave phase shift. Burke and Smith[5] relate $\delta_{m\ell m'}$ to the differential cross section and the integral cross section in terms of $\underset{\approx}{S}$ and $\underset{\approx}{T}$ matrix elements.

The system of equations symbolized by Eq. 2.11 is of infinite order. Even in cases where the expansions (Eqs. 2.3 and 2.12) are truncated (see section 2.3), the equations have only been applied to the simplest atomic cases. For the cases of elastic scattering or scattering which involves only vibrational or rotational excitation of the target, considerable simplification is obtained by analyzing the only motion of the incident electron moving in an "effective potential", $V(\underset{\sim}{r})$, describing its interaction with the target (9-13). The Schrödinger equation for this treatment is

$$[\nabla^2 + K^2 - V(\underset{\sim}{r})]\,\Psi(\underset{\sim}{r}) = 0 . \tag{2.13}$$

$\Psi(\underset{\sim}{r})$, the wavefunction for the incident electron, is expanded in terms of partial waves,

$$\Psi(\underset{\sim}{r}) = \sum_{\ell} \sum_{m=-\ell}^{\ell} A_{\ell m}\, Y_{\ell m}(\theta,\varphi)\, \phi_{\ell m}(r) . \tag{2.14}$$

Using the orthonormality of $Y_{\ell m}(\theta,\varphi)$ and for the case of axial symmetry one obtains a set of uncoupled differential equations given by

$$\frac{1}{r^2}\frac{d}{dr}\left(r^2 \frac{d\phi_\ell(r)}{dr}\right) + \left(K^2 - U(r) - \frac{\ell(\ell+1)}{r^2}\right)\phi_\ell(r) = 0 . \tag{2.15}$$

Again $\phi_\ell(r)$ must satisfy an asymptotic boundary condition

$$\phi_\ell(r) \underset{r\to\infty}{\sim} (1/Kr)\sin[Kr - (\pi\ell/2) + \delta_\ell(K)] . \tag{2.16}$$

The use of the effective potential reduced the coupled system of integro-differential equation found in Eq. 2.5 to a system of uncoupled equations. Also while Eq. 2.5 had non-local integral operators, in the form of coulomb and exchange integrals, which are very time consuming to numerically evaluate, Eq. 2.15 does not involve these entities. The effective potential $V(\underset{\sim}{r})$, which is sometimes termed the optical potential,[12] is often separated into several components.[10,11]

$$V(\underset{\sim}{r}) = V^{static}(\underset{\sim}{r}) + V^{exch}(\underset{\sim}{r},K) + V^{pol}(\underset{\sim}{r}) \qquad (2.17)$$

The static potential, $V^{static}(\underset{\sim}{r})$, models the electrostatic interaction between the scattering electron and the unperturbed ground electronic state charge distribution. The exchange potential, $V^{exch}(\underset{\sim}{r},K)$, models the effect of the exchange interaction between the incident electron and the target electrons. That interaction results from the possibility that the incident electron will interchange with one of the target electrons. For incident electrons with kinetic energies in the low (energy below electronic excitation threshold of target) and intermediate (energy above electronic excitation threshold but below several hundred eV where the Born approximation [see section 2.3.4] becomes valid) ranges a polarization potential, $V^{pol}(\underset{\sim}{r})$, is also included. The polarization potential takes into account the effects of target electron density distortion or polarization due to the presence of the incident electron. When the incident electron is in the inter-

mediate energy range, the possibility of electronic excitation may be included by adding a positive imaginary component to $V(\hat{r})$. This imaginary component will account for the loss of flux due to electronic excitation.[14]

While Eq. 2.15 represents a considerable simplification from Eq. 2.11, it is still an infinite set. Obviously infinite sets of equations cannot be solved entirely, so various approximations are required. These will be discussed in the next section.

2.3 Approximations to Expansion Results

2.3.1 Close Coupling

A simple approximation to Eqs. 2.11 and 2.15 is to truncate the expansion, including only a finite number of basis functions which are believed to be important for the scattering process being studied. Once the expansion is truncated it may no longer be a rigorous solution to the Schrödinger equation and hence does not satisfy Eq. 2.1. The method of optimizing the truncated expansion is based on satisfying variational criteria very similar to the bound state Hartree-Fock equation.[3,5,15] Wladowsky[15] has shown that for truncated expansions of Ψ in the form of Eq. 2.3 the following relations must be satisfied,

$$\langle \phi_n | H - E | \Psi \rangle = 0 \tag{2.18}$$

$$\langle \delta \phi_n | H - E | \Psi \rangle = 0 \tag{2.19}$$

$$\delta R_{\alpha\beta} = 0 \, . \tag{2.20}$$

$R_{\alpha\beta}$ represents elements of the $\underset{\approx}{R}$ matrix which can be related to the $\underset{\approx}{S}$ matrix by the expression[16]

$$\underset{\approx}{S} = \frac{I - \frac{1}{2} i \underset{\approx}{R}}{I + \frac{1}{2} i \underset{\approx}{R}} \, . \tag{2.21}$$

Satisfying Eqs. 2.18-2.20 yields a finite system of equations identical in form to Eqs. 2.11 and 2.15.

Close-coupling calculations have been performed for very simple

systems. For atomic hydrogen, the $1\,^2S \rightarrow 2\,^2P$ excitations have been studied using a basis consisting of 1s, 2s, and 2p states and $\ell \leq 7$ for each state.[17] These results are considered the most accurate for atomic hydrogen and are used for comparison with all other approximations. Within the effective potential scheme close-coupling calculations have been performed on atoms[9,18-21] for elastic scattering and on molecules[7,8,10,11,13,22-25] for elastic scattering, and rotational and vibrational inelastic scattering. However, due to the complexity of solving a finite but large set of coupled integro-differential equations, the close-coupling method does not seem to offer much promise for the problem of electronic excitations in electron-polyatomic molecule scattering.[7,8]

2.3.2 Two-State

As the name implies the two state approximation involves the assumption that only the initial state (ϕ_0) and the final state (ϕ_n) of the target molecule are important in the expansion of Eq. 2.3. All terms are neglected which do not directly couple $\phi_0 \rightarrow \phi_0$, $\phi_0 \rightarrow \phi_n$, or $\phi_n \rightarrow \phi_n$. This technique has been applied to electronic transitions in atoms[26] and may have potential usefulness in describing transitions in molecules between two close lying states.

2.3.3 Distorted Wave

The distorted wave approximation[27,28] reduces the system of equations represented by Eq. 2.5 to the following two equations when studying the excitation of the target from ϕ_0 to ϕ_m.

$$(\nabla_1^2 + K_0^2)\, F_0\,(\underset{\sim}{r}_1) = \frac{2m}{\hbar^2}\langle\phi_0 \,|\, V_{1\text{-mol}} \,|\, \phi_0\rangle\, F_0\,(\underset{\sim}{r}_1) +$$

$$(N\text{-}1)\langle\phi_0 \,|\, \phi_0\,(\nabla_2 + K_0^2 - \frac{2m}{\hbar^2} V_{2\text{-mol}})\, F_0\,(\underset{\sim}{r}_2)\rangle \qquad (2.22)$$

$$(\nabla_m^2 + K_m^2)\, F_m(\underset{\sim}{r}_1) = \frac{2m}{\hbar^2}\langle\phi_m \,|\, V_{1\text{-mol}} \,|\, \phi_m\rangle\, F_m(\underset{\sim}{r}_1) +$$

$$\frac{2m}{\hbar^2}\langle\phi_m \,|\, V_{1\text{-mol}} \,|\, \phi_0\rangle\, F_0\,(\underset{\sim}{r}_1) + (N\text{-}1)[\langle\phi_m \,|\, \phi_m(\nabla_2^2 + K_m^2 - \frac{2m}{\hbar^2} V_{2\text{-mol}})$$

$$F_m(\underset{\sim}{r}_2)\rangle + \langle\phi_m \,|\, \phi_0\,(\nabla_2^2 + K_0^2 - \frac{2m}{\hbar^2} V_{2\text{-mol}})\, F_0\,(\underset{\sim}{r}_2)\rangle\,] \,. \qquad (2.23)$$

These equations can be solved sequentially first for $F_0(\underset{\sim}{r})$ and then for $F_m(\underset{\sim}{r})$. This process is possible because the coupling between states 0 and m, which would have been in Eq. 2.22 if a two-state approximation had been made, has been neglected. Effectively the coupling terms in Eq. 2.23 distorts the $F_m(\underset{\sim}{r})$ from what it would have been if they were not included.

For low impact energies the distortion effects in $F_m(\underset{\sim}{r})$ are significant.[28] This technique has been applied to inelastic scattering in rare gas atoms (27) and is found to be greatly superior to the Born approximation (see section 2.3.4) for determining angular distributions. The distorted wave method has also been applied to elastic and rotationally inelastic scattering from H_2 and N_2.[29-31]

2.3.4 Born and Born-Oppenheimer Approximations

The Born and Born-Oppenheimer approximations[32,33] result, if in addition to all the previous assumptions it is assumed that all scattering, both elastic and inelastic, is small and the final state wavefunctions are simply products of plane waves and target eigenfunctions. Basically f_{on} and f_{oo} are set equal to zero in the asymptotic expression Eq. 2.7. Strictly speaking the Born approximation is used to determine the direct scattering process' scattering amplitude. The direct process is that for which the incident electron is also scattered. The Born-Oppenheimer approximation resulted from Oppenheimer's perception[34] that the incident electron could exchange with a target electron. This target electron would then appear as the outgoing scattered electron. These different processes show significantly different angular and incident energy dependences.

The Born expression for the direct scattering amplitude may be written as

$$f_{on}^{B} = -\frac{m}{2\pi\hbar^2}\langle e^{i\underset{\sim}{K}_n\cdot\underset{\sim}{r}_1}\,\phi_n(\underset{\sim}{r}_2,\ldots,\underset{\sim}{r}_N;\underset{\sim}{R})\,|\,V_{1\text{-mol}}\,|\times e^{i\underset{\sim}{K}_0\cdot\underset{\sim}{r}_1}\,\phi_0(\underset{\sim}{r}_2,\ldots,\underset{\sim}{r}_N;\underset{\sim}{R})\rangle\,, \tag{2.24}$$

where $\underset{\sim}{R}$ symbolizes all internuclear coordinates in the target. Performing the integration over $\underset{\sim}{r}_1$ yields

$$f_o^B = -\frac{me^2}{2\pi\hbar^2}\langle\phi_n(\underset{\sim}{r}_2,\ldots,\underset{\sim}{r}_N;\underset{\sim}{R})\Big|\sum_{m=2}^{N} e^{i\Delta\underset{\sim}{K}\cdot\underset{\sim}{r}_m}$$

$$-\sum_{h=1}^{N'} e^{i\Delta\underset{\sim}{K}\cdot\underset{\sim}{R}_n}\Big|\phi_o(\underset{\sim}{r}_2,\ldots,\underset{\sim}{r}_N;\underset{\sim}{R})\rangle\,, \qquad (2.25)$$

where $\Delta\underset{\sim}{K}$ is the difference between the momentum of the incident electron and the scattered electron. The second term vanishes for inelastic scattering due to the orthogonality of ϕ_o and ϕ_n. The differential cross section using the Born approximation is given by Eq. 2.8. Within the validity of the Born approximation it is evident that as $\Delta\underset{\sim}{K}$ becomes small, electron impact selection rules approach optical electric dipole selection rules. Expanding $e^{i\Delta\underset{\sim}{K}\cdot\underset{\sim}{r}_m}$ yields

$$f_{oB} = -\frac{2me^2}{\hbar^2}\langle\phi_n|\sum_{m=2}^{N}(1+\Delta\underset{\sim}{K}\cdot\underset{\sim}{r}_m+(\frac{\Delta\underset{\sim}{K}\cdot\underset{\sim}{r}_m}{2})^2+\ldots|\phi_o\rangle\,, \qquad (2.26)$$

where the first integral ($\langle\phi_n|\sum_{m=2}^{N}(1)|\phi_o\rangle$) is zero because ϕ_o and ϕ_n are orthogonal. $\Delta\underset{\sim}{K}$ becomes small at high impact energies and low scattering angle.

The exchange scattering amplitude, g_{on}^{BO}, given by the Born-Oppenheimer approximation is

$$g_{on}^{BO} = -\frac{m}{2\pi\hbar^2}\langle e^{i\underset{\sim}{K}_n\cdot\underset{\sim}{r}_2}\phi_n(\underset{\sim}{r}_1,\underset{\sim}{r}_3,\ldots\underset{\sim}{r}_N;\underset{\sim}{R}|V_{2\text{-mol}}|$$

$$\times e^{i\underset{\sim}{K}_o\cdot\underset{\sim}{r}_1}\phi_o(r_2,\ldots,r_N;R)\rangle\,. \qquad (2.27)$$

This scattering amplitude may be combined with the direct scattering amplitude to yield the total scattering amplitude, f_{on}^{tot}.

$$f_{on}^{tot} = \langle \chi_{initial}^{\Sigma u}(1,\ldots,N) \,|\, \chi_{final}^{'\Sigma u}(1,\ldots,N) \rangle_{spin} f_{on}^{B}$$

$$- (N-1)\langle \chi_{initial}^{\Sigma u}(2,1,\ldots,N) \,|\, \chi_{final}^{'\Sigma u}(1,\ldots,N) \rangle_{spin} g_{on}^{BO} \qquad (2.28)$$

In this equation, Σ is the eigenvalue of the total spin S^2, u is its axial projection, and the χ are the spin wavefunctions.

Both approximations suffer from the fact that replacing the scattered wave by a plane wave is only valid at high impact energies (>150 eV). Low impact energies (≤ 50 eV) are particularly interesting because spin forbidden transitions are more intense relative to spin allowed excitations and as the impact energy lowers the probability of exchange increases. So at the impact energies of greatest interest neither approximation is found to be extremely accurate. It is often the case that at low impact energy the Born-Oppenheimer approximation overestimates the integral cross section by an order of magnitude.[35,36] Also the Born approximation generates differential cross sections which drop off with scattering angle more rapidly than is experimentally observed.[17]

2.3.5 Ochkur-Rudge Modifications to the Born Oppenheimer approximation

The Born-Oppenheimer expression for the exchange scattering

amplitude is expected to be valid only when the incident and scattered electrons may be adequately described as plane waves. This is expected to be the case at relatively high impact energies ($\geq$ 150 eV). Unfortunately, at these energies the magnitude of exchange scattering is very small. Also attempts to extrapolate it to the domain of low energies lead to poor and often even quite meaningless results.[37]

With these thoughts in mind Ochkur[38] obtained an expansion for g_{on}^{BO} in terms of $1/K$, where $\hbar K$ is the incident electron's momentum. At high energies $|K| \gg 1$, the expansion may be truncated after the first term which is $O(1/K^2)$. Among the terms neglected are those corresponding to the interaction with target nuclei. The Ochkur expression for the exchange scattering amplitude is

$$g_{on}^{O} = -\frac{2me^2}{\hbar^2 K_0^2} \langle \phi_n(\underset{\sim}{r}_1, \underset{\sim}{r}_3, \ldots, \underset{\sim}{r}_N; \underset{\sim}{R}) \left| e^{i\Delta\underset{\sim}{K}\cdot\underset{\sim}{r}_2} \right|$$

$$\times \phi_0(\underset{\sim}{r}_2, \ldots, \underset{\sim}{r}_N; \underset{\sim}{R}) \rangle . \qquad (2.29)$$

Ochkur reasoned that use of this expression, which contained the portion of g_{on}^{BO} most valid at high incident energy, might yield more reasonable results at low energy than g_{on}^{BO}. It should be noted that g_{on}^{O} is quite similar to the Born approximation direct scattering amplitude (Eq. 2.24), except for the replacement of $\frac{(N-1)}{(\Delta\underset{\sim}{K})^2}$ by $\frac{1}{K_0^2}$. This difference leads to an angular dependence which is quite different from that of direct scattering.

In 1965 Rudge[39] pointed out that the Ochkur formula was not

consistent with variational principles. To correct this the Ochkur formula should be replaced by the expression

$$g_{on}^{OR} = - \frac{K_o^2}{[K_n - iA]^2} g_{on}^{O} , \tag{2.30}$$

where $A \equiv [2mI_i]^{\frac{1}{2}}/\hbar$, and I_i is the lowest ionization potential of the initial state of the target molecule. The Ochkur-Rudge expression does not satisfy the principle of detailed balance. Bely[39] has shown that the Ochkur-Rudge result can be corrected if the scattering amplitude is replaced by its absolute value.

Truhlar, Cartwright, and Kuppermann[40,41] have used the Ochkur-Rudge formula to calculate cross sections for the exchange processes in H and He. They found the cross sections to be fairly accurate. This approximation was used by the same authors to calculate integral and differential cross sections for excitations of the $a^3\Sigma_g^+$ and $b^3\Sigma_u^+$ states of H_2. Experimental results were compared to their theoretical calculations for differential cross sections at incident energies between 25 eV and 60 eV and scattering angles from 10° to 80°. The agreement between theory and experiment was quite good for incident energies of 35 eV and above. At 25 eV incident energy the agreement was considerably poorer. When attempting to apply the Ochkur-Rudge approximation, care should be taken because it is not based on a firm theoretical base. Its agreement with experimental results in the systems mentioned may be somewhat fortuitous.

2.3.6 Glauber and Eikonal Techniques

The Glauber approximation is a specific application of an entire class of Eikonal approximations for the scattering amplitude.[44] Eikonal approximations are semi-classical techniques and closely related to the JWKB approximation.[45] Development of the Glauber approximation from the Eikonal approximation will be shown below.

The Schrödinger equation for the potential scattering of a single particle can be written as

$$(-\frac{\hbar^2}{2m}\nabla^2 + V(\underset{\sim}{r}) - E)\psi(\underset{\sim}{r}) = 0 \ . \tag{2.31}$$

Write Ψ in the form

$$\Psi(\underset{\sim}{r}) = A(\underset{\sim}{r})\exp[iS(\underset{\sim}{r})], \tag{2.32}$$

where $A(\underset{\sim}{r})$ and $S(\underset{\sim}{r})$ are chosen to be purely real. After substitution of Eq. 2.32, the real and imaginary parts of Eq. 2.31 yield respectively

$$\nabla^2 A - A(\nabla S)^2 + (K^2 - U)A = 0 \tag{2.33}$$

and

$$2\nabla A \cdot \nabla S + A\nabla^2 S = 0 , \tag{2.34}$$

with

$$U(\underset{\sim}{r}) = \frac{2m\, V(\underset{\sim}{r})}{\hbar^2} \ . \tag{2.35}$$

Equation 2.33 cannot be solved without approximation. The fundamental Eikonal approximation is the assumption

$$\frac{\nabla^2 A}{A} \ll K^2 \ , \tag{2.36}$$

which is basically a high-energy approximation since K^2 is proportional to energy. With Eq. 2.36, Eq. 2.34 becomes

$$(\nabla S)^2 = K^2 - U \tag{2.37}$$

which has the solution

$$S(\underset{\sim}{r}) - S(\underset{\sim}{a}) = \int_{\underset{\sim}{a}(\underset{\sim}{r})}^{\underset{\sim}{r}} d\underset{\sim}{r}' \cdot \underset{\sim}{n}[K^2 - U(\underset{\sim}{r}')]^{\frac{1}{2}} \ . \tag{2.38}$$

$\underset{\sim}{a}(\underset{\sim}{r})$ is some initial point on the ray path through $\underset{\sim}{r}$, and at each point, $\underset{\sim}{r}' = \underset{\sim}{r}_0$, on the ray path the direction of $\underset{\sim}{n}(\underset{\sim}{r}_0)$ is perpendicular to the surface of constant S through $\underset{\sim}{r}_0$. Expanding the square root in Eq. 2.38 yields

$$S(\underset{\sim}{r}) - S(\underset{\sim}{a}) = \int_{\underset{\sim}{a}}^{\underset{\sim}{r}} d\underset{\sim}{r}' \cdot \underset{\sim}{n}(K - \tfrac{1}{2}\frac{U(\underset{\sim}{r}')}{K}) . \tag{2.39}$$

Equation 2.39 is to be integrated along the ray perpendicular to surfaces of constant $S(\underset{\sim}{r}')$. However, if the curvature is neglected, which in quantum mechanics implies small deflection angles of the incident electron, and the z direction is chosen to be $\underset{\sim}{r}_i$, the incident wave's propagation direction,then Eq. 2.39 reduces to

$$S(x,y,z) - S(x,y,a_z) = K(z - a_z) - \frac{m}{\hbar^2 K}\int_{a_z}^{z} dz'\, V(x,y,z'). \tag{2.40}$$

If we allow $a_z \rightarrow -\infty$ then we can set $S(x,y,a_z)$ equal to Ka_z which

allows writing $\Psi(\underset{\sim}{r})$ as

$$\Psi(\underset{\sim}{r}) = \exp(iK\underset{\sim}{n}_i \cdot \underset{\sim}{r}) \exp\left(-\frac{im}{\hbar^2 K} \int_{-\infty}^{z} dz' V(x,y,z)\right). \tag{2.41}$$

This result is Glauber's approximation to the wavefunction. The scattering amplitude is given by

$$A(\underset{\sim}{n}_i \rightarrow \underset{\sim}{n}_f) = -\frac{1}{4\pi} \frac{2m}{\hbar^2} T_{if} \tag{2.42}$$

where $\underset{\sim}{n}_i$ is the initial direction and $\underset{\sim}{n}_f$ is the final direction and T_{if} is given by[44]

$$T_{if} = \int d\underset{\sim}{r} \exp(-iK\underset{\sim}{n}_f \cdot \underset{\sim}{r}) V(\underset{\sim}{r}) \Psi(\underset{\sim}{r}) . \tag{2.43}$$

When the additional assumption that the component of the momentum transfer in the $\underset{\sim}{n}_i$ direction is negligible is made, the scattering amplitude may be written as

$$A(\underset{\sim}{n}_i \rightarrow \underset{\sim}{n}_f) = \frac{iK}{2\pi} \int d^2\underset{\sim}{b} \exp(i\underset{\sim}{\underset{\sim}{q}} \cdot \underset{\sim}{b}) \left[1-\exp\left(-\frac{im}{\hbar^2 K} \int_{-\infty}^{+\infty} dz V(x,y,z')\right)\right], \tag{2.44}$$

where $\underset{\sim}{b}$, with components (x, y) and $d^2\underset{\sim}{b} = dxdy$, can be regarded as the two-dimensional impact parameter vector in the plane perpendicular to z.

Both elastic and inelastic cross sections may be calculated within the formalism of the Glauber approximation.[44,46] While the Glauber approximation entirely neglects the exchange interaction it

seems to yield fairly accurate values for integral and differential cross sections at incident energies above 30 eV.[44,47] Generally these values are more accurate than Born approximation results. At incident energies above about 150 eV the Glauber and Born results are virtually the same. Applications have been limited to H, He, alkali atoms, and H_2.[44] However, Bartell[48] modified the Glauber theory to treat scattering of electrons by polyatomic molecules. For intermediate energies the Glauber approximation may prove to be useful for studying electron-molecule scattering.

2.4 Scattering Techniques Making Use of Green's Function Solutions of the Schrödinger Equation

2.4.1 Basis Set Approach to Nonspherical Scattering

The starting point for this technique is the Lippmann-Schwinger equation,[49]

$$\psi_a^{(+)}(\underset{\sim}{r},\boldsymbol{\mathcal{E}}) = \phi_a(\underset{\sim}{r},\boldsymbol{\mathcal{E}}) + G^{(+)}(\underset{\sim}{r}\boldsymbol{\mathcal{E}}|\underset{\sim}{r}'\boldsymbol{\mathcal{E}}')V\psi_a^{+}(\underset{\sim}{r},\boldsymbol{\mathcal{E}}) . \qquad (2.45)$$

Within this formalism, $\psi_a^{(+)}(\underset{\sim}{r},\boldsymbol{\mathcal{E}})$ represents a solution to the Schrödinger equation for a particle, located at $\underset{\sim}{r}$, scattering off a target, located at the origin of coordinates with internal degrees of freedom specified by $\boldsymbol{\mathcal{E}}$. $\phi_a(\underset{\sim}{r},\boldsymbol{\mathcal{E}})$ is the wavefunction for the system when the incoming particle is beyond interaction with the target and the target is in an initial eigenstate, a. $G^{(+)}(\underset{\sim}{r}\boldsymbol{\mathcal{E}}|\underset{\sim}{r}'\boldsymbol{\mathcal{E}}')$ is the Green's function for this system[33] with the superscript (+) indicating outgoing scattering waves. $G^{(+)}$ may be defined by the expression[50]

$$G^{(+)} \equiv \lim_{\epsilon \to 0^+} \frac{1}{E - H + i\epsilon} \qquad \begin{matrix} \mathrm{Im}\,\epsilon = 0 \\ \mathrm{Re}\,\epsilon > 0 \end{matrix} , \tag{2.46}$$

with E and H respectively being the total energy and Hamiltonian operator for the target + incident particle system. The superscript (+) on $\psi_a^{(+)}$ also represents that $\psi_a^{(+)}$ is composed of outgoing scattered waves. The interaction between the incident particle and the target is symbolized by V. Equation (2.45) represents an integral equation which $\psi_a^{(+)}$ must satisfy.

The Lippmann-Schwinger scattering operator, T, is given by

$$T(E) = V + V G^{(+)} T . \tag{2.47}$$

T, which is, as $G^{(+)}$, a function of E, may be written as

$$T = (1 - V G^{(+)})^{-1} V . \tag{2.48}$$

Rescigno, McCurdy, and McKoy[51,52] have used this formalism to study non-spherical elastic scattering. They first made the approximation that the exact potential V can be well represented by a NxN representation of V obtained by its projection onto the subspace spanned by N square-integrable basis functions $\{\phi_\alpha\}$. Similarly $G^{(+)}$ is written within this basis. For non-spherical potentials this technique appears to be significantly faster than more traditional methods.

For the elastic scattering of an electron from H_2 in the 8 eV to 21 eV range, Rescigno, McCurdy, and McKoy[53] have obtained results in good agreement with more expensive techniques. Klonover and Kaldor[54] have used the same technique to study inelastic rotational

excitation of H_2. Their results are found to be in good agreement with experiments.

2.4.2 Second Quantization Technique

Using Green's functions and the principle of second quantization Taylor and coworkers[55-58] have derived expressions for both elastic and inelastic electron scattering. The many-body technique allows uncoupling of the various exit channels for inelastic scattering. The resulting optical potential between two channels is in general energy-dependent, nonlocal and complex. Various approximations are discussed and application has been made to the calculation of elastic electron-helium scattering s, p, and d wave phase shifts.[58] Good agreement between experimental results and theoretical s and p wave phase shifts was observed. In a further study of the inelastic scattering of electrons from helium[59] in the incident electron energy range from 29.6 eV to 81.6 eV, Taylor and coworkers calculated both integral and differential cross sections for $1\,^1S$ to $2\,^1S$, $2\,^1P$, $2\,^3S$, and $2\,^3P$ excitations. Their results compare quite favorably with prior calculations and experimental results.[60]

The relation between the distorted wave approximation and the many-body approach of Taylor has been demonstrated by Rescigno et al.[61] Using many-body techniques in terms of the distorted-wave approximation, Rescigno et al.[62,63] have calculated cross sections for the excitation of H_2 to the $a\,^3\Sigma_g^+$ and $b\,^3\Sigma_u^+$ states. Their results display relatively isotropic differential cross sections and are in good agreement with the available experimental results.

References

1. J. K. Rice, Ph.D. thesis, California Institute of Technology, Pasadena, California (1969) pp. 14-21.
2. W. M. Flicker, Ph.D. thesis, California Institute of Technology, Pasadena, California (1976) p. 34.
3. I. C. Percival and M. J. Seaton, Proc. Cambridge Phil. Soc. 53, 654 (1957).
4. P. G. Burke and H. M. Schey, Phys. Rev. 126, 147 (1962).
5. P. G. Burke and K. Smith, Rev. Mod. Phys. 34, 458 (1962).
6. P. G. Burke, H. Schey, and K. Smith, Phys. Rev. 129, 1258 (1963).
7. P. G. Burke and N. Chandra, J. Phys. B: Atom. Molec. Phys. 5, 1696 (1972).
8. P. G. Burke, N. Chandra, and F. A. Gianturco, J. Phys. B: Atom. Molec. Phys. 5, 2212 (1972).
9. J. E. Purcell, R. A. Berg, and A. E. S. Green, Phys. Rev. A 2, 107 (1970).
10. M. A. Brandt, D. G. Truhlar, and F. A. Van-Catledge, J. Chem. Phys. 64, 4957 (1976).
11. D. G. Truhlar and M. A. Brandt, J. Chem. Phys. 65, 3092 (1976).
12. J. M. Paikeday, J. Chem. Phys. 65, 397 (1976).
13. Y. Itikana and K. Takayangi, J. Phys. Soc. Japan 27, 1293 (1969).
14. L. Schiff, Quantum Mechanics, 3rd ed., (McGraw-Hill Book Company, New York, 1968) p. 129.

15. I. Wladowsky, J. Chem. Phys. 58, 1826 (1973).

16. A. S. Davydov, Quantum Mechanics (Pergamon Press, New York, 1965) p. 436.

17. M. A. Brandt and D. G. Truhlar, Phys. Rev. A 11, 1340 (1975).

18. J. Callaway, R. W. LaBahn, R. T. Pu, and W. Duxler, Phys. Rev. 168, 12 (1968).

19. D. L. Walker, J. Phys. B: Atom. Molec. Phys., Ser. 2, 2, 356 (1969).

20. R. W. LaBahn and J. Callaway, Phys. Rev. A 2, 366 (1970).

21. D. Andrick and A. Bitsch, J. Phys. B: Atom. Molec. Phys. 8, 393 (1975).

22. S. Hara, J. Phys. Soc. Japan, 27, 1009 (1969).

23. M. A. Morrison, L. A. Collins, and N. F. Lane, Chem. Phys. Lett. 42, 356 (1976).

24. D. G. Truhlar, M. A. Brandt, A. Chutjian, S. K. Srivasta a, and S. Trajmar, J. Chem. Phys. 65, 2962 (1976).

25. N. Chandra and A. Temkin, J. Phys. Chem. 65, 4537 (1976).

26. B. L. Moiseiwitsch and S. J. Smith, Rev. Mod. Phys. 40, 238 (1968).

27. W. N. Shelton and E. S. Leherissey, J. Chem. Phys. 54, 1130 (1971).

28. H. S. W. Massey and E. H. S. Burhop, Electron and Ionic Impact Phenomena, Vol. 1 (Clarendon Press, Oxford, 1969) p. 525.

29. H. S. W. Massey and B. L. Moisewitsch, Proc. Roy. Soc. (London) 258, 147 (1960).

30. D. H. Sampson and R. C. Mjolsness, Phys. Rev. 140A, 1466 (1965).

31. K. Takayanagi and S. Geltman, Phys. Rev. 138A, 1003 (1965).

32. H. S. W. Massey and C. B. O. Mohr, Proc. Roy. Soc. A 132, 605 (1931).

33. Davydov, op. cit. pp. 406-421.

34. J. R. Oppenheimer, Phys. Rev. 32, 361 (1928).

35. K. L. Bell, H. Eissa and L. Moisewitsch, Proc. Phys. Soc. (London) 88, 57 (1966).

36. J. D. Jobe and R. M. St. John, Phys. Rev. 164, 117 (1967).

37. D. R. Bates, A. Fundaminsky, and H. S. W. Massey, Trans. Roy. Soc. (London) A243, 93 (1950).

38. V. I. Ochkur, Soviet Physics - JETP 18, 503 (1964).

39. O. Bely, Proc. Phys. Soc. (London) 87, 1010 (1966); Nuovo Cimento 49B, 66 (1967).

40. D. G. Truhlar, D. C. Cartwright and A. Kuppermann, Phys. Rev. 175, 113 (1968).

41. D. C. Cartwright, Ph.D. Thesis, California Institute of Technology, Pasadena, California (1967).

42. D. C. Cartwright and A. Kuppermann, Phys. Rev. 163, 86 (1967).

43. S. Trajmar, D. C. Cartwright, J. K. Rice, R. T. Brinkman and A. Kuppermann, J. Chem. Phys. 49, 5464 (1968).

44. E. Gerjuoy and B. K. Thomas, Rep. Prog. Phys. 37, 1345 (1974).

45. A. Messiah, Quantum Mechanics, Vol. I (North-Holland Publishing Co., Amsterdam. 1958), pp. 231-241.

46. V. Franco, Phys. Rev. A. 1, 1705 (1970).

47. H. Tai, R. H. Bassel, E. Gerjouy, and V. Franco, Phys. Rev. A 1, 1819 (1970).

48. L. S. Bartell, J. Chem. Phys. 63, 3750 (1975).

49. B. A. Lippmann and J. Schwinger, Phys. Rev. 79, 469 (1950).

50. A. Messiah, Quantum Mechanics, Vol. II (North-Holland Publishing Co., Amsterdam, 1958), p. 819.

51. T. N. Rescigno, C. W. McCurdy, and V. McKoy, Chem, Phys. Lett. 27, 401 (1974).

52. T. N. Rescigno, C. W. McCurdy, and V. McKoy, Phys. Rev. A10, 2240 (1974).

53. T. N. Rescigno, C. W. McCurdy, and V. McKoy, Phys. Rev. A11, 825 (1975).

54. A. Klonover and U. Kaldor, Chem. Phys. Lett. 51, 321 (1977).

55. B. Schneider, H. S. Taylor, and R. Yaris, Phys. Rev. A 1, 855 (1970).

56. G. Csanak, H. S. Taylor, and R. Yaris, Phys. Rev. A 3, 1322 (1971).

57. G. Csanak, H. S. Taylor, and D. N. Tripathy, J. Phys. B 6, 2040 (1973).

58. B. S. Yarlagadda, G. Csanak, H. S. Taylor, B. Schneider, and R. Yaris, Phys. Rev. A 7, 146 (1973).

59. L. D. Thomas, G. Csanak, H. S. Taylor, and B. S. Yarlagadda, J. Phys. B: Atom. Molec. Phys. 7, 1719 (1974).

60. R. I. Hall, G. Joyez, J. Mazeau, J. Rheinhardt, and C. Scherman, J. de Phys. 34, 824 (1973).

61. T. N. Rescigno, C. W. McCurdy, and V. McKoy, J. Phys. B 7, 2396 (1974).

62. T. N. Rescigno, C. W. McCurdy, and V. McKoy, J. Phys. B 8, L433 (1975).

63. T. N. Rescigno, C. W. McCurdy, V. McKoy, and C. F. Bender, Phys. Rev. A 13, 216 (1976).

3. EXPERIMENTAL

3.1 Introduction

Two electron impact spectrometers (EIS) were used to obtain the results presented in this thesis. Most of the molecules were studied using an instrument designed by Rice, Trajmar, and Kuppermann[1,2] in the late 1960's. This instrument is designated EIS I. The spectra of benzene, fluorobenzene and hexaflurobenzene were obtained using an improved version of the EIS I spectrometer, designated EIS II. The EIS I spectrometer has been described in great detail by J. K. Rice in his Ph. D. Thesis,[2] while EIS II is described in the Ph. D. theses of O. A. Mosher[3] and W. M. Flicker.[4]

This experimental section contains three parts in addition to the Introduction. The second sub-section describes briefly the EIS I spectrometer, while the third sub-section describes present data handling procedures. Finally, during the last several years, construction of a new electron impact spectrometer, EIS III, has progressed to near completion. Initial design work was performed by W. M. Flicker and is described in great detail in his Ph. D. Thesis.[4] While construction has progressed, certain changes in the design of EIS III have been made. These designed changes are summarized in the fourth part of this chapter.

3.2 Description of the EIS I Spectrometer

Figure 1 is a schematic drawing of EIS I. The instrument consists of an electron gun, two hemispherical electrostatic energy

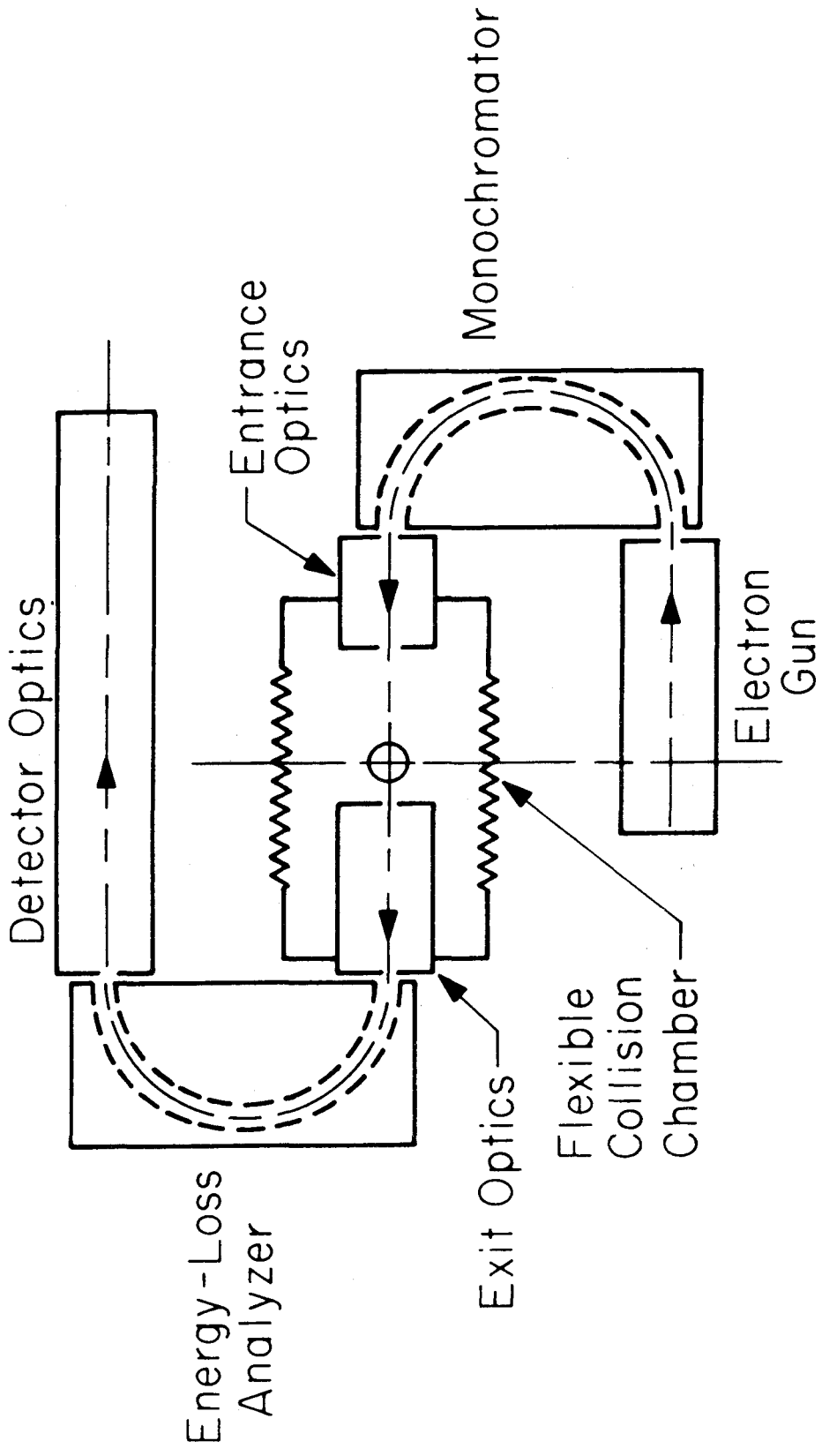

SPECTROMETER BLOCK DIAGRAM

Figure 1

analyzers (monochromator and energy loss analyzer), a scattering chamber, and a detector system.

The gun stage is identical to that used in EIS II and hence represents an improvement to the gun initially used by Rice.[2] This stage consists of four electrostatic lens elements. These lens elements are basically cylinders of oxygen-free high conductivity (OFHC) copper to which different electrical potentials are applied. The actual electron optical lens is formed in the region between two of the copper lens elements. In this region the electrical field changes from the potential of the first lens element to that of the second element.

Electrons are initially extracted from a 0.005" tungsten filament, operating between 1850° C and 2200° C.[3] These electrons have a thermal energy distribution with a full width at half maximum (FWHM) of approximately 0.63 eV.[2] The electron density in the region between the cathode housing and the first aperture, located in the Accelerator lens element, is space charge limited. These electrons are extracted by a two lens condensor system (Accelerator-High Voltage lens and High Voltage-Decelerator lens). The first aperture which is in the Accelerator lens element serves as an object (image) or window which illuminates the second gun stage aperture located in the Decelerator lens element. This aperture acts as the entrance window of the monochromator. In effect, it limits the field of view of the anode formed at the monochromator entrance plane. Also located within the Decelerator lens element, the third aperture is an angle defining aperture, which serves as the entrance pupil of the monochromator. Within the Accelerator, High Voltage, and Decelerator lens elements the

electron beam is moving with sufficient kinetic energy such that it is no longer space charge limited. This insures that the beam will be precisely defined by the second and third apertures.

The Decelerator and Herzog 1 lens elements form a 10 : 1 decelerator lens which slows the rapidly moving beam entering the Decelerator to a slowly moving (2 eV to 4 eV kinetic energy) beam which is again space charge limited and ready to enter the monochromator. This lens images the entrance window (second aperture) onto the entrance plane of the monochromator. In Herzog 1 is a fourth gun stage aperture. This is a "spatter" aperture, designed to intercept stray electrons scattered off lens element walls and apertures in the preceding stages, as well as any electrons produced in secondary emission.

In the Accelerator and the Decelerator lens elements are contained two deflectors and four deflectors, respectively. Potentials independent of the lens element within which they are contained may be applied to these deflectors. The deflectors allow slight corrections to the axial position of the electron beam within the gun stage.

The diameters for the four apertures within the gun are: #1 - 0.03", #2 - 0.016", #3 - 0.020", and #4 - 0.08". The gun stage lens elements along with the others in the rest of the instrument including the hemispherical electrostatic analyzers were goldplated. This relatively inert surface was found to be essential when studying reactive molecules such as UF_6 and WF_6. For similar reasons the most successful apertures were made of a platinum/10% irridium alloy fabricated by Engelhard Industries.[5] Potentials were applied to

lens elements using circuits described by Mosher[3] except the transistor emitter-follower stages were deleted.

The energy analyzers used in this study consist of inner and outer concentric hemispheres with a mean radius of 1.000" and a gap of 0.250" between the inner and outer surfaces. Rice[2] has described in detail the electrostatics and dynamics of this configuration. Only electrons with specific energies will be transmitted. The electron beam image formed on the entrance plane of the monochromator is reimaged on the exit plane. However, the exiting beam has an energy FWHM of 0.040 eV to 0.15 eV as compared to the incident thermal distribution.

Between the monochromator and the scattering chamber are three lens elements, Herzog 2, L2A, and L2B, collectively referred to as the entrance optics. Basically the entrance optics take the image at the exit plane of the monochromator and reimage it at the scattering center inside the scattering chamber. During this process, these lenses accelerate the electron beam from several electron volts to the full impact energy. The first lens element, Herzog 2, is used like all Herzog elements to minimize distortion of the electric field between the spheres. The H2-L2A elements and the L2A-L2B elements form a double aperture lens[6] (this lens type is different from the tube lenses used in the gun stage[7]) when L2B is held at the scattering chamber potential (generally ground potential). Actually, L2B's potential may be varied, providing an extra lens between it and the scattering chamber. This flexibility permits the angular properties of the beam within the scattering chamber to be better controlled,

as well as fixing the axial position of the beam focus.

After L2B there are two sets of perpendicular deflectors which are used to correct beam alignment. These deflectors are used to insure the electron beam passes through aperture 5 which is just at the entrance of the scattering chamber. Aperture 5 has a 0.030" diameter and minimizes gas flow out of the scattering chamber into the entrance optics. It does not perform an important function as far as electron-optical effects are concerned.

Currents entering the scattering chamber are measured using an electrometer attached to a Faraday Cup. The Faraday Cup may be remotely inserted and removed from the scattering center. In order to collect all of the incident electrons, the Faraday Cup is biased at +90 eV relative to ground. Typical currents detected at the Faraday Cup range from 20 namp to 150 namp. When currents drop below 20 namp, operation of the spectrometer is very difficult. Generally currents above 150 namp are unnecessary and resolution is often found to suffer.

The scattering chamber consists of two concentric, flexible bellows, each formed from about 700 S-shaped convolutions of 347 stainless steel which are welded together. This construction permits a wide bending range for the double bellows assembly. Due to mechanical constraints, the bellows was rotated $\pm 55°$, which permitted scattering angles from $-25°$ to $+85°$ to be studied. It should be mentioned explicitly that the first half elements (elements prior to scattering chamber) rest on a gear wheel which when rotated allows spectra to be taken at different scattering angles.

The optics located between the scattering center and the energy-loss analyzer are collectively termed the exit optics. Two apertures define the electron beam characteristics in the exit optics. The first aperture is located a short distance within the scattering chamber. The copper piece from which it is constructed is termed the "nose cone" and is the sixth aperture along the electron beam path in EIS I. At the rear of the nose cone element is the seventh aperture which is held in place by a grounded copper cylinder. These apertures both have 0.03" diameters and together define the acceptance angle of the exit optics. The sixth aperture acts as the entrance pupil while the seventh aperture is the entrance window of the exit optics.

The primary function of the exit optics is to focus an image of the entrance window (aperture 7) onto the entrance plane of the energy-loss analyzer. During the focusing process, the scattered electrons are also decelerated from a high velocity to a much lower velocity corresponding to a kinetic energy of several electron volts at the entrance of the energy-loss analyzer. To accomplish this, two decelerating lenses are used along with a third lens which gives the exit optics additional flexibility. The first lens is composed of the grounded copper cylinder and the L3A lens element. Together they form a variable-ratio decelerator. The next lens is an aperture-cylinder lens formed by the elements L3A and L3B. This lens allows the angular properties of the beam to be varied by shifting the exit pupil position. The final fixed-ratio decelerator is formed by L3B and Herzog 3. Herzog 3 also acts as a field matching lens between itself and the energy-loss analyzer.

The energy-loss analyzer is identical to the monochromator. By varying the potential at the analyzer's mean radius, electrons which have lost specific amounts of energy are transmitted. The potential variation is accomplished by sweeping all second-half (elements after the scattering chamber) element potentials uniformly. This sweep voltage corresponds to the energy lost by the electrons during the collision process with the target molecules.

The exit optics take the image from the exit plane of the energy-loss analyzer and focus it to the Spiraltron electron multiplier. These optics consist of Tube Lens 1, which acts primarily as the field matching lens after the energy-loss analyzer. The lens formed by the elements Tube Lens 1 and Tube Lens 2 focuses the real exit window of the analyzer, formed by the eighth aperture located in Tube Lens 2, onto the cone of the Spiraltron. Two final deflectors are included in Tube Lens 2 to aid in electron beam alignment. The diameter of the eighth aperture is 0.030".

The electron multiplier is a Spiraltron continuous dynode multiplier. The multiplier is positioned about 0.050" off the electron beam axis. This is essential because the electrons must strike the preamplifier cone of the Spiraltron before reaching the first amplifier stage of the multiplier. To aid in drawing electrons into the Spiraltron, its preamplifier cone is biased about +300 volts with respect to ground.

The output pulses of the Spiraltron containing between 10^7 to 10^8 electrons are amplified by a pulse amplifier designed by O. A. Mosher and D. Mason.[3] These pulses are taken to the Nuclear Data multichannel analyzer system. Each channel of the multichannel analyzer

corresponds to a specific energy-loss. The entire spectrum is punched out on paper tape. The format of the paper tape has been described by both Mosher[3] and Flicker.[4] The following section describes the present method of data handling.

3.3 Data Handling

The paper tapes which have the spectrum heading as well as the digitalized spectrum itself are typed in the following format. The heading portion is typed on the paper tape in USASCII while the data is in 6-character BCD. Each memory channel corresponds to three 8-bit lines on the paper tape. Each line has two 4-bit binary numbers which are the multipliers for particular decimal decades. Each channel contains a 6-digit integer number. When looking at the paper tape, the two least significant digits of a given channel appear on the first 8-bit line with the fifth digit as the left-most 4 bits and the sixth digit as the right-most 4 bits. Similarly digits three and four are on the second line, digit three on the left. Digits one and two (the two most significant digits) are in line three, digit one to the left.

Prior to 1976 paper tapes were put on magnetic tape in an IBM 370 compatible format using a SCC 4700 computer. However, in early 1976 this computer lost its ability to function in a predictable and reproducible manner, i.e., it died. This necessitated developing an alternative means of transferring data to the IBM system. In collaboration with Ronald Rianda, who performed a majority of both the conceptual and actual implementation work, a new method of data transfer was developed. It is based on transferring data initially to the Caltech

PDP-10 computer and then to the Caltech IBM 370 computer. Contact is made with the PDP-10 through a PDP-8 minicomputer which operates the Multiple Angle Photoelectron experiment and can be interfaced to the PDP-10.

IPIP is a PDP-10 assembler level program which reads paper tapes on the high speed tape reader of the PDP-8 computer and transfers exactly what is read to PDP-10 disk. At this point the DATACK Fortran IV program is used to determine if paper tapes were transferred successfully to disk. DATACK prints the heading and number of data bytes of each spectrum transferred. In most cases, if the spectrum heading is incorrect or the number of data bytes is wrong the spectrum should be reread onto disk. If only a minor heading error appears, this may be corrected using a PDP-10 system routine called FILDDT. Assuming that paper tapes appear to have successfully been transferred to disk, they may then be written onto magnetic tape on the PDP-10 system.

WRITE is an assembler language program which transfers the disk files to magnetic tape using a density of 800 bytes per inch (800 BPI). To check if the transfer to magnetic tape was successful, two other assembler level programs must be used. READ transfers the tape contents into disk file Munch. Munch may be read in 8-bit octal. Generally, only small portions of Munch are checked. WRITE and READ may be used at the PDP-8 minicomputer terminal after instructing the PDP-10 operator, via the Please command, to mount magnetic tape XXX 625 on a PDP-10 tape drive.

Assuming the magnetic tape appears correct, actual translation of this magnetic tape into a form usable by our other data analysis programs may proceed. The PDP-10 operators are instructed to take tape XXX 625 to the IBM 370. NDTOMT is a Fortran IV language program (this is not the NDTOMT program described by Flicker[4] for use on SCC 4700) which reads XXX 625, translating the spectrum headings, which are still in USASCII, to IBM-compatible EBCDIC and the data in BCD into an Integer *4 Fortran IV format. This translated information is stored temporarily on disk while all of the headings and spectra are printed. This print-out is carefully reviewed to locate any previously undetected errors. On occasion a spectrum is the right length but badly jumbled. In this case, the spectrum paper tape should be reread on the PDP-8 and WRITE and NDTOMT repeated, storing this spectrum in a file different from the main set of spectra. The spectra are still not in a form usable by our primary data handling programs.

SPEDIT is another Fortran IV program on the 370 which combines spectra from various files generated by NDTOMT. It then writes a new disk file which is in a format usable by our other data analysis programs. In addition to creating this file, headings may be changed and certain minor data errors may be corrected. Generally correcting data errors requires adding instructions to the SPEDIT program which then makes the specific corrections. SPTRANS is a short Fortran IV program which can further edit the output file of SPEDIT.

Finally, the WRITAPE Fortran IV program transfers the final SPEDIT disk file to the magnetic tape, EISDT1 (1600 BPI density). The spectra on the magnetic tape are currently separated into files each of which contains from one hundred to several hundred spectra. When using WRITAPE one must decide whether spectra are to be added to the file at the end of the filled portion of the tape or a new file should be created. The advantage to separating spectra into files is that when specific spectra are to be analyzed, specification of the file in which they are located limits the region of the magnetic tape over which programs must search for the spectra of interest.

The preceding paragraphs have given a short description of the procedure for transfering data from paper tape to IBM-compatible magnetic tape. A much more detailed description will appear in the thesis of Mr. R. Rianda. To use these programs efficiently, knowledge of both the PDP-10 and IBM systems is required.

The actual data analysis programs principally used have been previously described by Flicker.[4] They are all Fortran IV programs. Typically, ANDATA1 is run using the SPEDIT output disk file, eliminating expensive magnetic tape mounting. This program supplies large plots of these spectra. Also spectra before plotting are smoothed, noise spikes removed and background noise subtracted. To obtain areas under features observed in spectra, ANDATA2 is used. Integration regions are manually determined using the ANDATA1 output and areas within these regions computed. ANDATA2 punches ratios of feature areas with respect to the most intense feature's area and

and ratios with respect to the second most intense feature's area. These punched ratios are used by ANDATA3 to calculate differential cross sections which along with the area ratios may be plotted by this program.

ESSUBTR is a Fortran IV program which allows the subtraction of one spectrum from another. Both spectra and the difference spectrum are plotted. This technique is valuable when attempting to study spin-forbidden excitations overlapped by spin-allowed excitations. Generally a low-angle spectrum containing minimal spin-forbidden contributions is subtracted from a high-angle spectrum containing significant spin-forbidden contributions. Of course, before subtraction the low-angle spectrum is appropriately scaled by the program. The resulting difference spectrum should be primarily spin-forbidden structure. ESSUBTR replaces a similar subtraction routine in ANDATA2 which was found to be unreliable. The final data analys program is ESDATA. This program plots spectra in a form suitable for publication. Also it supplies gaussian least-squares fitting of a spectrum and further analysis based on this fitting.

3.4 EIS III Design Modification

The principal design work for the EIS III was performed by Dr. W. M. Flicker and has been previously described in his thesis.[4] During construction certain changes and additions have been made. This section will summarize these modifications.

The design modifications and additions can be separated into two groups: those dealing directly with the instrument and those involving the peripheral equipment. The major design modification involves thermal isolation of the body of the instrument from the sample inlet line. In order to study molecules with very low vapor pressures it is necessary to heat these samples. The design specification was to allow operation at sample temperatures up to 250° C.

In the molecular beam configuration this requires heating the sample inlet tube up to the molecular beam capillary array. The major portion of the instrument frame is constructed from aluminum. Since aluminum heated above 150° C may suffer irreversible deformation, the instrument frame should never be heated above this temperature. This possible permanent loss of alignment necessitated redesign to insure that the frame would not be subject to these temperatures. First, all instrument pieces within the differentially pumped central column were constructed from 316 stainless steel instead of aluminum. The heat conductivity of stainless steel is nearly an order of magnitude lower than aluminum. It is believed that any radiated heat will flow only slowly through the stainless steel pieces keeping the aluminum frame temperature within desired limits.

The actual sample tube was also redesigned so that it contacts the frame at only three locations within the instrument. Two of these contacts are through cylindrical steel bellows which, due to their thinness and numerous convolutions, have low heat conductivities. The bellows themselves contact stainless steel pieces which in turn

only then contact aluminum. The third contact location is a stainless steel alignment collar within the central column. This collar, termed a spider, was constructed in a way to minimize its cross sectional area and it again contacts only stainless steel. A 4-pin feed-through into the differentially pumped central column has been included so that an electrical heating element and a thermocouple may be attached to the sample tube.

Operating at elevated temperatures in the scattering chamber configuration should be possible but care must be exercised. The entire scattering chamber assembly is constructed of 316 stainless steel. It contacts the aluminum frame only through insulating materials such as boron nitride or Macor ceramic (at the present time contact is also made by viton O-rings which should be removed prior to high temperature operation). However, both the entrance and exit optics are contained within this assembly. Since these optics are constructed of oxygen-free high-conductivity copper and the delicate insulating pieces are made of boron nitride or Macor, differentials in the rates of thermal expansion may be a problem. Finally, expansion of the entire scattering chamber assembly relative to the remainder of the aluminum frame may cause unacceptably high stresses. This possibility must be considered prior to heating. Finally the gun stage electron optics are sometimes baked while the instrument is assembled. To allow this, the mounting piece which initially had been constructed from aluminum was remade out of stainless steel.

The Faraday cup design had not been formalized at the time of the writing of Dr. Flicker's thesis. The design finally accepted is usable in both the molecular beam and scattering chamber configurations. A Faraday cup which can be rotated in and out of the electron beam path enters through the lower portion of the scattering chamber assembly. Rotation is supplied by a cable which moves in and out and passes through a feed-through on the front flange allowing easy insertion and removal of the Faraday cup.

The final modification of the instrument itself involves optional installation of an additional set of deflectors after the final aperture in the detector stage. Initially it is suggested that the instrument be operated with these deflectors installed. If, as is expected, the detected signals are relatively independent of these deflectors they may be removed. Both the deflectors and a cylinder allowing for them have been constructed as has another cylinder which has no provision for deflectors.

A final design for the liquid nitrogen cyrotrap, which is to be used for pumping condensible substances, has been adopted. The cold trap itself consists of a hollow cylinder $2\frac{1}{2}$" in diameter and 7/8" thick which will contain liquid nitrogen. Two stainless steel tubes are connected to the cold trap. One tube is used to carry liquid nitrogen into the trap while the second acts as the exit line. These lines, which support the cryotrap, go through the main flange inside a larger cylinder which actually seals via O-rings at the feed-through. This larger tube is connected to a vacuum dewar in front of the main flange. As the main chamber is evacuated the vacuum dewar is also evacuated. The dewar

can contain approximately 10 liters of liquid nitrogen. This volume should last at least twelve hours. Moving the cryotrap in and out of the molecular beam path is accomplished by sliding the entire dewar assembly toward and away from the flange. The dewar assembly is supported by a frame attached directly to the front flange.

At the present time no construction has been initiated to allow installation of an additional pump on the top of the vacuum chamber. Initially an 80-liter/sec Vac-Ion pump was to be used when the cryotrap was moved out of the beam path; however, at present the main chamber diffusion pump will be the only other source of pumping for the molecular beam effluent. When a pump is installed it is suggested that it be an oil diffusion pump rather than a Vac-Ion pump. The 80-liter/sec pump will be used to pump the differential chambers. Formerly, a 30-liter/sec Vac-Ion pump was to be used for the differential chambers.

Finally, to accommodate EIS III's additional lens elements, the peripheral electronics have been expanded. They have been set up in such a way that both EIS III and EIS I can be controlled interchangeably. This has necessitated certain potential controls being active only when one instrument or the other is installed. By assuring this flexibility, if EIS III should ever need modification EIS I may be reinstalled in a short time.

References

1. (a) A. Kuppermann, J. K. Rice and S. Trajmar, J. Phys. Chem. 72, 3894 (1968); (b) S. Trajmar, J. K. Rice, and A. Kuppermann, Advan. Chem. Phys. 18, 15 (1970).
2. J. K. Rice, Ph.D. Thesis, California Institute of Technology, 1969.
3. O. A. Mosher, Ph.D. Thesis, California Institute of Technology, 1973.
4. W. M. Flicker, Ph.D. Thesis, California Institute of Technology, 1976.
5. Engelhard Industries Division, Engelhard Minerals and Chemical Corporation, 6001 Bandini Blvd., Los Angeles, Ca.
6. K. Spangenberg and L. M. Field, Elec. Comm. 21, 194 (1943).
7. C. Kuyatt, "Notes on Electron Optics", unpublished lecture notes (1967).

4. RESULTS AND DISCUSSION

4.1 Paper I: Excited Electronic States of Ketene

EXCITED ELECTRONIC STATES OF KETENE

Robert P. FRUEHOLZ, Wayne M. FLICKER and Aron KUPPERMANN

Arthur Amos Noyes Laboratory of Chemical Physics,
California Institute of Technology, Pasadena, California 91125

Received

The electron impact energy-loss spectrum of ketene has been measured at impact energies of 30 eV and 50 eV, and scattering angles varying from 5° to 80°. Transitions have been observed at 3.7, 5.3, and 5.86 eV. These values are in excellent agreement with recent high quality ab initio calculations. They are assigned, respectively, to an $n \rightarrow \pi^* \; \tilde{X}\,^1A_1 \rightarrow {}^1A_2$ transition, a $\pi \rightarrow \pi^* \; \tilde{X}\,^1A_1 \rightarrow {}^3A_1$ transition, and an $n \rightarrow 3s$ singlet → singlet Rydberg transition. The results do not preclude the existence of an $\tilde{X}\,^1A_1 \rightarrow {}^3A_2$ transition near 3.6 eV underlying the low-energy side of the $\tilde{X}\,^1A_1 \rightarrow {}^1A_2$ excitation. However, no evidence is found for the presence of a triplet state with maximum intensity transition energy lower than 3.4 eV.

Low-energy, variable-angle, electron-impact spectroscopy, which is a powerful method for studying both optically forbidden and optically allowed electronic transitions,[1] has been used to investigate the electronic spectrum of ketene. Previous optical studies[2-5] have not permitted an unambiguous interpretation[2,3,5] of the absorption spectrum of ketene, and in particular, the locations of low-lying triplet electronic states are uncertain. In this paper we report the detection of a previously unreported triplet in ketene at 5.3 eV excitation energy. We find no evidence for a triplet with maximum intensity at 3.35 eV, in disagreement with an earlier optical investigation.[2]

The experimental apparatus used in this study was similar to that described by Kuppermann et al.[1] The spectrometer consists basically of a multistage electron gun, a hemispherical electrostatic energy monochromator, a flexible bellows scattering chamber which contains the target gas, an energy-loss analyzer identical to the monochromator, and a Spiraltron electron multiplier. Pulses from the multiplier are amplified and shaped, and then counted with a 1024-channel scaler. In a typical experiment, the incident electron energy and scattering angle of detection are both fixed, and the energy-loss spectrum is scanned repeatedly, usually for a period of 4-8 hours. The energy-loss spectrum thus obtained is analogous to an optical absorption spectrum, except that optically-forbidden processes are much more readily detected.[1] For each impact energy, the scattering angle is then changed and the procedure repeated.

Information about the nature of the excited electron states observed in an electron-impact spectrum can be obtained by studying

the dependence of the intensity of each transition on impact energy and scattering angle.[1] Transitions which in optical spectroscopy are both electric dipole- and spin-allowed, in electron-impact spectroscopy have differential cross sections (DCS) which are forward peaked, for impact energies about 15 eV or more above excitation threshold.[1] In contrast, transitions involving changes in the molecular spin quantum number of unity, such as singlet → triplet excitations, have a more nearly isotropic DCS in the angular range 10° to 80°.[1] Such transitions occur by the mechanism of electron exchange.[6] Spin-allowed but electric dipole-forbidden processes are forward-peaked, but often not as much as fully allowed transitions.[7,8] Finally, for impact energies about 15 eV or more above threshold, optically forbidden processes, and in particular spin-forbidden ones, become more intense with respect to optically allowed ones as the impact energy is lowered.

In the present experiments, the electron-impact spectrum of ketene in the energy-loss range 0-15 eV was studied at impact energies of 30 eV and 50 eV and scattering angles from 5° to 80°. Sample pressures in the scattering chamber were typically 5 mtorr, as indicated by an uncalibrated Schulz-Phelps ionization gauge, while the incident electron beam current was approximately 150 namps. The energy resolution, as measured by the full width at half maximum (fwhm) of the elastically scattered peak, was set at about 0.16 eV. The ketene sample[9] was synthesized by low pressure pyrolysis of acetic anhydride at 500° C, and purified by passage through a dry ice-acetone cooled trap which collected involatile by-products and unreacted anhydride. Ketene was collected in a second trap at liquid

nitrogen temperatures and was further purified by additional bulb-to-bulb distillation at low temperatures.

Figure 1 shows the low energy-loss part of the electron-impact spectrum of ketene at an impact energy of 50 eV and scattering angles of 10° and 80°. The figure indicates the presence of at least three transitions having maximum intensities at 3.7, 5.3, and 5.86 eV energy loss. In fig. 2 we display the corresponding DCS's at an impact energy of 50 eV, obtained by a method previously described.[1]

The most intense feature in the energy-loss region shown in fig. 1 has a peak intensity at 5.86 eV. From fig. 2 one can see that its DCS is strongly forward-peaked. Its optical oscillator strength[5] is 9.9×10^{-3} and it has been assigned as an n → 3s Rydberg transition,[8] corresponding to the excitation of an electron from the nonbonding orbital of the oxygen to a 3s-like orbital on the adjacent carbon.

The feature having a maximum intensity at 5.3 eV and an apparent onset at 4.7 eV appears not to have been reported previously in the literature. As can be seen from fig. 2, the DCS of this transition is relatively independent of angle, varying by less than a factor of two from its mean value in the range 10° to 80°. Moreover, at each scattering angle studied, this transition was relatively more intense (with respect to the feature at 5.86 eV) at 30 eV impact energy than at 50 eV impact energy. As noted above, such behavior is characteristic of spin-forbidden processes and permits us to assign the 5.3 eV transition to a singlet → triplet excitation. Harding and Goddard[10] have recently made a high-quality ab initio GVB-CI calculation of the vertical excitation energies for the low-lying electronic states of ketene.

Their result for the $\tilde{X}\,^1A_1 \rightarrow {}^3A_1$ transition, corresponding to a $\pi \rightarrow \pi^*$ excitation in the carbon-carbon double bond, is 5.39 eV, in very good agreement with our measurement. This excitation has also been observed in a recent threshold electron impact study.[9] The $\tilde{X}\,^1A_1 \rightarrow {}^3A_1$ transition may be the one initially populated in the Hg $^3P_1$ photosensitized decomposition of ketene,[11] which is an important method for preparing triplet methylene.

The feature with the lowest observed transition energy has an apparent onset at 3.2 eV and a maximum intensity at 3.7 eV. As can be seen from fig. 2, the DCS for this transition decreases twenty-fold over the scattering angle range being considered. This decrease is in the range usually characteristic of spin-allowed transitions which, as stated above, are forward-peaked at the impact energy used. This transition has also been seen optically [5] with an oscillator strength of 2.3×10^{-4}, characteristic of spin-allowed but symmetry-forbidden optical transitions. The feature has been assigned[2] as an $\tilde{X}\,^1A_1 \rightarrow {}^1A_2$ transition, due to an $n \rightarrow \pi^*$ excitation in the carbonyl moiety, similar to that in formaldehyde.[12] The accurate ab initio calculations mentioned above[10] furnish a vertical transition energy of 3.69 eV, in excellent agreement with our measurement, and confirm its $n \rightarrow \pi^*$ character, which had been recently challenged.[13] All of this evidence supports the interpretation that the transition we observe at 3.7 eV is spin-allowed.

However, an anomalous aspect of the 3.7 eV feature is that its DCS is not nearly as forward-peaked as that for the 5.86 eV transition. This behavior may be indicative of the spin-allowed but symmetry-

forbidden nature of the $\tilde{X}\,^1A_1 \rightarrow {}^1A_2$ transition.[7,8] An alternate interpretation is also possible on the basis of the Harding and Goddard calculation.[10] Their lowest vertical excitation energy is 3.62 eV, corresponding to an $\tilde{X}\,^1A_1 \rightarrow {}^3A_2$ transition. The energy splitting of 0.07 eV between this transition and the $\tilde{X}\,^1A_1 \rightarrow {}^1A_2$ one is significantly smaller than the apparent Franck-Condon band width of the latter and would therefore not be observable in our experiments. However, at large scattering angles, a non-negligible fraction of the integrated area under the experimental 3.7 eV feature could be due to this underlying singlet → triplet transition, which would attenuate the forward-peaked character of the isolated singlet → singlet excitation.

One of the most interesting results of the present study is the fact that we find no evidence of a transition with a maximum intensity at 3.35 eV. This result disagrees with that of Dixon and Kirby,[2] who studied the optical absorption spectrum of ketene with a 24 m atm path length. They reported a weak band system with an onset at 2.62 eV and a maximum intensity at 3.35 eV, which they assigned to a $\tilde{X}\,^1A_1 \rightarrow {}^3A_2$ transition. However, Laufer and Keller,[3] using a wide variety of techniques, such as gas- and liquid-phase absorption spectroscopy, oxygen enhancement, and triplet-triplet absorption, were unable to detect such a band system. We cannot entirely eliminate the possibility that there exists an extremely weak singlet → triplet transition with an onset at 2.6 eV. However, such a transition, if it does indeed exist, must have an excitation function which not only rises sharply near threshold, but which also drops off unusually rapidly with increasing

impact energy. Our experience to date indicates, however, that this is an unlikely possibility. As a result, we believe that it is much more likely that the lowest-lying triplet state of ketene lies near 3.6 eV as predicted by the recent ab initio calculations.[10]

In conclusion, we have used the method of low-energy, variable-angle, electron-impact spectroscopy to clarify the nature of the low-lying excited states of ketene. A singlet → triplet transition has been observed at 5.3 eV, and evidence has been presented which indicates that another singlet → triplet transition may occur in the immediate vicinity of the 3.7 eV singlet → singlet transition. No lower-lying excitations were observed. These results agree well with recent ab initio calculations.

ACKNOWLEDGMENTS

We thank Dr. J. Vogt and Professor J. L. Beauchamp for providing us with the ketene sample and with the results of their experiments prior to publication. We also thank Mr. L. B. Harding and Professor W. A. Goddard III for communicating to us their theoretical results before publication, and for several stimulating discussions.

REFERENCES

1. A. Kuppermann, J. K. Rice and S. Trajmar, J. Phys. Chem. 72 (1968) 3094; S. Trajmar, J. K. Rice and A. Kuppermann, Advan. Chem. Phys. 18 (1970) 15.
2. R. N. Dixon and G. H. Kirby, Trans. Faraday Soc. 62 (1966) 1406.
3. A. H. Laufer and R. A. Keller, J. Am. Chem. Soc. 93 (1971) 61.
4. M. Grossman, G. P. Semeluk and I. Unger, Can. J. Chem. 47 (1969) 3079.
5. J. W. Rabalais, J. M. McDonald, V. Scherr and S. P. McGlynn, Chem. Rev. 71 (1971) 73.
6. J. R. Oppenheimer, Phys. Rev. 29 (1927) 433.
7. D. C. Cartwright, W. J. Hunt, W. Williams, S. Trajmar and W. A. Goddard III, Phys. Rev. A8 (1973) 2436.
8. O. A. Mosher, W. M. Flicker and A. Kuppermann, J. Chem. Phys. 62 (1975) 2600.
9. This sample was prepared for us by Dr. J. Vogt whom we thank. See J. Vogt, M. Jungen and J. L. Beauchamp, manuscript in preparation.
10. L. B. Harding and W. A. Goddard III, manuscript in preparation.
11. F. J. Duncan and R. J. Cvetanovic, J. Am. Chem. Soc. 84 (1962) 3593.
12. G. Herzberg, Molecular Spectra and Molecular Structure (Van Nostrand, Princeton, New Jersey, 1967) Vol. III, p. 530.

REFERENCES (continued)

13. J. E. Del Bene, J. Am. Chem. Soc. 94 (1972) 3713.

FIGURE CAPTIONS

Figure 1. Electron energy-loss spectrum of ketene at a scattering angle of (a) 10° and (b) 80°; 50 eV incident electron energy; 2×10^{-7} A incident beam current; 5.6 mtorr sample pressure reading from an uncalibrated Schulz-Phelps gauge; resolution approximately 0.16 eV (fwhm).

Figure 2. Differential cross sections of ketene as a function of scattering angle at an incident electron energy of 50 eV for elastic scattering (+) and for transitions to the excited states lying at 3.7 eV (○), 5.3 eV (◇), and 5.86 eV (△) above the ground state.

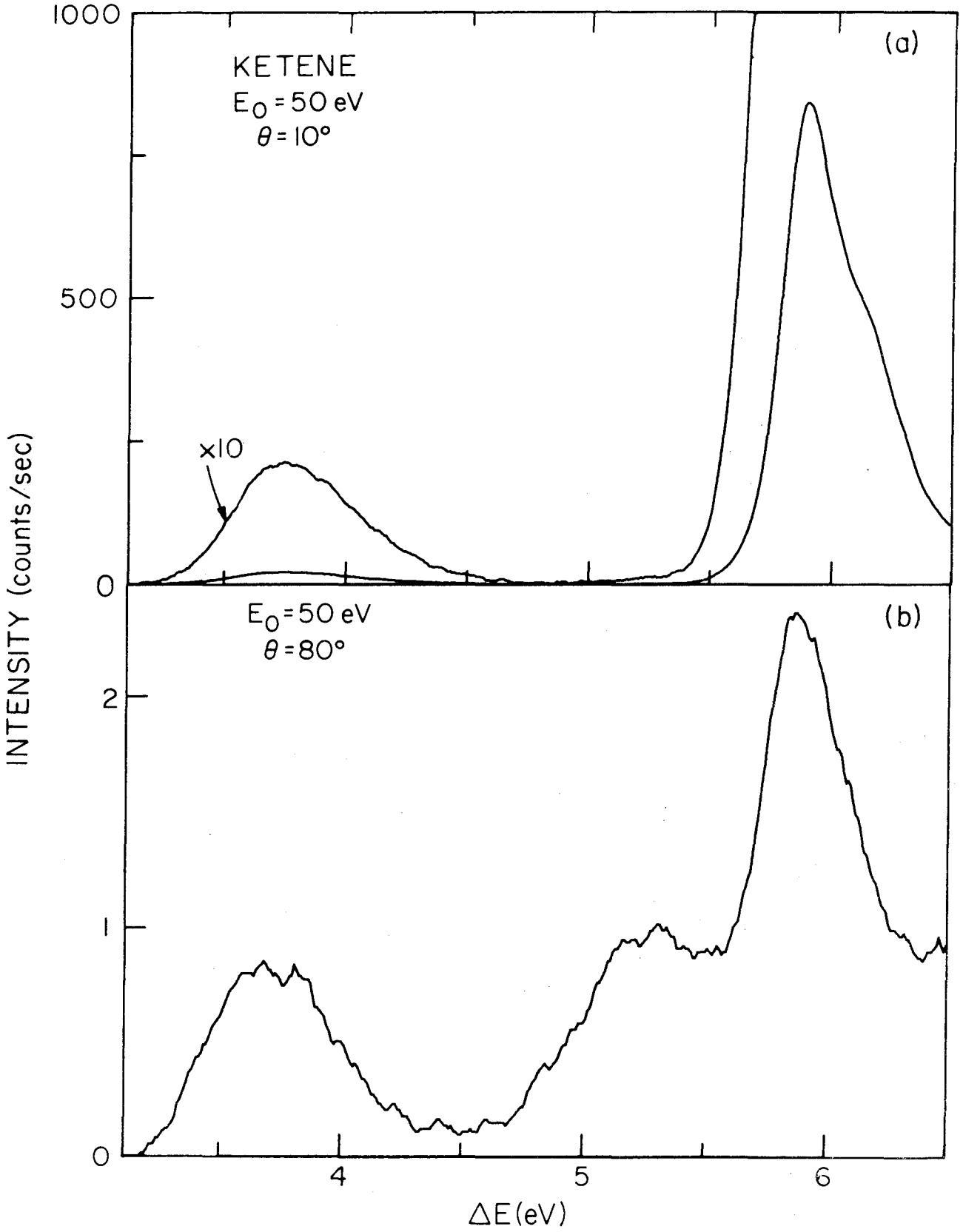
KETENE
E_0 = 50 eV
θ = 10°
(a)
×10
E_0 = 50 eV
θ = 80°
(b)
INTENSITY (counts/sec)
ΔE(eV)
1000
500
0
2
1
0
4
5
6

Figure 1

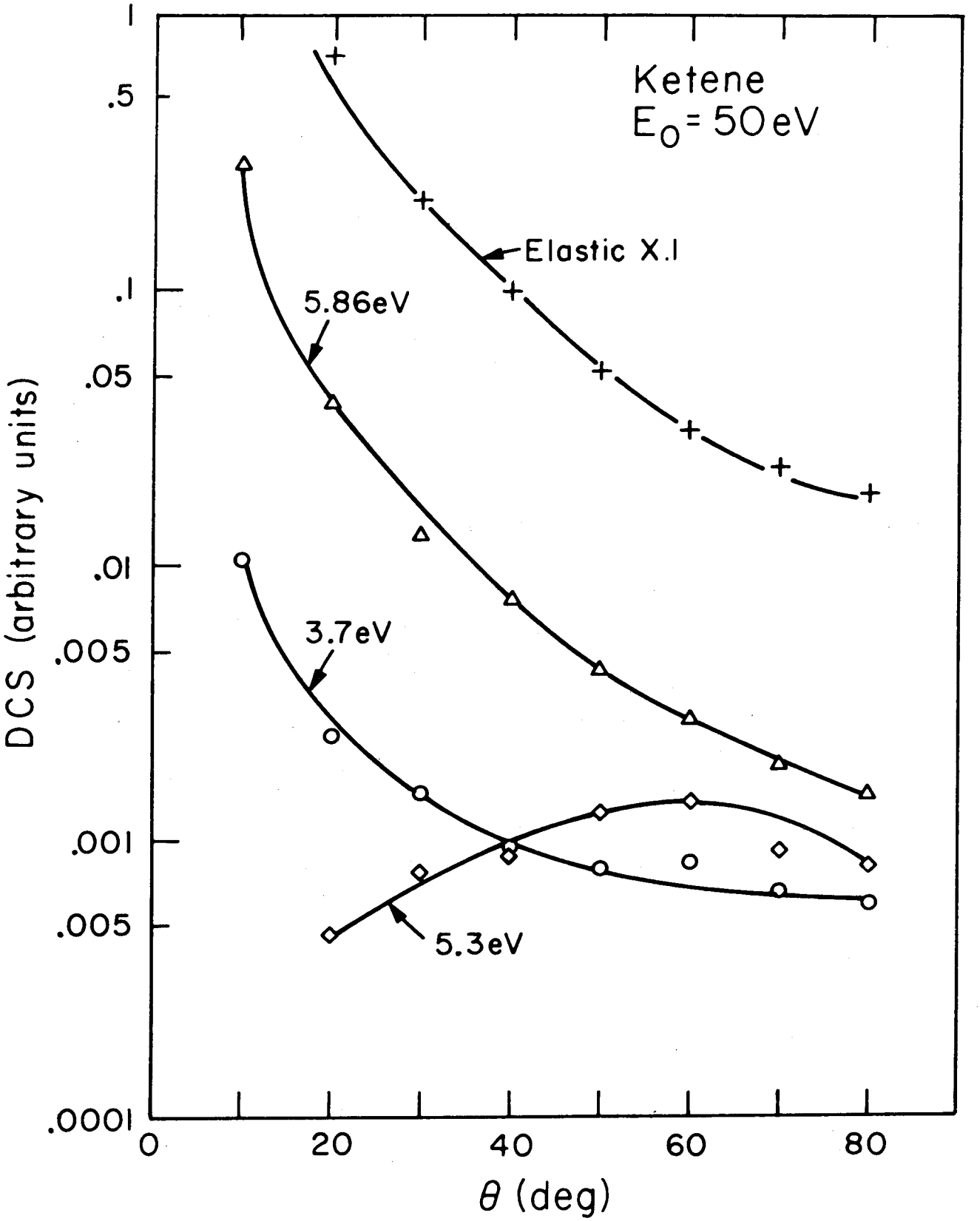
Ketene
E_0 = 50eV
Elastic X.1
5.86eV
3.7eV
5.3eV
DCS (arbitrary units)
1
.5
.1
.05
.01
.005
.001
.005
.0001
0
20
40
60
80
θ (deg)

Figure 2

4.2 Paper II: Electronic Spectroscopy of 1,3,5,7-Cyclooctatetraene by Low-Energy, Variable-Angle, Electron Impact

Electronic spectroscopy of 1,3,5,7-cyclooctatetraene by low-energy, variable-angle electron impact*

Robert P. Frueholz† and Aron Kuppermann

Arthur A. Noyes Laboratory of Chemical Physics,
California Institute of Technology, Pasadena, California 91125§

(Received)

The electron-impact energy loss spectrum of 1,3,5,7-cyclooctatetraene has been measured at electron impact energies of 30 eV, 50 eV, and 75 eV, and scattering angles varying from 5° to 80°. Three transitions with maxima at 3.05 eV, 4.05 eV, and 4.84 eV are identified as singlet → triplet excitations. The significance of the lowest lying of these triplet states in the quenching process of dye laser solutions (in particular rhodamine 6G) is discussed and an exciplex mechanism for triplet quenching is suggested. Singlet → singlet transitions are observed at 4.43 eV, 6.02 eV, and 6.42 eV. These spin-allowed transitions have been observed optically and are assigned as $\tilde{X}\,^1A_1 \rightarrow {}^1A_2$, $\tilde{X}\,^1A_1 \rightarrow {}^1E$, and $\tilde{X}\,^1A_1 \rightarrow {}^1E$ excitations. Three new, singlet → singlet transitions are observed at 6.99 eV, 8.41 eV and 9.05 eV and are tentatively assigned as the $\tilde{X}\,^1A_1 \rightarrow {}^1B_2$, $\tilde{X}\,^1A_1 \rightarrow {}^1E$, and $\tilde{X}\,^1A_1 \rightarrow {}^1E$, $\pi \rightarrow \pi^*$ excitations. Several super-excited features between 10 eV and 15 eV have been observed and are believed to involve excitations to autoionizing Rydberg states.

---

* This work was supported by a Contract (No. EY-76-S-03-767) from the Department of Energy. Report Code: CALT-767P4-163.

† Work performed in partial fulfillment of the requirements for the Ph.D. degree in Chemistry at the California Institute of Technology.

§ Contribution No. 5732.

I. INTRODUCTION

The 1,3,5,7-cyclooctatetraene (COT) molecule is an example of a non-aromatic,[1] cyclic, conjugated carbon-carbon double bond system. The ground electronic state, which has been studied by electron diffraction techniques,[2,3] was found to be non-planar and "tub" shaped. COT exhibits D_{2d} symmetry which may be seen from the following structure[2]

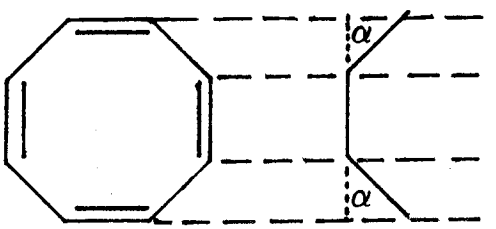

where the C=C, C-C and C-H bond lengths are 1.340 Å, 1.475 Å, and 1.100 Å, respectively, the C=C-C angle is 126.1°, the H-C=C angle is 117.6°, and α is 43.1°.

Due to its non-planar structure COT is an interesting molecule regarding σ-π interactions, through-bond interactions, and through-space interactions.[4-7] COT is also an efficient triplet quencher for several dye laser solutions[8-12] (e.g., rhodamine 6G and brilliant sulfaflavine). Moderate concentrations of this molecule ($\sim 1\times10^{-4}$ M/L)[11] in ethanol not only increase pulse length but increase the maximum pulse repetition rate of those lasers and also permit CW operation of some of them. One of the aims of the present investigation has been to obtain high-quality electronic band shapes and accurate locations of the intensity maxima for the low-lying singlet → triplet transitions

of COT by low-energy, variable-angle, electron-impact spectroscopy. This information should aid in the understanding of the effect of COT as a triplet quencher. A previous trapped electron study[13] has indicated the presence of several triplet excited states in the region from 3 eV to 4.5 eV and it was further hoped that our experiments would provide more detailed information and a better understanding of this energy-loss region.

II. SUMMARY OF PREVIOUS STUDIES

COT has 56 electrons which, in the ground state, occupy the following set of 28 molecular orbitals:[4] five a_1, two a_2, three b_1, four b_2, and seven doubly degenerate e orbitals. The ordering of the higher occupied molecular orbitals, from which low-lying excitations are expected is somewhat uncertain. Van-Catledge,[7] using the semi-empirical INDO formalism, places the highest orbital of each symmetry, with increasing energy, in the order: $4b_2(\pi)$, $3b_1(\sigma)$, $7e(\pi)$, and $5a_1(\pi)$. Batich et al.[4] have performed semi-empirical MINDO/2 calculations yielding a similar ordering. However, they feel that the $3b_1$ orbital has an erroneously high energy and support this opinion by referring to the ab initio results of Lehn and Wipf. The latter found, using several different gaussian-type orbital basis sets that the $3b_1$ orbital has a lower energy yielding the ordering $3b_1(\sigma)$, $4b_2(\pi)$, $7e(\pi)$, and $5a_1(\pi)$. Electronic transitions are expected to occur from these higher occupied orbitals to the following lower vacant molecular orbitals:[7] $3a_2(\pi)$, $8e(\pi)$, $4b_1(\pi)$, and $5b_2(\sigma)$. Table I summarizes the theoretical results for

transition energies. They are all semi-empirical, as no ab-initio values have been published so far. Unfortunately most calculations only consider singlet → singlet transitions; results for singlet → triplet excitations are limited.[13,14]

The optical absorption spectrum of COT[6] shows a broad weak band extending from 4.00 eV to 4.77 eV with a maximum at 4.39 eV assigned to be the $\tilde{X}\,^1A_1 \rightarrow {}^1A_2$ excitations.[15] In addition, an intense band at 6.42 eV (the upper transition energy limit of the experimental study) is assigned as $\tilde{X}\,^1A_1 \rightarrow {}^1E$, with another $\tilde{X}\,^1A_1 \rightarrow {}^1E$ excitation producing a pronounced inflection at 6.05 eV. Cope and Overberger[16] also observed a weak transition at 5.06 eV, which wasn't, however, detected in subsequent optical studies.[5,6] The trapped electron spectrum,[13] which measures a quantity proportional to the integral of the scattering cross section over a narrow energy band above the threshold energy, shows a broad peak from approximately 2.7 eV to 5.8 eV with several smaller peaks superimposed upon it. Several stronger transitions are observed between 5.8 eV and 10 eV. The features observed between 3.4 eV and 4.2 eV were assigned in that study to singlet → triplet transitions.

III. EXPERIMENTAL

The apparatus used in this study has previously been described in detail.[17,18] The low-energy, variable-angle, electron-impact spectrometer consists basically of an electron gun which injects a collimated beam of thermionically emitted electrons into a hemispherical electrostatic energy monochromator with a mean radius of 2.54 cm. The

energy-selected electron beam scatters off the target gas contained in a flexible bellows scattering chamber, and the scattered electrons are energy-analyzed by a second analyzer identical to the monochromator. A Spiraltron (continuous dynode) electron multiplier serves as the detector, and the output pulses are amplified, shaped, and stored in a 1024-channel multichannel scaler. In a typical experiment, the incident electron energy and scattering angle are both fixed, and the energy-loss spectrum is scanned repeatedly, usually for a period of 4 to 8 hours. The energy-loss spectrum thus obtained is analogous to an optical absorption spectrum, except that optically forbidden processes are much more readily detected.[17-19] For each impact energy, the scattering angle is then changed and the procedure repeated.

The method of low-energy, variable-angle, electron-impact spectroscopy has been used successfully to investigate spin-forbidden and other electric dipole-forbidden transitions in molecules.[17-19] Information about the nature of the excited electronic states observed in an electron-impact spectrum can be obtained by studying the dependence of the scattering intensity of each transition on impact energy and angle.[17,19] Transitions which in optical spectroscopy are both electric dipole and spin-allowed, have, at impact energies of 15 eV or more above threshold, electron impact differential cross sections (DCS's) which are forward peaked, decreasing by approximately 2 orders of magnitude as the scattering angle varies from 10° to 80°.[17,19] In contrast, transitions involving changes in the molecular spin quantum number of unity, such as singlet → triplet excitations, have a more

isotropic DCS (varying by less than about a factor of 3) over the angular range 10° to 80°. Such transitions occur by the mechanism of electron exchange.[20] Spin-allowed but electric-dipole forbidden processes are forward peaked, but often not as much as fully allowed transitions.[17-19] Finally, for impact energies about 15 eV or more above threshold, optically forbidden processes, and in particular spin-forbidden ones, become more intense with respect to optically allowed ones as the impact energy is lowered.

In the present experiments, the electron energy-loss spectrum of COT vapor was studied at impact energies, E_0, of 30 eV, 50 eV and 75 eV at scattering angles, θ, from 5° to 80°. Sample pressures in the scattering chamber ranged from 2 mTorr to 4mTorr, as indicated by an uncalibrated Schulz-Phelps ionization gauge, while the electron beam current incident into the scattering chamber was approximately 60 namps. The energy resolution, as measured by the full width at half maximum (FWHM) of the elastically scattered peak was electron-optically set in the range 0.10 eV to 0.13 eV. In these studies, two different samples of COT were used. One was obtained from the Aldrich Chemical Co., and has a specified purity of 98%, while another one was supplied by Professor Rowland Pettit of the University of Texas at Austin. Spectra obtained from both of these samples were identical. These samples were subjected to several liquid nitrogen freeze-pump-thaw cycles prior to use. When irradiated with a mercury vapor lamp COT is known to undergo various photochemical reactions including photoisomerization, decomposition into benzene and acetylene, and

formation of styrene.[22] In order to minimize the possibility of these undesirable reactions the samples were protected from room light.

IV. RESULTS AND DISCUSSION

Figure 1 shows the 2 eV to 7 eV energy loss region of the COT electron impact spectrum at 30 eV impact energy and scattering angles of 10° and 70°. DCS values at impact energies of 30 eV and 50 eV are presented in Figs. 2 and 3. The elastic DCS's in arbitrary units were determined by multiplying the observed count rates by the scattering volume correction[23] appropriate for each scattering angle and normalizing the results to an arbitrary value of 1.0 at $\theta = 40°$. The reproducibility of these elastic DCS values is about ±20%.

The sum of the DCS's of the two transitions at 6.04 eV and 6.42 eV (designated S_2 and S_3, respectively) was obtained by multiplying the ratio of the area under the corresponding peak to that of the elastic peak (as previously described)[18,24] by the elastic DCS at each θ. In addition for scattering angles of 30° and below the combined DCS of these transitions was determined without reference to the elastic peak using the same procedure as for the elastic DCS, except that the DCS at 20° was normalized to the value obtained by the ratio (to the elastic DCS) method at this angle. These two methods gave results within 6% of one another at 30°.

The DCS curves for the other inelastic features displayed in Figs. 2 and 3 were determined by the ratio method using the elastic DCS as a reference for angles of 20° and above, and the $S_2 + S_3$ DCS

below 20°. The estimated uncertainty in the inelastic DCS's is ±35%. The arbitrary units in Figs. 2 and 3 are the same for all curves at a given impact energy but differ from those of a different impact energy.

A. Triplet states

The lowest observed feature in the COT spectrum (Fig. 1) has an apparent onset at approximately 2.2 eV and an intensity maximum at 3.05 ± 0.05 eV. The DCS values for this transition at 50 eV impact energy do not vary by more than a factor of 3 over the angular range 20° to 80°. At 10° this feature is quite weak and contributions from the tails of adjacent transitions make it impossible to obtain an accurate DCS value. At an impact energy of 30 eV the DCS of this 3.05 eV electronic band varies by less than a factor of 2 over the angular range 10° to 80°. This behavior is indicative of a singlet→triplet transition and we designate it as $S_0 \rightarrow T_1$. The lowest singlet→singlet transition occurring with a maximum intensity at 4.43 eV, is assigned as $\tilde{X}\,^1A_1 \rightarrow {}^1A_2$ (see section 4.2). The $S_0 \rightarrow T_1$ transition probably corresponds, therefore, to the $\tilde{X}\,^1A_1 \rightarrow {}^3A_2$ excitation. The lowest singlet→triplet transition reported by Knoop et al.,[13] using a trapped electron technique, at 3.44 eV is not in good agreement with our studies.

In addition to the $\tilde{X}\,^1A_1 \rightarrow {}^1A_2$ ($S_0 \rightarrow S_1$) transition occurring at 4.43 eV, which is apparent at low scattering angles (Figs. 1a and 4), two other excitations are observed in this energy-loss region at larger scattering angles, occurring at 4.05 eV and 4.84 eV. These transitions are not visible at 10° and 20° (Figs. 1a and 4) due to the high intensity

of the $\tilde{X}\,^1A_1 \rightarrow {}^1A_2$ transition. However, at scattering angles of 40° and higher the DCS of this singlet → singlet transition has decreased so significantly that it is not clearly discernible, thereby making the transitions at 4.84 eV and 4.05 eV fully visible. These three transitions overlap each other appreciably and it is not possible to obtain accurate individual DCS values. Instead, the aggregate DCS for the energy-loss region from 3.4 eV to 5.4 eV has been plotted in Figs. 2 and 3 as the curve labeled $(T_2 + T_3 + S_1)$. At 50 eV impact energy this DCS decreases by less than a factor of two over the angular range 30° to 80° (compared to the $S_2 + S_3$ DCS which decreases by a factor of 8 over the same angular range). Between 20° and 30° the 50 eV $(T_2 + T_3 + S_1)$ DCS decreases by a factor of approximately 4. This yields a total variation of about a factor of 5 over the angular range 20° to 80°. If only 50% of the aggregate intensity at 20° is due to the $\tilde{X}\,^1A_1 \rightarrow {}^1A_2$ excitation, the two other transitions vary by a factor of 2.5 over the angular region 20° to 80°. This variation is most likely due to a singlet → triplet transition. The 50% contribution of the $\tilde{X}\,^1A_1 \rightarrow {}^1A_2$ is probably an underestimate, since the transitions at 4.05 eV and 4.84 eV are no longer distinguishable at the 20° scattering angle.

When the impact energy is lowered to 30 eV, the contributions of the transitions at 4.05 eV and 4.84 eV are more pronounced, the aggregate DCS varying by less than a factor of two over the angular range 20° to 80°. On the basis of these data it is possible to identify the transitions at 4.05 eV and 4.84 eV as singlet → triplet excitations and designate them $S_0 \rightarrow T_2$ and $S_0 \rightarrow T_3$. These results are again not in

good agreement with the trapped electron spectrum of Knoop et al.[13] As shown in Table 2, they report additional triplet states at 3.72 eV, 3.91 eV, and 4.11 eV, while a singlet state was reportedly observed at 4.82 eV.

B. Singlet states

Figure 4 shows the COT spectrum at 50 eV impact energy and a scattering angle of 10°. At this energy and angle the contribution of singlet → triplet transitions to the spectrum should be small and the observed transitions may be considered to be essentially singlet → singlet excitations.

Batich et al.[4] found that a parameterization of the molecular orbital energies based on a simple Hückel model agreed quite well with the observed photoelectron spectrum. This is surprising because not only does the HMO model assume complete $\sigma - \pi$ separation in this non-planar system but it also neglects through-space interactions between the opposite π orbitals. Batich et al.[4] believe that the satisfactory parameterization of their experimental results "is due to compensation of through-space interactions across the ring by through-band interactions with the lower lying σ orbitals." We have attempted to analyze the singlet → singlet excitation spectrum of COT in a similar manner.

The orbital ordering resulting from a Hückel calculation among the 8 p_π orbitals is shown in Fig. 5. In addition the highest energy occupied σ orbital, is also included. Energy spacings have been labeled α, β, γ, and δ as indicated in the figure. An approximate

spacing of levels may be obtained from the photoelectron spectrum[4] (vertical IP's 8.47 eV, 9.78 eV, 11.15 eV and 11.55 eV) by applying Koopmans' theorem.[25] Using the ionization potentials of that spectrum we obtain for β, γ and δ the values 1.3 eV, 1.37 eV and 0.40 eV, respectively. We also set α equal to the vertical excitation energy of the $\tilde{X}\,^1A_1 \rightarrow {}^1A_2$ transition, 4.43 eV. Considering only the symmetry-allowed transitions the following excitations are expected (orbital occupancy changes are given in parentheses): two transitions of the type $\tilde{X}\,^1A_1$ $(4b_2^2\ 7e^2\ 5a_1^2) \rightarrow {}^1E$ $(4b_2^2\ 7e^2\ 5a_1^1\ 8e^1$ and $4b_2^2\ 7e^1\ 5a_1^2\ 3a_2^1)$ at 5.69 eV, one $\tilde{X}\,^1A_1 \rightarrow {}^1B_2$ $(4b_2^2\ 7e^1\ 5a_1^2\ 8e^1)$ at 7.00 eV, and two $\tilde{X}\,^1A_1 \rightarrow {}^1E$ transitions $(4b_2^1\ 7e^2\ 5a_1^2\ 8e^1$ and $4b_2^2\ 7e^1\ 5a_1^2\ 4b_1^1)$ at 8.37 eV. In addition the degenerate sets of E states at 5.69 eV and 8.37 eV would be expected to interact and split thereby breaking their degeneracy.[26,27] We now associate these transitions with the observed spectrum.

Figure 4 shows the $\tilde{X}\,^1A_1 \rightarrow {}^1A_2$ transition at 4.43 eV and a strong absorption beginning at about 5.5 eV. A strong feature can be seen with an intensity maximum at 6.42 eV, having a shoulder at 6.02 eV. These values are in good agreement with previously reported optical results.[6] We believe the shoulder and peak correspond to the lower split set of E states. This assignment, besides qualitatively agreeing with the Hückel parameterization, is in good agreement with the semi-empirical calculation of Van-Catledge[7] who reports excitation energies of 5.88 eV and 6.34 eV. The transitions at 6.02 eV and 6.42 eV (designated S_2 and S_3) overlap heavily with each other and individual DCS's could not be obtained. The aggregate DCS for these transitions

decreases by a factor of about 130 at 50 eV impact energy as the scattering angle increases from 10° to 80°, while the relative intensities of the two E states remain approximately the same. At 30 eV impact energy a factor of 34 decrease in the DCS is observed over the same angular range. The sharply forward peaked behavior of this DCS is characteristic of the symmetry-allowed singlet → singlet nature of these transitions.[17-19]

At 6.99 eV another transition is observed. This excitation may be tentatively assigned as the $\tilde{X}\,^1A_1 \rightarrow {}^1B_2$ transition predicted by our Hückel parameterization to occur at 7.0 eV. This energy does not agree too well with Van-Catledge's[7] calculated value of 7.67 eV for $\tilde{X}\,^1A_1 \rightarrow {}^1B_2$ transition. This transition could alternately be assigned as a $5a_1 \rightarrow 4s$ Rydberg transition with a reasonable term value of 11,900 cm^{-1}.[28] It should be noted though, that we see no evidence of the $5a_1 \rightarrow 3s$ member of this series which would be expected near 5.2 eV,[29] or other transitions which could be assigned as higher members of this Rydberg series.

Two fairly intense transitions are observed at 8.41 eV and 9.05 eV, the latter being super-excited since it lies above the lowest IP of 8.47 eV. These transitions may be tentatively assigned as the two E states which we predicted above to lie at 8.5 eV by the Hückel parameterization. Complete DCS values were not obtained for these transitions; however, as would be expected for symmetry-allowed singlet → singlet transitions, their electronic band shapes relative to the lower E states change very little with respect to angle. The

tentative nature of these latter assignments should be emphasized as the corresponding transition energies calculated by Van-Catledge are 7.43 eV and 7.51 eV. The difference between these calculations and the experimental values could be due either to increasing inaccuracies in the semi-empirical method as one moves to higher energies or to mis-assignments of the observed transitions. There is also the possibility that these two transitions are members of Rydberg series converging to ionization potentials higher than 8.47 eV. However, they do not appear to fall into any well-defined series.

In some of our spectra we observe a very weak transition at 7.4 eV which could be related to the $\tilde{X}\,^1A_1 \rightarrow {}^1B_2\ (\pi \rightarrow \pi^*)$ excitation. However, this transition may well be the $(3b_1^2\ 4b_2^2\ 7e^2\ 5a_1^2 \rightarrow 3b_1^1\ 4b_2^2\ 7e^2\ 5a_1^2\ 3a_2^1)\ \tilde{X}\,^1A_1 \rightarrow {}^1B_2$, $\sigma \rightarrow \pi^*$ excitation which is predicted to have a transition energy of 7.51 eV by the Hückel parameterization. Several other weak transitions are observed with excitation energies above 10 eV. These transitions may be Rydberg super-excited states and their excitation energies are given in Table 2.

V. COT'S ROLE IN DYE LASER QUENCHING

Flashlamp-pumped or CW dye laser operation has been found to be inhibited by the intersystem crossing of dye molecules from singlet to triplet manifolds.[8,9,30] Once the lowest triplet state of the dye is populated, triplet → triplet excitations can occur. It has been suggested that this process quenches lasing in a few microseconds.[9,31] For this reason, triplet state quenchers such as COT are added to the dye solution. They usually increase both the laser pulse length and its maximum pulse repetition rate.[11] In the case of rhodamine 6G (R6G) the maximum triplet → triplet absorption occurs at approximately 2.0 eV[32,33] which is in the region of laser emission of this dye.[33]

Using ESR techniques, Yamashita and Kashiwagi[12] found that at 77°K COT effectively depopulated R6G's lowest triplet state. Dempster et al.[34] found the experimental rate constant for quenching, K_{exp}, of R6G by COT in ethanol solutions to be $(7 \pm 1) \times 10^8\ M^{-1}\ sec^{-1}$. The exact mechanism of quenching, whether through direct triplet → triplet energy transfer or via complex (exciplex) formation, is unknown. Our results furnish information about this mechanism.

Dexter[35] has proposed a theoretical model for triplet → triplet energy transfer rates in crystals due to exchange interactions. The transition probability rate for energy transfer between the neighboring donor and acceptor in a crystal, P_{da}^{cr}, is given by

$$P_{da}^{cr} = \frac{2\pi}{\hbar} Z^2 \int f_d(E)\, F_a(E)\, dE \qquad (1)$$

where Z^2 is related to the coulombic exchange integrals for the molecules, $f_d(E)$ is the normalized phosphorescence intensity distribution function of the donor (R6G) and $F_a(E)$ is the normalized singlet → triplet absorption intensity distribution function of the acceptor (COT). The value of $(2\pi/\hbar) Z^2$ may be estimated[35] to be approximately $1.0\ Y \frac{erg}{sec}$. Y is a dimensionless constant related to the nodal characteristics of the wavefunction and is much smaller than unity. Gas phase studies by Schmidt and Lee,[36] involving π-bonded molecules, indicate that the rate of triplet → triplet energy transfer is indeed proportional to the energy overlap of the donor molecule's phosphorescence spectrum with the $S_0 \rightarrow T_1$ absorption spectrum of the acceptor molecule. This overlap can be obtained either from direct or O_2-induced optical absorption measurements or from electron-impact spectroscopy.[18] This is consistent with Dexter's theoretical prediction for a crystal environment.

In attempting to estimate P_{da}^{cr} and subsequently the transition probability rate for solutions, P_{da}^{sol}, use may be made of our electron impact band shape for the $S_0 \rightarrow T_1$ transition in COT. The phosphorescence spectrum of R6G has been studied by Marling[37] but has not been published; its phosphorescence maximum occurs at 1.9 eV.[12] To estimate the spectral overlap we have assumed that the shape of the phosphorescence band is the same as that of the fluorescence intensity distribution of the lowest excited singlet state of R6G,[38]

with its maximum shifted to 1.9 eV. The resulting overlap integral has the value of approximately 3×10^{8} erg^{-1}, yielding a P_{da}^{cr} value of 3×10^{8} Y sec^{-1}.

From this theoretical value of P_{da}^{cr}, we wish to obtain a rate constant for quenching in solution which can be compared to the experimentally observed one. P_{da}^{cr} may be related to P_{da}^{sol} by

$$P_{da}^{sol} = P_{da}^{cr} \left\{1 - \left(\frac{[s]}{[A] + [s]}\right)^{n}\right\} , \qquad (2)$$

where n is the total number of solvent plus quencher molecules surrounding each donor molecule in solution, [A] is the concentration of the acceptor and [s] that of the solvent. The factor multiplying P_{da}^{cr} is an estimate of the fraction of the time that the donor has at least one acceptor molecule next to it in solution. Because the solvent is in great excess we may simplify (2) to

$$P_{da}^{sol} = P_{da}^{cr} \, n \frac{[A]}{[s]} . \qquad (3)$$

P_{da}^{sol} is related to the triplet quenching rate equation by

$$- \frac{1}{[D]} \frac{d[D]}{dt} = P_{da}^{sol} = K[a] , \qquad (4)$$

where [D] is the concentration of excited triplet donor. Using Eqs. 3 and 4, the theoretical rate constant is given by $K_{th} = P_{da}^{cr} \, n[s]^{-1}$. For the R6G-COT system in ethanol this results in a K_{th} value of

$6 \times 10^8 Y M^{-1} sec^{-1}$ (where n was estimated to be approximately 40 on the basis of size considerations).

Remembering that $Y \ll 1$, the theoretical rate constant is significantly smaller than the experimental rate constant of $7 \times 10^8 M^{-1} sec^{-1}$. While our method of estimation is admittedly crude, we feel that the difference in the orders of magnitude of the theoretical and experimental rate constants for quenching suffices to indicate the existence of another quenching mechanism beside direct triplet → triplet energy transfer. A reasonable second mechanism appears to be complex (or exciplex) formation.[39] The intimate interactions between molecules during the complex formation with the concurrent distortion of molecular geometries and possible changes in excited state energies provide another reasonable quenching mechanism. It is also interesting to compare the experimental triple quenching rate constant with the theoretical diffusion-limited value,[40] K_{dif}, of $8.8 \times 10^9 M^{-1} sec^{-1}$ obtained from the viscosity of ethanol. K_{dif} is about ten times greater than K_{exp}, which implies that each encounter of a triplet R6G molecule with a COT molecule does not result in deactivation of the R6G.

VI. SUMMARY AND CONCLUSIONS

The transition energies determined in this study are summarized in the last column of Table II. Optically undetected excitations to three low-lying triplet state were observed at 3.05 eV, 4.05 eV, and 4.84 eV (positions of band intensity maxima). The lowest of these overlaps with the lowest triplet phosphorescence band of rhodamine 6G suggesting that it plays an important role in quenching the rhodamine 6G triplet. A theoretical estimate of the rate constant for this quenching by direct triplet→triplet energy transfer leads to a value too low to account for the experimentally observed one, suggesting that exciplex formation may play an important role in the quenching mechanism. Several singlet→singlet transitions have been observed in the energy-loss region of 4 eV to 10 eV. The excitations above 7 eV have not been previously detected. Several superexcited states were identified in the 10 eV to 15 eV energy-loss region.

ACKNOWLEDGMENTS

We wish to thank Professor R. Pettit for providing us with one of our samples of 1,3,5,7-cyclooctatetraene. We also thank Dr. W. M. Flicker for several very helpful discussions.

TABLE I. Summary of semi-empirical theoretical calculations of transition energies

Electronic State	Contributing Configurations[a]	Symmetry[b] Character-ization	Calculated Energies (eV)				
			Van-Catledge[c]	Allinger[d]	Allinger[e]	Knoop[f]	Baird[g]
Not designated	$S_0 \rightarrow T_1$					3.41	1.37
" "	$S_0 \rightarrow T_2$					3.78	
" "	$S_0 \rightarrow T_3$					4.21	
$^1A_2$	$5a_1 \rightarrow 3a_2$	F	4.08	3.76	5.48	4.92	
^1E	$5a_1 \rightarrow 8e$, $7e \rightarrow 3a_2$	A (x, y)	5.88	5.56	6.71	6.60	
$^1B_2$	$3b_1 \rightarrow 3a_2$	A (z)	6.00				
$^1B_1$	$4b_2 \rightarrow 3a_2$, $5a_1 \rightarrow 4b_1$	F	6.26				
^1E	$5a_1 \rightarrow 8e$, $7e \rightarrow 3a_2$	A (x, y)	6.34	6.63	7.76	6.78	
$^1A_2$	$7e \rightarrow 8e$	F	6.72				
$^1B_1$	$5a_1 \rightarrow 4b_1$, $4b_2 \rightarrow 3a_2$	F	7.07				
$^1A_2$	$7e \rightarrow 8e$, $3b_1 \rightarrow 5b_2$	F	7.13				
^1E	$4b_2 \rightarrow 8e$, $7e \rightarrow 4b_1$	A (x, y)	7.43				
^1E	$4b_2 \rightarrow 8e$, $7e \rightarrow 4b_1$	A (x, y)	7.51				
$^1B_2$	$7e \rightarrow 8e$, $3b_1 \rightarrow 3a_2$	A (z)	7.67				

(Refs. to Table I)

---

[a]Singlet state contributing configurations are from Ref. 7 and represent excitation of a single electron from the first orbital to the second orbital.

[b]A stands for allowed and F for forbidden. The symbols x, y, z in parentheses after the A indicate the polarization of the corresponding transition. The O_z axis is the C_2 symmetry axis of the COT molecule perpendicular to the plane of four of its carbon atoms, and the other two axes are in the two molecular symmetry planes and are perpendicular to O_z.

[c]Ref. 7.

[d]Ref. 6.

[e]Ref. 5.

[f]Ref. 13.

[g]Ref. 14 provides $S_0 \rightarrow T_1$ energy for COT in planar configuration. This energy has been increased by inversion energy of COT ring (0.18 eV) from Ref. 6.

Table II. Summary of experimental observations of transition energies.

Nature of Transition	Possible Upper State	Energy of Transition (eV) Optical[a]	Trapped Electron[b]	Present Study[c]
Singlet → triplet	$^3A_2$ or	-	3.4	3.05
Singlet → triplet	^3E or	-	3.7	4.05
Singlet → triplet	^3E	-	3.9	4.84
Singlet → triplet	-	-	4.1	-
Symmetry forbidden singlet → singlet	$^1A_2$	4.39	4.4	4.43
Electric dipole allowed singlet → singlet	^1E	6.05[d]	5.88	6.02[d]
" "	^1E	6.42		6.42
" "	^1B			6.99
" "	^1E			8.41
" "	^1E			9.05
Super-excited state	Rydberg State			10.2
" "				10.6
" "				11.3
" "				12.2
" "				14.2

(Refs. to Table II)

---

[a]Ref. 6.

[b]Ref. 13.

[c]The accuracy of the transition energies below 9.1 eV is ± 0.05 eV and those for the super-excited states is ±0.1 eV.

[d]Feature appears as a shoulder.

REFERENCES

[1]M. Milun, Z. Sobotka, and N. Trinajstic, J. Org. Chem. 37, 139 (1972).

[2]M. Traetteberg, Acta Chem. Scand. 20, 1724 (1966).

[3]O. Bastiansen, L. Hedberg, and K. Hedberg, J. Chem. Phys. 27, 1311 (1957).

[4]C. Batich, P. Bischof, and E. Heilbronner, J. Electron Spectrosc. 1, 333 (1972/73).

[5]N. Allinger, J. Chow Tai, and T. Stuart, Theoret. Chim. Acta (Berl.) 8, 101 (1967).

[6]N. Allinger, M. Miller, L. Chow, R. Ford, and J. Graham, J. Am. Chem. Soc. 87, 3430 (1965).

[7]F. Van-Catledge, J. Am. Chem. Soc. 93, 4365 (1971).

[8]R. Pappalardo, H. Samelson, and A. Lempicki, Appl. Phys. Lett. 16, 267 (1970).

[9]J. Marling, D. Gregg, and L. Wood, Appl. Phys. Lett. 17, 527 (1970).

[10]J. Marling, L. Wood, and D. Gregg, IEEE J. Quantum Electron 7, 498 (1971).

[11]J. Weber, Z. angew. Physik 31, 7 (1971).

[12]M. Yamashita and H. Kashiwagi, J. Phys. Chem. 78, 2006 (1974).

[13]F. Knoop, J. Kistemaker, and L. J. Oosterhoff, Chem. Phys. Lett. 3. 73 (1969).

[14]N. Baird, J. Am. Chem. Soc. 94, 4941 (1972).

[15]U. V. Atlas of Organic Compounds, Vol. 1 (Butterworth Chemie Verlang, London, 1966).

[16]A. Cope and C. Overberger, J. Amer. Chem. Soc. 70, 1433 (1948).

[17](a) A. Kuppermann, J. K. Rice, and S. Trajmar, J. Phys. Chem. 72, 3894 (1968); (b) J. K. Rice, Ph.D. Thesis, California Institute of Technology, Pasadena, California (1969).

[18]O. A. Mosher, W. M. Flicker, and A. Kuppermann, J. Chem. Phys. 59, 6502 (1973).

[19]S. Trajmar, J. K. Rice, and A. Kuppermann, Adva. Chem. Phys. 18, 15 (1970).

[20]J. R. Oppenheimer, Phys. Rev. 32, 361 (1928).

[21]D. C. Cartwright, W. J. Hunt, W. Williams, S. Trajmar, and W. A. Goddard III, Phys. Rev. A8, 433 (1927).

[22]I. Tanaka and M. Okuda, J. Chem. Phys. 22, 1780 (1954).

[23]S. Trajmar, D. C. Cartwright, J. K. Rice, R. T. Brinkmann, and A. Kuppermann, J. Chem. Phys. 49, 5464 (1968).

[24]O. A. Mosher, W. M. Flicker, and A. Kuppermann, Chem. Phys. Lett. 19, 332 (1973).

[25]T. Koopmans, Physica 1, 104 (1934).

[26]G. Herzberg, Electronic Spectra of Polyatomic Molecules (Van Nostrand, Princeton, New Jersey, 1967) p. 403.

[27]M. Tinkham, Group Theory and Quantum Mechanics (McGraw-Hill Book Company, New York, 1964) p. 221.

[28]M. B. Robin, Higher Excited States of Polyatomic Molecules, Vol. I (Academic Press, New York, 1974) p. 51.

[29]For a Rydberg term value, $R/(n-\delta)^2$, of 11,900 cm^{-1} for the n = 4 transition, the quantum defect, δ, is found to be .97. Excitation energies, E, for other members of the Rydberg series may be predicted by use of the formula:

$$E = IP - R/(n-\delta)^2 .$$

[30]Topics in Applied Physics, Vol. 1, Dye Lasers, F. P. Schäfer, ed. (Springer-Verlag, New York, 1973) pp. 3 and 87.

[31]P. P. Sorokin, J. R. Lankard, V. L. Moruzzi, and E. C. Hammond, J. Chem. Phys. 48, 4726 (1968).

[32]V. I. Tomin, B. A. Bushuk, and A. N. Rubinov, Opt. Spectrosc. 32, 527 (1972).

[33]A. V. Aristov and Yu. S. Maslyukov, Opt. Spectrosc. 35, 660 (1973).

[34]D. N. Dempster, T. Morrow, and M. F. Quinn, J. Photochem. 2, 343 (1973/74).

[35]D. L. Dexter, J. Chem. Phys. 21, 836 (1953).

[36]a) M. W. Schmidt and E. K. C. Lee, J. Amer. Chem. Soc. 90, 5919 (1968); (b) M. W. Schmidt and E. K. C. Lee, J. Amer. Chem. Soc. 92, 3579 (1970).

[37]J. B. Marling, Ph.D. Thesis, University of California, 1971, cited in ref. 12.

[38]M. J. Weber and M. Bass, IEEE Journal of Quantum Electronics 5, 175 (1969).

[39](a) I. H. Kochevar and P. J. Wagner, J. Amer. Chem. Soc. 92, 5742 (1970); (b) I. H. Kochevar and P. J. Wagner, J. Amer. Chem. Soc. 94, 3859 (1972).

[40]A. D. Osborne and G. Porter, Proc. Roy. Soc. A, 284, 9 (1965).

FIGURE CAPTIONS

Fig. 1. Electron energy-loss spectrum of COT at a) $\theta = 10°$ and b) $\theta = 70°$; 30 eV incident energy; 5×10^{-9} A incident beam current; 4×10^{-3} torr sample pressure reading from an uncalibrated Schulz-Phelps gauge; resolution approximately .15 eV FWHM.

Fig. 2. Differential cross sections as a function of θ at an incident energy of 30 eV for elastic scattering (+) and for transitions to the following states: T1 (○), (T2 + T3 + S1) × 10 (◇), and $S_2 + S_3$ (△).

Fig. 3. Same as Fig. 2 for an incident energy of 50 eV. The elastic DCS has been multiplied by .1 before plotting.

Fig. 4. Electron energy-loss spectrum of COT at $\theta = 10°$, 50 eV incident beam energy; 7×10^{-9} A incident beam current; 3×10^{-3} torr sample pressure reading from an uncalibrated Schulz-Phelps gauge; resolution approximately .15 eV FWHM.

Fig. 5. COT valence orbital ordering. Orbitals below the dashed line are occupied in the ground state. The greek letters represent the energy spacing between the adjacent orbital levels. The ordering of occupied orbitals matches ab initio calculations of Lehn and Wipf while energy spacing is obtained via Koopman's theorem. The ordering and spacing

of the virtual orbitals was obtained from a Hückel calculation and the energy spacing of the occupied orbitals. α = 4.43 eV ($\tilde{X}\,^1A_1 \rightarrow {}^1A_2$ transition energy), β = 1.31 eV, γ = 1.37 eV, and δ = 0.40 eV.

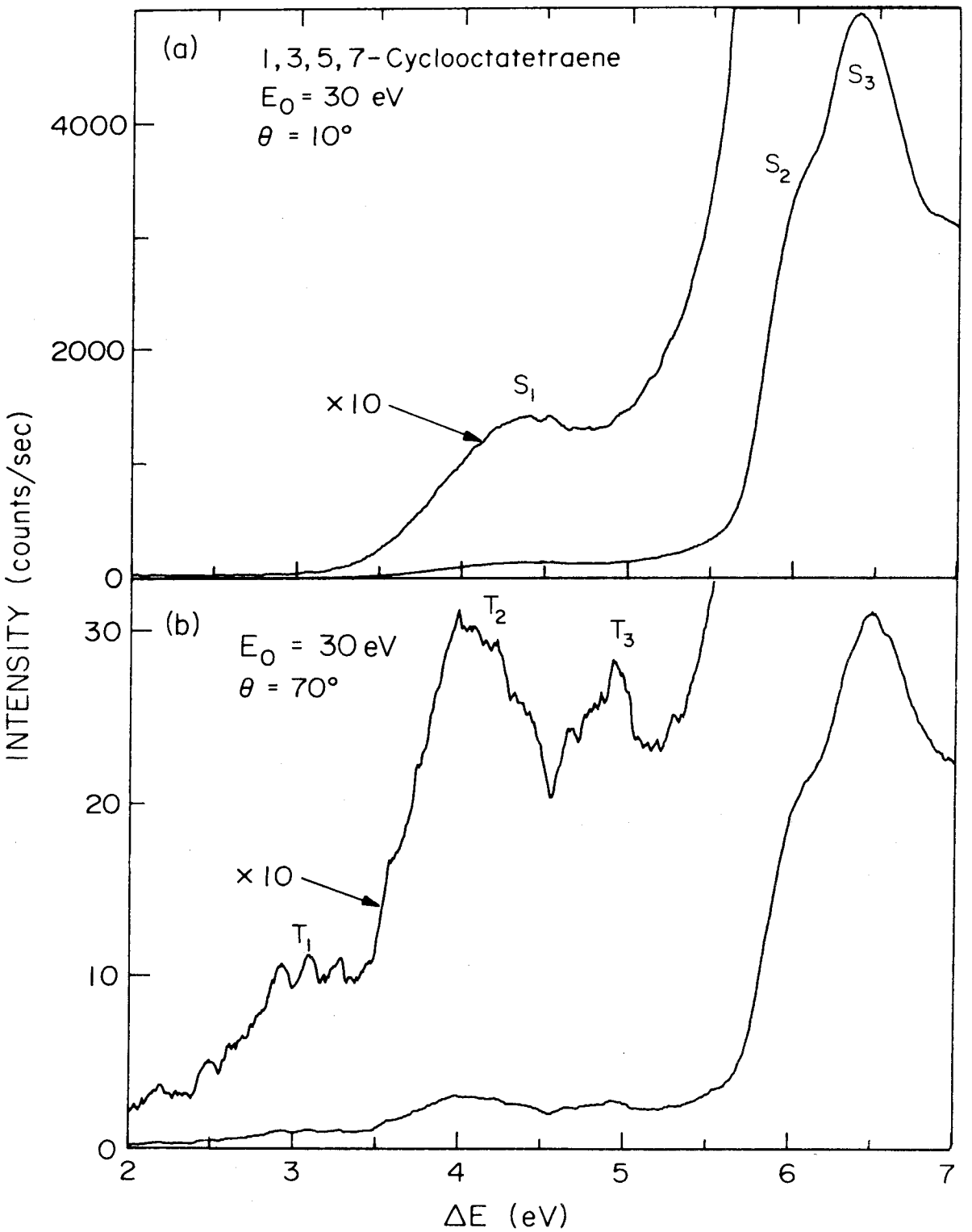
(a)
1,3,5,7-Cyclooctatetraene
E_0 = 30 eV
θ = 10°
S_1
S_2
S_3
×10
4000
2000
0
(b)
E_0 = 30 eV
θ = 70°
T_1
T_2
T_3
×10
30
20
10
0
INTENSITY (counts/sec)
2
3
4
5
6
7
ΔE (eV)

Figure 1

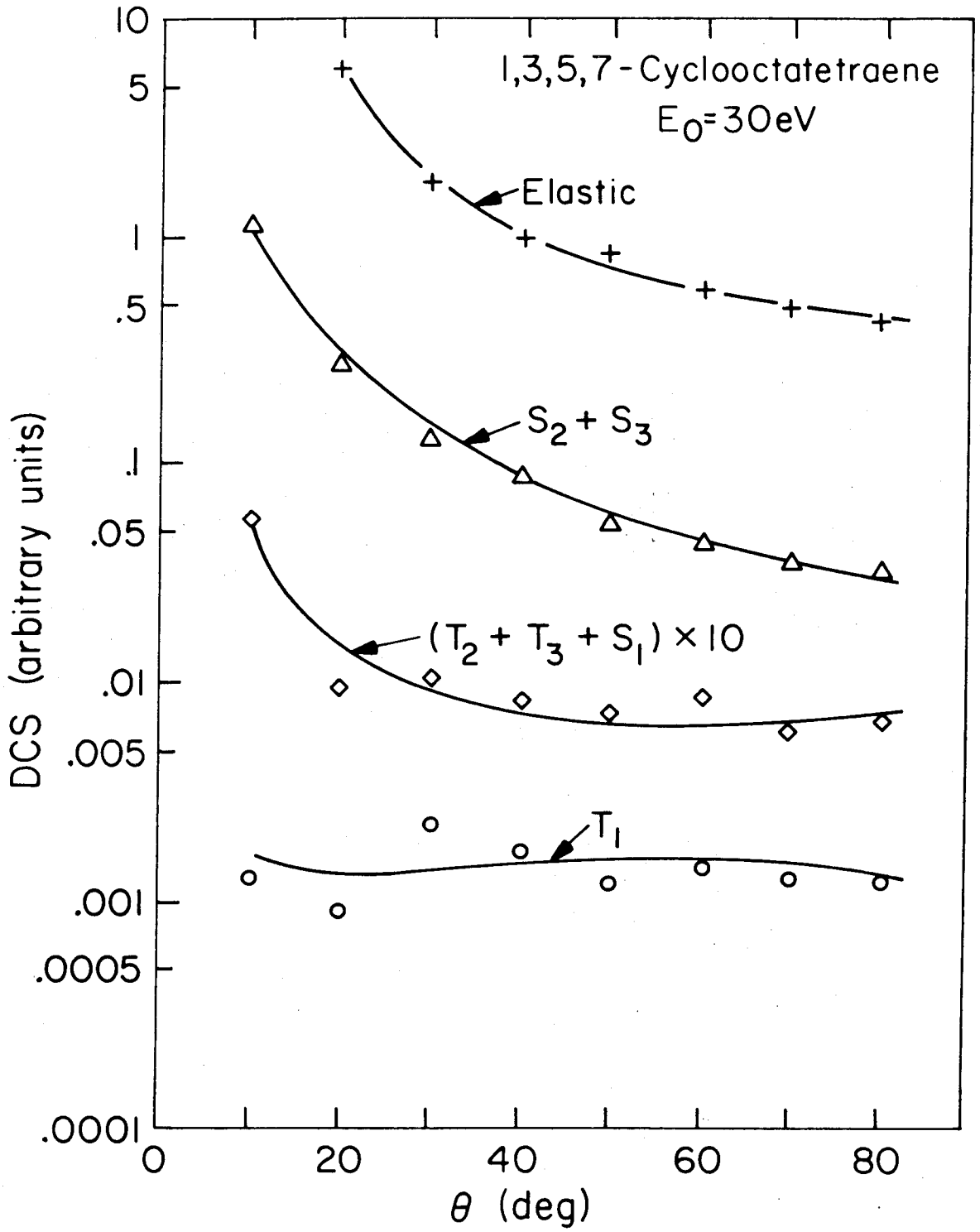
1,3,5,7-Cyclooctatetraene
E_0=30eV
Elastic
$S_2 + S_3$
$(T_2 + T_3 + S_1) \times 10$
T_1
DCS (arbitrary units)
10
5
1
.5
.1
.05
.01
.005
.001
.0005
.0001
0
20
40
60
80
θ (deg)

Figure 2

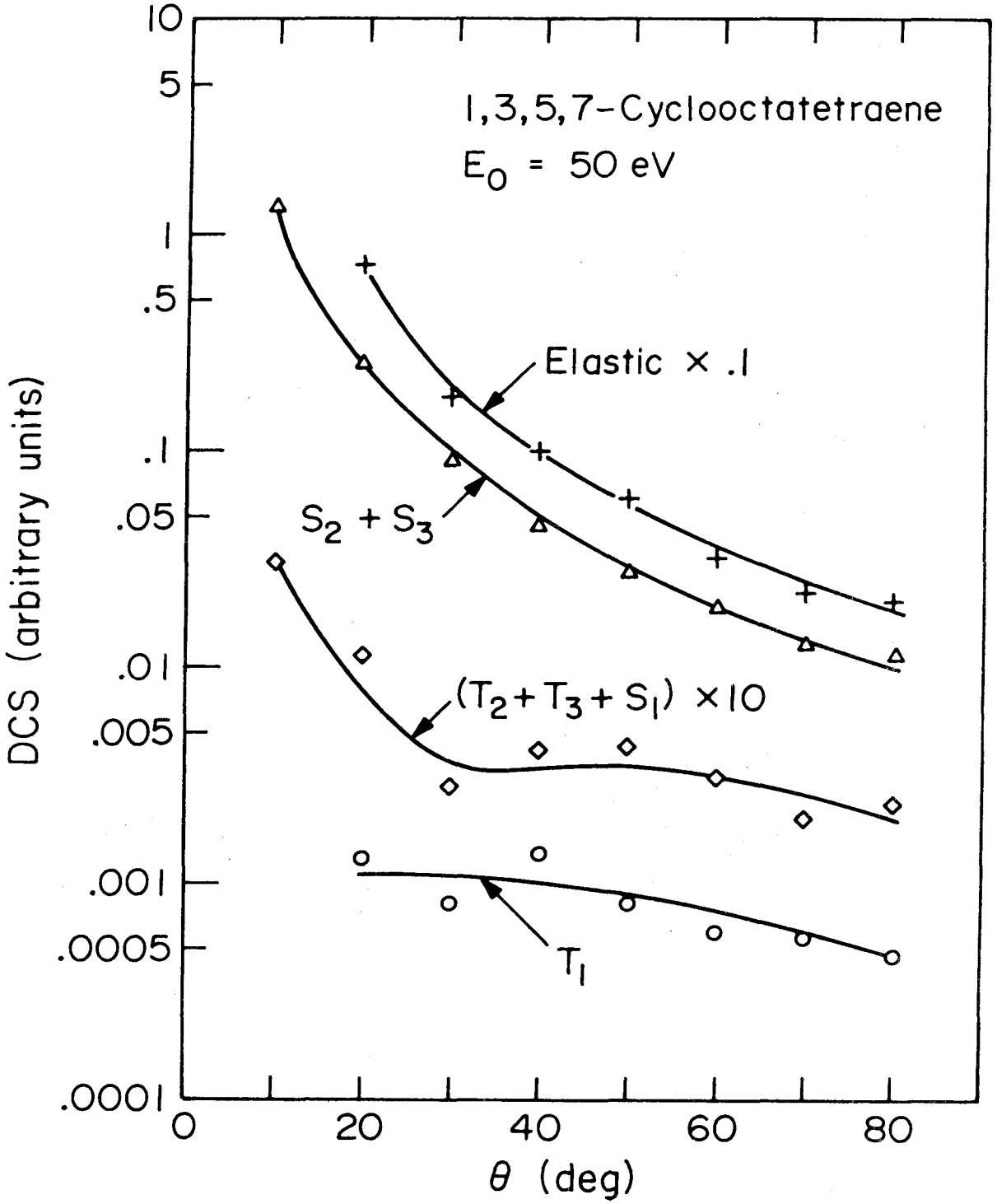
1,3,5,7-Cyclooctatetraene
E_0 = 50 eV
Elastic × .1
$S_2 + S_3$
$(T_2 + T_3 + S_1) \times 10$
T_1
DCS (arbitrary units)
θ (deg)
10
5
1
.5
.1
.05
.01
.005
.001
.0005
.0001
0
20
40
60
80

Figure 3

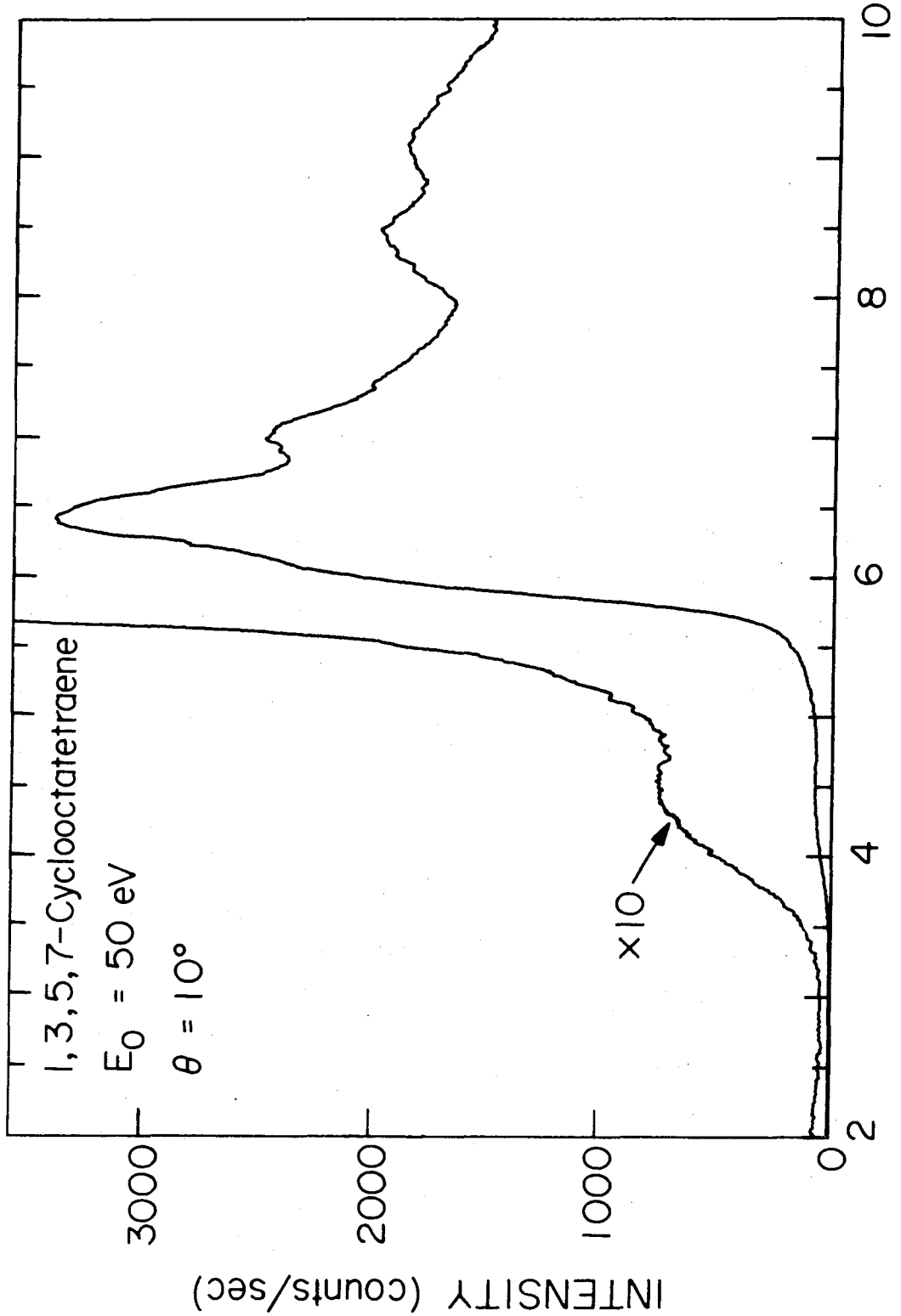
1,3,5,7-Cyclooctatetraene
E_0 = 50 eV
θ = 10°
×10
INTENSITY (counts/sec)
3000
2000
1000
0
2
4
6
8
10
ΔE (eV)

Figure 4

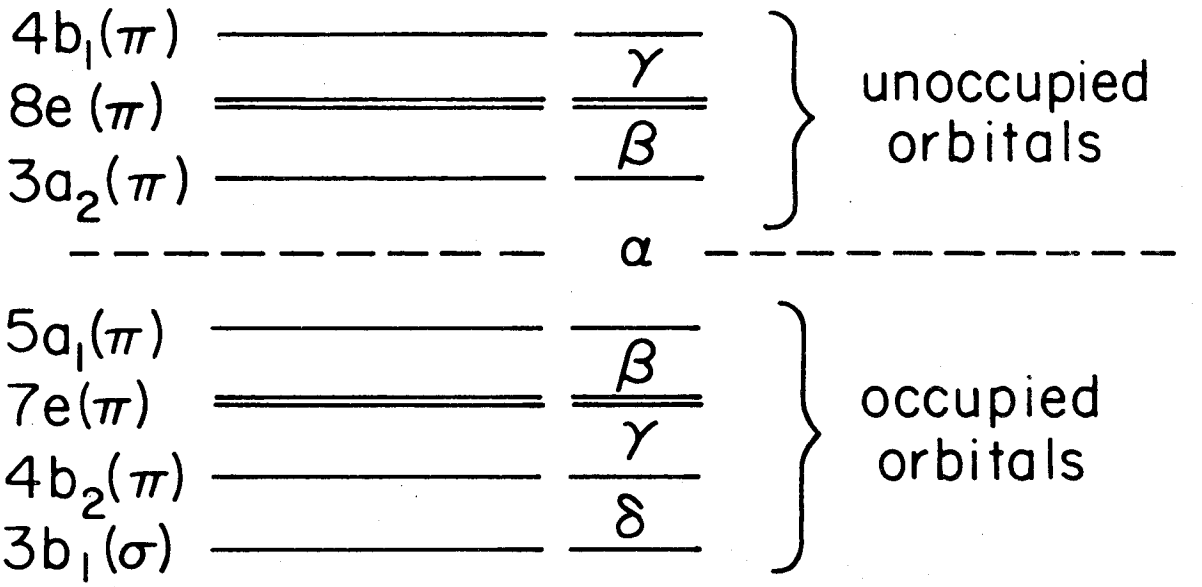
4b1(π)
8e(π)
3a2(π)
γ
β
unoccupied orbitals
α
5a1(π)
7e(π)
4b2(π)
3b1(σ)
β
γ
δ
occupied orbitals

Figure 5

4.3 Paper III: Excited Electronic States of 1,3,5-Cycloheptatriene

EXCITED ELECTRONIC STATES OF 1,3,5-CYCLOHEPTATRIENE*

Robert P. FRUEHOLZ,† Ronald RIANDA, and Aron KUPPERMANN

Arthur Amos Noyes Laboratory of Chemical Physics,‡

California Institute of Technology,

Pasadena, California 91125, USA

(Received)

The electron-impact energy-loss spectrum of 1,3,5-cycloheptatriene has been measured at impact energies of 30, 50, and 75 eV, and scattering angles varying from 5° to 80°. Singlet→triplet transitions were observed at 3.05 eV and 3.95 eV. No evidence for the very weak transition at 2.1 eV previously reported on the basis of threshold electron-impact studies was found. Singlet→singlet transitions were observed at 4.85 eV and 6.40 eV in good agreement with the optical spectrum and semi-empirical calculations.

---

* This work was supported in part by a contract (No. EY-76-S-03-767) from the Department of Energy. Report Code: CALT-767P4-160.

† Work performed in partial fulfillment of the requirements for the Ph.D. degree in Chemistry at the California Institute of Technology.

‡ Contribution No. 5712.

The electronic spectrum of 1,3,5-cycloheptatriene (CHT) has been investigated using low-energy, variable-angle, electron-impact spectroscopy. This has been shown to be a powerful technique for studying both optically forbidden and optically allowed electronic transitions [1]. The excitation energies and band shapes of the optically forbidden singlet → triplet transitions obtained are of particular interest since CHT was found to improve dye-laser performance (e.g., 7-diethyl-amino-4-methyl-coumarin, brilliant sulphaflavine, and kiton red) via what is believed to be quenching of the lowest triplet state [2] of the dye. Marling et al. [2] have proposed that CHT quenches the lowest dye triplet state via a collisional process in which CHT in its lowest triplet state (resulting from intersystem crossing with the excited singlet CHT state populated by the flash from the UV lamp) interacts with a dye molecule also in its lowest triplet state yielding a ground state dye molecule and by spin and energy conservation a CHT molecule in an excited singlet state.

The electronic spectrum of CHT has been studied previously by Knoop et al. [3] using the threshold-electron-impact technique. The excited states of CHT have also been studied theoretically by Knoop et al. [3] and by Van Catledge and Allinger [4] who investigated only the singlet excited states. Using electron diffraction techniques, Traetteberg [5] has determined the structure of CHT in the gas phase and found that it possesses C_s symmetry.

In the present experiments, the electron-impact spectrum of CHT in the energy loss range 0 – 15 eV was studied at impact energies of 30 eV, 50 eV and 75 eV, and scattering angles from 5° to 80°. Sample pressures in the scattering chamber were typically 4 mTorr, as indicated by an uncalibrated Schulz-Phelps ionization gauge, while the electron current incident into the scattering chamber was approximately 60 nA. The energy resolution, as measured by the full width at half maximum (fwhm) of the elastically scattered peak, was set electron-optically at 100 meV in general, while some spectra were obtained with a fwhm of 70 meV. The CHT sample was obtained from the Aldrich Chemical Company Inc. with a stated purity of 97% and was subjected to several liquid nitrogen freeze-pump-thaw cycles before use.

Figure 1 shows the low energy-loss part of the electron impact spectrum of CHT at an impact energy of 30 eV and scattering angles of 30° and 80°. The figure indicates the presence of at least four transitions having maximum intensities at 3.05 eV, 3.95 eV, 4.85 eV, and 6.40 eV. In figs. 2 and 3 we display the corresponding differential cross sections (DCS's) at impact energies of 50 eV and 30 eV. These DCS's were obtained by a method described previously [6].

The most intense feature in the energy -loss region shown in fig. 1 has a maximum intensity at 6.40 eV and an apparent inflection at 6.2 eV. The optical spectrum [7] of CHT in heptane has an absorption maximum (ϵ = 17,800 $\ell\,\mathrm{mole}^{-1}\,\mathrm{cm}^{-1}$) at 6.21 eV. In the threshold electron-impact spectrum of Knoop et al. [3] this transition is observed at 6.25 eV. The DCS's of this transition at 50 eV and 30 eV decrease by factors of 90 and 68, respectively, as the scattering angle varies

from 10° to 80°. These sharply forward peaked differential cross sections are characteristic of a fully allowed singlet → singlet transition. Van Catledge and Allinger's [4] semi-empirical calculations predict a $^1\pi \rightarrow {}^1\pi^*$ transition occurring at 6.60 eV. We assign the transition occurring at 6.40 eV to a singlet → singlet, $\pi \rightarrow \pi^*$, excitation and designate it $S_{6.4}$.

At 4.85 eV we observe a transition which is weaker than that at 6.40 eV. This excitation energy is in excellent agreement with Van Catledge and Allinger's [4] calculated result of 4.84 eV for a $\pi \rightarrow \pi^*$, singlet → singlet transition. For this transition the differential cross sections are again sharply forward-peaked, decreasing over the angular range 10° to 80° by factors of about 50 at both 50 eV and 30 eV impact energies. This angular behavior is consistent with a fully-allowed singlet → singlet excitation. In the optical spectrum [7], the absorption maximum for this transition occurs at 4.75 eV with ϵ = 3100 ℓ mole^{-1}cm^{-1}. The excitation is also observed in the threshold electron-impact spectrum at 4.60 eV. This transition is designated $S_{4.85}$. The fact that both this and the 6.40 eV singlet → singlet excitations display DCS's typical of fully-allowed transitions is consistent with CHT's belonging to the C_s point group for which all electronic transitions are symmetry allowed [8].

At excitation energies below 4.85 eV, we observe two additional transitions, with intensity maxima at 3.05 eV and 3.95 eV, which are designated $T_{3.05}$ and $T_{3.95}$. As can be seen from figs. 2 and 3, the DCS's of these transitions are relatively independent of scattering angle, varying by less than a factor of two from their mean values in

the angular range of 20° to 80°. Moreover, at each scattering angle studied these transitions were relatively more intense (with respect to the feature at 6.40 eV) at 30 eV impact energy than at 50 eV impact energy. This behavior is characteristic of a spin-forbidden process [1] and allows the assignment of these transitions to singlet → triplet excitations.

Our agreement with the threshold electron-impact spectrum of Knoop et al. [3] is not particularly good. They observe transitions, which they assign as singlet → triplet, at 3.68, 3.89, and 4.25 eV and possibly a weak excitation at 2.1 eV. In our spectra we do not observe the additional transitions at 3.68 eV, or 4.25 eV. In addition, below the 3.05 eV feature, which has an apparent onset at 2.4 eV, we find no evidence for another singlet → triplet transition. In fig. 4 the 1.5 eV to 4.5 eV energy-loss region of the CHT spectrum is displayed. Due to the weakness of the scattered signal and the relatively high noise level, this spectrum was digitally smoothed. The data in a given channel were replaced by the average of the data in adjacent channels corresponding to an energy range of 0.2 eV centered about the particular channel [9]. We cannot entirely eliminate the possibility that there exists an extremely weak singlet → triplet transition with intensity maximum at 2.1 eV. However, such a transition, if it does indeed exist, must have an excitation function which not only rises sharply near threshold but which also drops off unusually rapidly with increasing impact energy. Our experience to date indicates that this is an unlikely possibility. As a result, we believe that the lowest-lying triplet state of CHT occurs with a maximum intensity at 3.05 eV

and has an apparent onset at 2.4 eV.

Figure 5 shows the electron-impact spectrum of CHT above 6 eV energy-loss, with the first IP occuring at 8.57 eV [10], indicated by an arrow. Above 6.4 eV but below the first IP, three reproducible transitions are observed occurring at 6.93, 7.23, and 8.48 eV. Due to the fact that we can see these features at all at the relatively high 75 eV impact energy and the low 5° scattering angle, they may be assigned as singlet → singlet excitations. They may be valence excitations or transitions to Rydberg orbitals. Above 8.57 eV several previously unobserved super-excited states are detected. Their excitation energies are summarized in table 1.

In summary, we have used the method of low-energy, variable-angle, electron-impact spectroscopy to investigate the excited states of CHT. Two singlet → triplet excitations were observed at 3.05 eV and 3.95 eV, while no evidence was found for a singlet → triplet transition at 2.1 eV. Singlet → singlet transitions were observed at 4.85 and 6.40 eV in good agreement with the optical spectrum [7] and semi-empirical calculations [4]. Several previously unobserved super-excited states were observed above the first IP.

Table 1

1,3,5-Cycloheptatriene excitation energies eV (± .05 eV)

Nature of Transition	Present Results
Singlet → triplet	3.05
" "	3.95
Singlet → singlet	4.85
Singlet → singlet (shoulder)	6.2
Singlet → singlet	6.40
" "	6.93
" "	7.23
" "	8.48
Singlet → singlet (super-excited)	9.23
" "	9.98
" "	10.62
" "	11.35
" "	11.90
" "	12.47
" "	13.17
" "	14.16

References

[1] A. Kuppermann, J. K. Rice and S. Trajmar, J. Phys. Chem. 72 (1968) 3894; S. Trajmar, J. K. Rice and A. Kuppermann, Adv. Chem. Phys. 18 (1970) 15.

[2] J. B. Marling, D. W. Gregg and L. Wood, Appl. Phys. Lett. 17 (1970) 527; J. B. Marling, Ph.D Thesis, University of California, Davis (1971).

[3] F. W. E. Knoop, J. Kistemaker and L. J. Oosterhoff, Chem. Phys. Lett. 3 (1969) 73.

[4] F. A. Van-Catledge and N. L. Allinger, J. Am. Chem. Soc. 91 (1969) 2582.

[5] M. Traetteberg, Acta Chem. Scand. 86 (1964) 4265.

[6] O. A. Mosher, W. M. Flicker and A. Kuppermann, J. Chem. Phys. 62 (1975) 2600.

[7] U. V. Atlas of Organic Compounds, Vol. 4 (Butterworth Chemie Verlag, London, 1966).

[8] F. A. Cotton, Chemical Applications of Group Theory, 2nd ed. (Wiley-Interscience, New York, 1971) pp. 102-104.

[9] The spectra shown in figs. 1 and 5 were smoothed to a much lesser extent and by a different technique, using 5 to 15 point least square quadratic or cubic polynomial fits to introduce a correction at the midpoint [10].

[10] A. Savitzky and M. J. E. Golay, Anal. Chem. 36 (1964) 1627.

[11] C. Batich, P. Bischof and E. Heilbronner, J. Electron Spectrosc. 1 (1972/73) 333.

FIGURE CAPTIONS

Fig. 1. Electron energy-loss spectrum of CHT at a scattering angle of (a) 30° and (b) 80°; 30 eV incident electron energy; 5×10^{-8} A incident beam current; 4 mTorr sample pressure reading from an uncalibrated Schulz-Phelps gauge; resolution approximately 0.10 eV (fwhm). The spikes in the spectra below 4 eV energy loss are due to instrumental noise.

Fig. 2. Differential cross sections of CHT as a function of scattering angle at an incident electron energy of 50 eV; for elastic scattering (+) and for excited states: $T_{3.05}$ (○), $T_{3.95}$ (◇), $S_{4.85}$ (□), and $S_{6.4}$ (△). The elastic DCS was multiplied by 0.1 before plotting. The letters T and S stand for triplet and singlet upper states, respectively, and the index in these symbols represents the corresponding transition energies in eV.

Fig. 3. Differential cross sections of CHT as a function of scattering angle at an incident electron energy of 30 eV. The symbols for each transition are the same as in fig. 2. The elastic DCS was multiplied by 0.1 before plotting.

Fig. 4. Electron energy-loss spectrum of CHT over the 1.5 to 4.5 eV energy-loss region for the same experimental conditions as in fig. 1(b).

Fig. 5. Electron energy-loss spectrum of CHT at a scattering angle of 5°, 75 eV incident electron energy; 7×10^{-8} A incident beam current; 4 mTorr sample pressure as measured by an uncalibrated Schulz-Phelps gauge.

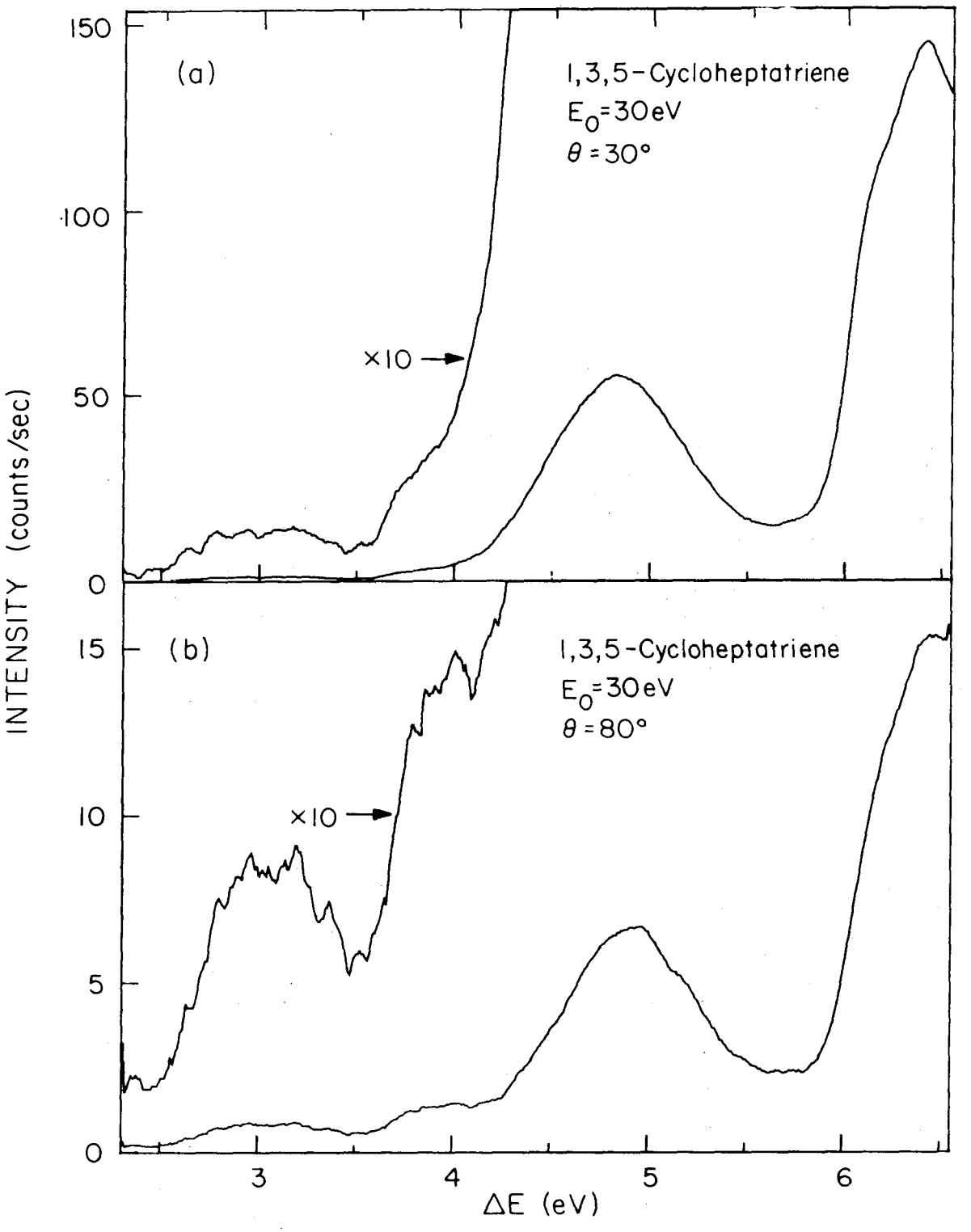
(a)
1,3,5-Cycloheptatriene
E_0=30eV
θ=30°
×10
(b)
1,3,5-Cycloheptatriene
E_0=30eV
θ=80°
×10
INTENSITY (counts/sec)
ΔE (eV)
150
100
50
0
15
10
5
0
3
4
5
6

Figure 1

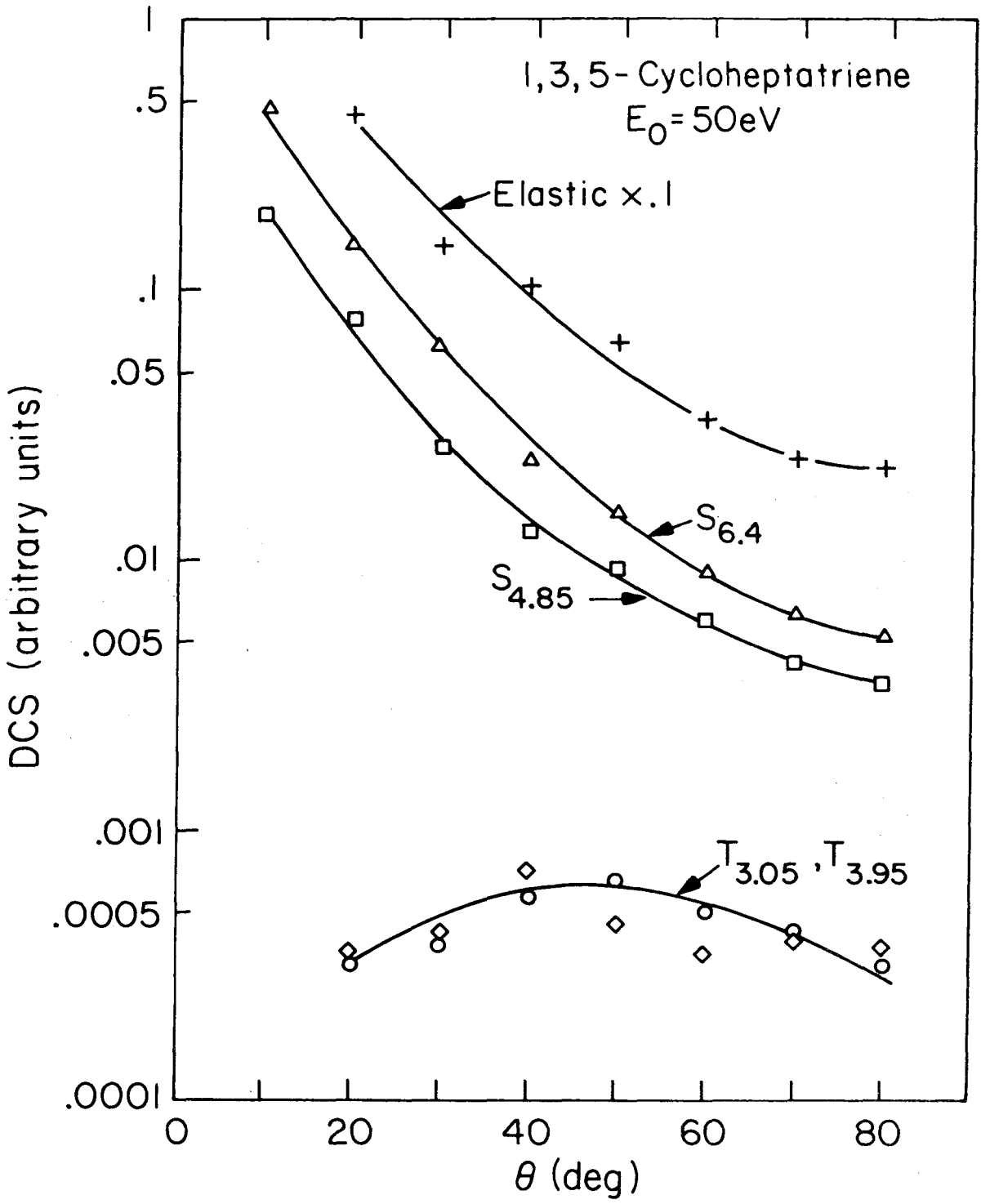
1,3,5-Cycloheptatriene
E_0=50eV
Elastic ×.1
$S_{6.4}$
$S_{4.85}$
$T_{3.05}$, $T_{3.95}$
DCS (arbitrary units)
θ (deg)
1
.5
.1
.05
.01
.005
.001
.0005
.0001
0
20
40
60
80

Figure 2

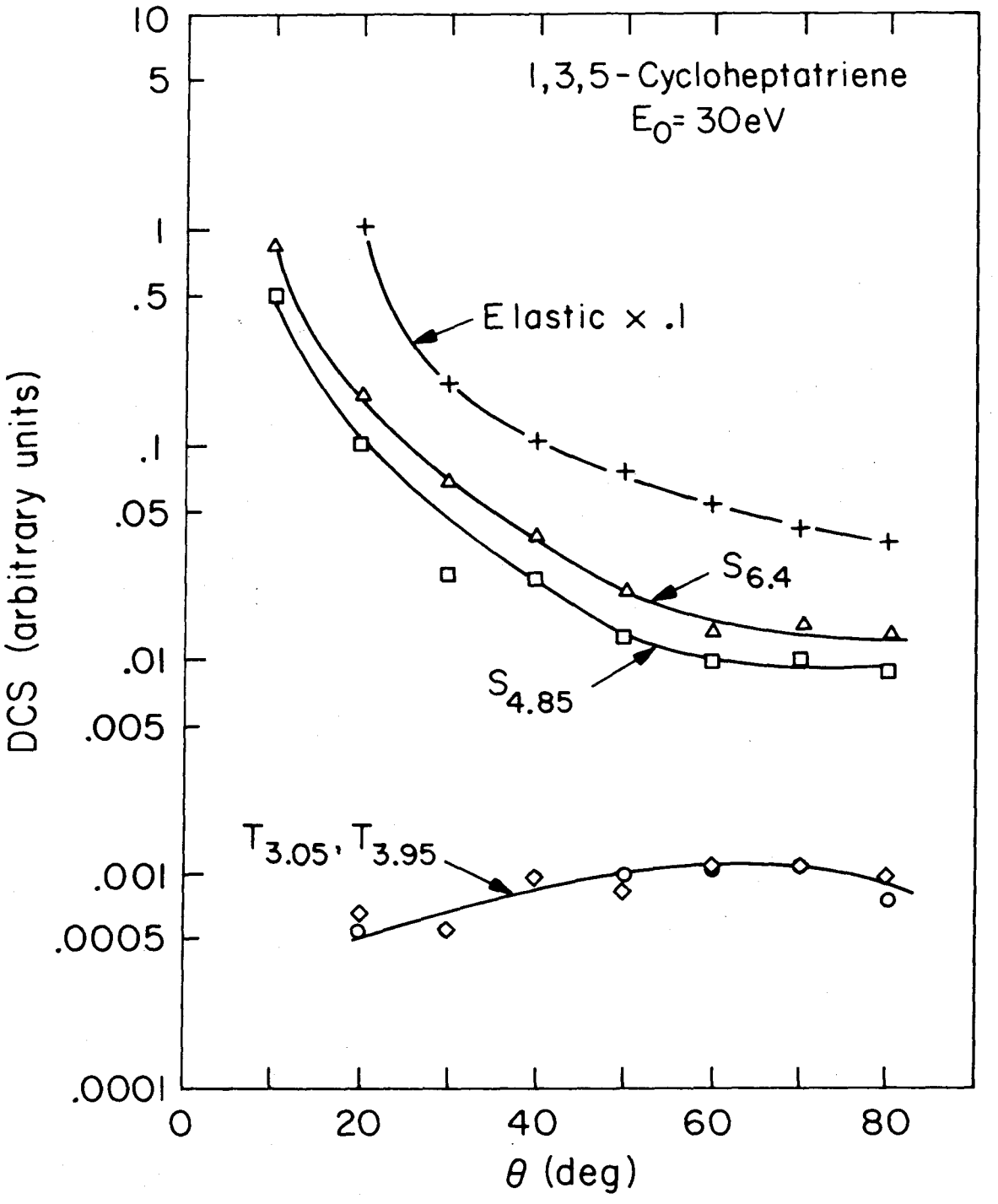
1,3,5-Cycloheptatriene
E_0= 30eV
Elastic × .1
$S_{6.4}$
$S_{4.85}$
$T_{3.05}$, $T_{3.95}$
DCS (arbitrary units)
θ (deg)
10
5
1
.5
.1
.05
.01
.005
.001
.0005
.0001
0
20
40
60
80

Figure 3

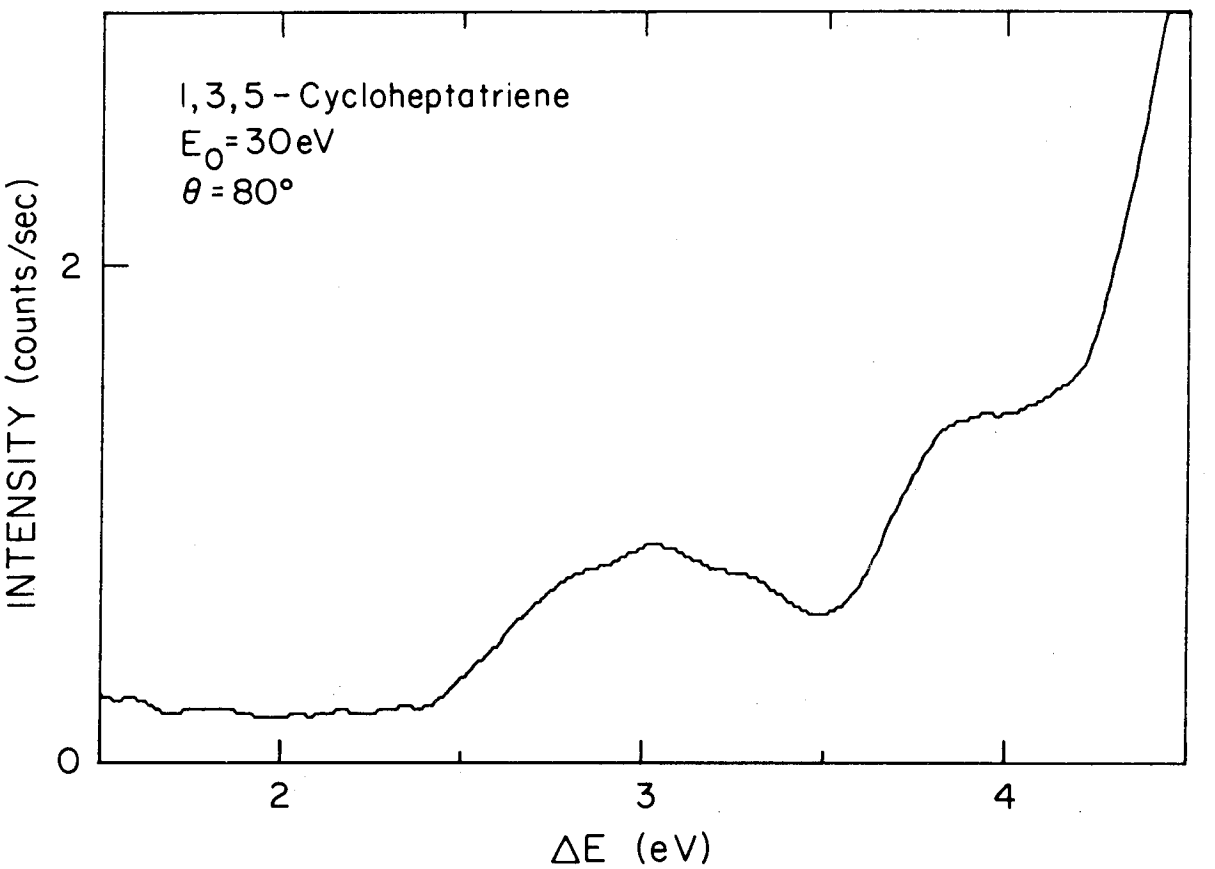
1,3,5 - Cycloheptatriene
E_0 = 30 eV
θ = 80°
INTENSITY (counts/sec)
2
0
2
3
4
ΔE (eV)

Figure 4

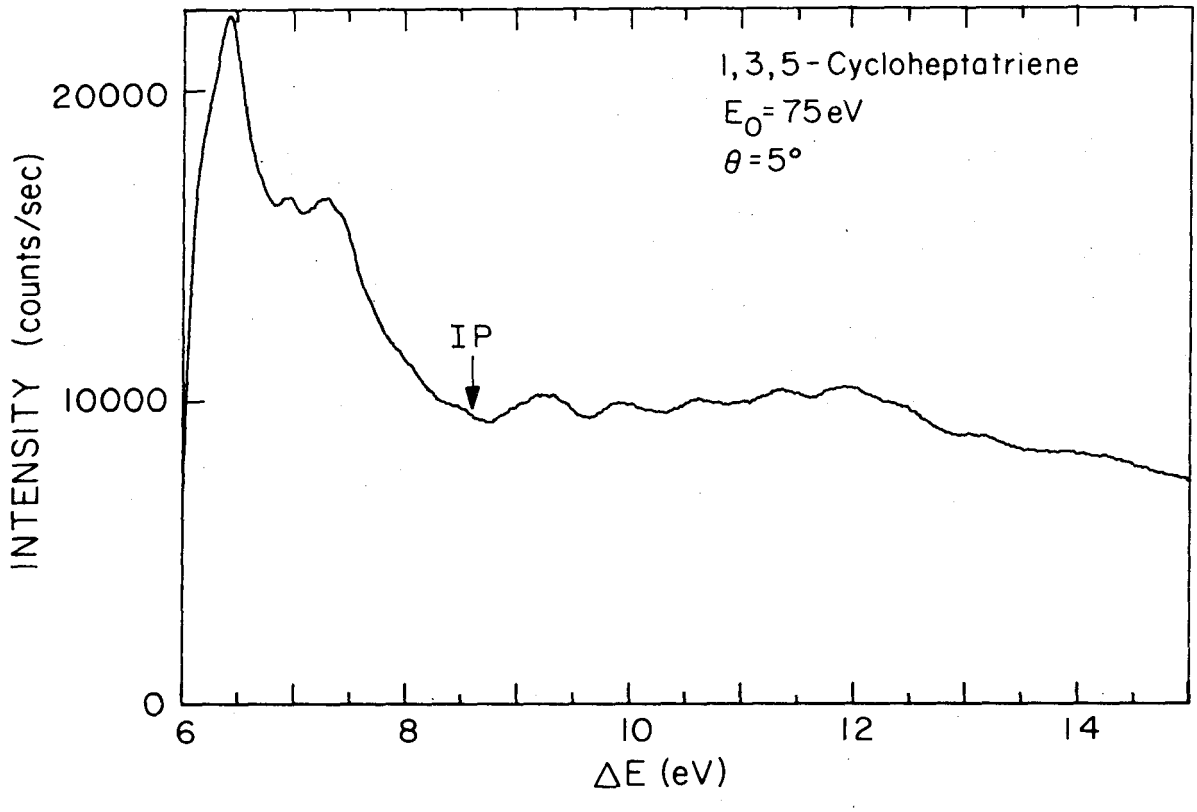
1,3,5-Cycloheptatriene
E_0= 75 eV
θ = 5°
IP
INTENSITY (counts/sec)
20000
10000
0
6
8
10
12
14
ΔE (eV)

Figure 5

4.4 Paper IV: Electronic Spectroscopy of Benzene and the Fluorobenzenes by Variable-Angle Electron Impact

Electronic spectroscopy of benzene and the fluorobenzenes by variable angle electron impact[a)]

Robert P. Frueholz,[b)] Wayne M. Flicker,[c)] Oren A. Mosher,[d)] and Aron Kuppermann

Arthur Amos Noyes Laboratory of Chemical Physics,[e)] California Institute of Technology, Pasadena, California 91125

(Received)

Electron-impact spectra of benzene and 11 fluorine-substituted derivatives have been obtained at impact energies of 75 eV, 50 eV, and either 25 eV or 30 eV, and scattering angles from 5° to 80°. Each molecule shows an absorption maximum at about 3.9 eV corresponding to a singlet→triplet, $\pi \rightarrow \pi^*$, transition. In benzene, fluorobenzene, o- and m-difluorobenzene, and 1,3,5-trifluorobenzene, an additional singlet→triplet excitation was detected at about 5.7 eV. Three singlet→singlet transitions analogous to the 4.90, 6.20, and 6.95 eV benzene excitations are seen in each of the fluorine-substituted molecules.

---

a) This work was supported in part by a contract (No. EY-76-S-03-767) from the Department of Energy. Report Code: CALT-767P4-169.

b) Work performed in partial fulfillment of the requirements for the Ph.D. in Chemistry at the California Institute of Technology.

c) Present address: Harvard-MIT Program in Health Sciences and Technology, Harvard Medical School, Boston, MA 02115.

d) Present address: Eagle Machinery Co. Ltd., 948 - 88th Avenue, Oakland, CA 94621.

e) Contribution No.

The more highly substituted compounds exhibit an additional singlet – singlet transition, which we designate as the C band system, that is most clearly observed in the hexafluorobenzene spectrum, where it has a peak at 5.32 eV. We briefly discuss the effects on relative transition strengths due to the different molecular symmetries of the various fluorobenzenes. We also report numerous superexcited states for each molecule studied.

I. INTRODUCTION

Extensive experimental and theoretical work has been performed in an attempt to understand the electronic spectroscopy of benzene and its derivatives, especially the halogenated derivatives. Historically, the bands resulting from excitation to the lowest singlet state of benzene represented the first extensive and clear cut example of electronic transitions forbidden by symmetry selection rules; their interpretation was achieved using vibronic selection rules.[1] In order to gain more information about the electronic spectroscopy of the simplest halogenated derivatives of benzene, we have applied the experimental technique of low-energy, variable-angle, electron-impact spectroscopy[2] in the present study to all possible fluorine-substituted benzenes except 1,2,3-trifluorobenzene.

The specific goals of this research were to locate singlet→triplet electronic transitions, to determine the shape of their Franck-Condon envelopes, and to investigate systematically the effects of fluorine substitution on the electronic transitions of the π-electron ring. Accurate triplet state energies allow a determination of singlet-triplet energy splittings that may be a factor in determining the value of the rate of intersystem crossing.[3] The maximum intensity locations (generally corresponding to the vertical transition energies) are useful for comparison with theoretical values. In addition, high-quality electronic band shapes of singlet→triplet transitions are important for analysis of photochemical electronic energy transfer experiments.[4-10] Investigation of the spectra of the fluorobenzenes is also inherently interesting because the replacement of hydrogen by fluorine in the benzene system

should perturb both σ and π orbitals.[11,12] Changes in transition energies, with varied fluorine substitution, will reflect the different effects of fluorine substitution on the ground and excited states.

In this paper, we report results obtained from the 3 eV to 18 eV energy-loss region of fluorobenzene, o-, m-, and p-difluorobenzene, 1,3,5- and 1,2,4-trifluorobenzene, 1,2,3,4-, 1,2,4,5-, and 1,2,3,5-tetrafluorobenzene, pentafluorobenzene, and hexafluorobenzene. In Sec. II we summarize the previous experimental and theoretical studies performed on the fluorobenzenes and in Sec. III we describe the present experiment. Results and their discussion are presented in Sec. IV. We conclude with a brief summary and statement of the conclusions in Sec. V.

II. SUMMARY OF BENZENE SPECTROSCOPY AND OF PREVIOUS FLUOROBENZENE STUDIES

The spectroscopy of the fluorobenzenes is intimately related to that of the parent molecule, benzene. The highest occupied molecular orbitals in benzene have the symmetries $e_{1g}(\pi_2, \pi_3)$, $e_{2g}(\sigma)$, and $a_{2u}(\pi_1)$ and have increasing ionization potentials.[11] Over the energy-loss region 3.0 to 8.5 eV, the gross features of the benzene spectrum include three singlet – singlet transitions, resulting from the excitation of an e_{1g} electron to an e_{2u} π^* orbital, occurring at energy losses of about 4.90 eV, 6.20 eV, and 6.95 eV.[13] The first and third singlet – triplet excitations can be assigned as the symmetry-forbidden, $\tilde{X}\ ^1A_{1g} \rightarrow 1\ ^1B_{2u}$, and the symmetry-allowed, $\tilde{X}\ ^1A_{1g} \rightarrow\ ^1E_{1u}$ excitations.[1,14]

The identity of the second singlet state is still somewhat uncertain. The most probable assignment appears to be the symmetry-forbidden, $\pi \rightarrow \pi^*$, $\tilde{X}\ ^1A_{1g} \rightarrow 1\ ^1B_{1u}$ excitation.[14,15] However, the low-angle electron-impact spectra of Lassettre et al.[13] and Doering[16] indicate the possibility of two transitions occurring in this region. On the basis of the variation of peak intensities with scattering angle, Lassettre et al.[13] suggested that vibronic peaks occurring at 6.31 eV, 6.41 eV, and 6.53 eV (the first being the most intense) belonged to an excitation other than the $\tilde{X}\ ^1A_{1g} \rightarrow 1\ ^1B_{1u}$ which they found at 6.20 eV. Further evidence in support of this suggestion comes from multiphoton ionization experiments.[17] In the multiphoton ionization spectrum, vibronic peaks were observed at transition energies including 6.33 eV, 6.42 eV, and 6.53 eV, with the 6.33 eV peak being the most intense of all transitions observed. No transition was observed at 6.20 eV, which is consistent

with the fact that the $\tilde{X}\ ^1A_{1g} \rightarrow 1\ ^1B_{1u}$ transition (which would be a two-photon resonance intermediate in the three-photon ionization) is forbidden by two-photon selection rules. The correlation between the results of these two different experimental techniques supports, very strongly, the existence of at least two electronic states of benzene in the excitation energy range of 6.2 eV to 6.7 eV. An additional $\pi \rightarrow \pi^*$ transition, $\tilde{X}\ ^1A_{1g} \rightarrow {}^1E_{2g}$, resulting from the excitation of an a_{2u} electron to the e_{2u} π^* orbital, is predicted by theoretical studies[18,19] to occur in the region of the intense, 6.95 eV, $\tilde{X}\ ^1A_{1g} \rightarrow {}^1E_{1u}$ excitation, but that transition has not yet been unambiguously identified.[14] It is possible that the excitation observed by Lassettre and co-workers[13] and by Johnson[17] is this $\tilde{X}\ ^1A_{1g} \rightarrow {}^1E_{2g}$ transition.

Doering,[16,20] who has studied benzene via low energy, variable angle, electron impact, assigned three other transitions occurring at 3.89 eV, 4.85 eV, and 5.69 eV as singlet $\rightarrow$ triplet transitions. The first and third may be assigned as $\tilde{X}\ ^1A_{1g} \rightarrow 1\ ^3B_{1u}$ and $\tilde{X}\ ^1A_{1g} \rightarrow 1\ ^3B_{2u}$ transitions,[18-20] while the second is believed to be the $\tilde{X}\ ^1A_{1g} \rightarrow 1\ ^3E_{1u}$ excitation.[18,19]

The electronic spectroscopy of the fluorobenzenes has also received significant attention.[12,21-26] The observed transitions, in the 3.0 eV to 8.5 eV energy-loss region, are quite similar to those observed in the benzene. Due to this similarity, these transitions are most easily discussed in terms of the benzene symmetry notation, even though it applies rigorously only to hexafluorobenzene. The lowest singlet $\rightarrow$ singlet excitation in the fluorobenzenes appears to be analogous to the $\tilde{X}\ ^1A_{1g} \rightarrow 1\ ^1B_{2u}$ transition in benzene. It has been studied optically by several authors.[12,21-23] The higher excited singlet $\rightarrow$ singlet

transitions, apparently corresponding to the $\tilde{X}\ ^1A_{1g} - 1\ ^1B_{1u}$ and $\tilde{X}\ ^1A_{1g} - {}^1E_{1u}$ excitations of benzene, have been investigated by Sandorfy and coworkers.[24] Spin-forbidden transitions have also been studied, but to a lesser extent. Evans,[25] using the oxygen-perturbation technique, obtained the $S_0 - T_1$ absorption spectrum of fluorobenzene, while Metcalfe et al.[26] investigated the $S_0 - T_1$ absorption spectra of 11 fluorobenzenes using the same method. However, the accuracy of the $S_0 - T_1$ absorption profiles and of the positions of the intensity maxima is limited in this technique because the $S_0 - T_1$ transition is partially masked by the diffuse charge-transfer band of the aromatic contact complex. Photochemists have also studied these states indirectly using the triplet state-induced cis-trans isomerization of cis-2-butene and the triplet photosensitized phosphorescence of biacetyl.[6-9]

In addition to experimental interest in the excited electronic states of the fluorobenzenes, there have been several theoretical studies of their excitation energies.[27-35] Unfortunately, these calculations have been limited to applications of various semi-empirical techniques. To our knowledge, no ab initio calculations have yet been performed on excited states of the fluorobenzenes. While the available semi-empirical excitation energies are generally within 1 eV of the experimental values, they are consistently below those values. As substitution is increased, the semi-empirical calculations predict a monotonic decrease in excitation energy of a given transition.[30,35] This is not consistent with the observed experimental results.[12,24,26] Duke et al.[35] explain this short-coming of the calculations as the result of an unrealistic lowering

of the energy of the π^* orbitals with fluorine substitition. While the semi-empirical calculations performed on the fluorobenzenes are limited in scope, high-quality ab initio configuration interaction (CI) calculations have been performed on benzene and its excited states by Hay and Shavitt.[18] Their detailed discussion of the transitions observed in the benzene spectrum is of value when considering the very similar transitions of the fluorobenzenes.

III. EXPERIMENTAL

The instrument used in these studies has been described in detail by Kuppermann et al.[2] The spectrometer consists basically of a multistage electron gun, a hemispherical electrostatic energy monochromator, a flexible bellows scattering chamber which contains the target gas, an energy-loss analyzer identical to the monochromator, and a Spiraltron electron multiplier. Pulses from the multiplier are amplified and shaped, then counted with a 1024 channel scaler. In a typical experiment, the incident electron-impact energy, E_0, and the scattering angle of detection, θ, are both fixed, and the energy-loss spectrum is scanned repeatedly, usually for a period of four to eight hours. The method of data reduction used to obtain both elastic and inelastic differential cross sections (DCS's) has also been described previously.[36]

The benzene and fluorobenzene used in these studies were obtained from Matheson, Coleman and Bell. The benzene sample was A.C.S. reagent grade with a boiling point range of 1 °C, while the fluorobenzenes used had a stated boiling point range of 1 °C. 1,3,5- and 1,2,4-trifluorobenzene were obtained from PCR Inc. with stated minimum purities of 97%. All other chemicals were obtained from the Aldrich Chemical Company. M-difluorobenzene and 1,2,3,5-tetrafluorobenzene had stated minimum purities of 97% and 99+%, respectively, while the other compounds had stated minimum purities of 98%. All samples were subjected to several freeze-pump-thaw cycles prior to use.

Spectra were taken for these molecules at impact energies of 75 eV, 50 eV, and either 25 eV or 30 eV. The energy-loss range scanned was 3.0 eV to 18 eV. Sample pressures in the scattering

chamber ranged from 2 mTorr to 8 mTorr, as indicated by an uncalibrated Schulz-Phelps ionization gauge. The instrumental resolution, as determined from the full width at half maximum (FWHM) of the elastic peak was set electron-optically in the range 0.10 eV to 0.16 eV.

IV. RESULTS AND DISCUSSION

A. Transitions below 8 eV

Table I summarizes the principal transition energies in the 3.0 to 8.5 eV energy-loss region obtained in the present experiments for benzene and the 11 fluorobenzenes studied. Figures 1 and 2 display the high angle spectra for all these molecules. These spectra were obtained at either 25 eV or 30 eV impact energy. The electronic band shapes do not change significantly between these two impact energies and can be compared with each other. Figure 3 displays the spectra of the three difluorobenzene isomers at 50 eV impact energy and 20° scattering angle, while Fig. 4 presents the corresponding spectra of 1,3,5- and 1,2,4-trifluorobenzene. Figure 5 shows those of the three tetrafluorobenzenes. Both elastic and inelastic DCS curves for selected fluorobenzenes are displayed in Figs. 6-11.

In the energy-loss region from 3.0 to 8.5 eV, the spectra of the mono-, di-, and trifluorinated molecules are quite similar to that of benzene. Each molecule possesses three transitions at approximately 4.8, 6.2, and 7.0 eV, which appear to be equivalent to the $\tilde{X}\ ^1A_{1g} \rightarrow 1\ ^1B_{2u}$, $\tilde{X}\ ^1A_{1g} \rightarrow 1\ ^1B_{1u}$, and $\tilde{X}\ ^1A_{1g} \rightarrow {}^1E_{1u}$ excitations in benzene. Each of these transitions possesses a differential cross section which is forward-peaked (see Figs. 6-8). This DCS behavior is characteristic of singlet → singlet transitions and is consistent with the commonly accepted nature of these transitions.[24] The DCS curves for the transitions occurring at about 4.8 eV are generally less forward-peaked than those

of the higher singlet states. This angular dependence is probably due to the presence of an underlying triplet state, as is the case in benzene where the second triplet overlaps the lowest-lying spin-allowed transition.[16] (In our benzene spectra the second singlet → triplet transition reported by Doering[16,20] was not distinguishable from the $\tilde{X}\ ^1A_{1g} \rightarrow 1\ ^1B_{2u}$ transition.)

Each of the six fluorinated molecules thus far considered has a transition occurring at about 3.9 eV. These transitions display essentially isotropic differential cross sections as a function of angle (Figs. 6-11), and their intensity relative to the singlet → singlet transitions just described increases as the impact energy decreases. This behavior is characteristic of singlet → triplet transitions, in agreement with previous assignments.[26] These excitations appear to be analogous to the $\tilde{X}\ ^1A_{1g} \rightarrow 1\ ^3B_{1u}$ transition observed in the benzene spectrum. In fluorobenzene, o- and m-difluorobenzene, and 1,3,5-trifluorobenzene, an additional weak transition was observed at about 5.7 eV. It was not possible to obtain reliable DCS values for this feature, due to its weakness and overlap with the $\tilde{X}\ ^1A_{1g} \rightarrow 1\ ^1B_{1u}$ excitation. However, the fact that it appeared principally in high-angle spectra, and increased in intensity relative to the singlet → singlet transitions as the impact energy decreased is consistent with a singlet → triplet assignment. These transitions appear to be analogous to the $\tilde{X}\ ^1A_{1g} \rightarrow 1\ ^3B_{2u}$ excitation in benzene which occurs at 5.69 eV.[16,18] The fact that this feature was not observed in the p-difluorobenzene and 1,2,4-trifluorobenzene spectra indicates that either its relative intensity is significantly weaker for these molecules or that the transition has shifted to higher energies. If the latter is the case, we estimate that the transition energies are higher

than 5.9 eV. This is the onset of the much more intense $\tilde{X}\ ^1A_{1g} - 1\ ^1B_{1u}$ transition which would obscure features whose strengths are comparable to those observed in the other mono-, di-, and trifluorobenzenes.

The electron-impact spectra of the tetra-, penta-, and hexafluorobenzenes are quite similar to the spectra of the less substituted fluorobenzenes. In the spectra of each of these molecules, the lowest energy transition observed occurs at about 3.9 eV. This is again a singlet → triplet excitation displaying, characteristically, a nearly isotropic DCS at both high and low impact energies (see Figs. 9 through 11). The excitation analogous to the third singlet → triplet transition of benzene is not detected in these molecules, due in part to the emergence of an additional singlet state, which will be discussed shortly. In hexafluorobenzene a transition is seen at 5.71 eV which might be due to the third singlet → triplet excitation. A small peak at this energy-loss, superimposed on the underlying singlet → singlet feature, is apparent in several spectra; however, it is seen at both high and low angles with approximately equal relative intensity with respect to the singlet → singlet intensities, which precludes its assignment as a spin-forbidden transition. This 5.71 eV transition may be due instead to a small amount of impurity.

The three singlet → singlet transitions analogous to those in benzene are still present at similar energy losses in the tetrafluorobenzenes, pentafluorobenzene, and hexafluorobenzene. The DCS curves of these transitions are all forward-peaked, which is consistent with the singlet → singlet nature of these excitations. In addition to these transitions, another feature emerges in the 5-6 eV region of the spectra. This new feature is clearly visible in the hexafluorobenzene spectrum

with an intensity maximum occurring at 5.32 eV. We designate this transition the C band system, for ease of reference.[37] Similar transitions in the spectra of penta- and the tetrafluorobenzenes discussed below are also designated C bands. The DCS of the C bands (see Fig. 11) is forward-peaked, permitting us to assign this excitation as singlet – singlet. In pentafluorobenzene a small peak is apparent with a maximum intensity at approximately 5.85 eV (see Fig. 1). The 6.36 eV transition heavily overlaps this feature and consequently we were not able to obtain a reliable DCS for it. However, the band shape of the transitions between 5.3 eV and 7.5 eV is approximately independent of angle, indicating that the DCS curves of the three transitions in this energy-loss region are quite similar. Therefore, we may assign the 5.85 eV feature as a singlet – singlet excitation. We believe that this transition is analogous to the feature observed in the hexafluorobenzene spectrum at 5.32 eV (C band). With decreasing fluorine substitution, the C band shifts to higher energy loss.

Analysis of the 5.5-7.0 eV region of the tetrafluorobenzene spectra is quite complicated. In 1, 2, 3, 4-tetrafluorobenzene there is a definite broadening on the low-energy side of the 6.51 eV feature ($\tilde{X}\,{}^1A_{1g} - 1\,{}^1B_{1u}$ in benzene notation) and the apparent onset is at lower energy than in molecules with fewer fluorine atoms. This broading appears to be due to the superposition of the C band (located at 5.85 eV in the penta compound), shifted to even higher energy losses, and the $\tilde{X}\,{}^1A_{1g} - 1\,{}^1B_{1u}$ excitation. In the 1, 2, 3, 5-tetrafluorobenzene spectra (see Fig. 5), the valley between the $\tilde{X}\,{}^1A_{1g} - 1\,{}^1B_{1u}$ and $\tilde{X}\,{}^1A_{1g} - {}^1E_{1u}$ transitions observed in the 1, 2, 3, 4-tetrafluorobenzene spectra (at 6.43 eV and 7.21 eV,

respectively) is not visible, indicating that the C band has shifted to somewhat higher excitation energy, approximately 6.5 eV. The spectrum of 1,2,4,5-tetrafluorobenzene also lacks the valley between the $\tilde{X}\ ^1A_{1g} \rightarrow 1\ ^1B_{1u}$ and $\tilde{X}\ ^1A_{1g} \rightarrow {}^1E_{1u}$ transitions and, in addition, displays a slope break on the low-energy side of the $\tilde{X}\ ^1A_{1g} \rightarrow {}^1E_{1u}$ excitation. This slope break is more apparent in spectra obtained at 30 eV impact energy and occurs at approximately 6.9 eV. Whether it is due to the superposition of the C band singlet → singlet feature observed in hexa-, penta-, and 1,2,3,4-tetrafluorobenzene and the $\tilde{X}\ ^1A_{1g} \rightarrow {}^1E_{1u}$ transition or is the result of an entirely different excitation is not obvious.

B. The nature of the C band

The C band singlet state observed in hexafluorobenzene at 5.32 eV and higher energy losses in the penta- and tetra-substituted molecules has also been observed in the hexafluorobenzene optical spectrum.[38] However, the character of this transition has been explicitly discussed only in our preliminary description of the fluorobenzene results.[39] One possibility is that these C band transitions may be related to the $\tilde{X}\ ^1A_{1g} \rightarrow {}^1E_{2g}$[18,19] transition of benzene. In hexafluorobenzene the excitation energy of the C band is near that of a weak vibronic system observed by Taleb et al.[40] and Morris and Angus,[41] who studied absorption and photoexcitation spectra, respectively, of benzene in rare gas matrices. The intensity maximum of this transition in the absorption spectrum[40] was located at approximately 5.77 eV and assigned to the $\tilde{X}\ ^1A_{1g} \rightarrow {}^1E_{2g}$[42] excitation. Two points should be considered when analyzing the possible relationship of this transition in benzene to the C bands in the fluorobenzenes. First, the possibility

exists that these vibronic peaks in the matrix spectra are due to impurities. Relative to the intensity of the $\tilde{X}\ ^1A_{1g} - {}^1B_{1u}$ transition, these $^1E_{2g}^-$ bands are at least ten times more intense in the absorption spectrum of Taleb et al. obtained using a perfluoro-n-hexane solvent at -85 °C than in the krypton film spectrum of Morris and Angus. In addition, this feature is not observed at all in the vapor phase high-resolution electron-impact spectrum of benzene obtained by Lassettre et al.[13] Secondly, assuming that the supposed $^1E_{2g}^-$ bands are indeed due to benzene, their valence assignment is inconsistent with the relatively large downward shift of 0.5 eV in the observed excitation energy of the C band in going from penta- to hexafluorobenzene when compared with those of the other valence singlet states. We conclude that the 5.77 eV excitation in the spectra of benzene in rare gas matrices does not correspond to the C band in the fluorobenzenes.

The C bands also seem not to be related to the transitions observed by Johnson[17] and Lassettre et al.[13] in the 6.3 eV to 6.7 eV energy-loss region (see Sec. II). If these excitations are valence transitions within the phenyl ring, the excitation energy behavior with varying fluorine substitution of the C bands is again inconsistent with this proposed assignment because of the relatively large shift between the penta and hexa compounds. The likelihood that the C bands are of the Rydberg type also appears to be small. The vertical ionization potentials of pentafluorobenzene and hexafluorobenzene are both 10.1 eV.[43] If the C bands are Rydberg-like, there should be a negligible difference in the corresponding excitation energies in these two molecules since the respective quantum defects should be approximately equal.

Still another possibility is that this 5.32 eV singlet → singlet transition involves an interaction of the fluorine substituents with the benzene ring. Two types of transitions of this kind appear to be plausible, in the sense of being able to explain the observed shifts in transition energy as the degree of fluorine substitution increases. The first may be described as a charge-transfer transition involving excitation of a fluorine p_π electron to a carbon p_{π^*} orbital. Kimura and Nagakura[28] have found significant differences between the optical spectra of benzene and other monosubstituted benzenes (e.g., -I, -Br, and -SH), involving changes in excitation energies and the appearance of additional electronic bands. They felt that charge-transfer configurations were important in a description of the excited states responsible for the extra bands. A discussion of the expected effect of charge transfer on the variation of C band transition energies with fluorine substitution is given below.

In 1940, Mulliken[44] suggested that the longest wavelength bands of the alkyl bromides and iodides are probably due to an $n_{\pi_X} \rightarrow \sigma^*_{C\text{-}X}$ (X = Br and I), $\sigma^2\pi_x^2\pi_y^2 \rightarrow \sigma^2\pi_x^2\pi_y\sigma^*$ excitation, rather than to a Rydberg transition. Kimura and Nagakura[45] have calculated oscillator strengths, using a simple LCAO technique, for both $n \rightarrow \sigma^*$ and n → Rydberg transitions in these molecules. A comparison of these oscillator strengths with experimental values indicates that the $n \rightarrow \sigma^*$ assignment is better than an n → Rydberg assignment. Similar bands have been observed in the spectra of chloromethanes.[46] These so-called A band transitions were not observed in the electron-impact spectroscopy of the fluoromethanes.[47] However, Robin[48] has suggested that these transitions in the fluoromethanes should be quite weak, lying at lower energies than the Rydberg transitions observed in these molecules.[47] Furthermore,

in methylchloride, -bromide, and -iodide these A band transitions are observed at 7.3 eV, 6.2 eV, and 4.8 eV.[49] These arguments would place the corresponding transitions in the fluoromethanes in the 7.5 eV to 12 eV range.

Robin[50] has tentatively assigned an additional transition observed in the hexachlorobenzene spectrum, at 4.71 eV, as the promotion of a chlorine lone-pair electron into the antibonding sigma molecular orbital formed from the chlorine atom and the adjacent carbon atom orbitals. This transition would then be similar to the A band transitions observed in haloalkanes. By analogy, one further possible explanation of the C band transition observed in the spectra of higher substituted fluorobenzenes is the excitation of a fluorine p_π electron into a C-F σ^* orbital.

Let us now analyze the expected effects of fluorine substitution on the excitation energies associated with the various fluorine ring-type transitions which we have suggested as possible explanations for the observed C bands. Let us first consider the effects of increasing fluorine substitution on the energy of the orbital into which the fluorine π-electron is excited. The σ^* orbital, being localized in the C-F region, should have an energy that is relatively independent of the presence of adjacent fluorines. The π^* orbital energy will probably also be relatively independent of fluorine substitution. On the basis of an analysis of ionization potentials, the highest π molecular orbital in these molecules is found to be stabilized by less than 1 eV when fluorine substitution is increased from benzene to hexafluorobenzene.[35] The lowest π^* orbitals should undergo a similarly small change in relative orbital energy because spatially they occupy a region quite similar to that of the π orbitals, differing primarily in the nodal pattern.[18]

The shifts in charge resulting from the fluorine interactions with the ring are of two primary types: the inductive effect of the fluorine through the σ bond and a back migration of the p_π electron density toward the ring.[12, 24, 25] As the fluorine p_π density is back-donated, there will be a repulsive electrostatic interaction between the fluorine p_π's and the ring p_π's. This should tend to destabilize the fluorine π orbitals. In addition, the fluorine π and the ring π orbitals are both doubly-occupied. The Pauli principle forces these orbitals to remain orthogonal, further raising the orbital energy of the fluorine π orbitals.

With increasing fluorine substitution, this destabilizing interaction should become increasingly important as the carbon p_π orbitals are less able to recede from the encroaching fluorine p_π orbitals. In pentafluorobenzene, for example, the carbon p_π cloud should be able to move outward, away from the fluorine clouds, along approximately one third of the periphery of the ring. However, upon substitution of the sixth fluorine, the freedom of in-plane distortion is eliminated. When this occurs, one would expect a sudden increase in the fluorine p_π orbital energies which might result in the 0.5 eV decrease in the transition energy of the C band.

The tetrafluorobenzene isomers are also interesting molecules to consider. In all of them, the fluorine p_π orbitals should be less affected by the electrostatic interactions and orthogonality constraints considered above than in pentafluorobenzene. This should result in higher C band excitation energies. Such a shift in excitation energy appears indeed to be observed, as can be seen from Table I. The C band, occurring at 5.85 eV in pentafluorobenzene, has shifted to higher excitation energy

in each of the tetrafluorobenzenes (see Figs. 1 and 5). In 1, 2, 3, 4-tetrafluorobenzene the carbon π system should be able to distort along nearly one half of the benzene ring, while in the 1, 2, 3, 5- and 1, 2, 4, 5-isomers this angular region of distortion should be close to 240°. It would be expected, on this basis, that the C band in 1, 2, 3, 4-tetrafluorobenzene should occur at a somewhat lower excitation energy than in the two other tetra isomers. Comparison of the energy-loss region between 5.5 eV and 6.5 eV in the spectra of each of the tetra isomers (see Fig. 5) shows an obvious difference between the shape of the absorption in 1, 2, 3, 4- and those of the tetra isomers. We attribute the shape of the 1, 2, 3, 4-tetrafluorobenzene spectrum in this region to the superposition of the $\tilde{X}\ ^1A_{1g} \rightarrow 1\ ^1B_{1u}$ excitation (using benzene symmetry notation) at 6.43 eV and the C band, which appears to have a maximum intensity located at about 6 eV. In the other tetra isomers, on the other hand, the C band has apparently shifted to somewhat higher energies (6.4 eV to 6.5 eV) whereas the maximum of the $\tilde{X}\ ^1A_{1g} \rightarrow 1\ ^1B_{1u}$ benzene-type transition seems to have shifted to somewhat lower energies (6.2 eV to 6.3 eV). The basis of this assignment is as follows. The relative intensities of the benzene-type transition and the C band are approximately the same in the penta and hexa compounds. In going to the tetra compounds one would therefore expect their ratios not to change significantly and to be approximately the same for all three isomers considered. This property is achieved by assuming that the order of the benzene-type transition and C bands in 1, 2, 3, 5- and 1, 2, 4, 5-tetrafluorobenzene is the reverse of the order in the 1, 2, 3, 4-isomer, as we have done.

In summary, the exact nature of the C bands is not known.

They appear not to be related to transitions among benzene ring-type orbitals. They do, on the other hand, seem to be associated with fluorine orbitals. The variation of the C band transition energy with the number of fluorine substituents as well as their isomeric configurations seems to be consistent with either a charge transfer excitation, i.e., fluorine p_π to carbon p_{π^*}, or a fluorine p_π to C-F σ^* transition. It is clear that further experimental and theoretical work is required to identify the C band.

C. Comparison between electron-impact and optical intensities of the transitions analogous to the benzene $\tilde{X}\,{}^1A_{1g} \rightarrow 1\,{}^1B_{2u}$ excitation

Study of the fluorobenzenes allows determination of the effects of varying molecular symmetry on the relative intensities of transitions in electron-impact spectra. For benzene the $\tilde{X}\,{}^1A_{1g} \rightarrow 1\,{}^1B_{2u}$ excitation, which is the first singlet $\rightarrow$ singlet transition, is symmetry-forbidden and is observed in optical spectra due to vibronic interactions.[1] In the fluorobenzene series investigated here, the analogous transition is symmetry-forbidden for only three molecules: benzene, 1,3,5-trifluorobenzene, and hexafluorobenzene. In Table II we display the optical oscillator strengths for these transitions relative to the one in benzene for the entire fluorobenzene series. We also display the R/R_B and R/R_{HFB} quotients, where R is the ratio of the integrated electron impact intensity of the $\tilde{X}\,{}^1A_{1g} \rightarrow 1\,{}^1B_{2u}$-type transition to that of the $\tilde{X}\,{}^1A_{1g} \rightarrow {}^1E_{1u}$-type transition (in benzene notation), while R_B and R_{HFB} are the values of this ratio for benzene and hexafluorobenzene.

These quotients of R values are approximately equal to corresponding

quotients of generalized oscillator strengths Indeed, let f^{EI} be the electron impact generalized oscillator strength [51] for the $\tilde{X}\,^1A_{1g} \rightarrow 1\,^1B_{2u}$-type transition of a given fluorobenzene and let f_B^{EI} and f_{HFB}^{EI} be the corresponding oscillator strengths for benzene and hexafluorobenzene. The $\tilde{X}\,^1A_{1g} \rightarrow {}^1E_{1u}$-type transition is optically allowed in benzene and in all of its fluorinated derivatives. The corresponding optical oscillator strengths are about 1.1.[24] The integrated electron impact intensities for the $\tilde{X}\,^1A_{1g} \rightarrow {}^1E_{1u}$-type and the $\tilde{X}\,^1A_{1g} \rightarrow 1\,^1B_{2u}$-type transitions in benzene and the fluorobenzenes used to determine the values of R, R_B and R_{HFB} were obtained from spectra at the same impact energy (50 eV) and scattering angle (10°). Furthermore, the shape of the variation of the corresponding DCS curves with scattering angle, at this impact energy, was nearly the same for all molecules and both transitions being considered. Under these conditions, f^{EI}/f_B^{EI} and f^{EI}/f_{HFB}^{EI} should be approximately equal to R/R_B and R/R_{HFB}, respectively.

The optical oscillator strength ratios (f/f_B) in the three molecules for which the transition is symmetry-forbidden are significantly smaller than for those which are symmetry-allowed, as can be seen from Table II. It is interesting to analyze the corresponding relative intensities in the electron-impact spectra. Rigorously speaking, these electron-impact transition intensities will only obey dipole selection rules when the Born approximation is valid. This occurs for relatively high incident electron energies, on the order of 200 eV.[52] As indicated above, we considered the intensity variation with fluorine substitution of the

first singlet – singlet transition in the fluorobenzenes for spectra taken at an impact energy of 50 eV and a scattering angle of 10°. We chose these parameters to minimize any contribution due to the triplet state which underlies the low-energy region of this singlet state excitation. The quantity R/R_B, which is approximately equal to f^{EI}/f_B^{EI}, displayed in column 6 of Table II, seems most appropriate for comparison with the ratio of optical oscillator strengths. Again, the dipole-allowed transitions are more intense than the dipole-forbidden excitations. The difference between the corresponding ratios in column 6 (for the electron-impact spectra) are smaller than those for column 5 (for the optical spectra), indicating that at 50 eV impact energies dipole selection rules are relaxed. One expects that these ratios will gradually approach the optical values as the impact energy increases.

Finally, we compare the electron-impact ratios of pairs of molecules which are related to one another by the replacement of fluorines by hydrogens and vice-versa, such as fluorobenzene and pentafluorobenzene. For this pair of molecules the appropriate comparison is between the f^{EI}/f_B^{EI} ratio for the first of these molecules and the f^{EI}/f_{HFB}^{EI} ratio for the second one. Similarly related ratios in columns 6 and 7 of Table II are connected by double-headed arrows. It is seen that the corresponding ratios are close to one another, indicating the importance of molecular symmetry independently of whether the benzene symmetry is broken by F-atom substitution or that of hexafluorobenzene is broken by H-atom substitution.

D. Transitions above 8 eV

We have obtained electron-impact spectra for excitation energies up to 18 eV. Transitions in the energy region above 8 eV are believed to be primarily due to excitations to Rydberg-like orbitals, forming Rydberg series converging to various ionization potentials. Transitions belonging to series converging to the first ionization potential for several fluorobenzenes have been assigned previously[53-56] on the basis of term values[47,57] as well as vibrational spacings. While assignments of transitions converging to first ionization potentials appear to be reliable, those for transitions converging to higher ionization potentials are less certain. We have been unable to classify uniquely the term values of any of the transitions we observe in the 10 eV to 18 eV range as being associated with one of the several known ionization potentials of the molecules being considered.[35,43,53-56,58] Spectra of these molecules in the 9 to 17 eV energy-loss range are presented in Figs. 12 through 15. The transition energies of the more prominent excitations above 8 eV are summarized in Table III.

V. SUMMARY

We have investigated the electronic spectra of benzene and 11 of its fluorine-substituted derivatives. In each molecule, the location and electronic band shape of the lowest triplet state has been accurately determined. For fluorobenzene, o- and m-difluorobenzene, and 1,3,5-trifluorobenzene, a second triplet, apparently analogous to the $1\,^3E_{1u}$ state of benzene, was detected. Each of the fluorobenzenes studied has three singlet – singlet transitions that are analogous to the well-known features in the benzene spectra at 4.90, 6.20, and 6.95 eV. An additional spin-allowed transition, which we have designated the C band system, is observed in 1,2,3,4-tetrafluorobenzene at about 6.0 eV as a broadening on the low-energy side of the 6.43 eV feature. In the other two tetrafluorobenzenes it appears to occur at the slightly higher energy loss of about 6.4 eV. This transition is more clearly observed in the spectra of pentafluorobenzene and hexafluorobenzene, with a maximum intensity at 5.85 eV and 5.32 eV, respectively. The identity of this transition is uncertain but the dependence of its transition energy on increasing fluorine substitution is best rationalized by assigning it to a charge-transfer $F_{p_\pi} \rightarrow C_{p_{\pi^*}}$ excitation or to a $F_{p_\pi} \rightarrow C\text{-}F_{\sigma^*}$ transition.

The intensity dependence of the lowest singlet – singlet transition in the several fluorobenzene spectra was discussed. Dipole selection rules were found to be obeyed less rigorously in the electron-impact spectra than in the corresponding optical spectra. Finally, numerous transitions at high excitation energies, including transitions to super-excited states, were observed. These are believed to be primarily transitions to Rydberg-like orbitals.

TABLE I. Transition energies of the fluorobenzenes

Molecule	Transition Energies (eV)[a]											
	Singlet – Triplet				Singlet – Singlet[b]							
	$(\tilde{X}\ ^1A_{1g} - 1\ ^3B_{1u})$[c]		$(\tilde{X}\ ^1A_{1g} - 1\ ^3B_{2u})$[c]		$(\tilde{X}\ ^1A_{1g} - 1\ ^1B_{2u})$[c,d]		C band		$(\tilde{X}\ ^1A_{1g} - 1\ ^1B_{1u})$[c]		$(\tilde{X}\ ^1A_{1g} - {}^1E_{1u})$[c]	
Benzene	3.90	(3.89)[e]	5.59	(5.69)[e]	4.80	(4.89)[e]				(6.2)[e]	6.95	(6.95)[e]
Fluorobenzene	3.90	(3.88)[f]	5.72		4.78				6.23		6.99	
o-Difluorobenzene	3.92	(3.88)[f]	5.67		4.76				6.22		7.02	
m-Difluorobenzene	3.91	(3.84)[f]	5.72		4.79				6.17		6.96	
p-Difluorobenzene	3.85	(3.77)[f]			4.67				6.18		7.02	
1,3,5-Trifluorobenzene	3.95	(3.92)[f]	5.62		4.87				6.20		6.94	
1,2,4-Trifluorobenzene	3.89	(3.82)[f]			4.72				6.20		7.04	
1,2,3,4-Tetrafluorobenzene	3.95	(3.82)[f]			4.85		~6.0[g]		6.43		7.21	
1,2,3,5-Tetrafluorobenzene	3.93	(3.91)[f]			4.79			(6.4)[h]	6.2 (± 0.1)		7.10	
1,2,4,5-Tetrafluorobenzene	3.93	(3.73)[f]			4.69			(6.5)[h]	6.3 (± 0.1)		7.25	
Pentafluorobenzene	3.90	(3.88)[f]			4.79		5.85		6.36		7.12	
Hexafluorobenzene	3.86	(3.81)[f]			4.80		5.32	(5.31)[i]	6.36		7.10	

[a] These are the locations of intensity maxima to an accuracy of ± 0.05 eV, unless otherwise indicated.

[b] Our excitation energies for singlet – singlet transitions are in good agreement with values obtained optically; see Refs. 12 and 24.

[c] The symmetry designations correspond to transitions for benzene.

[d] According to Doering's results,[16] this feature consists of two overlapping transitions, a singlet – singlet transition with maximum intensity at 4.89 eV and a singlet – triplet transition which peaks at 4.85 eV.

[e] Excitation energies in parentheses were obtained from the electron-impact studies, Ref. 16.

[f] Excitation energies in parentheses were obtained from oxygen perturbation optical spectra, Ref. 26.

[g] Appears as broadening on the low energy side of 6.43 eV feature.

[h] Location approximate.

[i] Reference 37.

TABLE II. Comparison between electron-impact and optical allowedness of $\tilde{X}\,^1A_{1g} - 1\,^1B_{2u}$ transition

Molecule	Molecular Point Group	Excited State Symmetry	Transition Symmetry Allowed?	f/f_B f = optical oscillator strength	R/R_B [a] $\cong f^{EI}/f^{EI}_B$	R/R_{HFB} [a] $\cong f^{EI}/f^{EI}_{HFB}$
Benzene	D_{6h}	B_{2u}	No	1.0 [b]	1.0	0.8
Fluorobenzene	C_{2v}	B_1	Yes	5.6 [b]	2.5	2.1
o-Difluorobenzene	C_{2v}	B_1	Yes		3.6	3.0
m-Difluorobenzene	C_{2v}	B_1	Yes	6.0 [b]	2.0	1.7
p-Difluorobenzene	D_{2h}	B_{3u}	Yes	14.0 [b]	7.3	6.1
1,3,5-Trifluorobenzene	D_{3h}	A_1'	No	1.3 [b]	0.7	0.6
1,2,4-Trifluorobenzene	C_s	A'(?)	Yes	12.0 [b]	5.7	4.8
1,2,3,4-Tetrafluorobenzene	C_{2v}	B_1	Yes	3.9 [c]	3.6	3.0
1,2,3,5-Tetrafluorobenzene	C_{2v}	B_1	Yes	4.2 [c]	2.6	2.2
1,2,4,5-Tetrafluorobenzene	D_{2h}	B_{3u}	Yes	15.0 [c]	7.3	6.1
Pentafluorobenzene	C_{2v}	B_1	Yes		2.7	2.3
Hexafluorobenzene	D_{6h}	D_{6h}	No	1.9 [d]	1.2	1.0

[a] R is the ratio of the area of the $\tilde{X}\,^1A_{1g} - 1\,^1B_{2u}$-type transition (in benzene notation) to the ares of the $\tilde{X}\,^1A_{1g} - {}^1E_{1u}$ transition at $\theta = 10°$ and $E_0 = 50$ eV for the molecule being considered. R_B and R_{HF} are the equivalent ratios for benzene and hexafluorobenzene, respectively. f^{EI} is the electron-impact generalized oscillator strength for the $^1A_{1g} - 1\,^1B_{2u}$-type transition for the molecule being considered, and the f^{EI}_B and f^{EI}_{HFB} are the corresponding oscillator strengths in benzene and hexafluorobenzene, respectively.

[b] Ratios obtained from data presented in Ref. 12.

[c] Tetrafluorobenzene oscillator strength estimated from optical spectrum in Ref. 9.

[d] Hexafluorobenzene oscillator strength estimated from optical spectrum in Ref. 37.

TABLE III. Transition energies in eV from ground to excited electronic states of the fluorobenzenes in the energy-loss region above 8 eV.[a]

Benzene	Fluorobenzene	o-Difluoro-benzene	m-Difluoro-benzene	p-Difluoro-benzene	1,2,4-$C_6H_3F_3$	1,3,5-$C_6H_3F_3$	1,2,3,4-$C_6H_2F_4$	1,2,3,5-$C_6H_2F_4$	1,2,3,5-$C_6H_2F_4$	C_6HF_5	C_6F_6
8.14	8.87	8.14	7.94	8.04	8.13	8.20	8.13	9.07	8.07	9.91	9.82
8.41	9.73	8.46	8.28	8.50	8.52	8.56	8.43	9.92	8.26	11.11	10.26
8.72	10.75	9.60	8.46	9.49	9.18	8.73	9.05	11.02	8.59	11.61	10.99
8.88	11.38	9.93	9.06	9.98	9.42	9.43	9.90	11.82	9.14	12.35	11.14
9.50	11.72	10.73	9.78	11.13	9.53	9.56	10.40	12.62	10.16	13.41	11.39
9.76	12.33	11.39	10.31	11.98	10.23	10.40	10.90	13.06	11.06	14.25	11.72
9.90	12.73	12.13	10.79	12.67	10.40	11.33	11.91	14.00	12.39	15.58	12.49
10.01	13.93	12.99	11.76	13.23	10.83	12.51	12.58	15.32	13.26	16.40	12.79
10.51	14.63	14.09	12.21	14.03	10.98	13.08	13.08	16.00	13.64		13.46
11.08	15.27		12.84	15.40	11.40	13.55	13.58		13.96		13.89
11.61	16.97		13.84		11.50	13.96	14.33		14.49		15.81
12.15			15.31		11.62	15.16	15.50		15.62		16.32
13.08			17.01		12.13		16.31				
13.96					12.90		17.21				
14.26					13.20						
15.21					14.30						
15.81					15.47						
17.45					17.47						

[a] The accuracy in the location of the peaks of the reported transitions is ± 0.05 eV.

REFERENCES

1. G. Herzberg, Molecular Spectra and Molecular Structure (Van Nostrand-Rheinhold Co., New York, 1966), Vol. III, pp. 555-561.
2. (a) A. Kuppermann, J. K. Rice, and S. Trajmar, J. Phys. Chem. 72, 3894 (1968); (b) S. Trajmar, J. K. Rice, and A. Kuppermann, Adv. Chem. Phys. 18, 15 (1970).
3. K. F. Freed, Fortschr. Chem. Forsch. 31, 105 (1972).
4. M. W. Schmidt and E. K. C. Lee, J. Am. Chem. Soc. 90, 5919 (1968).
5. M. W. Schmidt and E. K. C. Lee, J. Am. Chem. Soc. 92, 3579 (1970).
6. O. A. Mosher, W. M. Flicker, and A. Kuppermann, J. Chem. Phys. 59, 6502 (1973).
7. G. Das Gupta and D. Phillips, J. Phys. Chem. 76, 3668 (1972).
8. I. Unger, J. Phys. Chem. 68, 4284 (1965).
9. B. H. Scholz and I. Unger, Can. J. Chem. 48, 2324 (1970).
10. G. P. Semeluk and R. D. S. Stevens, Can. J. Chem. 49, 2452 (1971).
11. C. Brundle, M. B. Robin, and N. A. Kuebler, J. Am. Chem. Soc. 94, 1466 (1972).
12. H. Sponer, J. Chem. Phys. 22, 234 (1954).
13. E. N. Lassettre, A. Skerbele, M. A. Dillon, and K. J. Ross, J. Chem. Phys. 48, 5066 (1968).
14. M. B. Robin, Higher Excited States of Polyatomic Molecules (Academic Press, New York, 1975), Vol. II, p. 210.
15. B. Katz, M. Brith, B. Sharf, and J. Jortner, J. Chem. Phys.

52, 88 (1970).

16. J. P. Doering, J. Chem. Phys. 67, 4065 (1977).
17. P. M. Johnson, J. Chem. Phys. 62, 4562 (1975).
18. P. J. Hay and I. Shavitt, J. Chem. Phys. 60, 2865 (1974).
19. J. Karwowski, J. Mol. Struct. 19, 143 (1973).
20. J. P. Doering, J. Chem. Phys. 51, 2866 (1969).
21. C. D. Cooper, J. Chem. Phys. 22, 503 (1954).
22. K. N. Rao and H. Spooner, Can. J. Phys. 35, 332 (1957).
23. P. D. Singh and A. N. Pathak, Indian J. Pure Appl. Phys. 7, 39 (1969).
24. R. Gilbert, P. Sauvageau and C. Sandorfy, Can. J. Chem. 50, 543 (1972).
25. D. F. Evans, J. Chem. Soc. 27 (1959).
26. J. Metcalfe, M. G. Rockley, and D. Phillips, J. Chem. Soc. Faraday Trans. 270, 1660 (1974).
27. J. Petruska, J. Chem. Phys. 34, 1120 (1961).
28. K. Kimura and S. Nagakura, Mol. Phys. 9, 117 (1964).
29. B. Ford, Theor. Chim. Acta 10, 342 (1968).
30. O. Chalvet and C. Leibovici, Theor. Chim. Acta 13, 297 (1969).
31. P. C. Mishra and D. K. Rai, Int. J. Quantum Chem. 6, 47 (1972).
32. J. S. Yadav, P. C. Mishra, and D. K. Rai, Mol. Phys. 26, 193 (1973).
33. A. I. Kiss and A. Martin, Chem. Phys. Lett. 19, 104 (1973).
34. A. Martin and A. I. Kiss, Chem. Phys. Lett. 22, 390 (1973).
35. C. B. Duke, K. L. Yip, G. P. Ceasar, A. W. Potts, and D. G. Streets, J. Chem. Phys. 66, 256 (1977).

36. O. A. Mosher, W. M. Flicker, and A. Kuppermann, J. Chem. Phys. 62, 2600 (1975).

37. For simplicity we will hereafter refer to this band system as the C band. The letter C is arbitrary, chosen to avoid confusion with the A, B, and E-type irreducible representations of the D_{6h} point group.

38. S. H. Bauer and C. F. Aten, J. Chem. Phys. 39, 1253 (1963).

39. R. P. Frueholz, W. M. Flicker, O. A. Mosher, and A. Kuppermann, Chem. Phys. Lett. 52, 86 (1977).

40. A. M. Taleb, I. H. Munro, and J. B. Birks, Chem. Phys. Lett. 21, 454 (1973).

41. G. C. Morris and J. G. Angus, J. Mol. Spectrosc. 45, 271 (1973).

42. $^1E_{2g}^-$ is a term symbol in the "alternant symmetry notation" which arises from semi-empirical calculations where two states, $^1E_{2g}^-$ and $^1E_{2g}^+$, are found. In ab initio calculations, no distinction is made between $^1E_{2g}^+$ and $^1E_{2g}^-$ yielding only the single state, $^1E_{2g}$.[18]

43. D. W. Turner, C. Baker, A. D. Baker, and C. R. Brundle, Molecular Photoelectron Spectroscopy (Wiley-Interscience, New York, 1970), pp. 316, 320.

44. R. S. Mulliken, J. Chem. Phys. 8, 382 (1940).

45. K. Kimura and S. Nagakura, Spectrochim. Acta 17, 166 (1961).

46. C. R. Zobel and A. B. F. Duncan, J. Am. Chem. Soc. 77, 2611 (1955).

47. W. R. Harshbarger, M. B. Robin, and E. N. Lassettre, J. Electron Spectrosc. 1, 319 (1972/73).

48. See Ref. 14, Vol. I, p. 191.

49. Ref. 14, p. 156.

50. Ref. 14, p. 230.

51. E. N. Lassettre, A. Skerbele, and M. A. Dillon, J. Chem. Phys. 50, 1829 (1969).

52. H. J. Blaauw, F. J. de Heer, R. W. Wagenaar, and D. H. Barends, J. Phys. B 10, L299 (1977).

53. D. R. Smith and J. W. Raymonda, Chem. Phys. Lett. 12, 269 (1971).

54. R. Gilbert, P. Sauvageau, and C. Sandorfy, Chem. Phys. Lett. 17, 465 (1972).

55. C. Sluse-Goffart and J. Momigny, Chem. Phys. Lett. 25, 231 (1974).

56. R. Gilbert and C. Sandorfy, Chem. Phys. Lett. 27, 457 (1967).

57. W. R. Harshbarger, N. A. Kuebler, and M. B. Robin, J. Chem. Phys. 60, 345 (1974).

58. I. D. Clark and D. C. Frost, J. Am. Chem. Soc. 89, 244 (1967).

FIGURE CAPTIONS

FIG. 1. Electron-impact energy-loss spectra of benzene and six fluorine-substituted derivatives in the 3.4 eV to 8.5 eV energy-loss region. Typical experimental parameters for these spectra and those presented in later figures are: sample pressures ranging from 2 mTorr to 8 mTorr as measured with an uncalibrated Schulz-Phelps ionization gauge, incident electron beam currents of approximately 50 namp, and resolution in the range 120 meV to 160 meV FWHM.

Fig. 2. Electron-impact energy-loss spectra of benzene and five fluorine substituted derivatives. Experimental conditions as in Fig. 1.

FIG. 3. Electron-impact energy-loss spectra of the difluorobenzenes in the 4 eV to 11 eV energy-loss region. Experimental conditions as described in Fig. 1.

FIG. 4. Electron-impact energy-loss spectra of 1,3,5-trifluorobenzene and 1,2,4-trifluorobenzene in the 4 eV to 11 eV energy-loss region. Experimental conditions as described in Fig. 1.

FIG. 5. Electron-impact energy-loss spectra of the tetrafluorobenzenes in the 4 eV to 11 eV energy-loss region. Experimental conditions as described in Fig. 1.

FIG. 6. Relative elastic and inelastic differential cross sections for fluorobenzene at an incident electron energy of 25 eV. These differential cross sections are in arbitrary units set by normalizing the elastic differential cross section to 1.0 at $\theta = 40°$. The arbitrary units are the same for all transitions of a given molecule at a particular impact energy. The arbitrary units are not the same for different molecules or for the same molecule at different impact energies.

FIG. 7. Relative elastic and inelastic differential cross sections for p-difluorobenzene at an incident electron energy of 25 eV. The normalization procedure for the arbitrary ordinate units is the same as for Fig. 6.

FIG. 8. Relative elastic and inelastic differential cross sections for 1,3,5-trifluorobenzene at an incident electron energy of 50 eV. The normalization procedure for the arbitrary ordinate units is the same as for Fig. 6.

FIG. 9. Relative elastic and inelastic differential cross sections for 1,2,3,5-tetrafluorobenzene at an incident electron energy of 50 eV. The normalization procedure for the arbitrary ordinate units is the same as for Fig. 6.

FIG. 10. Relative elastic and inelastic differential cross sections for pentafluorobenzene at an incident electron energy of 50 eV. The normalization procedure for the arbitrary ordinate units is the same as for Fig. 6.

FIG. 11. Relative elastic and inelastic differential cross sections for hexafluorobenzene at an incident electron energy of 25 eV. The normalization procedure for the arbitrary ordinate units is the same as for Fig. 6.

FIG. 12. Electron-impact energy-loss spectra of benzene, fluorobenzene, pentafluorobenzene, and hexafluorobenzene in the 9 eV to 17 eV energy-loss region. Experimental conditions as described in Fig. 1.

FIG. 13. Electron-impact energy-loss spectra of the difluorobenzenes in the 9 eV to 17 eV energy-loss region. Experimental conditions as described in Fig. 1.

FIG. 14. Electron-impact energy-loss spectra of 1,3,5-trifluorobenzene and 1,2,4-trifluorobenzene in the 9 eV to 17 eV energy-loss region. Experimental conditions as described in Fig. 1.

FIG. 15. Electron-impact energy-loss spectra of the tetrafluorobenzenes in the 9 eV to 17 eV energy-loss region. Experimental conditions as described in Fig. 1.

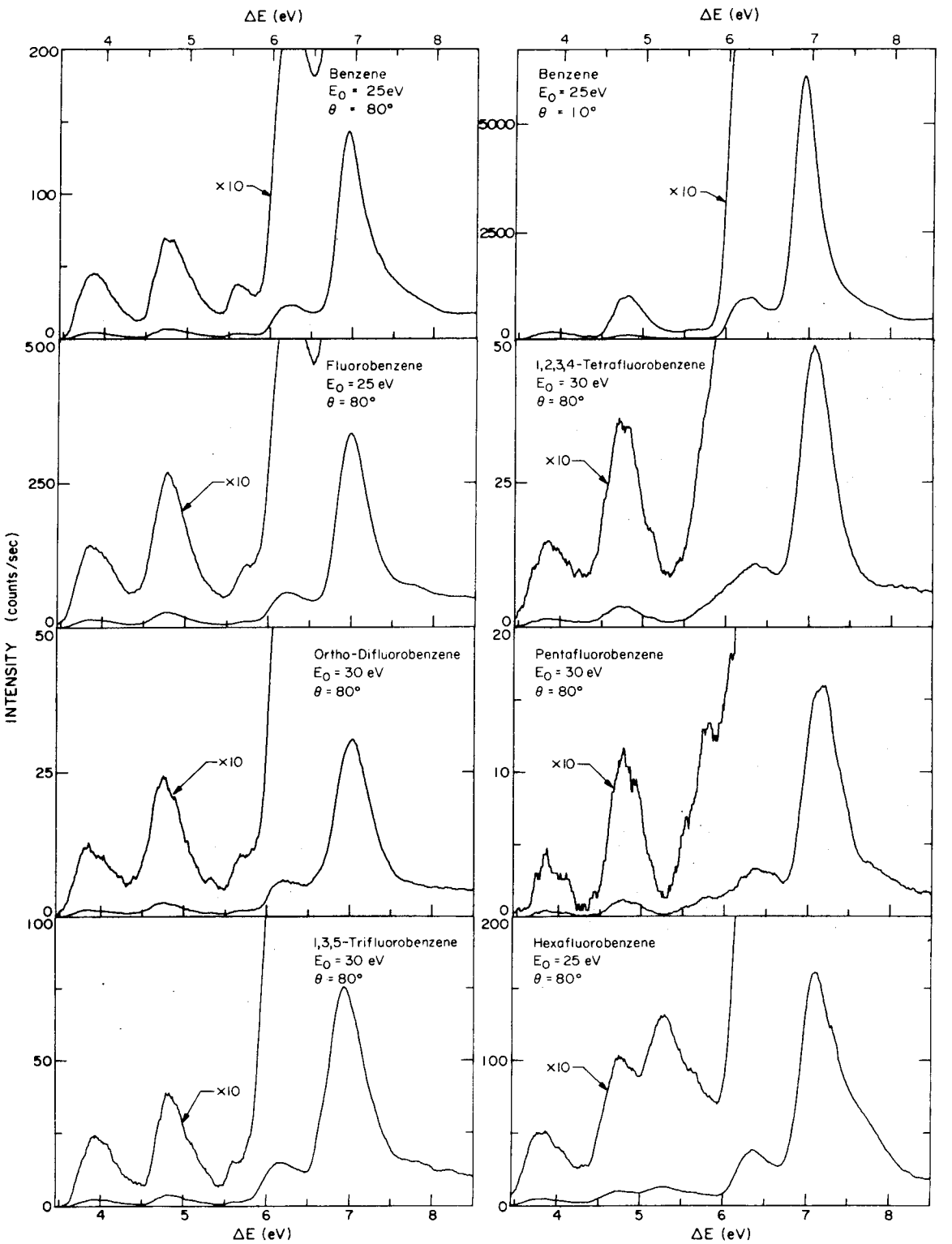
ΔE (eV)
INTENSITY (counts/sec)
Benzene
E0 = 25eV
θ = 80°
Benzene
E0 = 25eV
θ = 10°
Fluorobenzene
E0 = 25 eV
θ = 80°
1,2,3,4-Tetrafluorobenzene
E0 = 30 eV
θ = 80°
Ortho-Difluorobenzene
E0 = 30 eV
θ = 80°
Pentafluorobenzene
E0 = 30 eV
θ = 80°
1,3,5-Trifluorobenzene
E0 = 30 eV
θ = 80°
Hexafluorobenzene
E0 = 25 eV
θ = 80°
×10

Figure 1

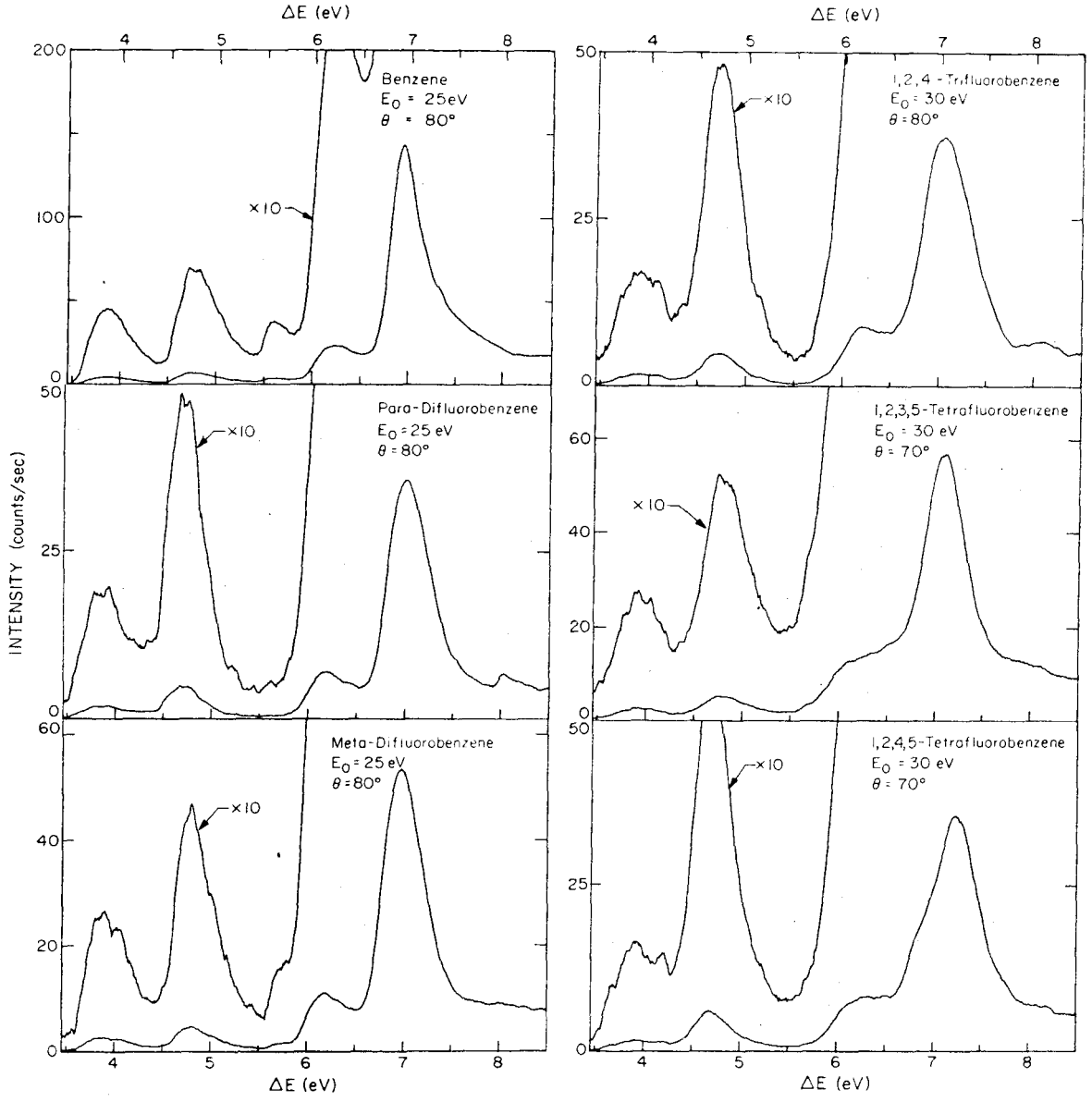
ΔE (eV)
INTENSITY (counts/sec)
Benzene
E_0 = 25eV
θ = 80°
×10
Para-Difluorobenzene
E_0 = 25 eV
θ = 80°
Meta-Difluorobenzene
E_0 = 25 eV
θ = 80°
1,2,4 - Trifluorobenzene
E_0 = 30 eV
θ = 80°
1,2,3,5-Tetrafluorobenzene
E_0 = 30 eV
θ = 70°
1,2,4,5-Tetrafluorobenzene
E_0 = 30 eV
θ = 70°

Figure 2

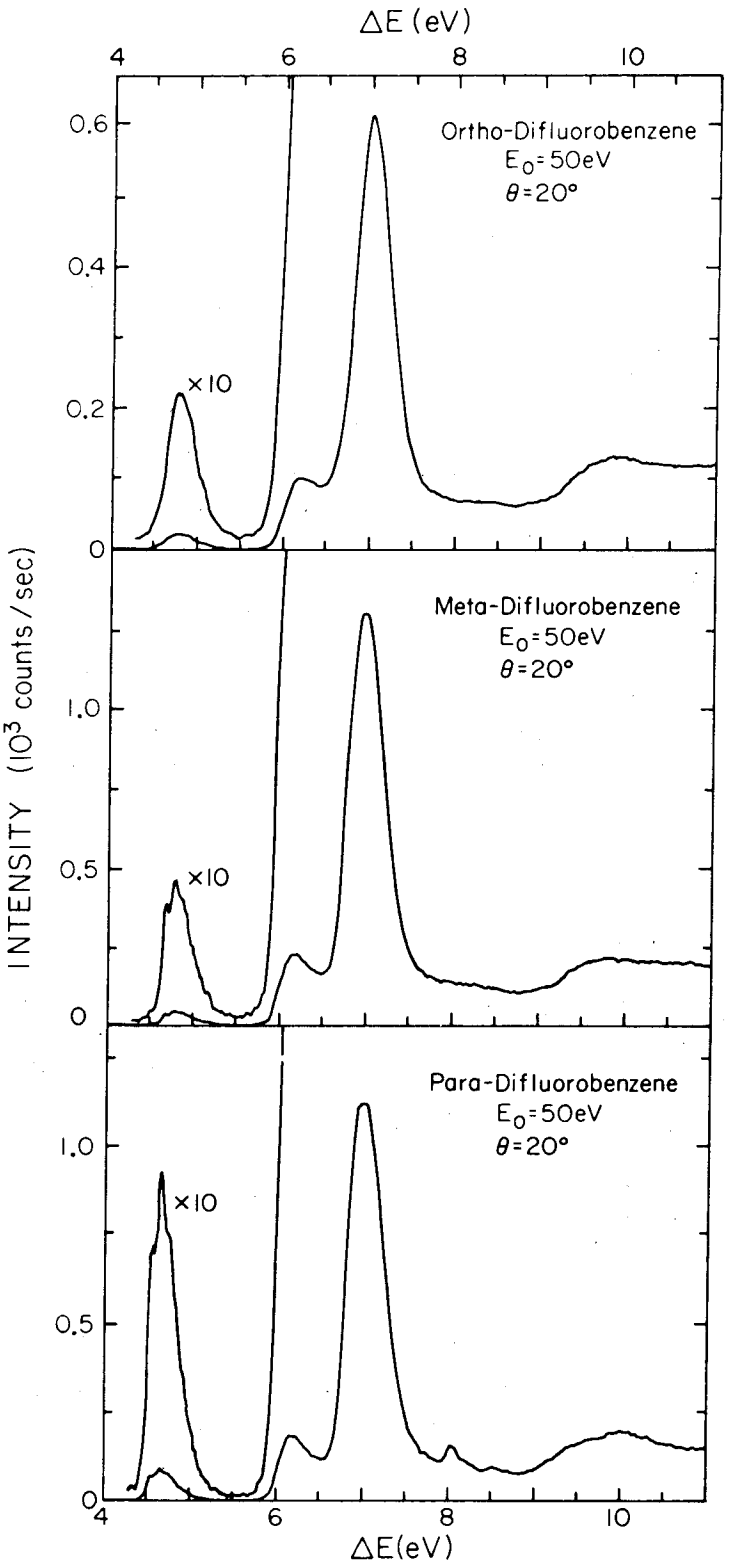
ΔE (eV)
4
6
8
10
Ortho-Difluorobenzene
E_0=50eV
θ=20°
×10
Meta-Difluorobenzene
E_0=50eV
θ=20°
×10
Para-Difluorobenzene
E_0=50eV
θ=20°
×10
INTENSITY (10^3 counts/sec)
0.6
0.4
0.2
0
1.0
0.5
0
1.0
0.5
0
4
6
8
10
ΔE(eV)

Figure 3

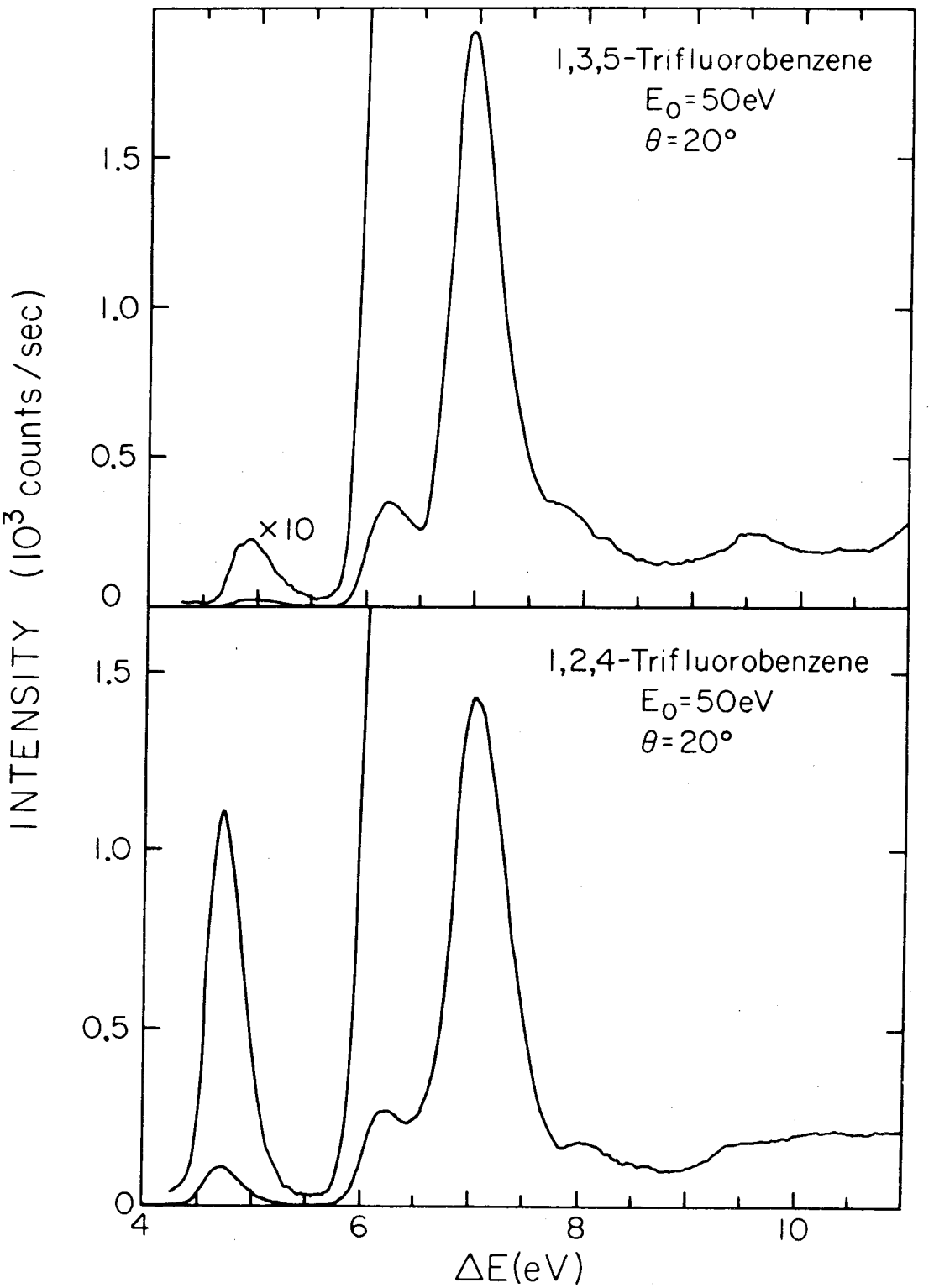
1,3,5-Trifluorobenzene
E_0=50eV
θ=20°
×10
1,2,4-Trifluorobenzene
E_0=50eV
θ=20°
INTENSITY (10³ counts/sec)
ΔE(eV)
0
0.5
1.0
1.5
4
6
8
10

Figure 4

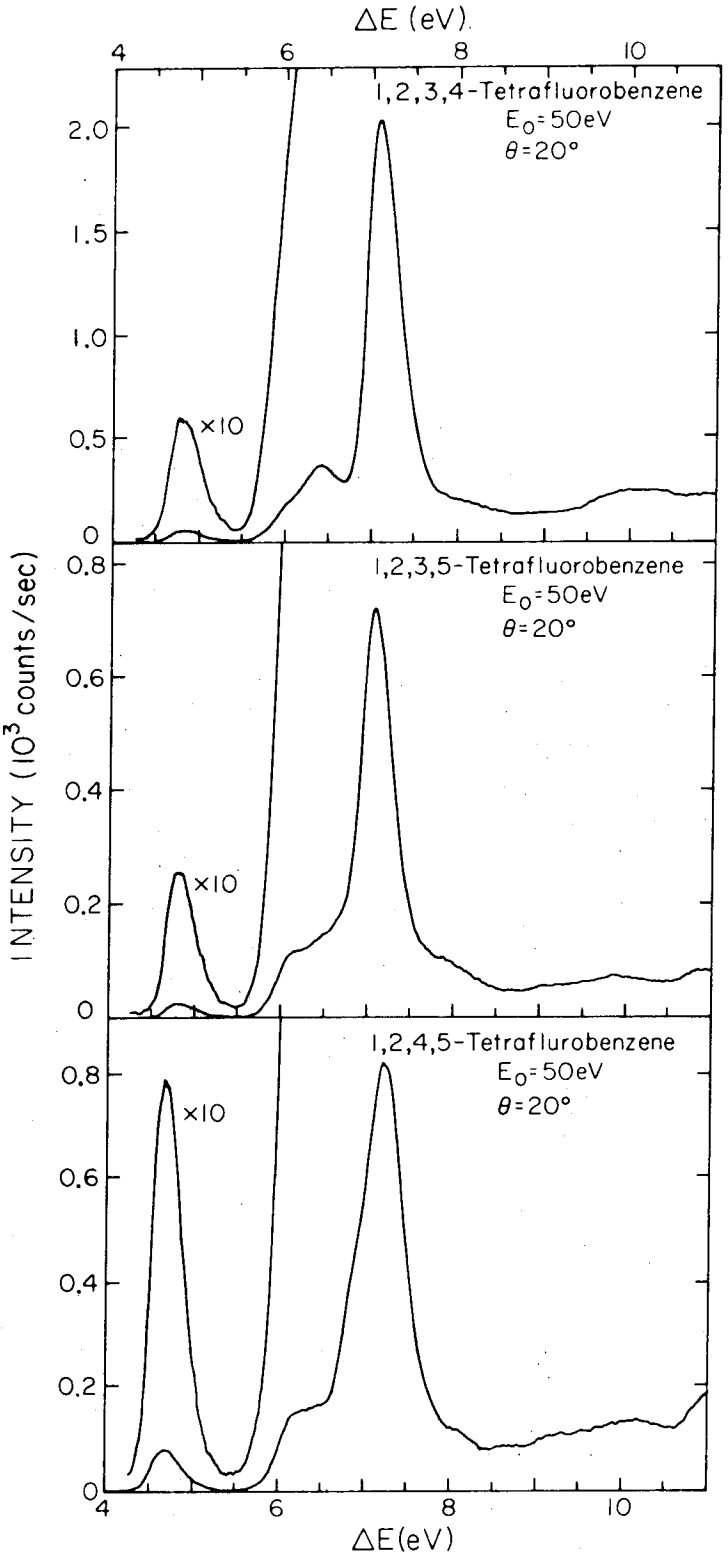
ΔE (eV)
4
6
8
10
1,2,3,4-Tetrafluorobenzene
E0=50eV
θ=20°
×10
1,2,3,5-Tetrafluorobenzene
E0=50eV
θ=20°
×10
1,2,4,5-Tetraflurobenzene
E0=50eV
θ=20°
×10
INTENSITY (10³ counts/sec)
0
0.5
1.0
1.5
2.0
0.2
0.4
0.6
0.8
ΔE(eV)

Figure 5

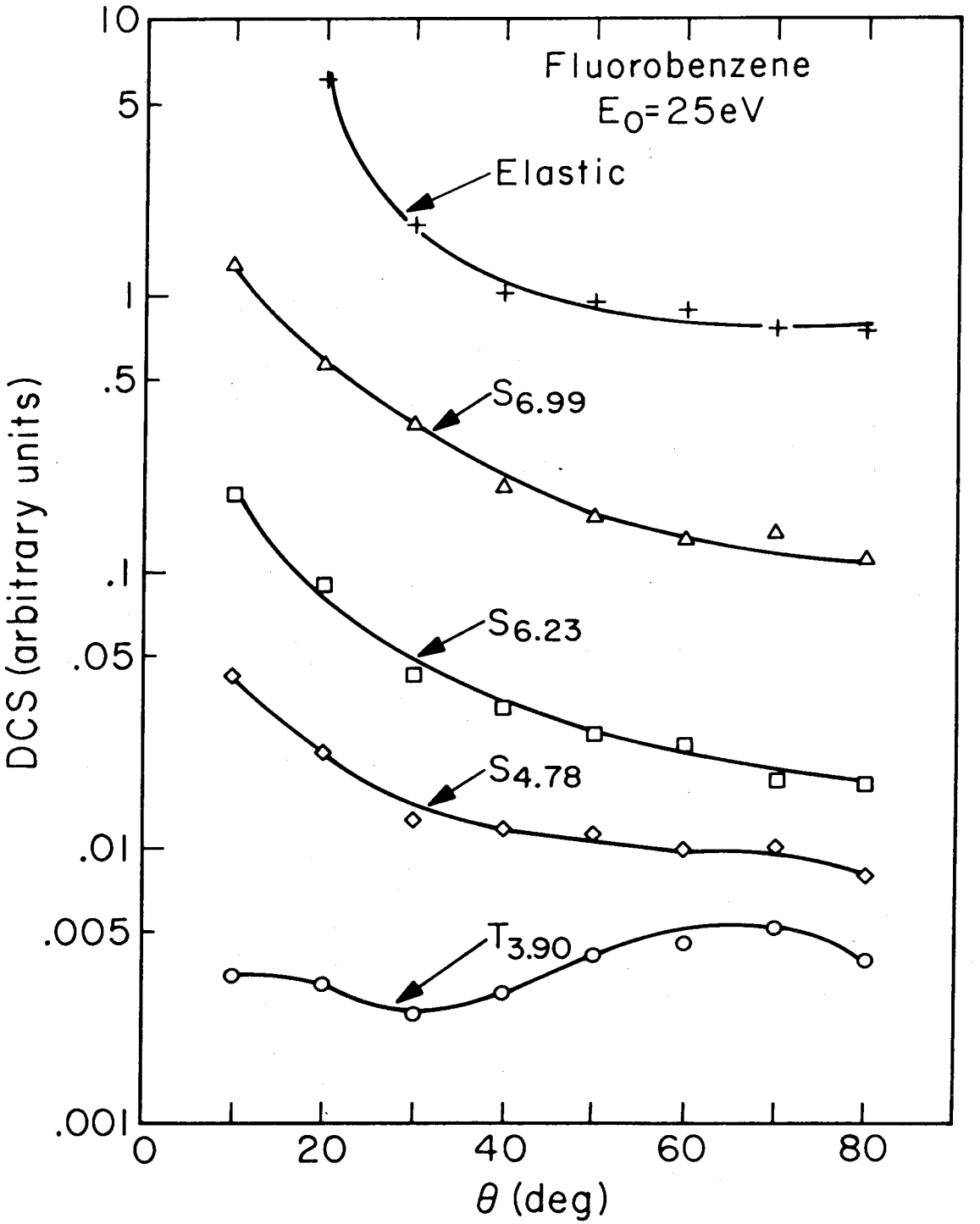
Fluorobenzene
E_0=25eV
Elastic
$S_{6.99}$
$S_{6.23}$
$S_{4.78}$
$T_{3.90}$
DCS (arbitrary units)
10
5
1
.5
.1
.05
.01
.005
.001
0
20
40
60
80
θ (deg)

Figure 6

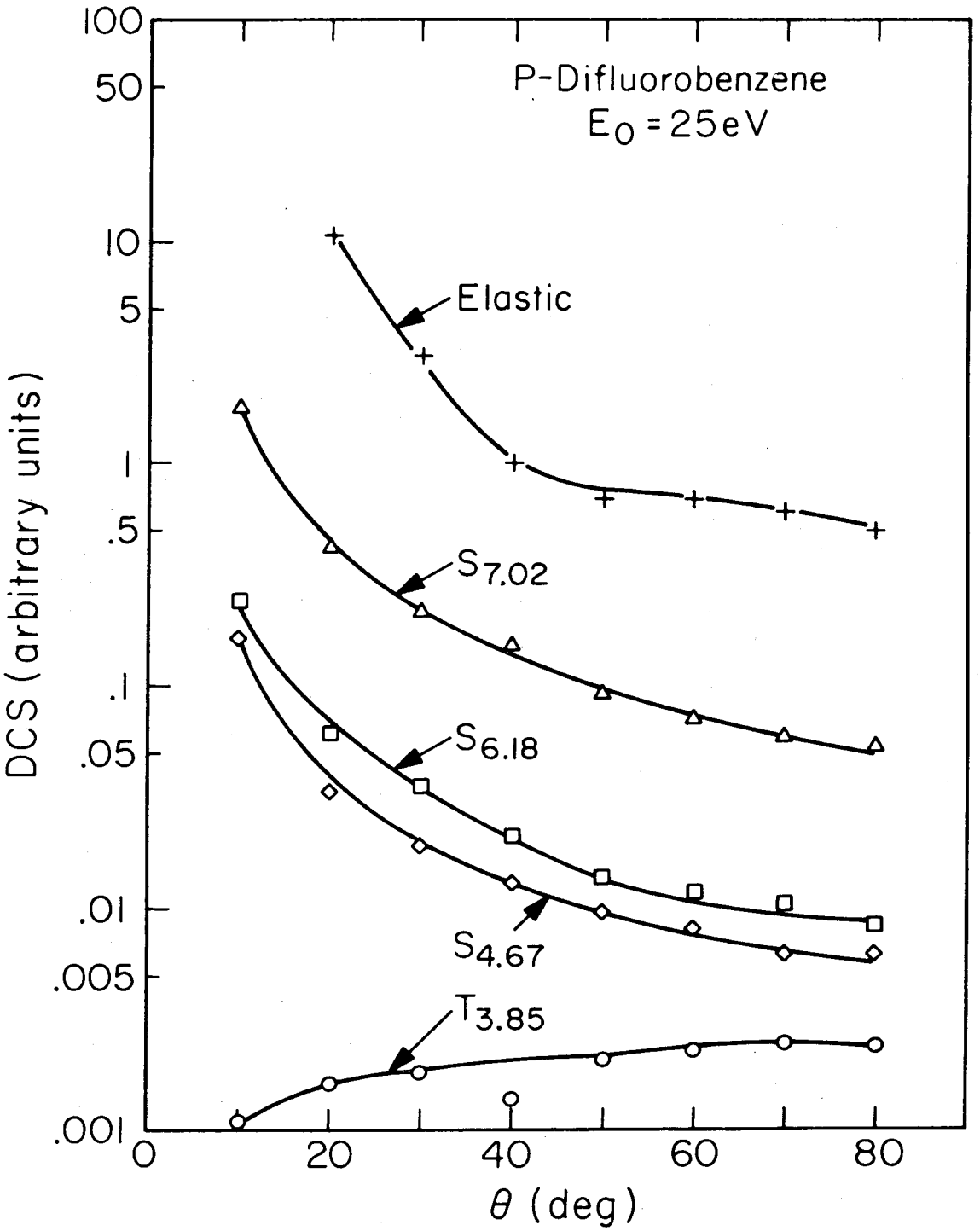
P-Difluorobenzene
$E_0 = 25eV$
Elastic
$S_{7.02}$
$S_{6.18}$
$S_{4.67}$
$T_{3.85}$
DCS (arbitrary units)
100
50
10
5
1
.5
.1
.05
.01
.005
.001
0
20
40
60
80
θ (deg)

Figure 7

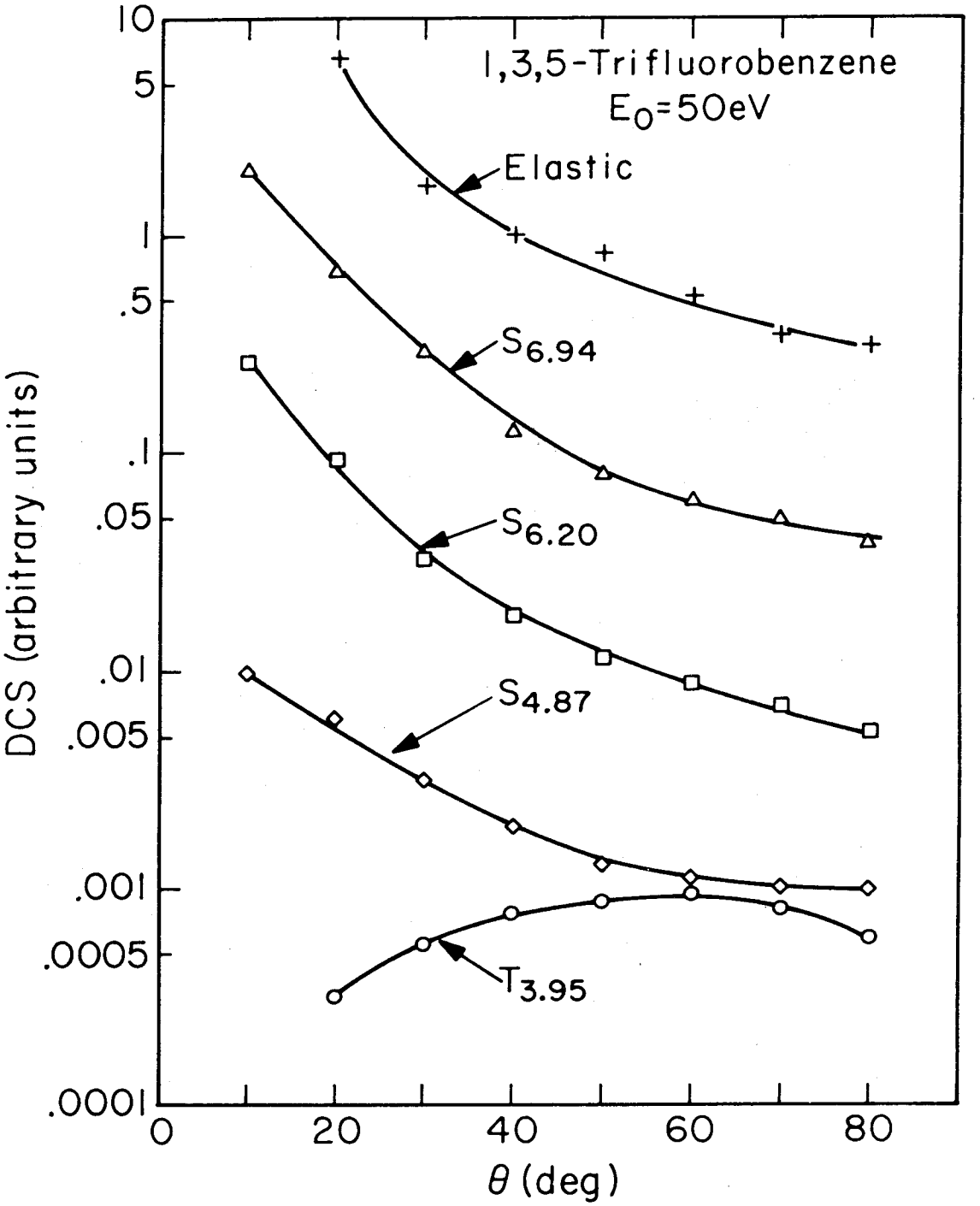
1,3,5-Trifluorobenzene
E_0=50eV
Elastic
$S_{6.94}$
$S_{6.20}$
$S_{4.87}$
$T_{3.95}$
DCS (arbitrary units)
10
5
1
.5
.1
.05
.01
.005
.001
.0005
.0001
0
20
40
60
80
θ (deg)

Figure 8

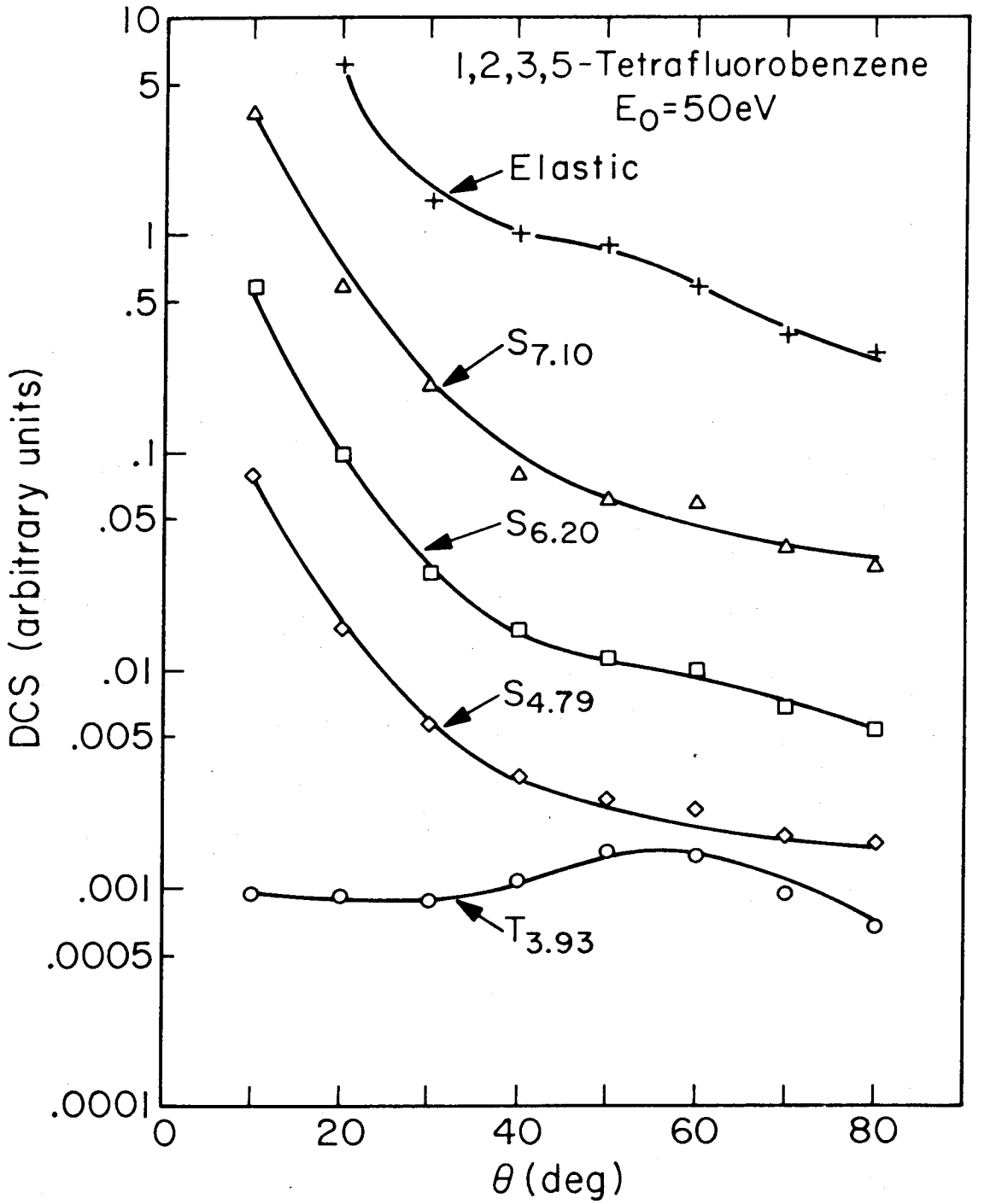
1,2,3,5-Tetrafluorobenzene
E_0=50eV
Elastic
$S_{7.10}$
$S_{6.20}$
$S_{4.79}$
$T_{3.93}$
DCS (arbitrary units)
10
5
1
.5
.1
.05
.01
.005
.001
.0005
.0001
0
20
40
60
80
θ (deg)

Figure 9

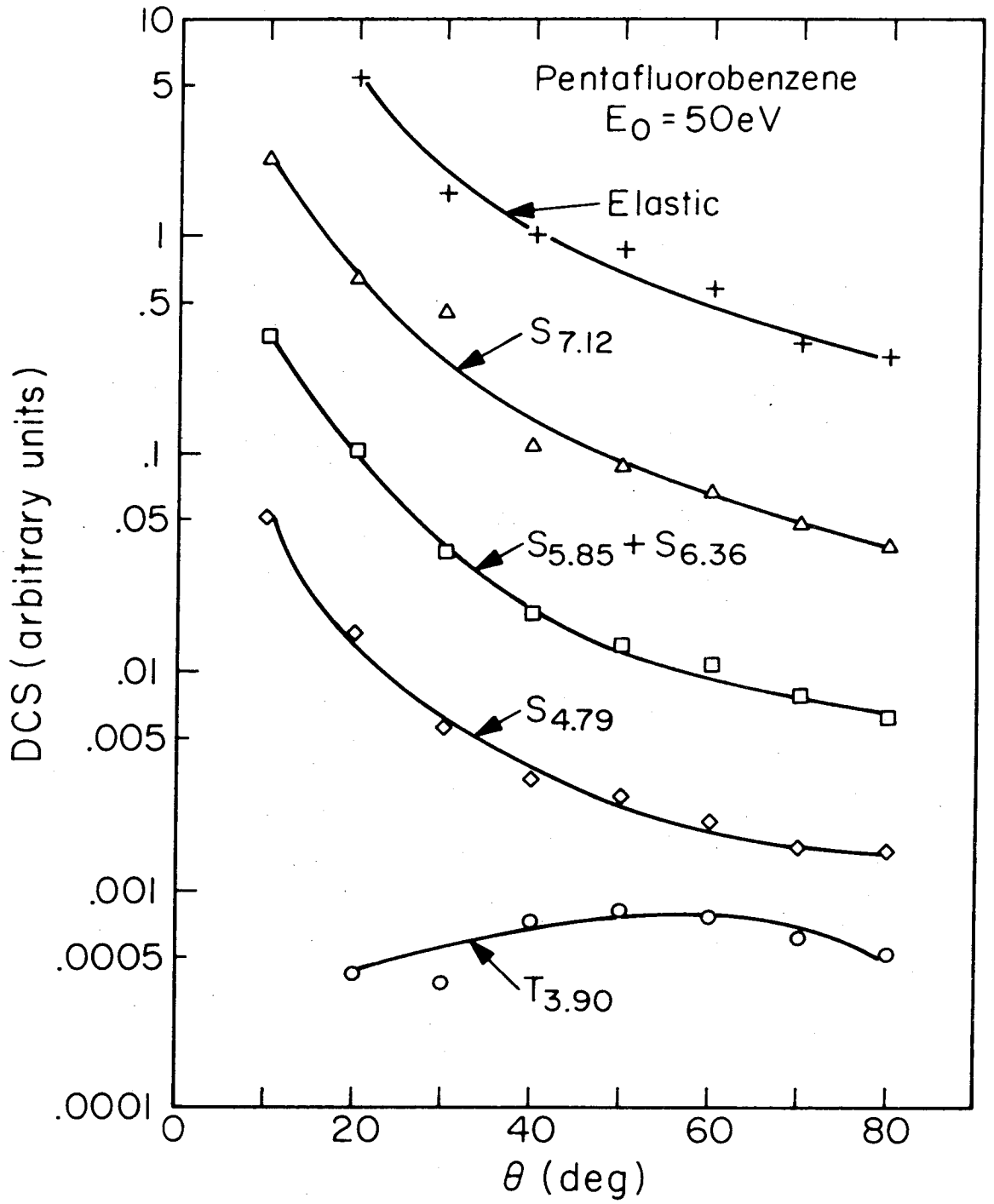
Pentafluorobenzene
E_0 = 50eV
Elastic
$S_{7.12}$
$S_{5.85} + S_{6.36}$
$S_{4.79}$
$T_{3.90}$
DCS (arbitrary units)
θ (deg)
10
5
1
.5
.1
.05
.01
.005
.001
.0005
.0001
0
20
40
60
80

Figure 10

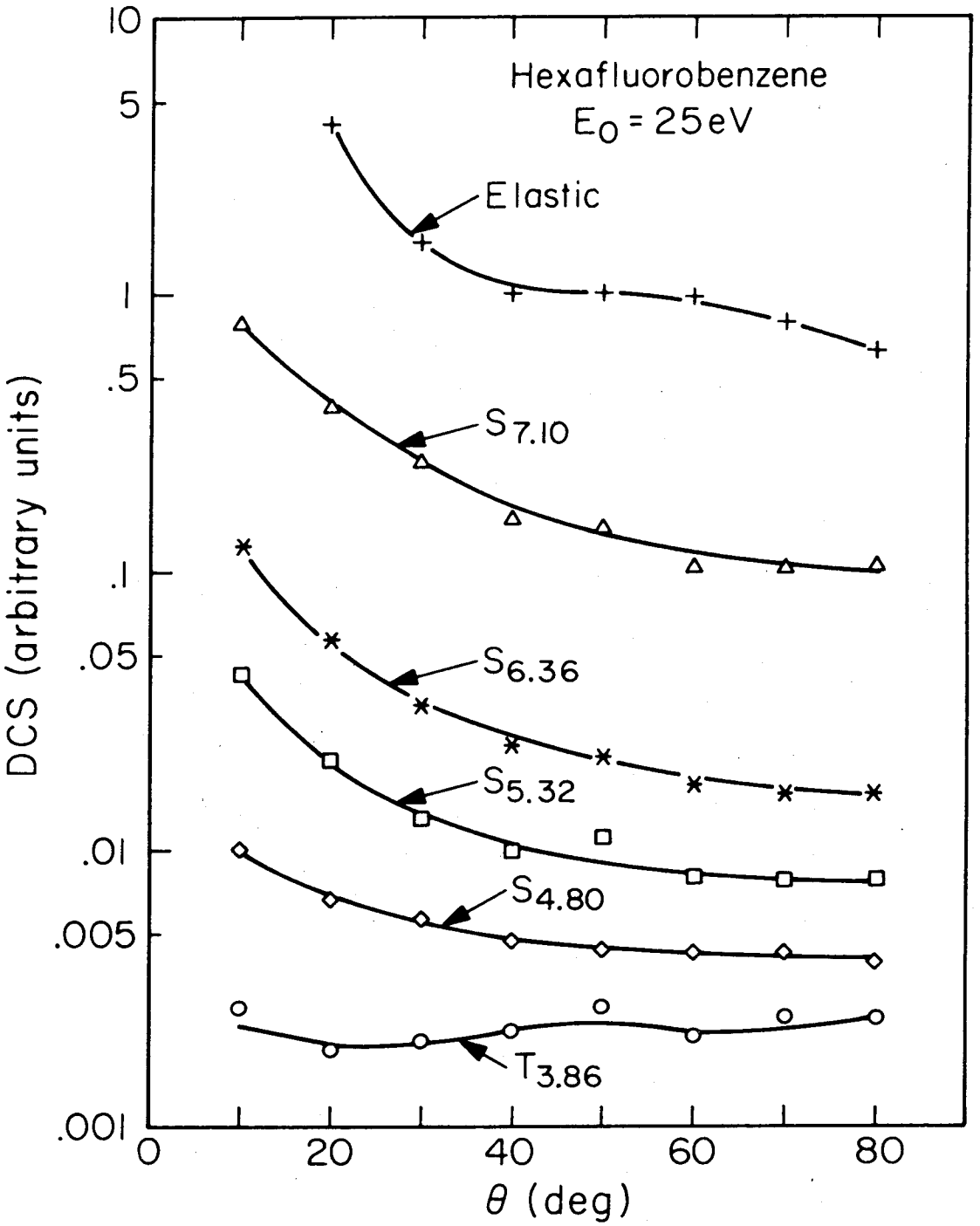
Hexafluorobenzene
E_0 = 25eV
Elastic
$S_{7.10}$
$S_{6.36}$
$S_{5.32}$
$S_{4.80}$
$T_{3.86}$
DCS (arbitrary units)
10
5
1
.5
.1
.05
.01
.005
.001
0
20
40
60
80
θ (deg)

Figure 11

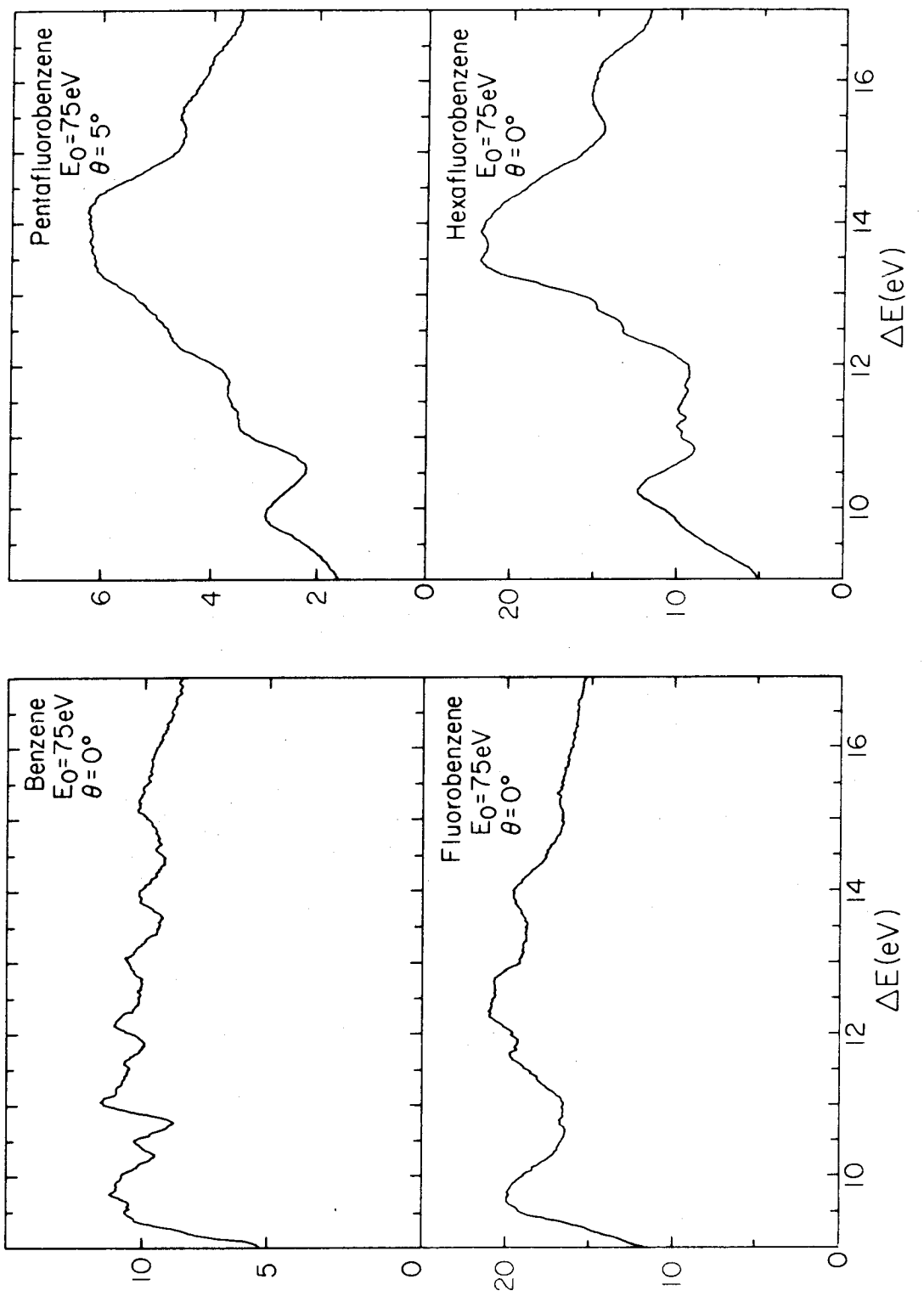
Benzene
E0=75eV
θ=0°
Fluorobenzene
E0=75eV
θ=0°
Pentafluorobenzene
E0=75eV
θ=5°
Hexafluorobenzene
E0=75eV
θ=0°
ΔE(eV)
ΔE(eV)
INTENSITY (10³ counts/sec)

Figure 12

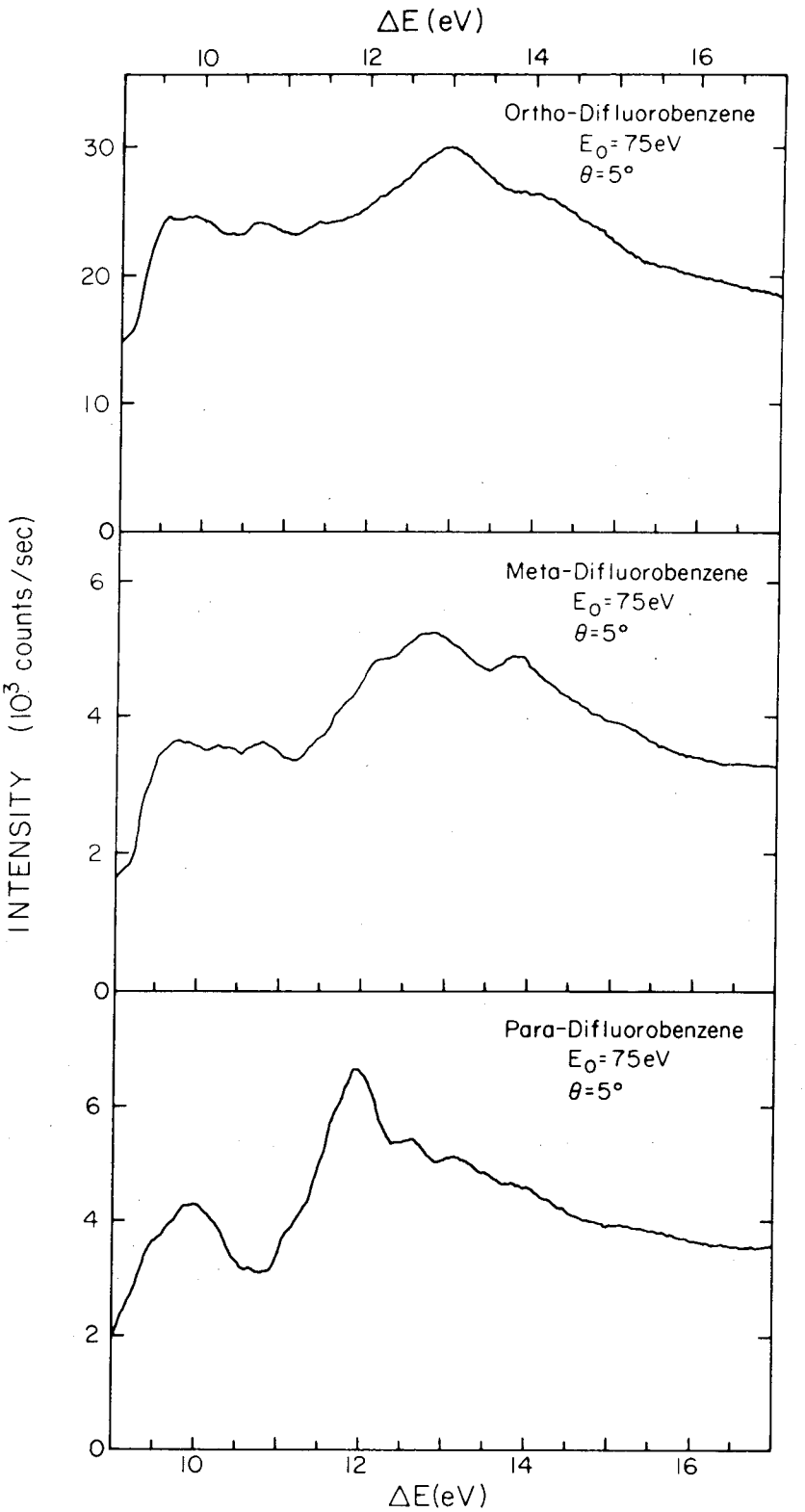
ΔE (eV)
10
12
14
16
Ortho-Difluorobenzene
E_0=75eV
θ=5°
30
20
10
0
Meta-Difluorobenzene
E_0=75eV
θ=5°
6
4
2
0
Para-Difluorobenzene
E_0=75eV
θ=5°
6
4
2
0
10
12
14
16
ΔE(eV)
INTENSITY (10³ counts/sec)

Figure 13

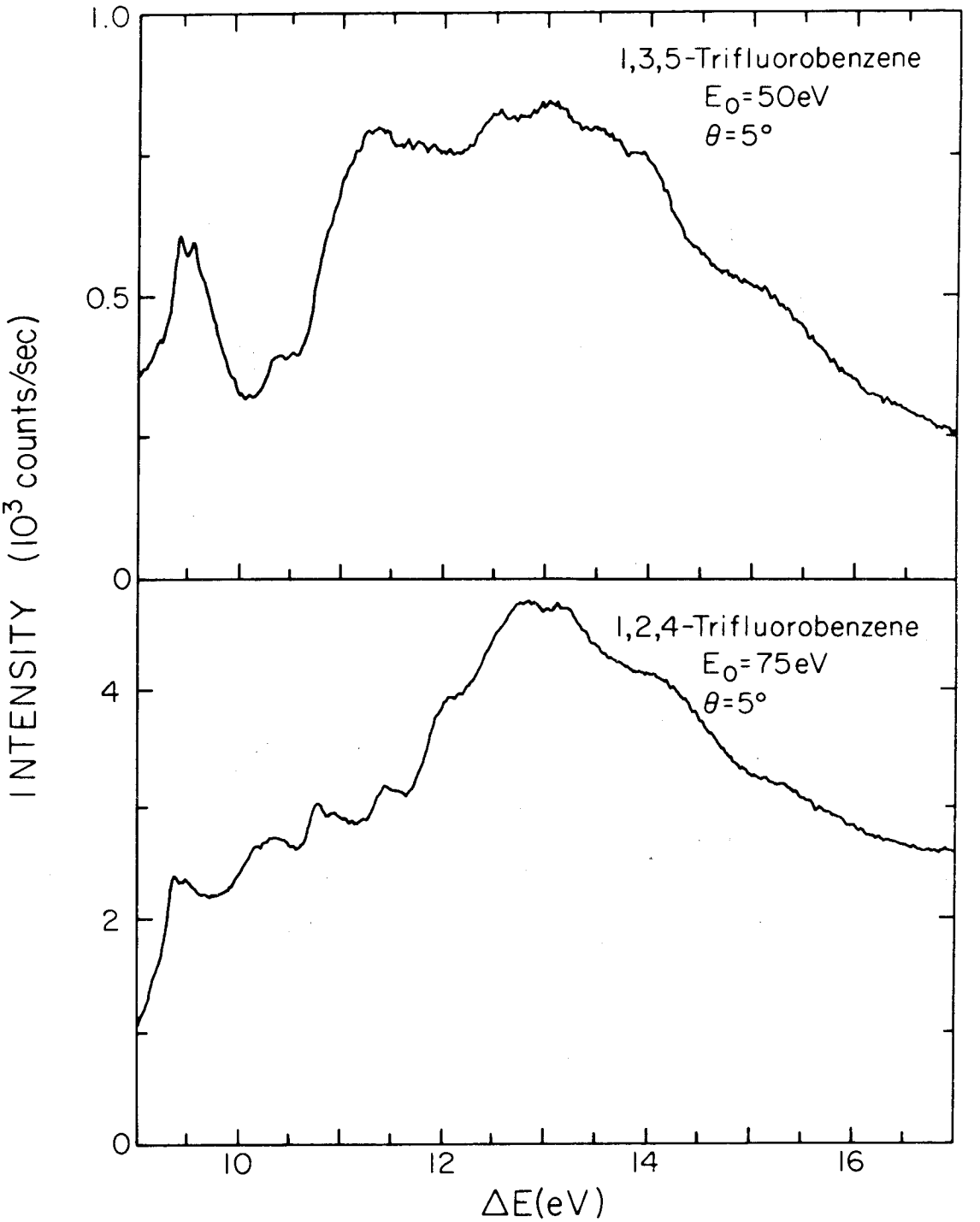
1,3,5-Trifluorobenzene
E_0=50eV
θ=5°
1,2,4-Trifluorobenzene
E_0=75eV
θ=5°
INTENSITY (10^3 counts/sec)
ΔE(eV)
1.0
0.5
0
4
2
0
10
12
14
16

Figure 14

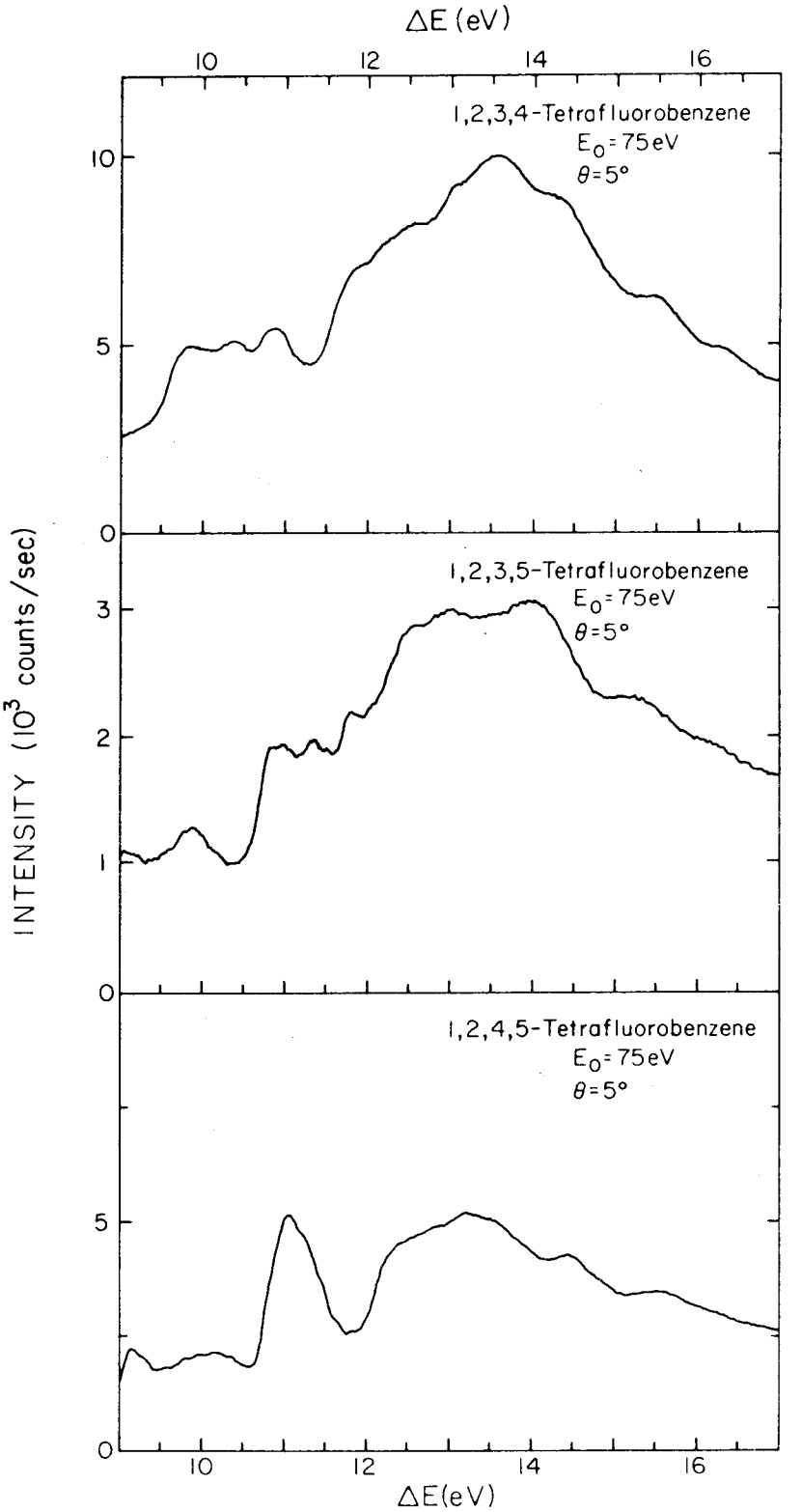
ΔE (eV)
10
12
14
16
1,2,3,4-Tetrafluorobenzene
E_0 = 75eV
θ=5°
1,2,3,5-Tetrafluorobenzene
E_0 = 75eV
θ=5°
1,2,4,5-Tetrafluorobenzene
E_0 = 75eV
θ=5°
INTENSITY (10^3 counts/sec)
ΔE(eV)

Figure 15

4.5 Paper V: Electronic Spectroscopy of 1,3-Cyclopentadiene, 1,3-Cyclohexadiene, and 1,3-Cycloheptadiene by Electron Impact

Electronic spectroscopy of 1,3-cyclopentadiene, 1,3-cyclohexadiene, and 1,3-cycloheptadiene by electron impact[a)]

Robert P. Frueholz,[b)] Wayne M. Flicker,[c)] Oren A. Mosher,[d)] and Aron Kuppermann

Arthur Amos Noyes Laboratory of Chemical Physics,[e)]
California Institute of Technology, Pasadena, California 91125

(Received)

The electronic spectra of three conjugated cis-dienyl systems, 1,3-cyclopentadiene, 1,3-cyclohexadiene, and 1,3-cycloheptadiene have been investigated using electron-impact spectroscopy. Spectra were obtained at impact energies ranging from 20 eV to 75 eV and scattering angles from 5° to 80°. A single singlet → triplet transition was observed for each molecule at 3.10, 2.94, and 2.99 eV, respectively. Accurate electronic system profiles were obtained for these transitions. The $N \rightarrow V_1$ and $N \rightarrow V_2, V_3$ transitions were also observed in each substance. Rydberg structure was observed in these spectra and is discussed.

---

a) This work was supported in part by a contract (EY-76-S-03-767) from the Department of Energy. Report Code: CALT-767P4-172.

b) Work performed in partial fulfillment of the requirements for the Ph.D. in Chemistry at the California Institute of Technology.

c) Present address: Harvard-MIT Program in Health Sciences and Technology, Harvard Medical School, Boston, MA 02115.

d) Present address: Eagle Machinery Co., Ltd., 948 - 88th Avenue, Oakland, CA 94621.

e) Contribution No.

Several previously unreported super-excited states lying above the first ionization potential are reported.

I. INTRODUCTION

The electronic spectra of three cyclic conjugated dienes, 1,3-cyclopentadiene, 1,3-cyclohexadiene, and 1,3-cycloheptadiene, have been investigated by the method of low-energy variable angle electron impact.[1-3] Previously these dienyl systems have been the object of numerous photochemical[4-15] and spectroscopic studies.[16-26] Due to the cyclic nature of these compounds, the two double bonds are locked in the cis conformation. The planes of the double bonds in 1,3-cyclopentadiene and 1,3-cycloheptadiene are the same while those of 1,3-cyclohexadiene intersect at an angle of 18°.[27-29] Figure 1 shows the ground state configurations of the molecules studied as obtained from electron diffraction and microwave rotational studies.[27-29]

Over the last forty years several groups of researchers have used ultraviolet spectroscopy to investigate the excited states of these molecules.[16-22] Also high energy electron impact has been used to study spin-allowed electronic transitions.[23] Spin-forbidden, singlet → triplet transitions in these molecules have been studied to a much lesser extent. Researchers have used both the O_2 perturbation technique and external heavy atom perturbations to increase the optical intensity of singlet → triplet transitions.[22,25,26]

Investigations of the stereochemical aspects of the photosensitized cycloaddition to cyclopentadiene, in the presence of various photochemical sensitizers, have been made.[4-7] It is believed that after photoexcitation of the sensitizer and a subsequent intersystem crossing to an excited triplet state this energy is collisionally trans-

ferred to cyclopentadiene resulting in a reactive cyclopentadiene triplet intermediate.[4] The photochemical reactions of 1,3-cyclohexadiene are of interest because they are typical of those of the vitamin D system.[8,9,11] Photolysis of gas phase 1,3-cyclohexadiene with ultraviolet light leads to 1,3,5-hexatriene, benzene, H_2, and other products.[10,11] The photoisomerization of 1,3-cycloheptadiene has also been investigated.[15]

The location and band shapes of singlet → triplet excitations are important when attempting to interpret results of photochemical experiments involving triplet-triplet energy transfer, as is the case in cyclopentadiene.[4-7] According to a theory for the solid,[30] and as applied to gases,[3a,31-33] the rate of triplet-triplet energy transfer due to exchange interactions is dependent upon the energy overlap of the $S_0 \rightarrow T$ absorption spectrum of the acceptor and the phosphorescence spectrum of the donor.

The method of low-energy, variable angle, electron-impact spectroscopy has been used successfully to investigate spin-forbidden and other dipole-forbidden transitions in molecules.[1-3] With this technique high-quality band shapes of singlet→triplet transitions may be measured. Information about the nature of the excited electronic states observed in an electron-impact spectrum can be obtained from the dependence of the intensity of each transition on impact energy and scattering angle.[1,2] Transitions which in optical spectroscopy are both electric dipole and spin allowed have, in electron impact

spectroscopy, differential cross sections (DCS's) which are forward peaked. For impact energies 15 eV or more above excitation threshold these DCS's decrease by 1 to 2 orders of magnitude as the scattering angle varies from 10° to 80°.[1,2] In contrast, transitions involving changes in the electron spin quantum number of unity, such as singlet → triplet excitations, have a more nearly isotropic DCS, which varies by a factor smaller than 3 over that angular range. Such transitions occur by the mechanism of electron exchange.[34] Spin-allowed but electric dipole-forbidden processes are forward peaked, but often not as much as fully allowed transitions.[2,3b,35] Finally, for impact energies about 15 eV or more above threshold, optically forbidden processes, and in particular spin-forbidden ones, become more intense with respect to optically allowed ones as the impact energy is lowered.

II. SUMMARY OF PREVIOUS STUDIES

A. Introduction

In the first approximation the interacting ethylenic groups produce two filled π molecular orbitals (MO's) and two antibonding MO's. The four lowest $\pi \rightarrow \pi^*$ singlet $\rightarrow$ singlet transitions were designated by Mulliken[36] as $N \rightarrow V_1$, V_2, V_3, and V_4, respectively. The symmetry of the cyclic dienes makes these excitations be electric dipole-allowed. Experimentally, all these dienes exhibit the $N \rightarrow V_1$ transitions and at higher excitation energies an intense region of absorption has been attributed by Robin[37] to the overlapping of the $N \rightarrow V_2$ and $N \rightarrow V_3$ transitions. In addition to valence excitations, transitions from the highest π orbital to Rydberg-like orbitals are expected with the Rydberg series converging to the first ionization potential.

B. Theoretical calculations

Calculations of the electronic spectrum of cyclic cis-dienes have thus far been limited to semi-empirical investigations. For cyclopentadiene, which has C_{2v} symmetry, the V_1, V_2, V_3, and V_4 states transform according to the $^1B_2$, $^1A_1$, $^1A_1$, and $^1B_2$ irreducible representations of that symmetry group. Del Bene and Jaffé[38] performed semi-empirical CNDO calculations yielding the following transition energies from the ground ($\tilde{X}\,^1A_1$) to the indicated excited state: $^1B_2$ - 4.8 eV, $^1A_1$ - 6.2 eV, $^1B_1$ ($\sigma \rightarrow \pi^*$) - 7.5 eV, and $^1A_1$ - 7.9 eV.

More recent CNDO/2 calculations performed by Hayashi and Nakajima[39] yield $\pi \rightarrow \pi^*$ excitation energies of $^1B_2$ - 5.11 eV, $^1A_1$ - 6.36 eV, $^1B_1$ - 7.27 eV, and $^1A_1$ - 8.12 eV. In addition $\sigma \rightarrow \pi^*$ excitations were calculated to occur at 6.01 eV, 6.29 eV, 6.94 eV, and 8.03 eV.[39] The excitation energy of the lowest triplet state of cyclopentadiene ($N \rightarrow T_1$, $\tilde{X}\,^1A_1 \rightarrow {}^3B_2$) was calculated by Barfield, using a semi-empirical valence bond technique, to lie at 3.4 eV.[40] Allinger, Tai, and Stuart[41] performed semi-empirical variable electronegativity self-consistent field (VESCF) configuration interaction calculations on the π system of 1,3-cyclohexadiene. Singlet → singlet transitions were predicted to occur at 5.21 eV and 5.71 eV while the two lowest-lying triplet states were calculated to have excitation energies of 3.01 eV and 4.61 eV. The lowest excited singlet state (V_1) energy of cycloheptadiene was calculated by Allinger and Miller[42] using the Pariser-Parr method in conjunction with the corresponding energies of the other cyclic 1,3-dienes. These calculated excitation energies were found to be 5.0 eV, 5.1 eV, and 5.4 eV, for 1,3-cyclopentadiene, 1,3-cyclohexadiene, and 1,3-cycloheptadiene, respectively. Table I summarizes the results of the calculations done so far.

In addition to the theoretical investigations on the molecules being considered, ab initio SCFCI calculations were performed by Buenker and Whitten[43] and Shih, Buenker, and Peyerimhoff[44] on s-cis-1,3-butadiene. Their results should be useful for comparison with those of the cyclic cis-dienes, particularly if the diene portion of

the ring is more important in determining the transition energy than the overall ring size and conformation. Recent results by Shih et al.[44] indicate that the lowest excited singlet state is the $^1B_2$ one and that the $^1A_1$ state is 0.31 eV above it. These results are different from those of an earlier investigation[42] which had placed the $^1A_1$ state below the $^1B_2$ one. For the trans configuration of butadiene Buenker et al.[45] found that the lowest $^1B_2$ state had significant diffuse character and may correspond to a Rydberg excitation observed at 6.66 eV.[46] The observed N → V_1 transition may be due to a non-vertical valence excitation to a "n $^1B_1$" state.[46]

For s-cis-1,3-butadiene Shih et al.[43] have predicted singlet → triplet transitions with excitation energies of 2.95 eV ($\tilde{X}\,^1A_1 \rightarrow 1\,^3B_2$) and 4.90 eV ($\tilde{X}\,^1A_1 \rightarrow 1\,^3A_1$). The quality of these calculations is expected to be quite good. Similar investigations[43] for trans-butadiene yield triplet excitation energies of 3.24 eV and 4.95 eV, which are in excellent agreement with the electron impact measurements of Mosher, Flicker, and Kuppermann,[3a] who observed singlet → triplet excitations at 3.22 eV and 4.91 eV.

C. Previous experimental results

The optical spectrum of 1,3-cyclopentadiene has been previously studied by Scheibe and Grieneisen,[16] Pickett, Paddock, and Sackter,[17] and Price and Walsh.[18] The first observed singlet → singlet transition was designated N → V_1 ($\tilde{X}\,^1A_1 \rightarrow {}^1B_2$) by Mulliken.[35] Absorption begins at about 4.75 eV and continues to 5.90 eV with the absorption maximum

located at 5.34 eV. Superimposed on the low-energy side of the $N \rightarrow V_1$ transition, both Scheibe and Grieneisen[16] and Pickett et al.[17] observe weak although sharp transitions. On the high-energy side of the $N \rightarrow V_1$ feature an additional set of five excitation peaks is observed. The next region of absorption occurs from 6.20 eV to 6.90 eV. This region consists of a complicated system of vibronic bonds. Price and Walsh[18] have interpreted these in terms of a single electronic transition while Picket et al.[17] assigned them to two superimposed electronic excitations. At higher transition energies four additional features are observed[18] and were suggested to be members of a Rydberg series ($\delta = 0.28$) converging to the first ionization potential, 8.566 eV (vert.).[47] These features appear to be superimposed on a broad region of intense absorption which has its onset at approximately 7.32 eV. Derrick et al.[47] have arranged these transitions and those occurring at about 6.3 eV into three Rydberg series. The lowest triplet state of 1,3-cyclopentadiene was studied by Evans[25] using the high pressure O_2 perturbation technique. An absorption maximum was observed at 3.1 eV in an oxygen and chloroform solution and the 0-0 band of this transition was placed at 2.53 eV.

The spectrum of 1,3-cyclohexadiene has been studied previously both optically[18-22] and by high-incident energy electron impact spectroscopy.[23] An intense transition is observed with onset at about 4.4 eV and an absorption maximum at 4.95 eV.[21] It has been assigned by Mulliken[35] as the $N \rightarrow V_1$ (or $\tilde{X}\,^1A_1 \rightarrow {}^1B_2$ in C_{2V} symmetry notation)[48] transition analogous to its counterpart in 1,3-cyclopentadiene. The

earlier optical spectra of Henri and Pickett[20] showed this peak to have some vibrational structure. Subsequent studies[21,22,49] though, have shown only a smooth feature. The previous vibrational structure was shown to be that of 1,3,5-hexatriene produced by photochemical conversion of the 1,3-cyclohexadiene sample.[21] Three peaks are observed above the $N \rightarrow V_1$ transition centered at 6.22 eV[18,19,22] and are believed to correspond to the vibronic components of a single Rydberg transition. High incident energy electron impact studies by Killat[23] have provided information about the more energetic excitations. Below the first vertical ionization potential of 8.25 eV,[50] several transitions were assigned as having Rydberg character while at 8.04 eV a strong excitation has been attributed to a combination of the $N \rightarrow V_2$ and V_3 ($\tilde{X}\,^1A_1 \rightarrow {}^1A_1$ and $^1A_1$) excitations. In an O_2 plus chloroform solution Evans[25] detected the lowest singlet $\rightarrow$ triplet transition of 1,3-cyclohexadiene, with maximum absorption intensity occurring at 2.9 eV and the 0-0 band at 2.32 eV. In a methyl iodide solution the intensity maximum shifted downwards to 2.79 eV.[22]

The spectrum of 1,3-cycloheptadiene has received considerably less attention than those of the other molecules. The $N \rightarrow V_1$ transition is observed to have an onset at approximately 4.5 eV with an absorption maximum at 5.00 eV.[24] No singlet $\rightarrow$ triplet transitions have been reported. The previously obtained experimental and theoretical results are summarized in Table I.

III. EXPERIMENTAL METHODS

The electron impact spectrometer used in these studies has been described previously by Kuppermann et al.[1] In summary, a beam of electrons generated by a tungsten filament at about 2100° C is injected into a hemispherical electrostatic energy analyzer where it is monochromatized and is afterwards accelerated to an impact energy E_0. This beam is then scattered off the target gas contained in a flexible, metal bellows scattering chamber. The scattered electrons are energy-analyzed by another hemispherical device identical to the previous one. A continuous dynode electron multiplier serves as the detector. Its output pulses are amplified, shaped, and stored in a 1024 channel scalar.

In the present experiments, the electron impact spectra of 1,3-cyclopentadiene, 1,3-cyclohexadiene, and 1,3-cycloheptadiene were obtained at impact energies of 30 eV and 50 eV, 20 eV and 40 eV, and 25 eV and 50 eV, respectively, over scattering angles ranging from 5° to 80°. Electron beam intensities incident into the scattering chamber were typically 4.0×10^{-8} A while sample pressures ranged from 3 mtorr to 6 mtorr, as indicated by an uncalibrated Schulz-Phelps ionization gauge. The energy resolution, as measured by the full width at half maximum (FWHM), was usually chosen to lie in the range 0.10 eV to 0.15 eV; some spectra were obtained at higher resolutions of 0.07 eV to 0.09 eV.

The 1,3-cyclopentadiene used in these studies was prepared by cracking dicyclopentadiene obtained from the Matheson, Coleman and

Bell Co. with a stated purity of 95%. As a check on the cracking procedure and to allow detection of any dicyclopentadiene generated while the spectra were being obtained, several independent spectra of dicyclopentadiene were also obtained. No structure in any of the 1,3-cyclopentadiene results could be attributed to excitations in the spectrum of dicyclopentadiene. The samples of 1,3-cyclohexadiene and 1,3-cycloheptadiene, with stated purities of 99% and 97%, respectively, were obtained from the Aldrich Chemical Co. The 1,3-cyclohexadiene sample was used as soon after its arrival as possible to minimize build-up of benzene, cyclohexene, or 1,3,5-hexatriene impurities.[12] The cycloheptadiene sample was kept in an ice bath prior to its use and its spectra showed no change with sample age over the period of two weeks during which these spectra were obtained.

IV. RESULTS AND DISCUSSION

Figures 2-4 display the low-energy portion of the spectra of the three cyclic-dienes at both high and low scattering angles. Figure 5 shows the higher energy loss region of the spectra of these molecules. The differential cross sections (DCS) for the elastic peak and various transitions are shown for both high and low impact energies in Figs. 6 - 11. The technique for obtaining these differential cross sections has been described previously.[1,3] The DCS's are given in terms of arbitrary units specified by setting the elastic DCS at $\theta = 40°$, for a given impact energy, equal to unity. The arbitrary units thus determined are different for each molecule and impact energy but are the same for all curves of a given molecule at a given energy.

A. Spectral features

1. 1,3-Cyclopentadiene

The lowest energy transition observed in the 1,3-cyclopentadiene spectrum has an effective vertical Franck-Condon region (outside of which we can no longer detect the transition) extending from 2.5 eV to 3.9 eV, with the intensity maximum occurring at 3.10 eV. The DCS of this transition at 30 eV impact energy (see Fig. 6) is much more isotropic than are the other DCS's of Fig. 6a, decreasing monotonically by less than a factor of 5 over the angular range 10° to 80°. At 50 eV impact energy this transition is relatively more intense with respect to the other transitions of Fig. 6b and its DCS is also much

more isotropic than are the DCS's for the other transitions in that figure. This DCS behavior permits us to assign this transition as a singlet → triplet excitation.[1,2] Our value of 3.10 eV for the excitation energy corresponding to the intensity maximum is identical to that obtained by Evans[25] using the oxygen perturbation technique. It is also in good agreement with the value of 3.4 eV predicted by the semi-empirical calculations of Barfield[40] and very close to the ab initio result of 2.95 eV for the first triplet in cis-butadiene.[44] On this basis we assign this transition as the $\tilde{X}\,^1A_1 \rightarrow 1\,^3B_2$ ($N \rightarrow T_1$) excitation.

At 5.26 eV (see Figs. 2a and 5a) we observe an intensity maximum of a broad transition. The DCS of this excitation at 50 eV impact energy (see Fig. 6a) decreases by a factor of 90 as the scattering angle increases from 10° to 80°, while at 30 eV impact energy (see Fig. 6b) the corresponding change in the DCS is greater than a factor of 100. This forward peaked behavior of the DCS is characteristic of a singlet → singlet symmetry allowed transition, and is consistent with its assignment as the optically observed $\tilde{X}\,^1A_1 \rightarrow 1\,^1B_2$ ($N \rightarrow V_1$) excitation. Both Scheibe and Grieneisen[16] and Pickett et al.[17] observed five weak peaks separated by approximately 0.095 eV on the low-energy side of the $N \rightarrow V_1$ absorption. The resolution we used in obtaining these spectra, of about 0.15 eV, did not permit us to observe this structure. On the high-energy side of the $N \rightarrow V_1$ transition, between 5.5 eV and 6 eV energy loss, we observe several apparently superimposed peaks which have been previously reported in optical studies.[16-18] They will be discussed in Section IV-B.

Between 6.15 eV and 6.7 eV (see Fig. 5a), there is another intense feature with resolvable peaks at 6.28 eV and 6.41 eV. In the corresponding optical spectra[17,18] (see Section II-C), complex higher resolution vibronic structure has been obtained and interpreted in terms of either a single or two different transitions. At 50 eV impact energy, the DCS of this feature increases by a factor of nearly 200 as the scattering angle decreases from 80° to 10°. In addition, the ratio of this DCS to that of the $N \rightarrow V_1$ excitation changes by a factor of only two over the same angular range. The observed band shape shows no discernible change over the angular region studied. This behavior is consistent with a single electronic transition,[51] or with two superimposed transitions which have essentially the same angular dependence. As a result, we cannot differentiate between these two possibilities.

The region of the most intense inelastic scattering in the 1,3-cyclopentadiene spectrum occurs from approximately 7.2 eV to 8.6 eV with an intensity maximum at 7.84 eV. This feature appears to be due to a broad and structureless transition with smaller peaks superimposed on it. Robin[37] has suggested that the corresponding feature in the optical spectra results from the superposition of the $N \rightarrow V_2$ ($\tilde{X}\,^1A_1 \rightarrow {}^1A_1$) and $N \rightarrow V_3$ ($\tilde{X}\,^1A_1 \rightarrow {}^1A_1$) excitations. For cis-butadiene these transitions are calculated to occur at 6.66 eV and 7.89 eV.[44]

2. 1,3 Cyclohexadiene

Figure 3 shows the lower energy-loss portion of the 1,3-cyclohexadiene spectrum. With an effective vertical Franck-Condon region

extending from 2.1 eV to 3.8 eV, the lowest energy, electronic transition is observed to have an intensity maximum at 2.94 eV. As seen in Fig. 7 the DCS's for this transition at both 20 eV and 40 eV impact energies are nearly isotropic over the angular range, 20° to 80°. This behavior is typical of a singlet → triplet transition. The close correlation between the observed excitation energy and that calculated for cis-butadiene by Shih et al.[44] (2.95 eV) and Allinger et al.[41] (4.01 eV), confirm the expected assignment of this transition as the $N \rightarrow T_1$ ($\tilde{X}\,^1A_1 \rightarrow 1\,^3B_2$) excitation. There is also excellent agreement between our result and that obtained from O_2 perturbation (2.9 eV).[25] The intense transition peaking at 4.94 eV was assigned to the $N \rightarrow V_1$ ($\tilde{X}\,^1A_1 \rightarrow 1\,^1B_2$) transition by Mulliken.[36]

The DCS curves for this excitation (see Fig. 7) are forward peaked decreasing by factors of 16 and 80, as the scattering angle increases from 10° to 80°, at impact energies of 20 eV and 40 eV. On the high energy side of the $N \rightarrow V_1$ transition there is a slight indication of vibrational structure suggesting the possibility of the presence of a very small amount of 1,3,5-hexatriene. At higher energy losses three peaks are observed at 6.05 eV, 6.20 eV, and 6.39 eV. These transitions were also observed in previous optical studies.[18,19,22] The next transition is observed at 6.90 eV. A peak is seen at about 7.0 eV in a recent optical study[22] and at 6.9 eV in a 50 KeV incident electron energy electron impact study.[23] However, an earlier optical study showed a feature peaking at 6.81 eV and smooth continuous absorption in the 6.85 eV to 7.1 eV region. Benzene is known to have

an extremely intense (f = 1, 2) transition peaking at 6.93 eV.[52] At low scattering angles the intensity ratio in the electron-impact spectrum between two singlet → singlet transitions is of the same order as that of their optical oscillator strength. Consequently, the observed ratio of the area under the N → V_1 transition to that of the 6.90 eV transition could result from the presence of as little as a 2% benzene contamination, since the f number for the N → V_1 excitation in 1,3-cyclohexadiene is 0.13.[22] This 6.90 eV peak may therefore be the result of a benzene inpurity. On the other hand, the intensities of the transitions observed at 7.0 eV in the optical study[22] at 6.90 eV in the high incident energy electron impact spectra,[23] and at 6.90 eV in our 40 eV, 0° spectra relative to the other transitions in those spectra are about the same. If those transitions were attributed to a benzene impurity, this would require the concentration of this impurity to be approximately the same in all three studies. While such a coincidence is possible, it seems unlikely. Nevertheless, to determine more reliably whether this feature is due to a benzene impurity requires further experimental study in which special care is taken with respect to sample purity. As in 1,3-cyclopentadiene, a broad, intense transition, which has been suggested to be due to N → V_2, V_3 excitations,[37] is observed between approximately 7.2 eV and 8.8 eV. Several distinct peaks appear to be superimposed on this transition.

3. 1,3-Cycloheptadiene

Figures 4 and 5 show both the low and high energy-loss portions of the 1,3-cycloheptadiene spectrum. At 2.99 eV the intensity maximum

of a low-lying transition is observed. This transition has an effective vertical Franck-Condon region extending from 2.4 eV to 3.9 eV. The DCS for this transition is essentially isotropic at both 25 eV and 50 eV impact energies (Fig. 8). This allows us to assign this excitation to the N → V_1 singlet → triplet transition, analogous to similar transitions observed in 1,3-cyclopentadiene and 1,3-cyclohexadiene.

The next feature in the 1,3-cycloheptadiene spectrum is a broad excitation with an intensity maximum occurring at 5.08 eV. The DCS of this transition decreases by factors of 80 and 36 at impact energies of 50 eV and 25 eV as the scattering angle increases from 10° to 80°. This transition is analogous to the corresponding excitations observed in the other two molecules. We can assign it as the N → V_1 ($\tilde{X}\,^1A_1 \rightarrow 1\,^1B_2$) excitation. We also observe two weaker peaks superimposed on the high-energy side of the N → V_1 transition with estimated intensity maxima occurring at 5.41 eV and 5.61 eV. The available optical spectrum extends to 5.46 eV,[24] but does not show the first additional feature just mentioned. This optical spectrum was obtained in the liquid phase and if the transitions being considered correspond to Rydberg excitations, we would expect that under these conditions they would be less intense than in the gas phase. The spacing of 0.20 eV ($\sim$1600 cm^{-1}) between those two transitions is in the range expected for vibrational splittings, since for the ground state of 1,3-cycloheptadiene the symmetric and asymmetric C=C-C fundamental vibration wavenumbers are 1613 cm^{-1} and 1646 cm^{-1}, respectively.[53] This spacing is consistent with features which are different vibronic peaks

of the same electronic transition. Their electronic nature is discussed in Section IV-B.

Several additional transitions occur above the $N \rightarrow V_1$ excitation. Between 5.9 eV and 7.0 eV, six sharp although weak transitions are observed (see Fig. 5c). These appear to correspond to two different electronic excitations each with three vibronic components occurring at 5.95 eV, 6.13 eV, and 6.27 eV and 6.65 eV, 6.79 eV and 6.97 eV, respectively. Possible assignments of these features are discussed in Section IV-B. The region of most intense absorption above the $N \rightarrow V_1$ transition occurs between 7.2 eV and 8.6 eV. It is analogous to the $N \rightarrow V_2, V_3$ features observed at 8.03 eV and 7.88 eV in 1,3-cyclopentadiene and 1,3-cyclohexadiene, respectively. There appear to be several smaller peaks superimposed on this absorption.

B. Rydberg transitions

In each of the three molecules studied, in this investigation, we have observed many transitions in addition to the $N \rightarrow V_1$ and apparent $N \rightarrow V_2, V_3$ excitations. These additional transitions appear to have fairly sharp structure and occur as both isolated peaks and superimposed on other peaks. Specific assignment of them is quite difficult. McDiarmid[54] recently completed a new interpretation of the ultraviolet spectrum, and in particular the Rydberg states, of trans-1,3-butadiene. The analysis was based on the separation of electronic origins and an assignment of the vibronic transitions related to each origin by studying the spectra of different deuterium substituted molecules. This procedure for assignment of Rydberg series is much more reliable than

basing the entire interpretation on the spectrum of a single isotopic molecule. In our own studies we also lack the higher resolution obtainable in optical experiments. Rather than attempting to make definitive assignments of Rydberg series we will discuss the likely assignments of the more apparent of these transitions.

Although these excitations are most likely Rydberg in nature, the possibility that they are valence transitions cannot be entirely ruled out. An $N \rightarrow V_4$ transition is expected to occur above the $N \rightarrow V_1$ excitation in the spectra of these molecules.[36] In both 1,3-cyclopentadiene (vert IP = 8.566 eV[47]) and 1,3-cycloheptadiene (vert IP = 8.31 eV[50]) the structure we observed superimposed on the high-energy side of the $N \rightarrow V_1$ transition has term values of about 23,000 cm^{-1}. This value is quite appropriate for a $\pi \rightarrow 3s$ Rydberg excitation.[55,56] In the 1,3-cyclohexadiene (vertical IP 8.25 eV),[48] we also observe structure in the equivalent energy-loss region but in this case it could be due to a small amount of 1,3,5-hexatriene impurity.[21,22,49] Transitions are clearly observed at 6.4 eV, 6.3 eV and 6.2 eV in 1,3-cyclopentadiene, 1,3-cyclohexadiene and 1,3-cycloheptadiene, respectively. The corresponding term values lie between 17,000 cm^{-1} and 18,000 cm^{-1} which is reasonable for $\pi \rightarrow 3p$ Rydberg excitations.[55,56] In addition high pressure and crystal spectra of 1,3-cyclohexadiene obtained by Robin[37] indicate that the transition at 6.3 eV is definitely Rydberg in nature.

In each of the molecules studied some structure is observed superimposed on the $N \rightarrow V_2, V_3$ features. In the spectra of 1,3-cyclohexadiene and 1,3-cycloheptadiene. These transitions are quite weak

and appear to be higher elements of Rydberg series. However, in 1,3-cyclopentadiene (see Fig. 5a) this structure is quite pronounced. Let us discuss the question of whether this structure corresponds to vibronic components of the (apparent) $N \rightarrow V_2, V_3$ transitions or is Rydberg in nature. Byrne and Ross[57] arrive at the empirical rule that the lowest singlet excited state of a polyatomic molecule in the gas phase will exhibit the sharpest vibronic structure. The higher states tend to show much more diffuse vibrational structure due to the many means of intramolecular relaxation available which shorted the excited state lifetime, leading to major uncertainty broadening. They also point out that Rydberg transitions may be exceptions to this rule because they are only weakly coupled to the valence manifold and their relaxation times are consequently longer. With this information and noting that $N \rightarrow V_1$ transition is structureless, we feel that the peaks on the apparent $N \rightarrow V_2/V_3$ transitions of 1,3-cyclopentadiene are probably Rydberg in nature. In all of these molecules broad autoionization excitations were observed above the first ionization potential. These superexcited state transition energies are summarized in Table I.

C. Discussion

The data obtained in this study clearly demonstrate that there are many similarities between the spectra of these three cyclic dienes. As indicated in Table I, each molecule exhibits an $N \rightarrow T_1$, $(\tilde{X}\,^1A_1 \rightarrow {}^3B_2)$ transition near 3,0 eV with quite similar effective vertical Franck-

Condon envelopes. Since the N → T_2 ($\tilde{X}\,^1A_1 \rightarrow 1\,^3A_2$) excitation is predicted to occur at 4.90 eV in cis-1,3-butadiene.[44] A second spin-forbidden transition should exist at approximately this energy in each of the cyclic-dienes. This transition has not been observed and probably is hidden under the N → V_1 excitations. However, we can at least estimate a lower band above which this transition should lie. In 1,3-cyclopentadiene we would not be able to observe the N → T_2 transition if it lay above 4.7 eV (due to masking by the N → V_1 transition), while in the other two molecules this limit is 4.5 eV.

Each molecule exhibits a strong structureless N → V_1 transition as well as the even more intense feature presumed to be the N → V_2, V_3 excitations. We also see (Fig. 5) that as the ring size increases, the N → V_1 transition becomes more intense relative to the N → V_2, V_3 feature. The relative insensitivity of the valence transitions to increasing ring size is consistent with excitations being localized to the dienyl portion of the molecule, and therefore somewhat insensitive to overall molecular geometry. Although the suggested assignments of Rydberg transitions in these molecules are tentative it appears that the term value of the 3s and 3p Rydberg states vary little with ring size.

It is also interesting to compare the present results for the triplet states of 1,3-cyclopentadiene with those from previous investigations of furan (C_4H_4O), thiophene (C_4H_4S), and pyrrole (C_4H_4NH),[58,59] three heterocycles which also contain two conjugated double bonds locked into a cis conformation. In these molecules, two low-lying triplets (T_1 and T_2) were observed, with excitation energies listed in Table 2. The

locations of these triplet states and the energy splitting between them are similar to those of the first two triplet states of benzene.[60] This correlation suggests that for these valence transitions, the five-membered heterocycles may be considered to have appreciable aromatic character, resulting from partial participation of two formally nonbonding electrons on the heteroatom in the resonance π electron system.

In contrast, the lowest triplet state in 1,3-cyclopentadiene occurs 0.85 eV below either the corresponding state in benzene or the average of those states in furan, thiophene, and pyrrole. Furthermore, the splitting between T_1 in 1,3-cyclopentadiene and the unobserved T_2 is probably greater than 1.6 eV, which is considerably larger than the 0.80 eV T_1-T_2 splitting in benzene, or the 1.0 eV average splitting in the five-membered heterocycles. These results indicate that 1,3-cyclopentadiene can be regarded as a typical conjugated diene, and that to a first approximation hyperconjugation of the π orbitals' double bonds with the CH_2 orbitals does not play an important role in determining the excitation energies of the lowest triplet states.

V. SUMMARY

A single, low-lying triplet state has been observed near 3 eV in cyclic 1,3-diene with 5, 6, and 7 carbon atoms. $N \rightarrow V_1$ and presumed $N \rightarrow V_2, V_3$ singlet $\rightarrow$ singlet transitions were also observed in each molecule. The excitation energies of these valence transitions are relatively insensitive to the ring size and geometry. This behavior is consistent with the belief that these transitions are localized in the dienyl region of the molecule. Several previously unreported states lying above the first ionization potential have been located. Assignments of transitions to 3s and 3p Rydberg states have been made on the basis of the term values of these features. Comparison of the location of the two lowest lying triplet states in 1,3-cyclopentadiene with those in furan, thiophene, pyrrole and benzene indicate that the former is a typical dienyl π electron system and that hyperconjugation of the CH_2 orbitals to the dienyl π electron system is negligible in those states.

ACKNOWLEDGMENT

The authors would like to thank Mr. R. Rianda for his assistance in obtaining some of the 1,3-cycloheptadiene data.

TABLE I. Transition energies (in eV) for 1,3-cyclopentadiene, 1,3-cyclohexadiene, and 1,3-cycloheptadiene.[a]

Transitions[b]	Previous Theoretical Results				Previous Experimental Results			Present Experimental Results		
	cis-butadiene[c]	C_5H_6	C_6H_8	C_7H_{10}	C_5H_6	C_6H_8	C_7H_{10}	C_5H_6	C_6H_8	C_7H_{10}
$N \rightarrow T_1(\tilde{X}\,^1A_1 \rightarrow {}^3B_2)$	2.95	3.4[d]	3.01[h]		3.1[i]	2.9[i]		3.10(2.5 – 3.9)[p]	2.94(2.1 – 3.8)[p]	2.99(2.4 – 3.9)[p]
$N \rightarrow T_2(\tilde{X}\,^1A_1 \rightarrow {}^3A_1)$	4.90		4.61[h]					Above 4.7	Above 4.5	Above 4.5
$N \rightarrow V_1(\tilde{X}\,^1A_1 \rightarrow {}^1B_2)$	6.35	4.8[e], 5.11[h], 5.0[g]	5.21[h], 5.1[g]	5.4[g]	5.34[j]	4.95[m]	5.00[o]	5.26	4.94	5.08
$N \rightarrow V_2(\tilde{X}\,^1A_1 \rightarrow {}^1A_1)$	6.66	6.3[e], 6.36[f]	5.71[h]		8.06[l]	8.04[h]		8.03	7.88	8.24
$N \rightarrow V_3(\tilde{X}\,^1A_1 \rightarrow {}^1A_1)$	7.89	7.9[e], 8.12[f]								
$N \rightarrow V_4(\tilde{X}\,^1A_1 \rightarrow {}^1B_2)$	8.53	7.27[f]								
$\pi - 3s$					5.68, 5.77, 5.8, 5.94, 5.99[j]			5.68, 5.77, 5.94		5.41, 5.61
$\pi - 3p$					6.24, 6.35, 6.43, 6.49[j]	6.05, 6.22, 6.40[k]		6.28, 6.41	6.05, 6.20, 6.39	5.95, 6.13, 6.27
					7.88[k]	6.90[n]		6.80	6.90[q]	6.65
					8.13[k]	7.23[n]		7.05	7.21	6.79
					8.28[k]	7.46[n]		7.61	7.42	6.97
					8.36[k]	7.75[n]		7.84	7.73	7.18
						8.5[n]		8.03	7.88	7.38
						8.95[n]		8.19	8.05	7.66
		Apparent Rydberg Transitions				10.49[n]		9.2	9.05	7.86
						12.28[n]		10.4		8.24
						15.5[n]		11.8		8.80
						18.8[n]		14.0		9.52
										10.00
										11.33
										13.78

Footnotes to Table I

---

[a]The uncertainty in the location of these intensity maxima is ±0.05 eV.

[b]None of the experimental identifications are definite. They represent an assignment based on analysis of experiments and theoretical calculations. Symmetry designations are those appropriate for the C_{2V} point group.

[c]Ref. 44.

[d]Ref. 40.

[e]Ref. 38.

[f]Ref. 39.

[g]Ref. 42.

[h]Ref. 41.

[i]Ref. 25.

[j]Ref. 17.

[k]Ref. 18.

[l]Ref. 37.

[m]Ref. 21.

[n]Ref. 23.

[o]Ref. 24.

[p]Values in parentheses are the effective vertical Franck-Condon regions.

[q]This feature may be due to a small benzene impurity ($\lesssim$ 2%).

TABLE II. Heterocycle Triplet Excitation Energies

	T_1	T_2
Benzene	3.95[a]	4.75[a]
Furan	3.99[b]	5.22[b]
Thiophene	3.75[b]	4.62[b]
Pyrrole	4.21[b]	5.1[c]
1,3-Cyclopentadiene	3.10	>4.7[d]

[a]Ref. 60.

[b]Ref. 58.

[c]Ref. 59.

[d]The second singlet → triplet transition in 1,3-cyclopentadiene is estimated to lie above this value in the present study.

REFERENCES

1. (a) A. Kuppermann, J. K. Rice, and S. Trajmar, J. Phys. Chem., 72, 3894 (1968); (b) S. Trajmar, J. K. Rice, and A. Kuppermann, Adv. Chem. Phys. 18, 15 (1970).
2. A. Kuppermann, W. M. Flicker, and O. A. Mosher, Acc. Chem. Res., submitted for publication.
3. (a) O. A. Mosher, W. M. Flicker, and A. Kuppermann, J. Chem. Phys. 59, 65092 (1973); (b) ibid. 62, 2600 (1975).
4. B. D. Kramer and P. D. Bartlett, J. Am. Chem. Soc. 94, 3934 (1972).
5. P. D. Bartlett, R. Helgeson, and O. A. Wersel, Pure Appl. Chem. 16, 187 (1968).
6. P. D. Bartlett, Lecture at 23rd International Congress of Pure and Applied Chemistry, Boston, Mass.; Pure Appl. Chem., Suppl. 4, 281 (1971).
7. T. S. Cantrell, J. Org. Chem. 39. 3063 (1974).
8. R. Srinivasan, Adv. Photochem. 4, 113 (1966).
9. E. Havinga and J. L. M. A. Schlatmann, Tetrahedron 16, 146 (1961).
10. R. Srinivasan, J. Am. Chem. Soc. 82, 5063 (1960).
11. R. Srinivasan, J. Am. Chem. Soc. 83, 2806 (1961).
12. R. J. DeKock, N. G. Minnaard, and E. Havinga, Rec. Trav. Chim. Pays-Bas 79, 922 (1960).
13. Y. L. Bahurel, D. J. MacGregor, T. L. Penner, and G. S. Hammond, J. Am. Chem. Soc. 94, 637 (1972).

14. N. G. Minnard and E. Havinga, Rec. Trav. Chim. Pays-Bas 92, 1315 (1973).

15. W. G. Dauben and R. L. Cargill, Tetrahedron 12, 186 (1961).

16. G. Scheibe and H. Grieneisen, Z. Phys. Chem. B25, 52 (1934).

17. L. W. Pickett, E. Paddock, and E. Sackter, J. Am. Chem. Soc. 63, 1073 (1941).

18. W. C. Price and A. D. Walsh, Proc. R. Soc. Lond. 179A, 201 (1941).

19. E. P. Carr and H. Stucklen, J. Chem. Phys. 6, 55 (1938).

20. V. Henri and L. W. Pickett, J. Chem. Phys. 7, 439 (1939).

21. H. Schüler, E. Lutz, and G. Arnold, Spectrochim. Acta 17, 1043 (1961).

22. N. G. Minnaard and E. Havinga, Rec. Trav. Chim. Pays-Bas 92, 1179 (1973).

23. U. Killat, Z. Phys. 270, 169 (1974).

24. P. Pesch and S. L. Friess, J. Am. Chem. Soc. 72, 5756 (1950).

25. D. F. Evans, J. Chem. Soc. 1960, 1735.

26. R. E. Kellog and W. T. Simpson, J. Am. Chem. Soc. 87, 4230 (1965).

27. L. H. Scharpen and V. W. Laurie, J. Chem. Phys. 43, 2765 (1965).

28. M. Traetteberg, Acta Chem. Scand. 22, 2305 (1968).

29. K. Hagen and M. Traetteberg, Acta Chem. Scand. 26, 16 (1972).

30. D. L. Dexter, J. Chem. Phys. 21, 836 (1953).

31. M. W. Schmidt and E. K. C. Lee, J. Am. Chem. Soc. 90, 5919 (1968).

32. M. W. Schmidt and E. K. C. Lee, J. Am. Chem. Soc. 92, 3579 (1970).

33. G. L. Loper and E. K. C. Lee, J. Chem. Phys. 63, 264 (1975).

34. J. R. Oppenheimer, Phys. Rev. 29, 433 (1927).

35. D. C. Cartwright, W. J. Hunt, W. Williams, S. Trajmar, and W. A. Goddard III, Phys. Rev. A 8, 533 (1927).

36. R. S. Mulliken, J. Chem. Phys. 7, 121 (1939).

37. M. B. Robin, Higher Excited States of Polyatomic Molecules (Academic Press, New York, 1975), Vol. II, pp. 166-176.

38. J. Del Bene and H. Jaffé, J. Chem. Phys. 48, 4050 (1968).

39. T. Hayashi and T. Nakajima, Bull. Chem. Soc. Jap. 48, 980 (1975).

40. M. Barfield, J. Chem. Phys. 47, 3831 (1967).

41. N. L. Allinger, J. C. Tai, and T. W. Stuart, Theor. Chim. Acta 8, 101 (1967).

42. N. L. Allinger and M. A. Miller, J. Am. Chem. Soc. 86, 2811 (1964).

43. R. J. Buenker and J. L. Whitten, J. Chem. Phys. 49, 5381 (1968).

44. S. Shih, R. J. Buenker, and S. D. Peyerimhoff, Chem. Phys. Lett. 16, 244 (1972).

45. R. J. Buenker, S. Shih, and S. D. Peyerimhoff, Chem. Phys. Lett. 44, 385 (1976).

46. G. Herzberg, Molecular Spectra and Molecular Structure (Van Nostrand, Princeton, 1966), Vol. III, p. 656.

47. P. J. Derrick, L. Asbrink, O. Edquist, B.-O. Johnsson, and E. Lindholm, Int. J. Mass Spectrom. Ion Phys. 6, 203 (1971).

48. As indicated by electron diffraction studies neither the ground-state symmetry of 1,3-cyclohexadiene nor that of the cis-dienyl portion of the molecule has truly C_{2V} symmetry. However, for clarity throughout this discussion we will refer to transitions observed in these cis-dienyl systems in terms of the C_{2V} symmetry point group.

49. G. R. De Mare, J. Chem. Phys. 55. 3057 (1971).

50. P. Bischof and E. Heibronner, Helv. Chim. Acta 53, 1677 (1970).

51. E. N. Lassettre, A. Skerbele, M. A. Dillion, and K. J. Ross, J. Chem. Phys. 48, 5066 (1968).

52. L. W. Pickett, M. Muntz, and E. M. McPherson, J. Am. Chem. Soc. 73, 4862 (1951).

53. E. V. Sobolev, V. T. Aleksanyan, E. M. Mil'vitskaya, and M. A. Pryanishnikova, Zh. Strukt. Khim. 4, 189 (1963).

54. R. McDiarmid, J. Chem. Phys. 64, 514 (1976).

55. M. B. Robin, Higher Excited States of Polyatomic Molecules (Academic Press, New York, 1974), Vol. I, pp. 7-30.

56. C. Sandorfy, J. Mol. Struct. 19, 183 (1973).

57. J. P. Byrne and I. G. Ross, Aust. J. Chem. 24, 1107 (1971).

58. W. M. Flicker, O. A. Mosher, and A. Kuppermann, J. Chem. Phys. 64, 1315 (1976); Chem. Phys. Lett. 38, 489 (1976).

59. E. H. Van Veen, Chem. Phys. Lett. 41, 535 (1976).

60. J. P. Doering, J. Chem. Phys. 51, 2866 (1969).

FIGURE CAPTIONS

FIG. 1. Molecular geometries and symmetries of 1, 3-cyclopentadiene, 1, 3-cyclohexadiene, and 1, 3-chcloheptadiene.

FIG. 2. Electron energy-loss spectrum of 1, 3-cyclopentadiene at a scattering angle of (a) 20° and (b) 80°; 30 eV incident electron energy; 5×10^{-8} A incident beam current; 8 mTorr sample pressure reading from an uncalibrated Schulz-Phelps gauge; resolution approximately 0.15 eV (fwhm). Flat sections in the 80° spectrum are the result of computer roundoff.

FIG. 3. Electron energy-loss spectrum of 1, 3-cyclohexadiene at a scattering angle of (a) 20° and (b) 80°; 40 eV incident electron energy; 4×10^{-8} A incident beam current; 5 mTorr sample pressure reading from an uncalibrated Schulz-Phelps gauge; resolution approximately 0.12 eV (fwhm). Flat sections in the spectra are the result of computer roundoff.

FIG. 4. Electron energy-loss spectrum of 1, 3-cycloheptadiene at a scattering angle of (a) 20° and (b) 80°; 25 eV incident electron energy; 3×10^{-8} A incident beam current; 4 mTorr sample pressure; resolution approximately 0.09 eV (fwhm). The dashed line represents our estimate for the $S_0 - T_1$ band system profile.

FIG. 5. Electron energy-loss spectra of 1, 3-cyclopentadiene, 1, 3-cyclohexadiene, and 1, 3-cycloheptadiene over the energy-loss region 4 to 10 eV. Experimental conditions for each molecule are those given in the captions of Figs. 2 through 4.

FIG. 6. Relative differential cross sections of 1,3-cyclopentadiene as a function of scattering angle at an incident energy of (a) 30 eV and (b) 50 eV. The elastic DCS was multiplied by 0.1 before plotting. The error bar beneath the heading represents the uncertainty (± 30%) for an inelastic DCS value.

FIG. 7. Same as Fig. 6 except for 1,3-cyclohexadiene at (a) 20 eV and (b) 40 eV. The $N \rightarrow R_{3p}$ is the DCS for the $\pi \rightarrow 3\pi$ Rydberg transition occurring at about 6.3 eV.

FIG. 8. Same as Fig. 6 except for 1,3-cycloheptadiene at (a) 25 eV and (b) 50 eV.

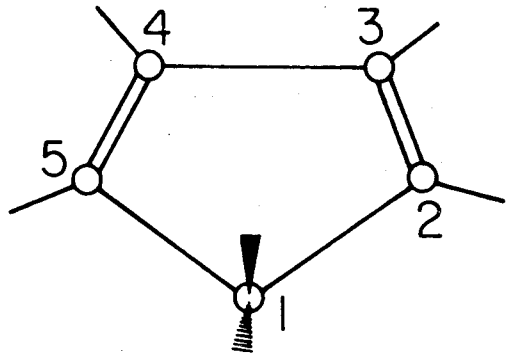

1,3-Cyclopentadiene (C_{2v})

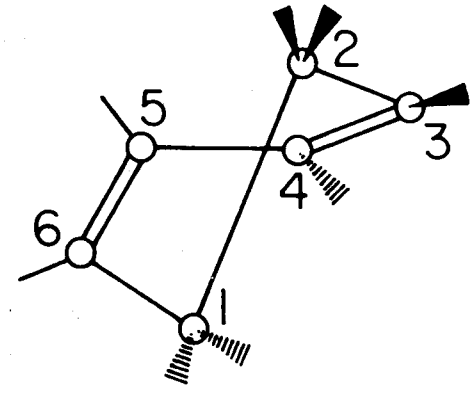

1,3-Cyclohexadiene (C_2)

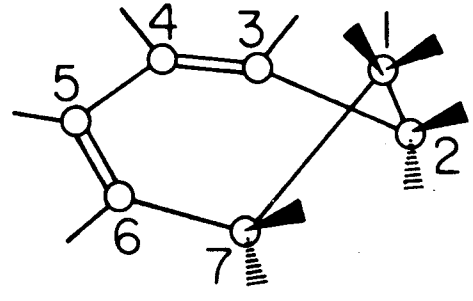

1,3-Cycloheptadiene (C_S)

Figure 1

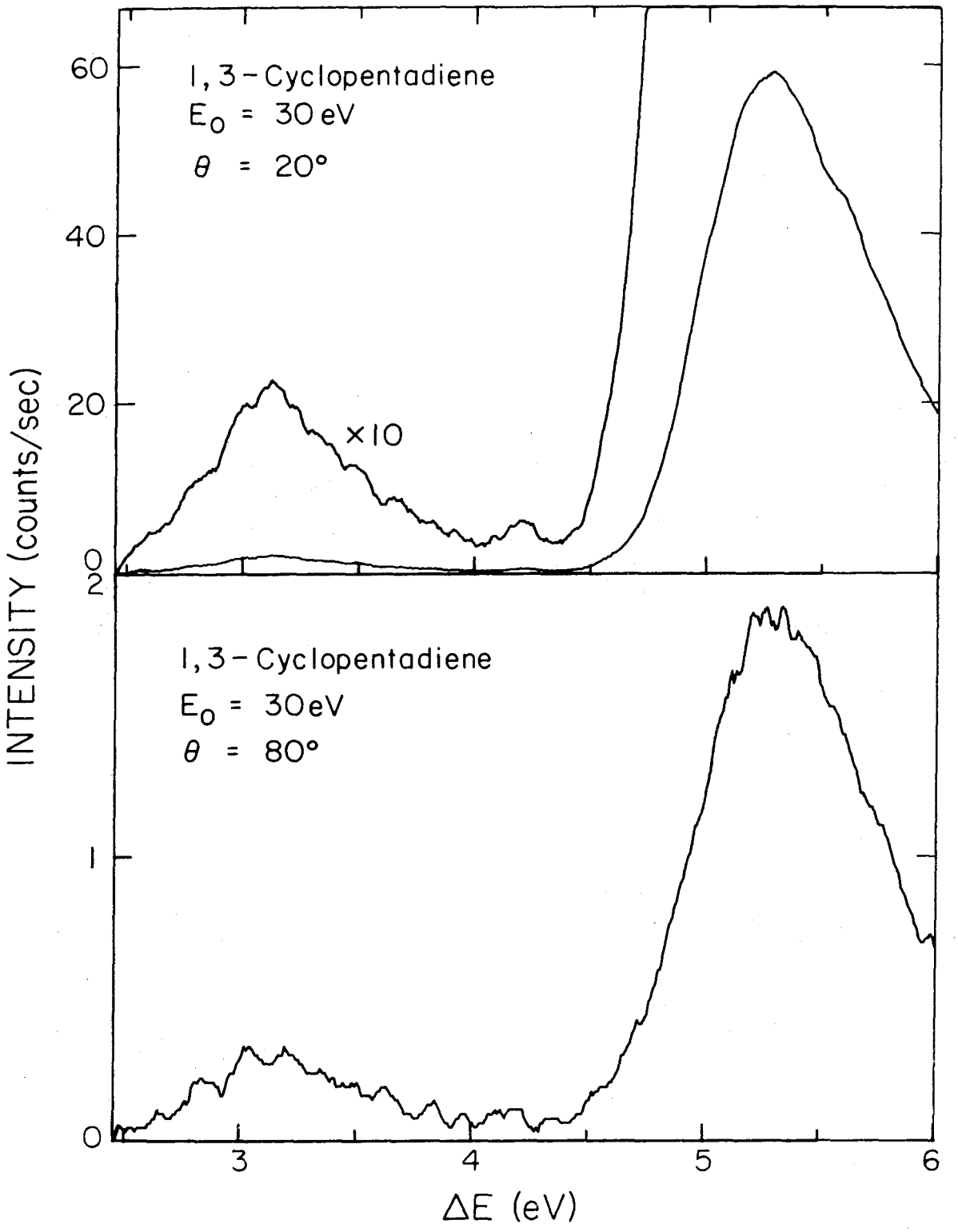
1, 3 - Cyclopentadiene
E_0 = 30 eV
θ = 20°
×10
1, 3 - Cyclopentadiene
E_0 = 30eV
θ = 80°
INTENSITY (counts/sec)
60
40
20
0
2
1
0
3
4
5
6
ΔE (eV)

Figure 2

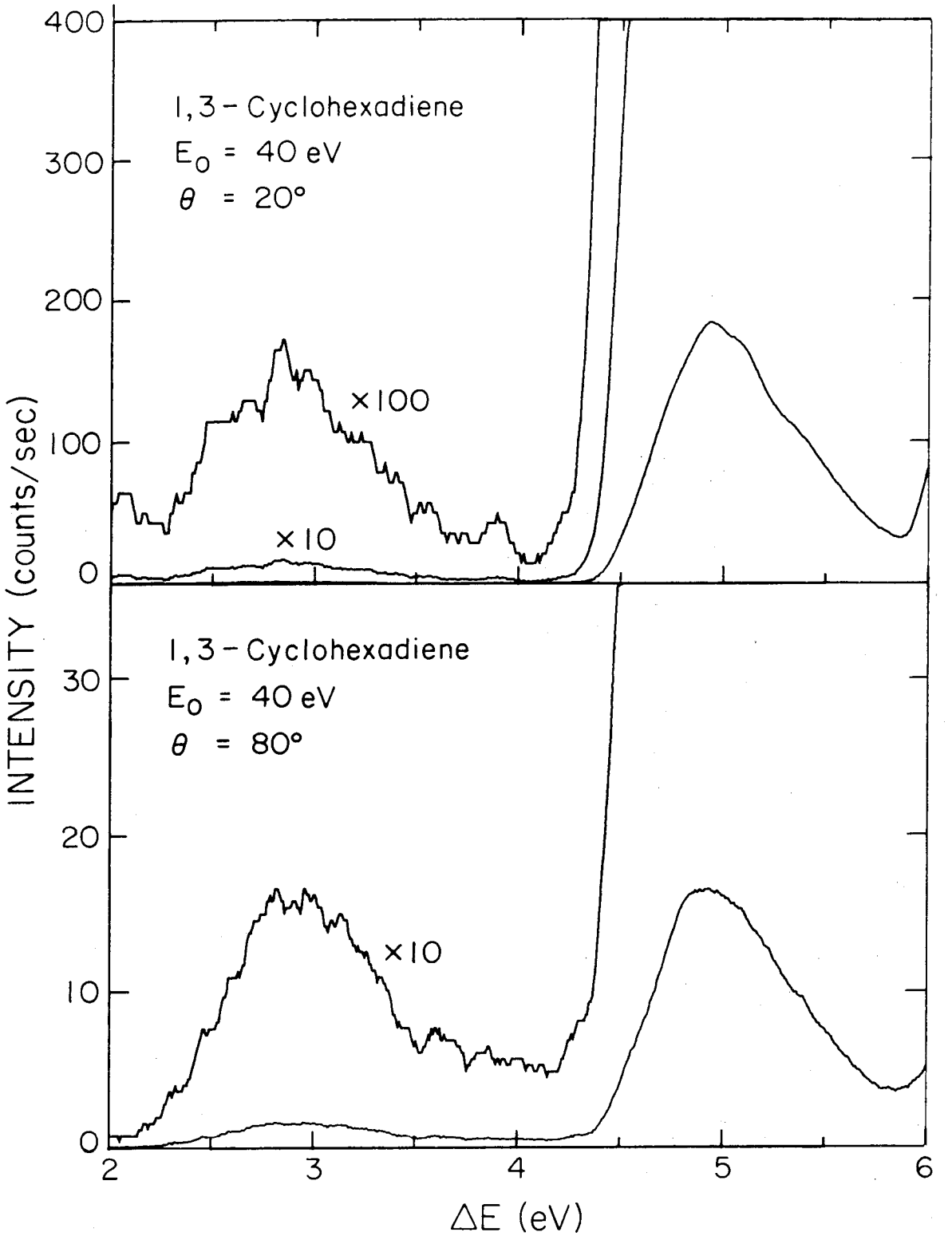
1,3 - Cyclohexadiene
E_0 = 40 eV
θ = 20°
×100
×10
1,3 - Cyclohexadiene
E_0 = 40 eV
θ = 80°
×10
INTENSITY (counts/sec)
ΔE (eV)

Figure 3

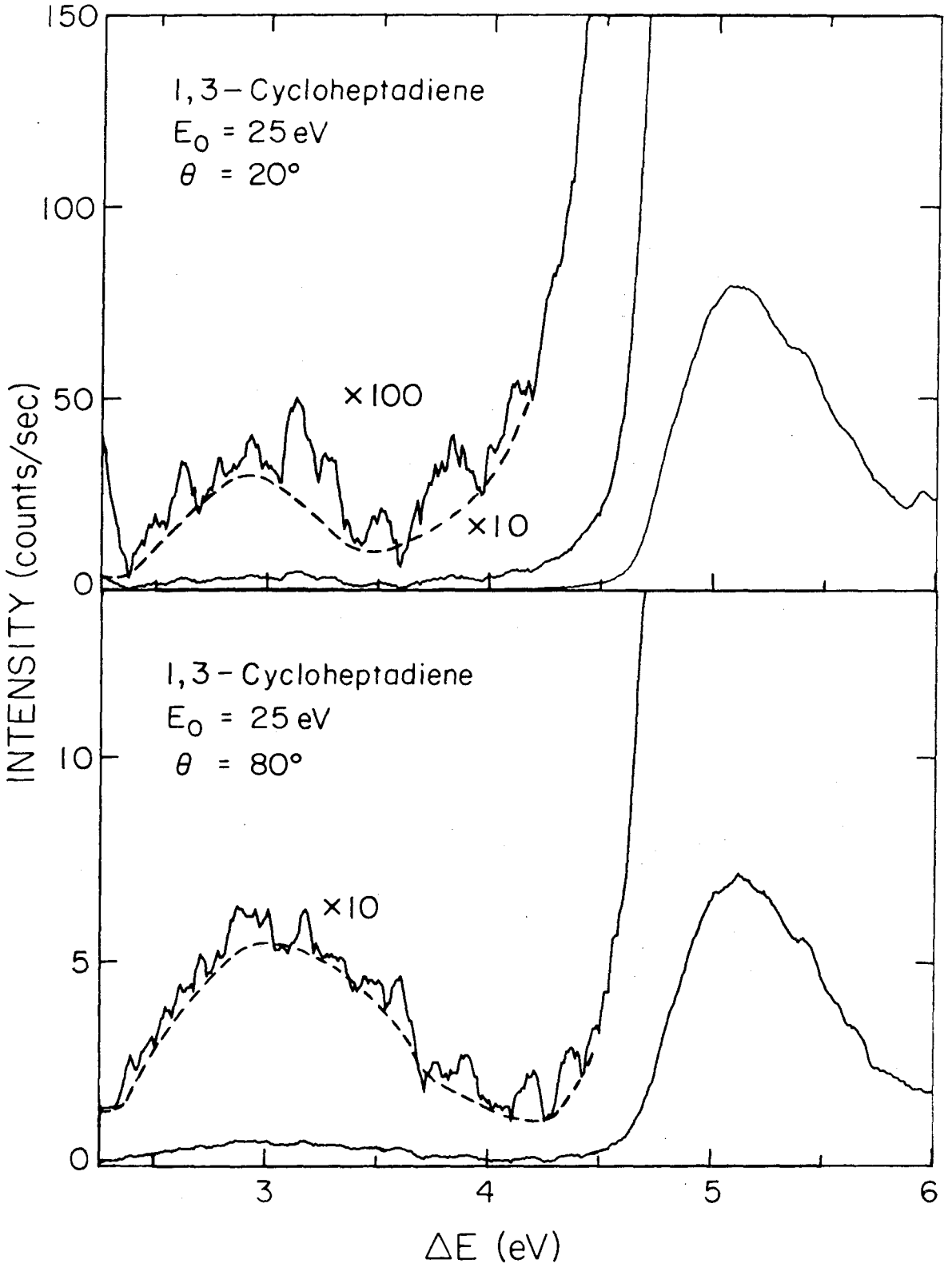
1,3-Cycloheptadiene
E_0 = 25 eV
θ = 20°
×100
×10
1,3-Cycloheptadiene
E_0 = 25 eV
θ = 80°
×10
INTENSITY (counts/sec)
ΔE (eV)
150
100
50
0
10
5
0
3
4
5
6

Figure 4

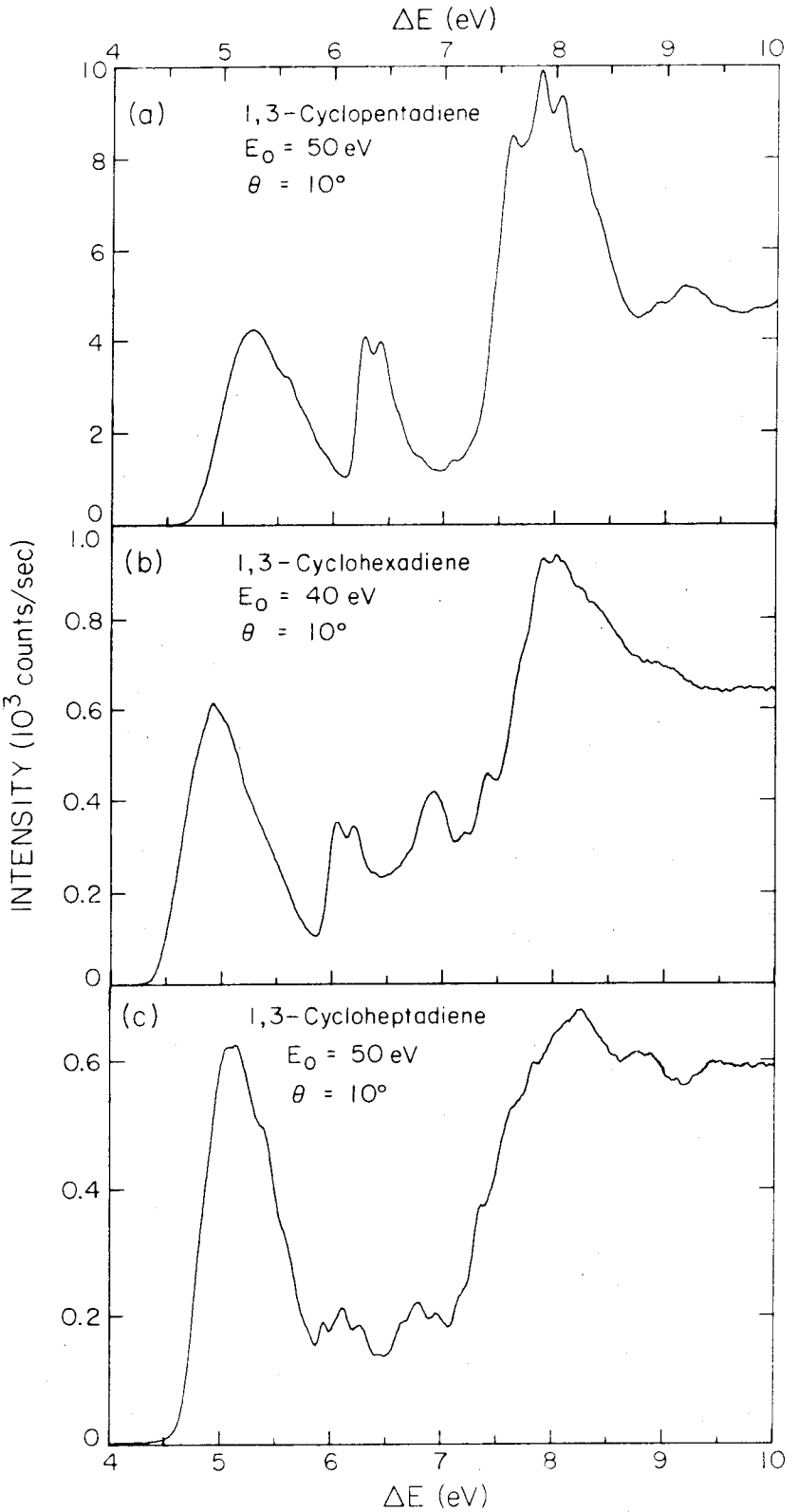
ΔE (eV)
(a) 1,3-Cyclopentadiene
E_0 = 50 eV
θ = 10°
(b) 1,3-Cyclohexadiene
E_0 = 40 eV
θ = 10°
(c) 1,3-Cycloheptadiene
E_0 = 50 eV
θ = 10°
INTENSITY (10^3 counts/sec)
ΔE (eV)

Figure 5

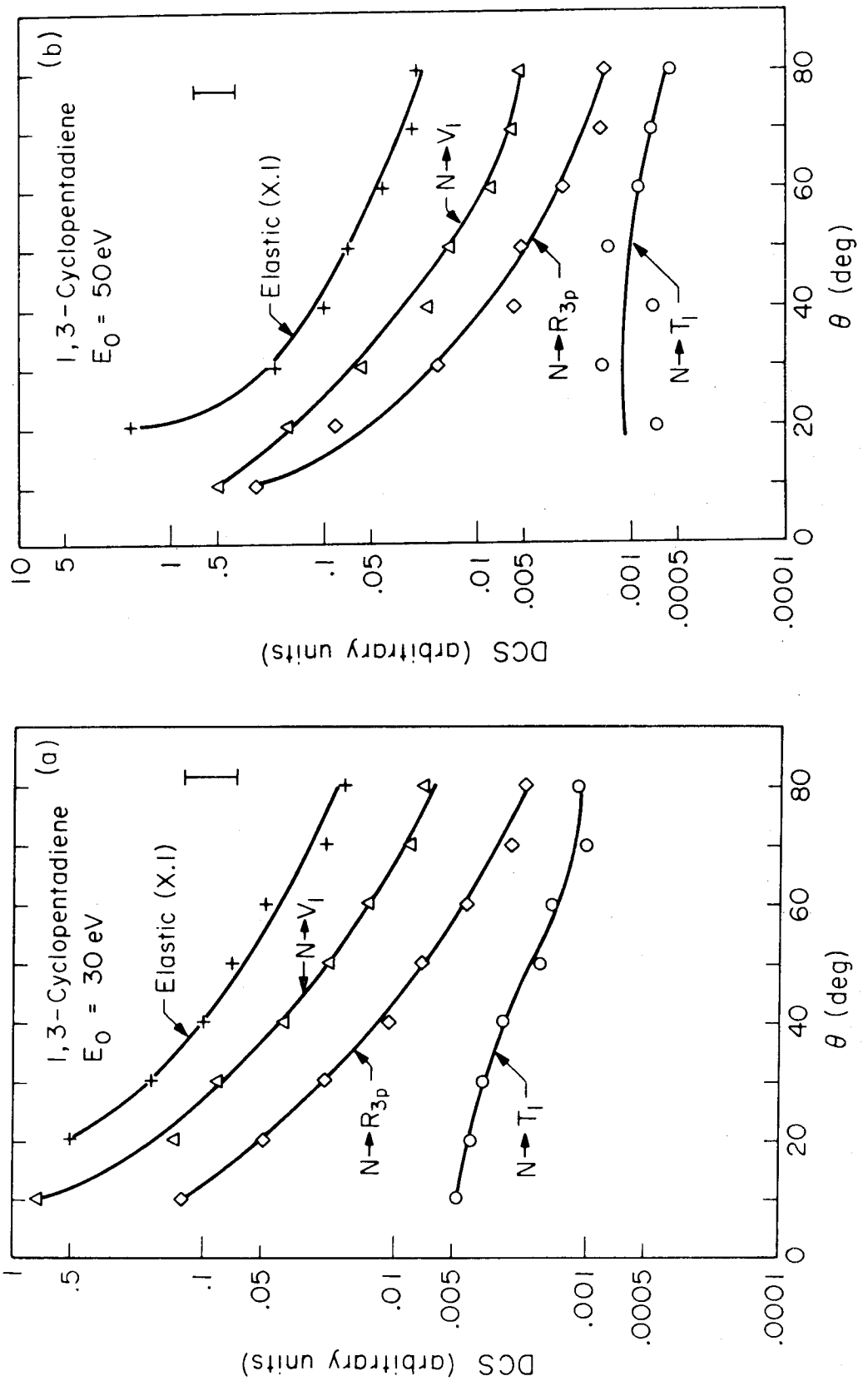
1, 3-Cyclopentadiene
E_0 = 30 eV
(a)
Elastic (X.1)
N→V_1
N→R_{3p}
N→T_1
DCS (arbitrary units)
θ (deg)
1, 3-Cyclopentadiene
E_0 = 50 eV
(b)
Elastic (X.1)
N→V_1
N→R_{3p}
N→T_1
DCS (arbitrary units)
θ (deg)

Figure 6

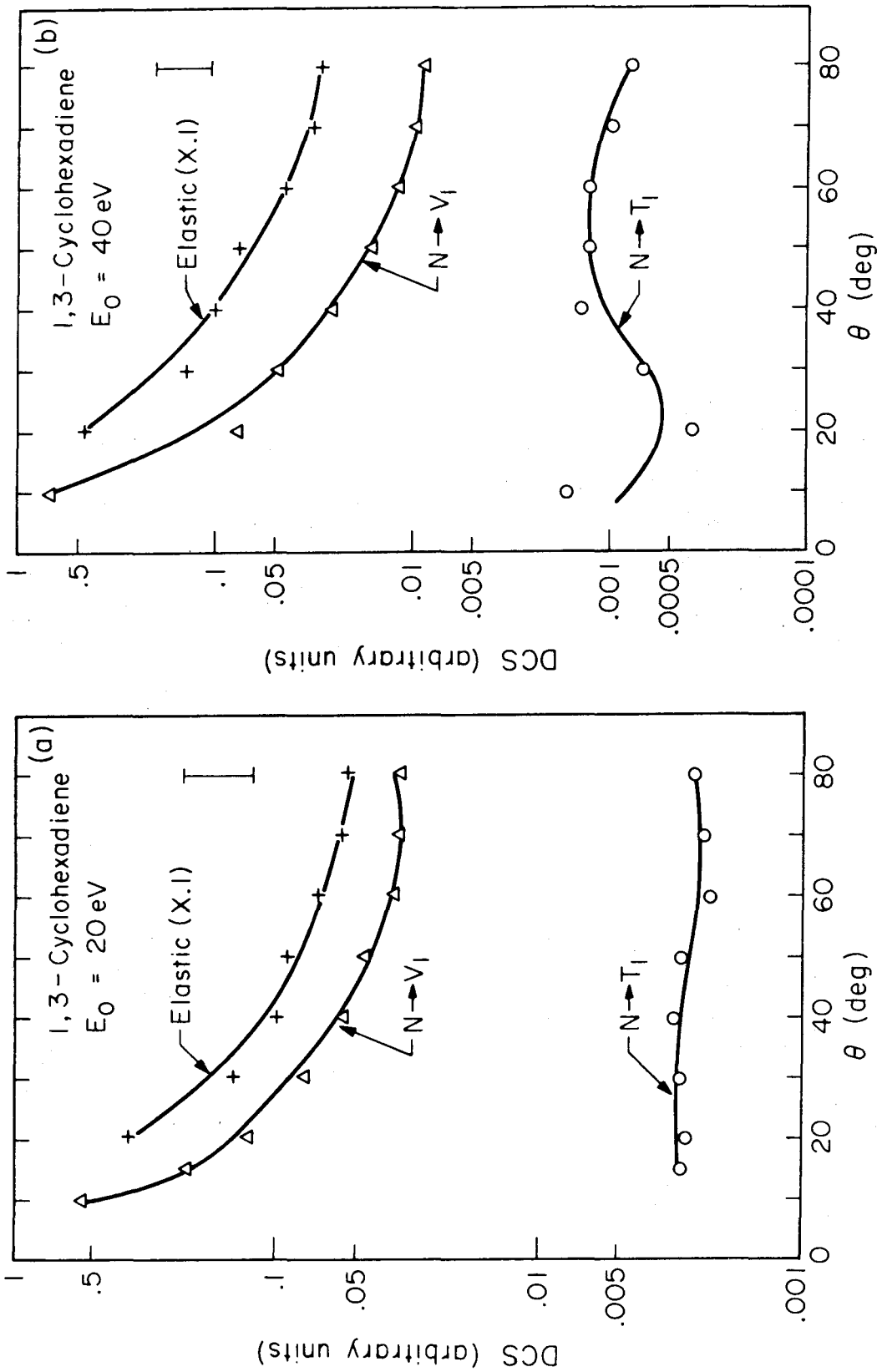
(a)
1,3-Cyclohexadiene
E_0 = 20 eV
Elastic (X.1)
N→V_1
N→T_1
DCS (arbitrary units)
θ (deg)
(b)
1,3-Cyclohexadiene
E_0 = 40 eV
Elastic (X.1)
N→V_1
N→T_1
DCS (arbitrary units)
θ (deg)

Figure 7

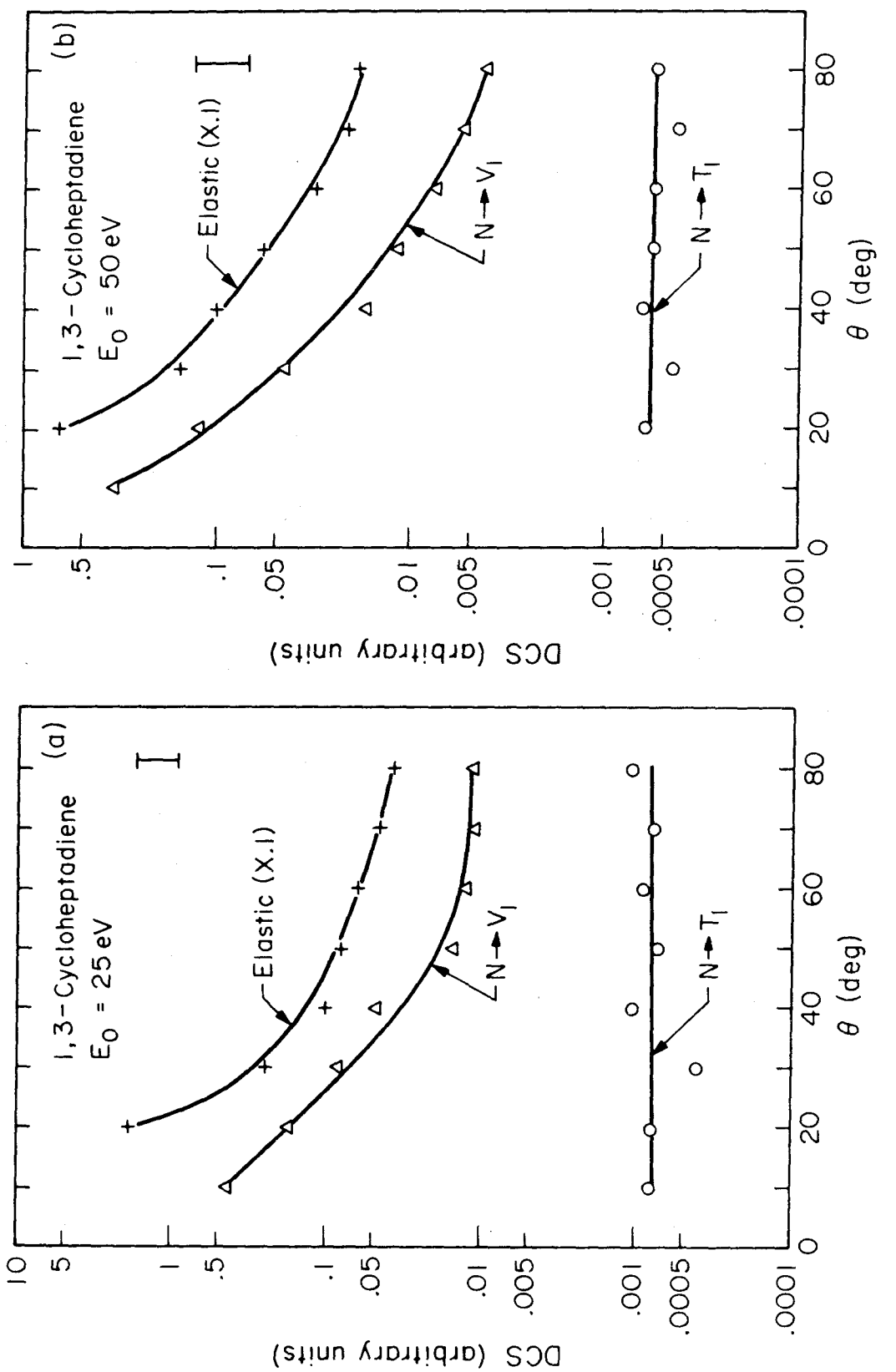
(a)
1,3-Cycloheptadiene
E_0 = 25 eV
Elastic (X.1)
N→V_1
N→T_1
DCS (arbitrary units)
θ (deg)
(b)
1,3-Cycloheptadiene
E_0 = 50 eV
Elastic (X.1)
N→V_1
N→T_1
DCS (arbitrary units)
θ (deg)

Figure 8

4.6 Paper VI: Excited Electronic States of Cyclohexene, 1,4-Cyclohexadiene, Norbornene, and Norbornadiene as Studied by Electron Impact Spectroscopy

Excited electronic states of cyclohexene, 1,4-cyclohexadiene, norbornene and norbornadiene as studied by electron impact spectroscopy[a)]

Robert P. Frueholz,[b)] Wayne M. Flicker,[c)] Oren A. Mosher,[d)] and Aron Kuppermann

Arthur A. Noyes Laboratory of Chemical Physics,[e)]
California Institute of Technology, Pasadena, California 91125

(Received)

The excited electronic states of cyclohexene, 1,4-cyclohexadiene, norbornene (bicyclo[2.2.1]-2-heptene), and norbornadiene (bicyclo-[2.2.1]-2,5-heptadiene) have been studied by electron impact at scattering angles from 5° to 80°, and impact energies of 30 eV and 50 eV. Low-lying features with intensity maxima at 4.24 eV in cyclohexene and 4.10 eV in norbornene are identified as singlet → triplet transitions. Similar features in the spectra of 1,4-cyclo-hexadiene and norbornadiene with intensity extending from 3.4 eV

---

a) This work was supported in part by a contract (EY-76-S-03-767) from the Department of Energy. Report Code: CALT-767P4-173.

b) Work performed in partial fulfillment of the requirements for the Ph.D. degree in Chemistry at the California Institute of Technology.

c) Present address: Harvard-M.I.T. Program in Health Sciences and Technology, Harvard Medical School, Boston, MA 02115.

d) Present address: Eagle Machinery Co., Ltd., 948 - 88th Avenue, Oakland, CA 94621.

e) Contribution No.

to 5.4 eV and 2.9 eV to 4.5 eV, respectively, are believed to result from superposition of two low-lying singlet → triplet transitions in each molecule. For norbornadiene these features have estimated intensity maxima at 3.4 eV and 3.9 eV, while in 1,4-cyclohexadiene they appear to be more highly overlapped, yielding a single intensity maximum at 4.29 eV. The singlet → singlet excited state spectra of these molecules are discussed from the point of view of a model in which ethylene units interact via through-bond and through-space effects. In each of these four molecules, transitions to several super-excited states are observed.

I. INTRODUCTION

Low-energy, variable angle, electron-impact spectroscopy is a powerful technique for studying both optically forbidden and optically allowed electronic transitions.[1,2] Using this technique, we have investigated the electronic spectra of cyclohexene, 1,4-cyclohexadiene, norbornene (bicyclo[2.2.1]-2-heptene), and norbornadiene (bicyclo-[2.2.1]-2,5-heptadiene). In this paper we report the observation of the lowest singlet → triplet transition in each of these molecules and discuss the effects of ground-state molecular geometry on the excited state manifold. This geometry is indicated below.

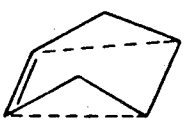

Cyclohexene

1,4 Cyclohexadiene

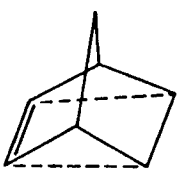

Norbornene

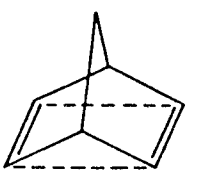

Norbornadiene

All four molecules have a boat-shaped six-membered carbon ring with either one double bond or two double bonds on opposite sides of the planar or nearly planar 4-carbon portion of that ring (indicated

with the help of the dashed lines, which do not represent bonds). In addition, for the norborna- compounds there is a one-carbon, two-bond bridge connecting the two carbons of the six-membered ring on the bow and stern of the boat.

Spectroscopic investigation of both the singlet and triplet excited states of norbornadiene and 1,4-cyclohexadiene permits us to probe the interaction of non-conjugated ethylenic units. These two molecules represent, respectively, systems in which through-space and through-bond interactions are believed to be important.[3,4] Norbornene and cyclohexene have been studied to provide a comparison between the isolated double-bond and the dienyl systems. In addition, the spectra of norbornene and cyclohexene are interesting when compared to those of methyl-substituted ethylenes.[5]

Information about the nature of the excited electronic states observed in an electron-impact spectrum can be obtained by studying the dependence of the intensity of each transition on the impact energy (E_0) and scattering angle (θ).[1,2] In electron-impact spectroscopy at impact energies about 15 eV or more above the excitation threshold, the differential cross sections (DCS's) of transitions which are both electric dipole- and spin-allowed are sharply forward peaked, decreasing by approximately one to two orders of magnitude as the scattering angle increases from 10° to 80°.[1,2] In contrast, transitions involving changes of unity in the molecular spin quantum number, such as singlet → triplet excitations, have a more nearly isotropic DCS over the same angular region.[1,2] Such transitions occur by the mechanism of electron exchange.[6] Excitations which are spin-allowed

but electric dipole-forbidden display DCS's which are forward peaked, but often not as much as fully allowed transitions.[7,8] Finally, for impact energies about 15 eV or more above threshold, optically forbidden processes, and in particular spin-forbidden ones, become more intense with respect to optically allowed ones as the impact energy is lowered.[1,2]

II. EXPERIMENTAL

The apparatus used in this study has been described previously by Kuppermann and coworkers.[1,2] In the present experiments, the electron-impact spectra of cyclohexene, 1,4-cyclohexadiene, norbornene, and norbornadiene in the energy-loss region 0 to 13 volts were studied at impact energies of 30 eV and 50 eV, and scattering angles from 5° to 80°. Sample pressures in the scattering chamber were typically 7 mTorr, as indicated by an uncalibrated Schulz-Phelps ionization gauge, while the incident electron beam current was approximately 100 nA. The energy resolution, as measured by the full width at half maximum (FWHM) of the elastically scattered peak was set at about 0.15 eV. The norbornene and norbornadiene samples were obtained from Aldrich Chemical Company, with stated purities of 99%. Two samples of cyclohexene, from Aldrich Chemical Co. (99% stated purity) and Chemical Sample Co. (99.8% stated purity) were used. Structure due to trace impurities was observed in the cyclohexene spectra at scattering angles less than 20° when using the Aldrich sample. This structure was not present when using the sample

supplied by Chemical Samples Co. Samples of 1,4-cyclohexadiene were obtained from Aldrich Chemical Co. (97% stated purity) and from PCR Inc. (99% stated purity). The sample from Aldrich was used for only a few spectra because a benzene impurity gave a noticeable peak at 6.93 eV. Most of the spectra were taken with the PCR sample where the benzene peak was not discernible. All samples were subjected to several liquid nitrogen freeze-pump-thaw cycles prior to use. The data were analyzed and the DCS values were calculated as described previously.[8]

III. RESULTS AND DISCUSSION

A. Cyclohexene and Norbornene

Figures 1 and 2 show spectra of cyclohexene and norbornene at both low and high scattering angles. These spectra are quite similar to those of the methyl-substituted ethylenes, in which three principal transitions, due to excitations from the carbon double bond, are observed.[5] These three principal kinds of transitions are: $\pi \rightarrow \pi^*$, singlet $\rightarrow$ triplet valence excitations, designated N $\rightarrow$ T; the corresponding $\pi \rightarrow \pi^*$, singlet $\rightarrow$ singlet transitions, designated N $\rightarrow$ V; and $\pi \rightarrow$ 3s Rydberg transitions, designated N $\rightarrow$ R.[5,9] The lowest energy excitations of the two molecules being considered occur with maximum intensity at 4.24 eV in cyclohexene and 4.10 eV in norbornene. Figures 3 and 4 give the DCS's at 30 eV impact energy for several of the transitions observed in their spectra. The DCS's of the 4.24 eV and 4.10 eV excitations are relatively independent of angle. As noted

previously, this behavior allows us to assign them as singlet → triplet transitions. For comparison, the N → T transition intensity maxima in the methyl substituted ethylenes fall between 4.32 eV and 4.10 eV.[5] The excitations presently reported are undoubtedly the analogous $\pi \rightarrow \pi^*$, N → T transitions of cyclohexene and norbornene.

The next detected transition in the cyclohexene spectrum occurs with intensity maximum at 6.11 eV. Upon close study of the low angle spectrum (Fig. 1), three vibronic peaks are observed at 5.92, 6.07, and 6.22 eV. These have been seen optically, and are believed to result from the excitation of zero, one, and two quanta of C=C vibrations.[10] Initially this transition was assigned by Potts[11] as the N → T excitation; however, subsequent optical studies, involving the effects of high pressure nitrogen performed by Evans,[12] led to the $\pi \rightarrow 3s$, N → R, Rydberg assignment. Our results leave no doubt as to the singlet → singlet nature of this transition: the DCS of this feature, shown in Fig. 3, is sharply forward peaked.

The most intense feature in both the cyclohexene and norbornene spectra is the N → V transition occurring respectively at 6.85 eV and 6.35 eV in these two molecules. These transitions, as expected for singlet → singlet excitations, have sharply forward peaked DCS's. The positions of their intensity maxima are in good agreement with optical studies which give energies of 6.79 eV for cyclohexene[11] and 6.34 eV for norbornene.[13] In cyclohexene shoulders appear on both the low and high energy sides of the N → V transition. These are most likely either vibronic components of the N → V transition or

superimposed Rydberg structure. At higher energies additional transitions, which appear to be singlet → singlet in nature, are observed in both molecules; they are listed in Table I. The exact nature of those excitations is unknown; it seems likely that they are elements of various Rydberg series converging to the first and higher ionization potentials. In norbornene, optical studies with inherently higher resolution than our electron impact spectra, reveal a sharp absorption at 48,150 cm^{-1} (5.97 eV) followed by a second peak 280 cm^{-1} higher in energy.[13] These have been assigned to the $\pi \rightarrow 3s$ Rydberg transition.[10] We do not observe these features.

It is interesting to note that while the N → R transitions in norbornene and cyclohexene occur at 5.97 and 6.07 eV, respectively, and have nearly identical term values of 3.00 eV and 3.05 eV, the N → V transition intensity maxima differ by 0.50 eV. It seems that in norbornene the excited state is stabilized relative to the ground state as compared to cyclohexene. This stabilization cannot be presently explained and further theoretical studies would be desirable.

B. 1,4-cyclohexadiene and norbornadiene

1. Introduction

When discussing the spectroscopy of these molecules the interaction of the ethylenic units must be considered. Hoffmann and coworkers[3,4] give a summary of the interactions of orbitals through space and through bonds. When the geometry of a molecule permits direct spatial overlap of the orbitals on each of the chromophores the interaction is of the through-space type. Norbornadiene provides an

example of this form of interaction.[3,4] It splits both sets of degenerate π and π^* orbitals of the isolated ethylenic moieties. This splitting is evidenced by a comparison of the vertical π ionization potential of norbornene, 8.97 eV[14] and the vertical π ionization potentials of norbornadiene, 8.69 eV and 9.57 eV.[14]

The through-space interaction is expected to be small in 1,4-cyclohexadiene because the molecule is almost planar. The dihedral angle of 1,4-cyclohexadiene is 159.3°[15] compared to 115.6° for norbornadiene.[16] This near planar geometry gives poor direct overlap between the p-type π orbital lobes. However, a through-bond interaction, via hyperconjugative effects of the σ_{CH} bonds, can couple the ethylenic π systems. This through-bond interaction leads to two separate π ionization potentials. Indeed, whereas the lowest (vertical) π ionization potential of cyclohexene is 9.12 eV, the corresponding photoelectron state in 1,4-cyclohexadiene splits into two levels at 8.80 eV and 9.80 eV.[3]

The effects of these interactions are expected to manifest themselves in the electronic spectrum of norbornadiene and 1,4-cyclohexadiene (Figs. 5-7). The resulting spectra should be significantly different from their monoethylenic counterparts. Following the simple procedure used by Mulliken[17] in discussing the spectra of cis- and trans-1,3-butadiene, in the first approximation the interaction of the two ethylenic units should result in four molecular orbitals. In the C_{2v} point group of 1,4-cyclohexadiene and norbornadiene these orbitals belong, in order of increasing orbital energy, to the A_1, B_1, A_2, and B_2 irreducible representations. In the ground state both the a_1 (π_1) and b_1 (π_2)

orbitals are doubly-occupied. Four excited singlet states result by excitation of single electrons to the a_2 and b_2 orbitals belonging, in order of increasing energy, to the irreducible representations A_2, B_2, B_2, and A_2. Transitions from the ground state (A_1) to the A_2 states are symmetry forbidden while transitions to the B_2 states are symmetry allowed. Mulliken[17] has designated these transitions, in order of increasing energy, as $N \rightarrow V_1$, V_2, V_3, V_4. Four corresponding excited triplet states should also occur.

Unfortunately a correlation between these simple ideas and our experimental results will be shown to be difficult to establish. One source of difficulty is the possibility of other transitions in addition to those within the π system. Transitions to Rydberg excited states are observed and $\sigma \rightarrow \pi^*$ transitions may also be possible.

2. Singlet – triplet transitions

The lowest energy feature in the spectrum of norbornadiene has an apparent Franck-Condon region extending from 2.9 eV to 4.5 eV. As shown in Fig. 8, the DCS of this feature (labeled $T_1 + T_2$) is nearly isotropic. It is also observed that the intensity of this feature relative to the remainder of the spectrum, becomes more intense at a given scattering angle as the impact energy is lowered. This behavior is characteristic of a singlet – triplet transition. The band shape of this feature (Fig. 5) seems to indicate the presence of two overlapping singlet – triplet transitions. We estimate the locations of the intensity maxima of these transitions to be approximately 3.4 eV and 3.9 eV, yielding a splitting between the two lowest triplet states of norborna-

diene, T_1 and T_2, of about 0.5 eV. This splitting seems reasonable when we remember that the interaction of the two ethylenic units resulted in two π ionization potentials of 8.69 eV and 9.57 eV.[3] The feature occurring between 2.9 eV and 4.5 eV in the spectrum of norbornadiene is therefore suggested to be due to the superposition of the $N \rightarrow T_1$ and $N \rightarrow T_2$, singlet $\rightarrow$ triplet transitions.

The lowest feature in the 1,4-cyclohexadiene spectrum extends from 3.4 eV to 5.4 eV with maximum intensity occurring at 4.29 eV. The DCS of this feature (see Fig. 9, $T_1 + T_2$ curve) varies by about a factor of 3 over the angular range 10° to 80°. This behavior is characteristic of a spin-forbidden transition. This feature could be due to a single transition. However, the two lowest π ionization potentials for 1,4-cyclohexadiene are split by about 1.0 eV. This fact and the splitting of the two lowest triplets in norbornadiene, suggest that this low-lying 1,4-cyclohexadiene feature may be due to the superposition of the $N \rightarrow T_1$ and $N \rightarrow T_2$ singlet $\rightarrow$ triplet transitions, having approximately equal intensity, and split by about 0.3 eV to 0.4 eV. Brongersma[18] has also observed this feature with intensity maxima occurring at 4.3 eV. The experimental results are in fair agreement with the theoretical calculations of Allinger et al.[19] which place the lowest triplet state of 1,4-cyclohexadiene at 4.07 eV.

3. Singlet $\rightarrow$ singlet transitions

The next feature in the spectrum of 1,4-cyclohexadiene has an intensity maximum at 6.15 eV. The DCS of this transition, (Fig. 9), is forward peaked, indicating that it is a singlet $\rightarrow$ singlet excitation.

This feature is also observed in the optical spectrum at 6.20 eV,[19] in the threshold electron impact spectrum at 6.3 eV,[18] and in high impact energy electron impact at 6.23 eV.[20] The theoretical calculations of Allinger et al.[19] predict a forbidden, $\pi \rightarrow \pi^*$, singlet → singlet transition at 6.42 eV. The intensity of this feature relative to the fully allowed transition occurring at 7.95 eV is consistent with this assignment. The possibility also exists that this could be a $\pi_2 \rightarrow$ 3s Rydberg transition similar to the N → R excitation observed in cyclohexane and norbornene. The term value of this excitation (IP-Excitation energy), 21,300 cm^{-1} (2.64 eV), is consistent with that expected for a 3s Rydberg transition.[21] Superimposed on the low energy side of the 7.95 eV feature is weak structure. This also may be due to transitions to Rydberg-like excited states.

The most intense feature found in 1,4-cyclohexadiene occurs at 7.95 eV. The DCS of this transition at 30 eV impact energy (see Fig. 9) decreases by a factor of 27 as the scattering angle increases from 10° to 80°. This sharply forward peaked behavior is characteristic of a fully allowed excitation. As discussed earlier in this section, this feature probably does not correspond to the first $\pi \rightarrow \pi^*$ transition, which is expected to be symmetry forbidden. It may instead be the second or third $\pi \rightarrow \pi^*$ transition. This transition is observed at 8.1 eV in the threshold electron impact spectrum[18] and 7.9 eV in the high incident energy electron impact spectrum.[20] The only available theoretical calculations are those of Allinger et al.,[19] which predict that the lowest optically allowed $\pi \rightarrow \pi^*$ transition should occur at

7.37 eV. This is in relatively poor agreement with the experimental results.

The singlet-state spectrum of norbornadiene is as complicated as that of 1,4-cyclohexadiene. The intensity maximum of the first singlet → singlet transition in our norbornadiene spectra occurs at 5.23 eV (Figs. 5 and 6). Unlike the optical spectrum, where only a shoulder is observed at 5.4 eV,[22] we detect a well defined peak. Figure 8 shows that the DCS of this transition is sharply forward peaked, indicating its singlet → singlet nature. The assignment of this excitation is uncertain. Its term value, 30,000 cm^{-1} (3.72 eV) is large enough to rule out the possibility of a Rydberg identification. A semi-empirical Pariser-Parr type calculation by Hermann[23] places the lowest $\pi \rightarrow \pi^*$ transition at 5.50 eV, while a second calculation using different empirical parameters increases this excitation energy to 5.98 eV. It seem reasonable to suggest that this is the lowest $\pi \rightarrow \pi^*$, symmetry-forbidden, $\tilde{X}\ ^1A_1 \rightarrow {}^1A_2$ excitation predicted by simple arguments. If this is the case, this excitation is probably analogous to the feature occurring at 6.15 eV in the 1,4-cyclohexadiene spectrum.

The next feature in the present norbornadiene spectra occurs at 5.95 eV. Its DCS behavior with respect to angle indicates that it is a singlet → singlet transition. Robin and Kuebler[24, 25] have observed it optically at 5.89 eV. Their vibronic study indicates that this is an

allowed transition. The effects of high pressure helium on the optical spectrum and the characteristics of its rare gas matrix spectrum and neat film low temperature spectrum indicate that this feature is due to a Rydberg transition, most likely the $\pi_2 \rightarrow 3s$ excitation. Its term value is 21,700 cm^{-1} (2.74 eV).

This assignment of the 5.95 eV transition in norbornadiene as $\pi_2 \rightarrow 3s$ has implications for the interpretation of the 6.15 eV transition in 1,4-cyclohexadiene. The similarity between the term values for the $\pi \rightarrow 3s$ Rydberg transitions in cyclohexene and norbornene suggest an equivalent similarity between cyclohexadiene and norbornadiene. The lowest π ionization potential in 1,4-cyclohexadiene is 8.80 eV, which is 2.65 eV above the 6.15 eV transition. At the beginning of the present sub-section we suggested the possibility that the latter was due to a $\pi_2 \rightarrow 3s$ Rydberg excitation. It is seen that this is consistent with the 2.74 eV term value for the corresponding $\pi_2 \rightarrow 3s$ excitation in norbornadiene.

In the same excitation energy region, Robin and Kuebler[25] found that underlying the $\pi_2 \rightarrow 3s$ Rydberg transition in norbornadiene was a second transition which they assigned as the lowest $\pi \rightarrow \pi^*, N \rightarrow V_1$ excitation. This assignment must be viewed with care for two reasons. First, they also observed similar structure underlying the $N \rightarrow V$ transition in norbornene, for which no additional $\pi \rightarrow \pi^*$ transition is expected. Secondly, if this underlying excitation is indeed $\pi \rightarrow \pi^*$ in nature it is more likely the $N \rightarrow V_2$ ($\tilde{X}\,^1A_1 \rightarrow {}^1B_2$) transition, because, as indicated above, the $N \rightarrow V_1$ ($\tilde{X}\,^1A_1 \rightarrow {}^1A_2$) transition probably occurs at 5.23 eV in norbornadiene.

The most intense feature in the norbornadiene spectrum has an intensity maximum at 6.85 eV and also exhibits a DCS characteristic of a singlet → singlet transition. This excitation is also observed optically at 6.88 eV.[24] It is probably related to the symmetry allowed N → V_3 ($\tilde{X}^1A_1 \rightarrow {}^1B_2$) transition. Hermann's[23] calculations place an $\tilde{X}^1A_1 \rightarrow {}^1B_2$ transition at 7.13 eV or 6.61 eV depending on the choice of parameters. These energies are consistent with the observed value.

We also observe structure superimposed on top of the 6.85 eV feature. More detailed vibronic structure is detected in the optical spectrum.[24] It is probably due to a superimposed Rydberg excitation whose term value with respect to the first π ionization potential is 14,800 cm^{-1}. This value does not seem to be consistent with this structure being part of either an s or p Rydberg series converging to the first I.P. However, the term value with respect to the second π ionization potential of norbornadiene is 21,900 cm^{-1}. This value is quite similar to the $\pi_2 \rightarrow 3s$ term values and hence a possible assignment of this structure is the $\pi_1 \rightarrow 3s$ Rydberg transition. We might expect a similar transition to occur in the 1,4-cyclohexadiene spectrum. Using the 21,900 cm^{-1} term, the $\pi_1 \rightarrow 3s$ transition would be expected to be present about 7.08 eV. Examination of 1,4-cyclohexadiene's spectrum reveals two weak features at 7.1 eV and 7.3 eV. These features may be due to vibronic components of the $\pi_1 \rightarrow 3s$ Rydberg excitation. Finally a weak feature in 1,4-cyclohexadiene occurring at 6.4 eV with a term value, relative to the first ionization potential of 19,300 cm^{-1} may be the $\pi_2 \rightarrow 3p$ Rydberg feature. Several additional excitations in both 1,4-cyclohexadiene and norbornadiene occur at energy-losses

above that of their most intense feature. The corresponding positions are listed in Table I. These relatively weak peaks are probably elements of Rydberg series converging to the first or higher ionization potentials.

There are similarities between the supposed valence singlet → singlet portions of the spectra of 1,4-cyclohexadiene and norbornadiene. If the spectrum of norbornadiene is shifted upwards by approximately 1 eV it becomes similar to the spectrum of 1,4-cyclohexadiene. This similarity would be expected if the simple model of interacting ethylene units is valid. The upward shift seems to indicate that the valence-excited states of norbornadiene are somewhat stabilized with respect to those of 1,4-cyclohexadiene. This behavior is similar to the lowering of the N → V transition energy by 0.5 eV in going from cyclohexene to norbornene. The stabilization of the norbornadiene levels with respect to the 1,4-cyclohexadiene ones, as well as that of the norbornene levels with respect to the cyclohexene ones is not readily explained. Appropriate theoretical studies of these systems would be useful.

IV. SUMMARY AND CONCLUSION

The band shapes and locations of the lowest singlet → triplet transitions in each of the four molecules studied have been obtained. In norbornadiene and 1,4-cyclohexadiene the features occurring of the lowest excitation energies are believed to be the result of the superposition of two singlet → triplet transitions. For norbornadiene these

features have estimated intensity maxima occurring at 3.4 eV and 3.9 eV. The singlet state spectra have also been discussed in terms of interacting ethylenic units. While the lower excitation energy region of norbornene and cyclohexene is fairly well understood, the equivalent region in the spectrum of norbornadiene and 1,4-cyclohexadiene is not. The states of norbornene and norbornadiene are stabilized with respect to the corresponding states in cyclohexene and 1,4-cyclohexadiene by about 0.5 eV and 1.0 eV, respectively. This stabilization is not presently understood.

TABLE I. Transition energies of cyclohexene, norbornene, 1,4-cyclohexadiene, and norbornadiene[a]

	N → T	N → R	N → V	Additional Singlet → Singlet transitions
Cyclohexene	4.24(3.4-5.3)[b]	5.92[c], 6.07[c], 6.22[c]	6.85	7.40, 8.10, 8.40, 8.93, 9.50, 10.35
		(6.10)[d]	(6.79)[e]	11.07, 11.85, 12.15, 13.60, 13.95
				14.65
Norbornene	4.10(3.4-5.1)[b]		6.35	7.4, 8.25, 8.97, 9.62, 10.3, 11.90
		(5.97)[f]	(6.34)[f]	12.8

	$N \rightarrow T_1 + T_2$	$N \rightarrow V_1/\pi_2 \rightarrow 3s$	$N \rightarrow V_2$ $\pi_2 \rightarrow 3p$	$\pi_1 \rightarrow 3s$	$N \rightarrow V_3$	
1,4-Cyclohexadiene	4.29(3.4-5.4)[b]	6.15	6.4	7.1[c], 7.3[c]	7.95	9.00, 9.25, 9.90, 10.30, (10.14)[h], (10.45)[h]
	(4.3)[g]	(6.20)[g]			(8.1)[g]	11.30, 12.05, 12.95
						(11.3)[h] (12.0)[h] (13.0)[h]

	$N \rightarrow T_1 + T_2$	$N \rightarrow V_1$	$N \rightarrow V_2/\pi_2 \rightarrow 3s$	$N \rightarrow V_3/\pi_1 \rightarrow 3s$	
Norbornadiene	3.4, 3.9	5.23	5.95	6.85	7.2, 7.5, 7.9, 8.8, 9.8
	(2.9-4.5)[b]	(5.39)[i]	(5.89)[i]	(6.88)[j]	10.4, 11.45, 13.0

[a] Transition energies listed correspond to intensity maxima. The estimated accuracy of these values is ± 0.05 eV.

[b] Apparent Franck-Condon region observed in present study.

[c] These are believed to be vibronic components of the same electronic transition.

[d] Reference 10.

[e] Reference 11.

[f] Reference 13.

[g] Reference 20.

[h] Reference 22.

[i] Appears as a shoulder in the optical spectrum of Ref. 24.

[j] Reference 26.

References

1. A. Kuppermann, J. K. Rice, and S. Trajmar, J. Phys. Chem. 72, 3894 (1968).
2. A. Kuppermann, W. M. Flicker, and O. A. Mosher, Acc. Chem. Res., submitted for publication.
3. R. Hoffmann, E. Heilbronner, and R. Gleiter, J. Am. Chem. Soc. 92, 706 (1970).
4. R. Hoffmann, Acc. Chem. Res. 4, 1 (1971).
5. W. M. Flicker, O. A. Mosher, and A. Kuppermann, Chem. Phys. Lett. 36, 56 (1975).
6. J. R. Oppenheimer, Phys. Rev. 32, 361 (1928).
7. D. C. Cartwright, W. J. Hunt, W. Williams, S. Trajmar and W. A. Goddard III, Phys. Rev. A 8, 2436 (1973).
8. O. A. Mosher, W. M. Flicker, and A. Kuppermann, J. Chem. Phys. 62, 2600 (1975).
9. A. J. Merer and R. S. Mulliken, Chem. Rev. 69, 639 (1969).
10. M. B. Robin, Higher Excited States of Polyatomic Molecules (Academic Press, New York, 1975), Vol. I, pp. 20-40.
11. W. J. Potts, Jr., J. Chem. Phys. 23, 65 (1955).
12. D. F. Evans, Proc. Chem. Soc. Lond. 378 (1963).
13. S. Stokes and L. W. Pickett, J. Chem. Phys. 23, 258 (1955).
14. P. Bischof, J. A. Hoshmall, E. Heilbronner, and V. Hornung, Helv. Chim. Acta 52, 110 (1969).
15. H. Oberhammer and S. H. Bauer, J. Am. Chem. Soc. 91, 10 (1969).

16. A. Yokozeki and K. Kuchitsu, Bull. Chem. Soc. Jap. 44, 2356 (1971).

17. R. S. Mulliken, J. Chem. Phys. 7, 121 (1939).

18. H. H. Brongersma, Ph.D. Thesis, University of Leiden, Leiden, The Netherlands (1968), pp. 52-54.

19. N. L. Allinger, J. Chow Tai, and T. W. Stuart, Theor. Chim. Acta 8, 101 (1967).

20. U. Killat, Z. Phys. 270, 169 (1974).

21. M. B. Robin, Higher Excited States of Polyatomic Molecules (Academic Press, New York, 1974), Vol. I, p. 29.

22. B. C. Roquitte, J. Phys. Chem. 69, 2475 (1965).

23. R. B. Hermann, J. Org. Chem. 27, 441 (1962).

24. M. B. Robin and N. A. Kuebler, J. Chem. Phys. 44, 2664 (1966).

25. M. B. Robin and N. A. Kuebler, J. Mol. Spectrosc. 33, 274 (1970).

Figure Captions

Figure 1. Electron energy-loss spectrum of cyclohexene at scattering angles of 10° and 70°, 30 eV incident electron energy; 6×10^{-8} Å incident beam current; 6×10^{-3} torr sample pressure as indicated by an uncalibrated Schulz-Phelps ionization gauge.

Figure 2. Electron energy-loss spectrum of norbornene at scattering angles of 20° and 70° at scattering; 30 eV incident electron energy; 7×10^{-8} Å incident beam current; 8×10^{-3} torr sample pressure as indicated by an uncalibrated Schulz-Phelps ionization gauge.

Figure 3. Relative elastic and inelastic differential cross sections for cyclohexene at an incident electron energy of 30 eV. These differential cross sections are in arbitrary units set by normalizing the elastic differential cross section to 1.0 at 40°. The arbitrary units for all transitions of a given molecule at a particular impact energy are the same. The arbitrary units are not the same for different molecules or the same molecule at different impact energies. The error bar beneath the heading represents the uncertainty (± 30%) for an inelastic DCS value.

Figure 4. Relative elastic and inelastic differential cross sections for norbornene at an incident electron energy of 30 eV. The normalization procedure for the arbitrary ordinate units is the same as for Fig. 3. The error bar beneath the heading represents the uncertainty (± 30%) for an inelastic DCS value.

Figure 5. Electron energy-loss spectrum for norbornadiene at scattering angles of 30° and 70°; 30 eV incident energy; 9×10^{-8} Å incident beam current; 8×10^{-3} torr sample pressure as indicated by an uncalibrated Schulz-Phelps ionization gauge.

Figure 6. Electron energy-loss spectrum for norbornadiene at a scattering angle of 20° and 50 eV incident energy. Experimental conditions as described in Fig. 5.

Figure 7. Electron energy-loss spectrum for 1,4-cyclohexadiene at scattering angles of 20° and 80°; 30 eV incident electron energy; 4×10^{-8} Å incident beam; 6×10^{-3} torr sample pressure as indicated by an uncalibrated Schulz-Phelps ionization gauge.

Figure 8. Relative elastic and inelastic differential cross sections for norbornadiene at an incident electron energy of 30 eV. The normalization procedure for the arbitrary ordinate units is the same as for Fig. 3. The error bar beneath the heading represents the uncertainty (± 30%) for an inelastic DCS value.

Figure 9. Relative elastic and inelastic differential cross sections for 1,4-cyclohexadiene at an incident electron energy of 30 eV. The normalization procedure for the arbitrary ordinate units is the same as for Fig. 3.

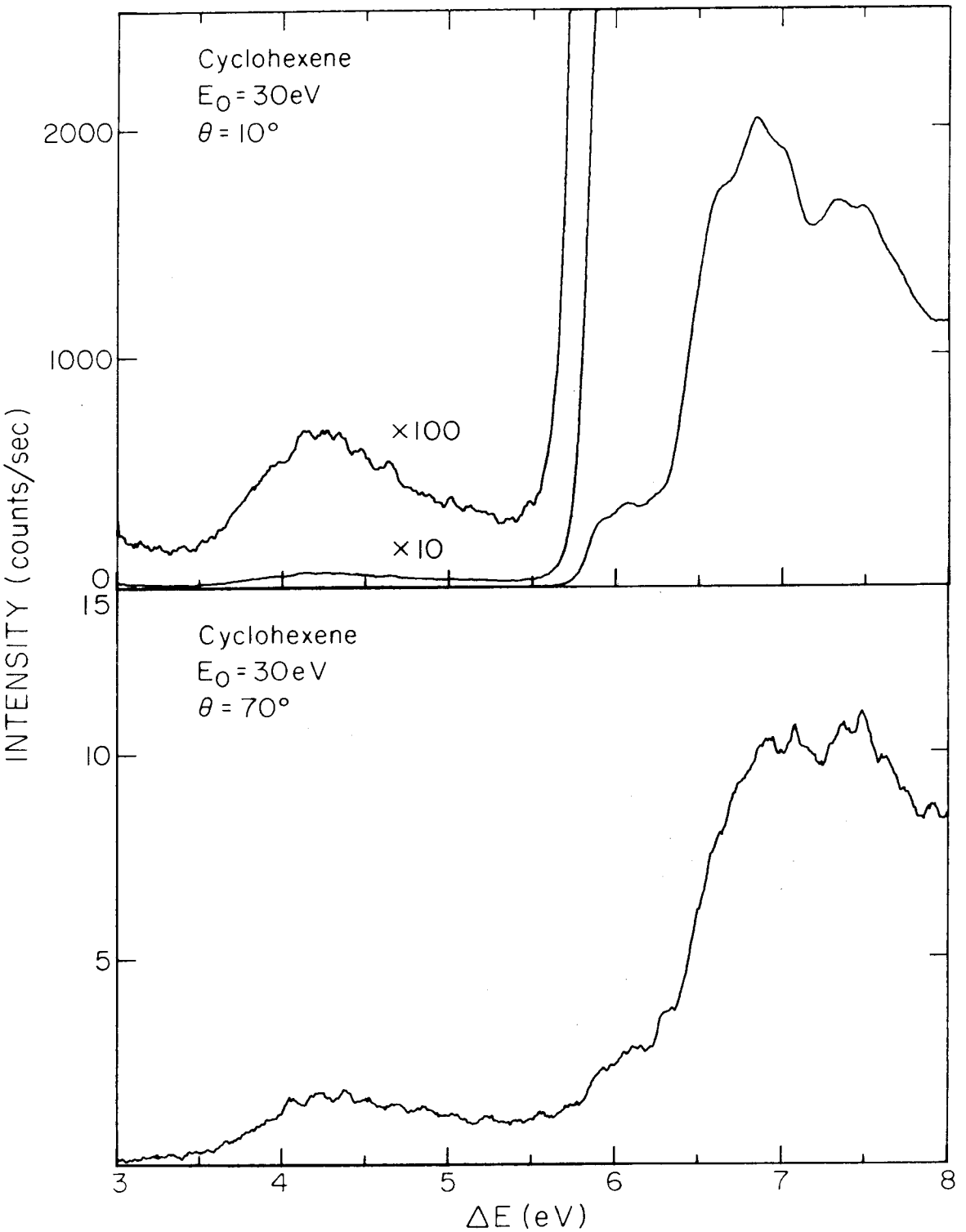
Cyclohexene
E_0 = 30eV
θ = 10°
2000
1000
0
×100
×10
Cyclohexene
E_0 = 30eV
θ = 70°
15
10
5
3
4
5
6
7
8
ΔE (eV)
INTENSITY (counts/sec)

Figure 1

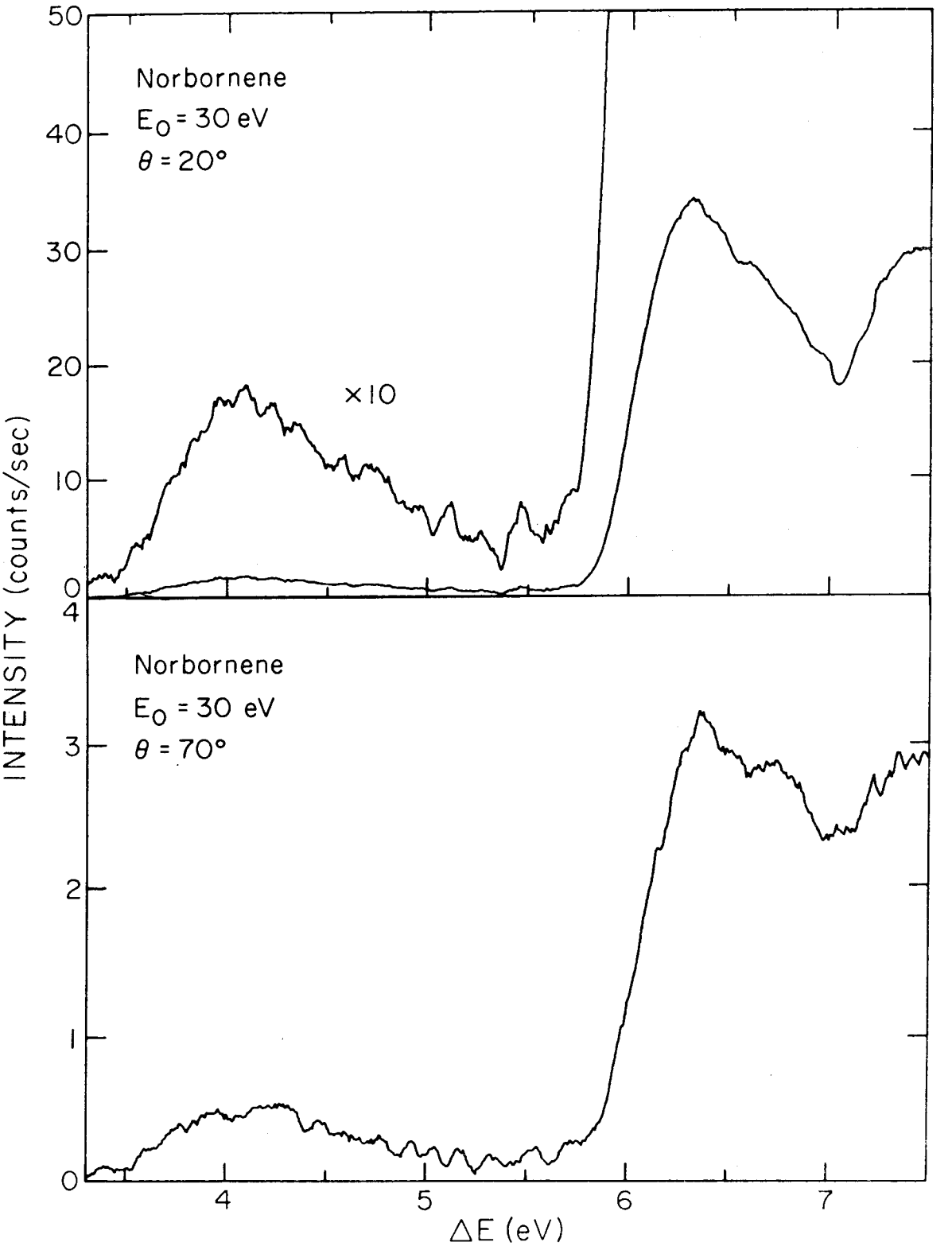
Norbornene
E_0 = 30 eV
θ = 20°
×10
Norbornene
E_0 = 30 eV
θ = 70°
INTENSITY (counts/sec)
ΔE (eV)
50
40
30
20
10
0
4
3
2
1
0
4
5
6
7

Figure 2

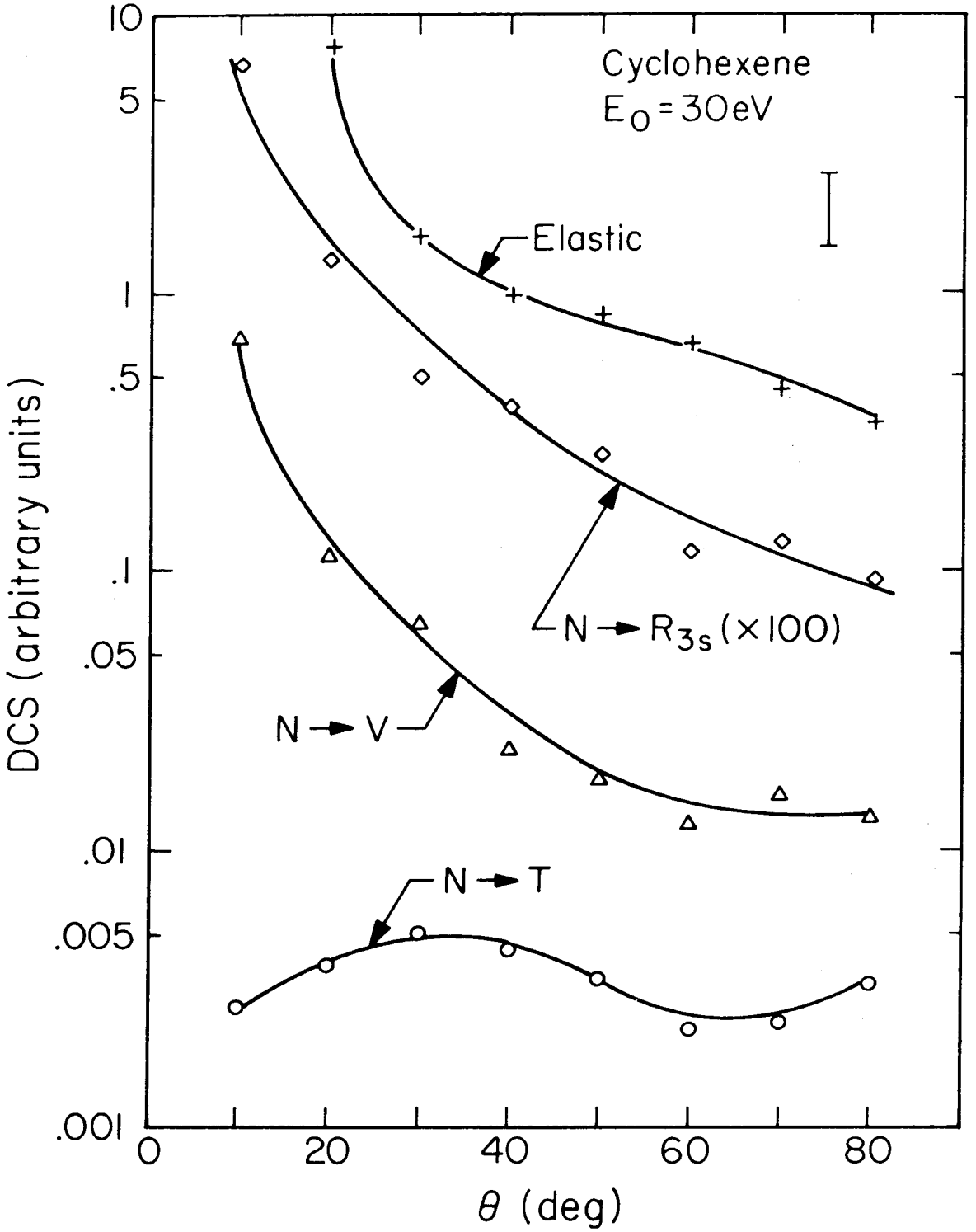
Cyclohexene
$E_0 = 30eV$
Elastic
$N \rightarrow R_{3s}$ (×100)
$N \rightarrow V$
$N \rightarrow T$
DCS (arbitrary units)
θ (deg)
10
5
1
.5
.1
.05
.01
.005
.001
0
20
40
60
80

Figure 3

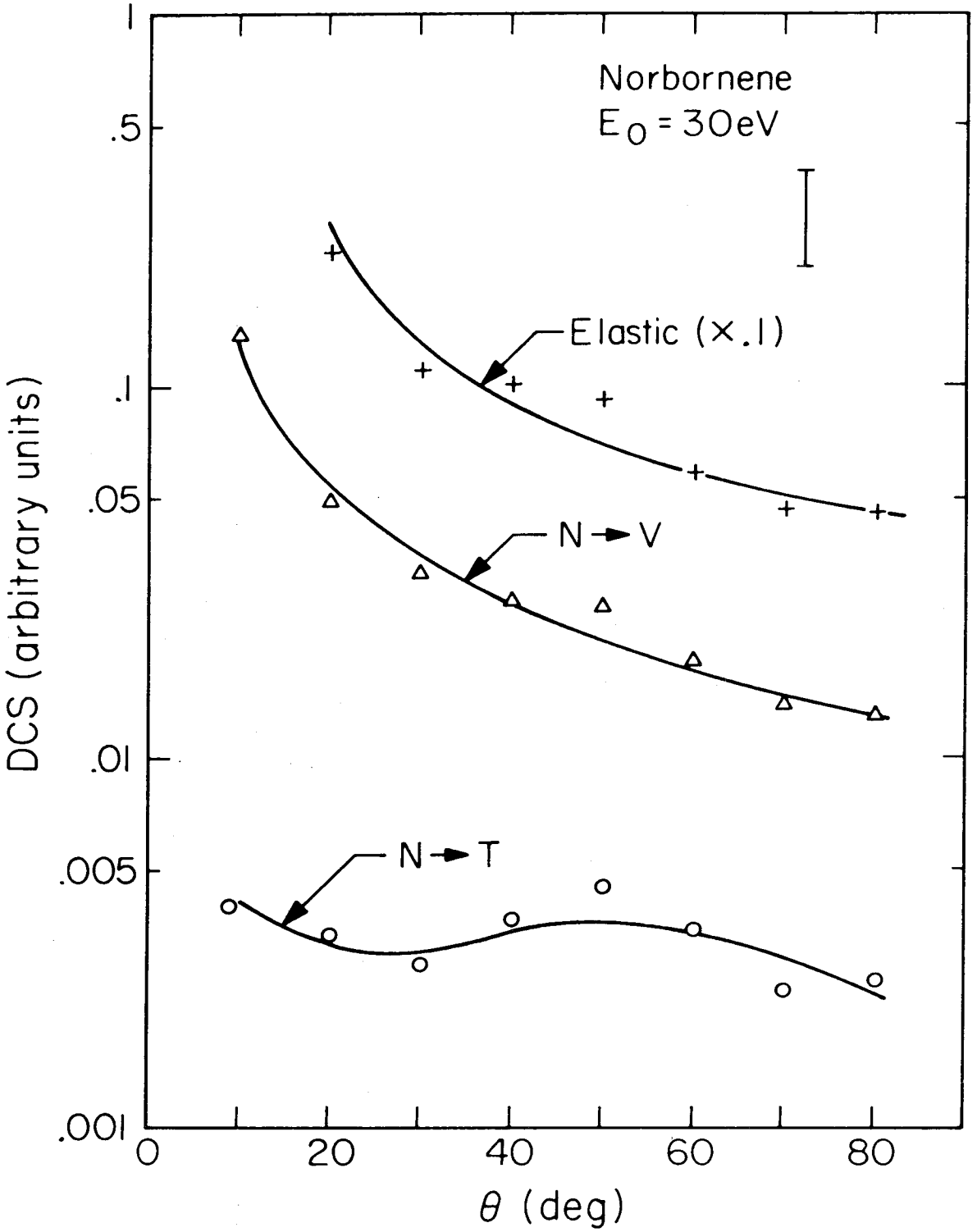
Norbornene
E_0 = 30eV
Elastic (×.1)
N → V
N → T
DCS (arbitrary units)
θ (deg)
1
.5
.1
.05
.01
.005
.001
0
20
40
60
80

Figure 4

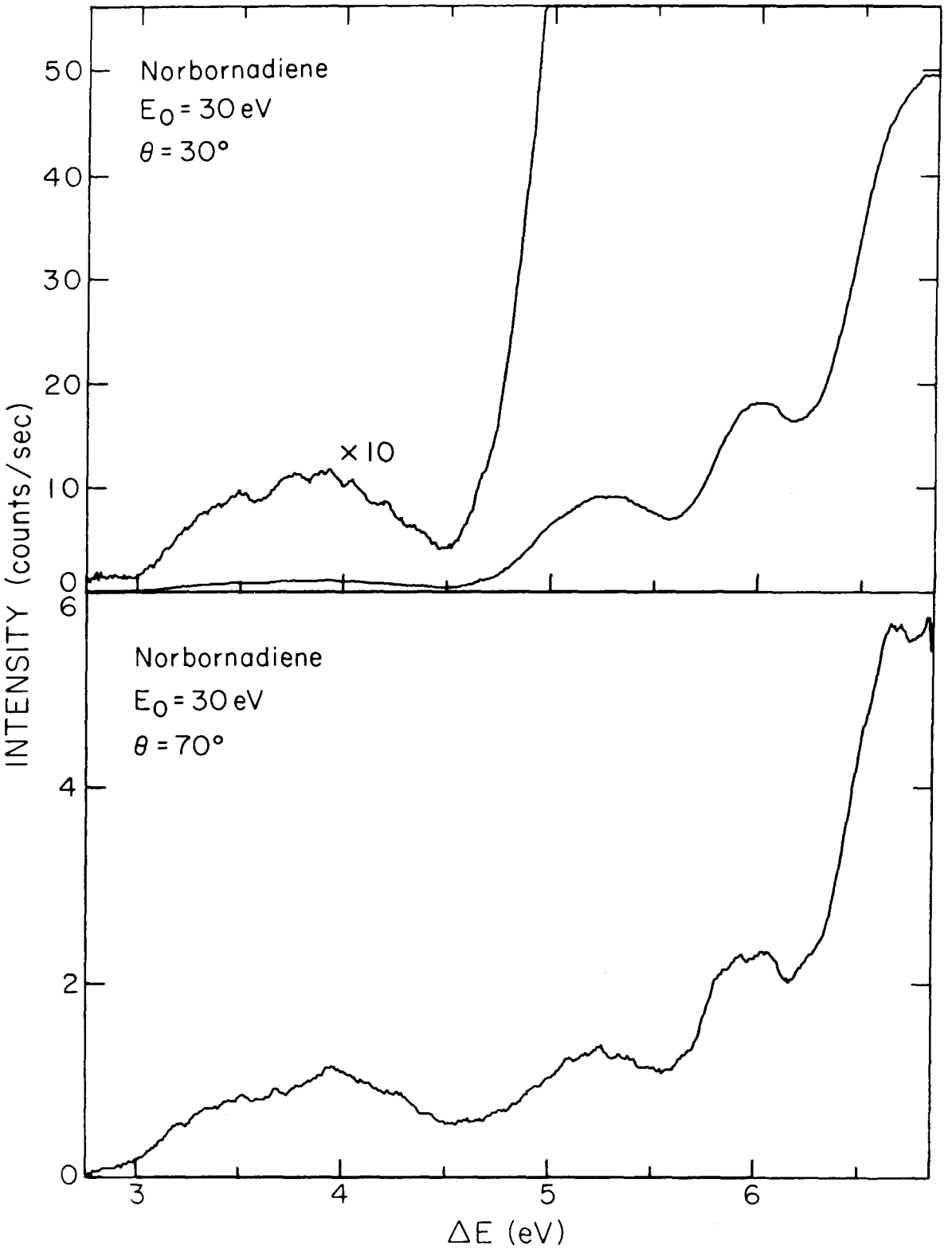
Norbornadiene
E_0 = 30 eV
θ = 30°
× 10
Norbornadiene
E_0 = 30 eV
θ = 70°
INTENSITY (counts/sec)
ΔE (eV)
0
10
20
30
40
50
0
2
4
6
3
4
5
6

Figure 5

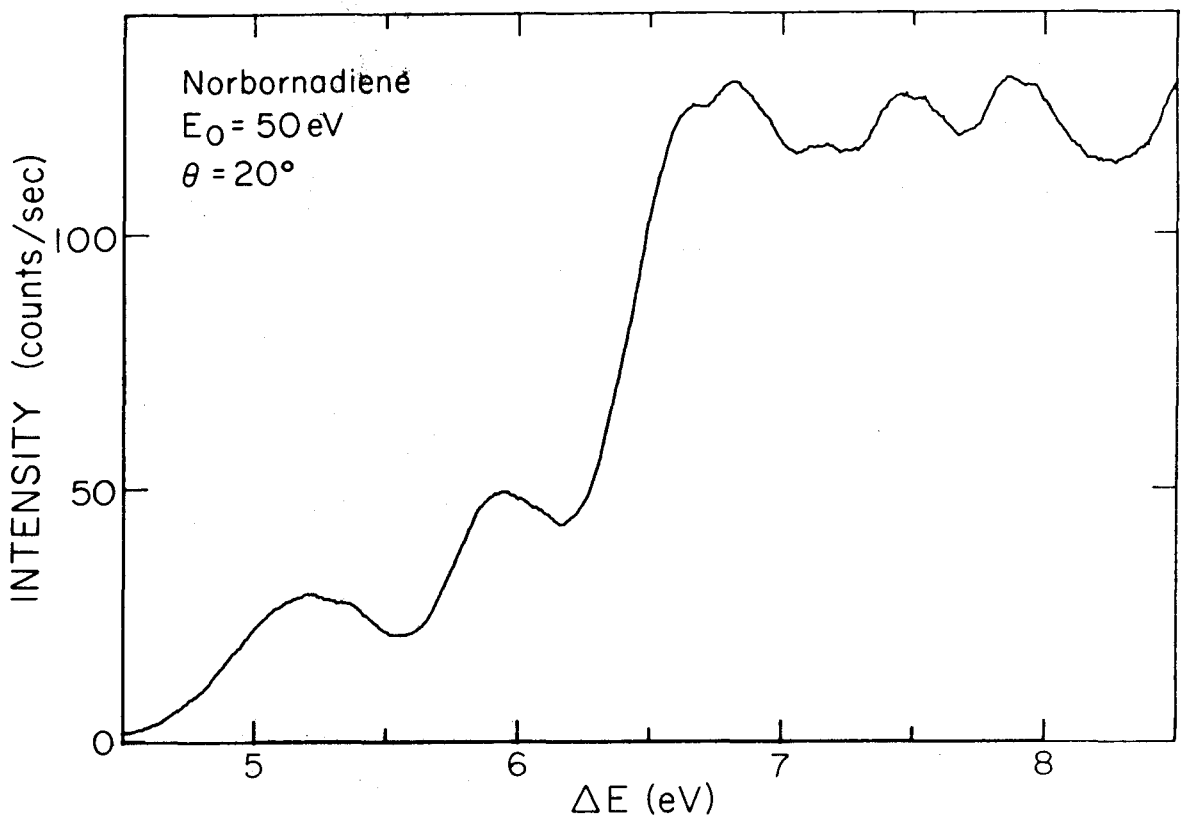
Norbornadiene
E_0 = 50 eV
θ = 20°
INTENSITY (counts/sec)
100
50
0
5
6
7
8
ΔE (eV)

Figure 6

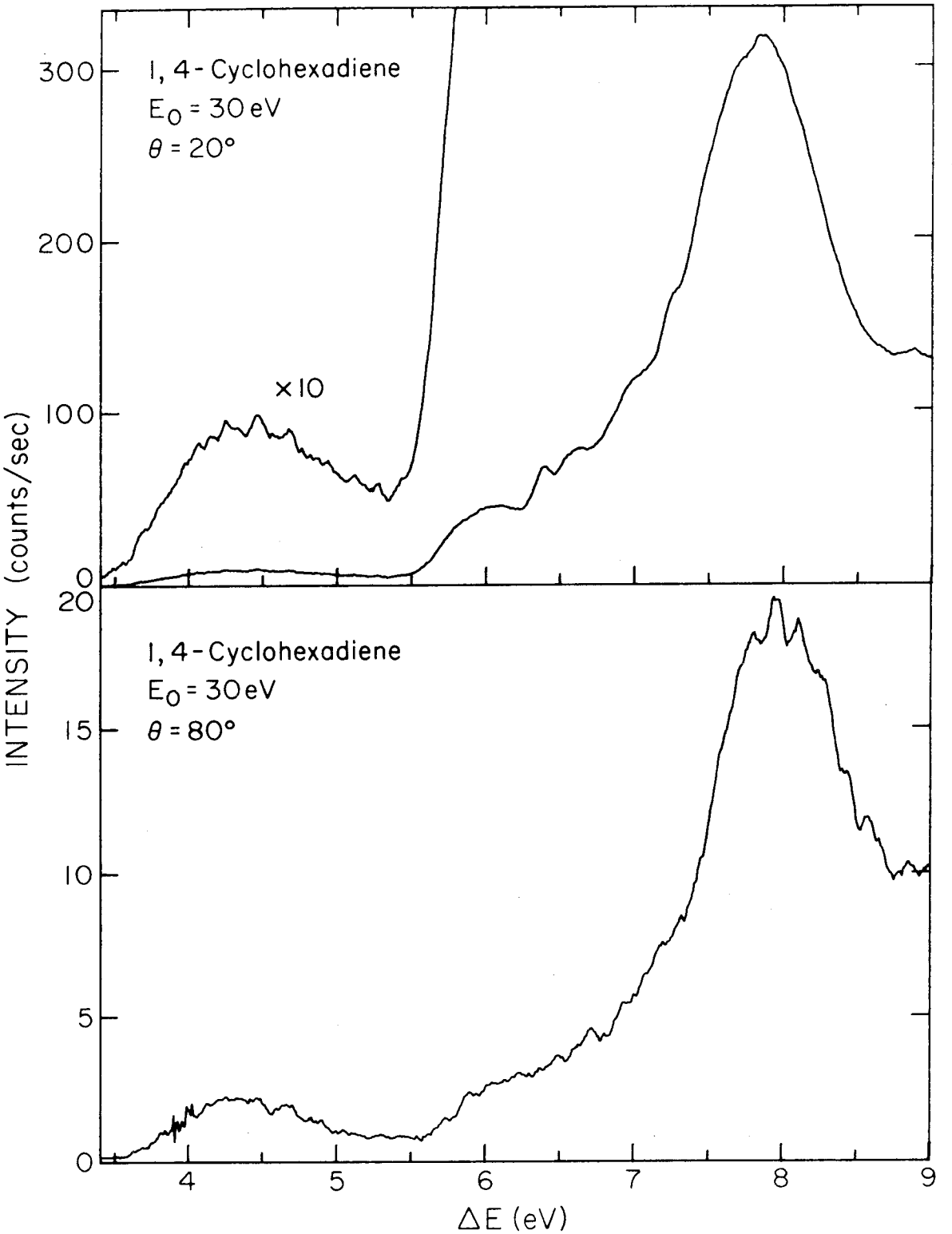
1, 4 - Cyclohexadiene
E_0 = 30 eV
θ = 20°
×10
1, 4 - Cyclohexadiene
E_0 = 30 eV
θ = 80°
INTENSITY (counts/sec)
ΔE (eV)

Figure 7

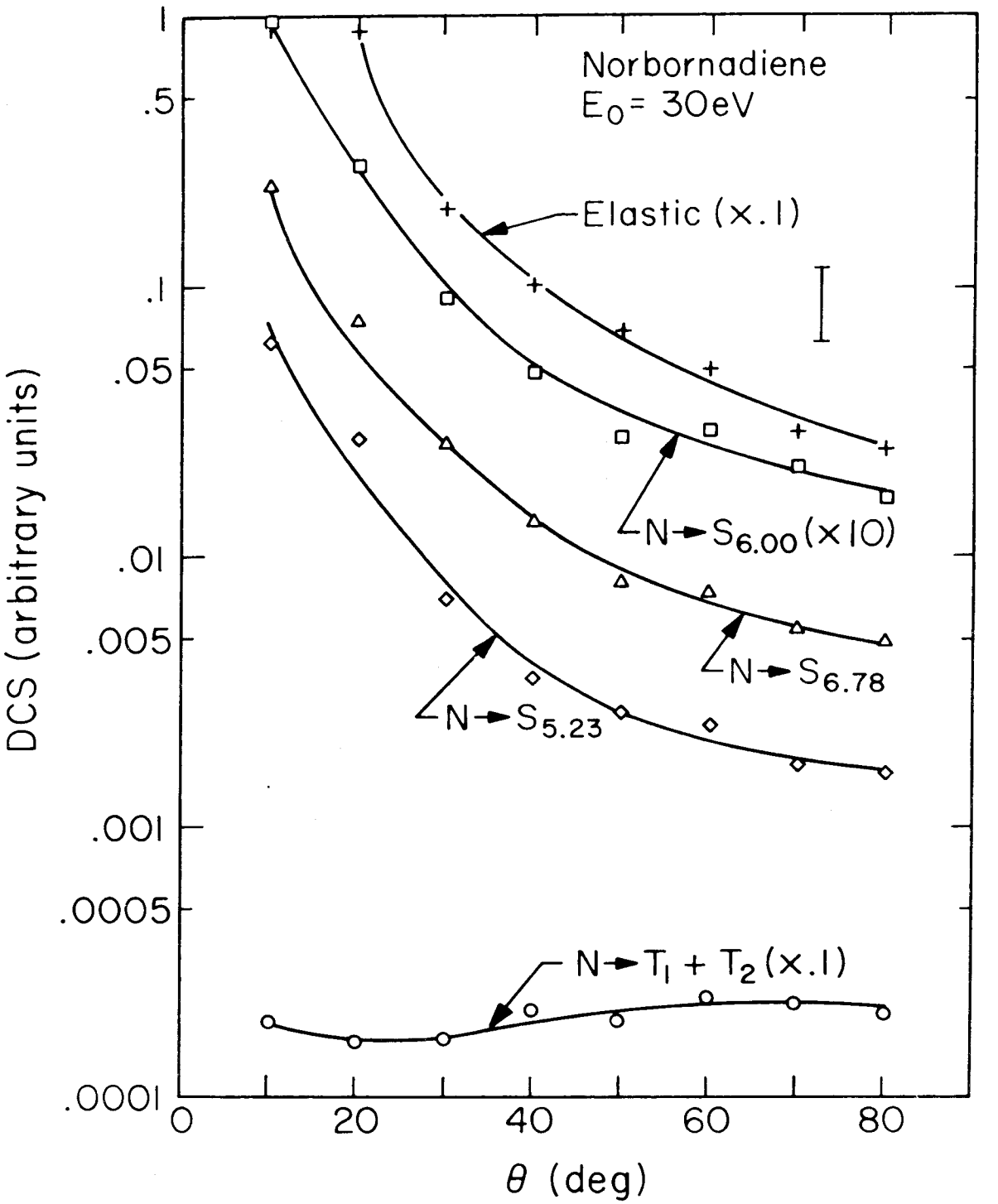
Norbornadiene
E_0 = 30eV
Elastic (×.1)
N→$S_{6.00}$ (×10)
N→$S_{6.78}$
N→$S_{5.23}$
N→T_1 + T_2 (×.1)
DCS (arbitrary units)
θ (deg)
1
.5
.1
.05
.01
.005
.001
.0005
.0001
0
20
40
60
80

Figure 8

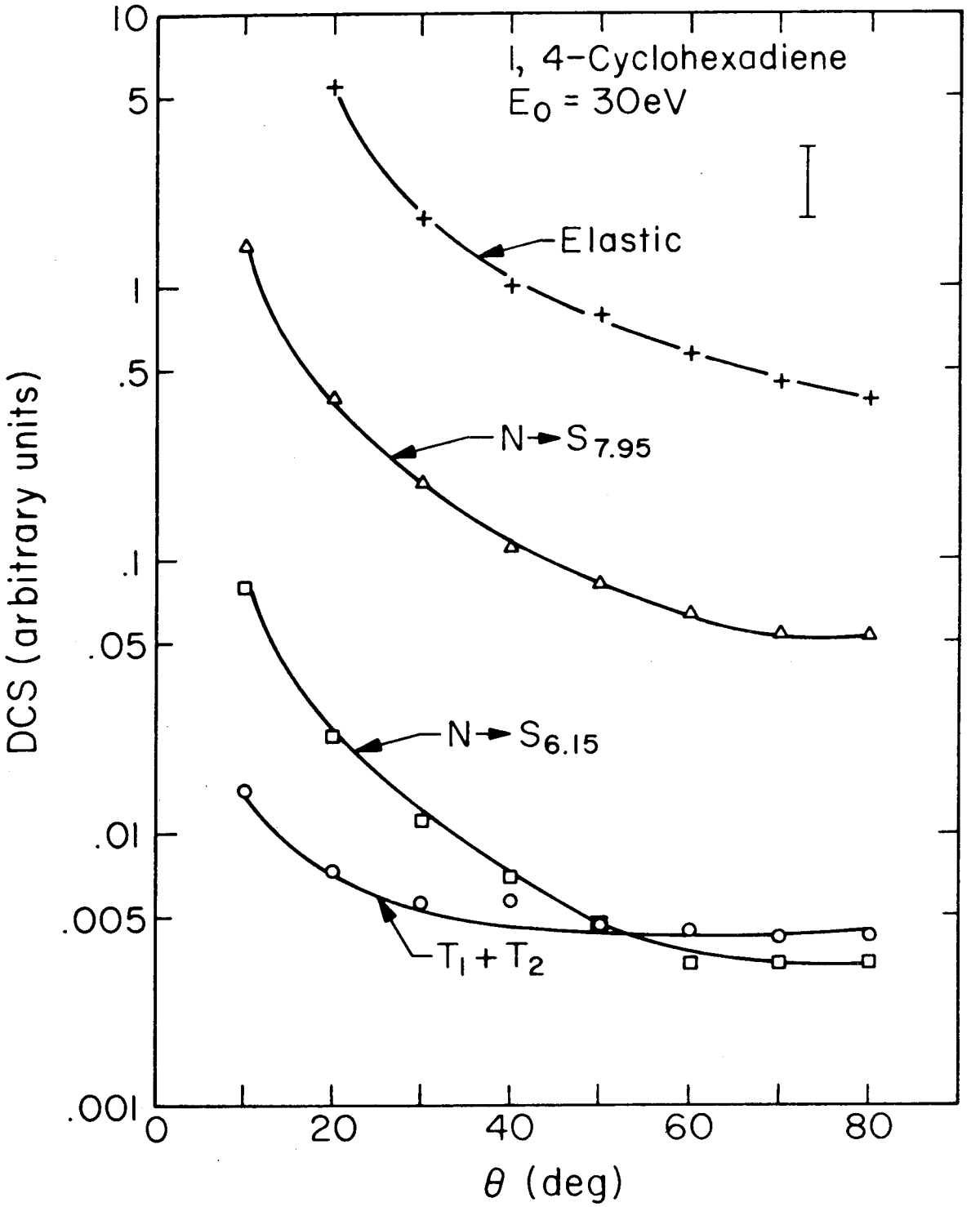
1, 4-Cyclohexadiene
E_0 = 30eV
Elastic
N→$S_{7.95}$
N→$S_{6.15}$
$T_1 + T_2$
DCS (arbitrary units)
θ (deg)
10
5
1
.5
.1
.05
.01
.005
.001
0
20
40
60
80

Figure 9

5. CONCLUSIONS

The technique of low-energy, variable-angle, electron impact spectroscopy has been used to study the electron spectra of several groups of molecules. In addition to inherent spectroscopic interest in these molecules, elucidation of the electronic spectra of the compounds studied is also of chemical interest.

A molecule of particular photochemical interest is ketene (H_2CCO). It has been found to be a source of both singlet and triplet methylene when irradiated by ultraviolet light. The ratio of singlet to triplet methylene was also found to be dependent on the wavelength of the irradiating light. On the basis of spin conservation it is believed that one source of triplet methylene is triplet ketene. Prior to our studies the locations of the low-lying triplet states were not definitely established. We assigned the transition occurring at 5.3 eV as the $\tilde{X}\,^1A_1 \rightarrow {}^3A_2$, $\pi \rightarrow \pi^*$ excitation. The lowest energy singlet → triplet transition, the $\tilde{X}\,^1A_1 \rightarrow {}^3A_2$, $n \rightarrow \pi^*$ excitation, in the ketene spectrum is believed to underlie its corresponding singlet state, the $\tilde{X}\,^1A_1 \rightarrow {}^1A_2$ transition which occurs at 3.7 eV.

Both 1,3,5,7-cyclooctatetraene and 1,3,5-cycloheptratriene are of practical interest. They have been found to be efficient dye laser quenchers. Dye molecules in metastable triplet states are known to inhibit lasing action. Dye laser quenchers undergo an energy transfer process in which the triplet state energy of the dye molecule is given to the quencher. Again prior to our studies the location of the low-lying triplet states of these molecules were uncertain. In 1,3,5-cyclo-

heptatriene two low-lying singlet → triplet excitations occurring at 3.05 eV and 3.95 eV were located. Three low-lying singlet → triplet transitions were detected in the spectrum of 1,3,5,7-cycloocta-tetraene. By studying the band shape for absorption of 1,3,5,7-cyclooctatetraene's lowest triplet state and an approximation to the triplet → singlet emission band of the rhodamine 6G laser dye we have been able to investigate the energy transfer mechanism. Our conclusion is that in addition to a direct triplet → triplet energy transfer between the dye molecule and cyclooctatetraene, an additional mechanism, most likely exciplex formation, is required to explain the experimentally observed quenching rate.

Study of the fluorobenzenes has provided information about both spin-forbidden and spin-allowed excitations of these molecules. In addition to spectroscopic information concerning locations and band shapes of the low-lying, spin-forbidden excitations we have gained information concerning the effects of varying molecular symmetry on transition intensities. The lowest singlet → singlet transitions occurring in the fluorobenzenes are equivalent to the $\tilde{X}\,^1A_{1g} \rightarrow 1\,^1B_{2u}$ benzene excitation. Both benzene and hexafluorobenzene have D_{6h} symmetry. Whether the benzene symmetry is broken by fluorines or that of hexafluorobenzene by hydrogens, the resulting symmetry is more important than the substituent (fluorine or hydrogen) in determining this transition's intensity.

A singlet → singlet transition not occurring in the spectrum of benzene was observed in the spectra of hexafluorobenzene, pentafluoro-

benzene, and the tetrafluorobenzenes. This transition occurred at 5.32 eV in hexafluorobenzene, 5.85 eV in pentafluorobenzene, and about 6.0 eV in 1,2,3,4-tetrafluorobenzene. By studying the excitation energy dependence of this feature with changing fluorine substitution we have formulated an opinion as to the nature of this transition. Its excitation energy behavior appears most consistent with either a charge transfer fluorine p_{π} to carbon $p_{\pi*}$ transition or a fluorine p_{π} to carbon-fluorine $\sigma*$ excitation.

The conjugated cyclic dienes, 1,3-cyclopentadiene, 1,3-cyclohexadiene, and 1,3-cycloheptadiene were also investigated. These molecules are also of photochemical interest. The results of these studies were the location of the lowest singlet → triplet excitation in each molecule and investigation of the spin-allowed portion of the spectra. Several conclusions are reached in this study. First the spectra of these molecules are most effectively discussed in terms of two interacting ethylene units. The dienyl portion is most important in determining the electronic spectrum of each molecule. The spectra display a relative insensitivity to ring size or conformation. Also 1,3-cyclopentadiene's spectrum was compared to those of furan, thiophene, and pyrrole. The three heterocycles display spectra having appreciable aromatic character while that of 1,3-cyclopentadiene is not particularly similar and is best described in terms of its cis-dienyl structure.

The study of 1,4-cyclohexadiene and norbornadiene probes the interaction of non-conjugated ehtylenic units. These molecules represent, respectively, systems in which through-bond and through-

space interactions are believed to be important. Norbornene and cyclohexene were studied to provide a comparison between the isolated double-bond and the dienyl systems. In both cyclohexene and norbornene a single low-lying triplet state was detected. The dienyl counterparts also exhibited low-lying singlet → triplet absorption. However, for these two molecules the features are believed to be due to the superposition of two triplet states resulting from the interactions of the ethylenic units. This superposition is most apparent in norbornadiene and intensity maxima are estimated to occur at approximately 3.4 eV and 3.9 eV. This interaction between ethylenic units is also visible in the singlet excited state spectra where several singlet → singlet transitions, believed to be primarily $\pi \rightarrow \pi^*$ in nature, are observed.

Appendix I: Doublet-Quartet Transitions in Nitric Oxide by Low-Energy, Variable-Angle, Electron Scattering

Doublet-quartet transitions in nitric oxide by low-energy, variable-angle electron scattering[a)]

Robert P. Frueholz, Ronald Rianda,[b)] and Aron Kuppermann

Arthur Amos Noyes Laboratory of Chemical Physics,[c)]
California Institute of Technology, Pasadena, California 91125

(Received)

ABSTRACT

The electron impact spectrum of nitric oxide between 4 eV and 10 eV energy loss has been studied in detail at impact energies of 25, 35, and 50 eV and at scattering angles between 5° and 80°. Weak structure occurring between 5.22 eV and 5.60 eV has been assigned as vibronic bands belonging to the $X\,^2\Pi \rightarrow a\,^4\Pi$ transition. Structure with an apparent Franck-Condon envelope extending from 5.70 eV to approximately 7 eV with intensity maximum at 6.29 eV was assigned to the $X\,^2\Pi \rightarrow b\,^4\Sigma^-$ transition. Additional higher lying transitions have been tentatively assigned as doublet → quartet in nature. These represent the first direct observation of doublet → quartet excitations in the gas phase. Several previously unobserved doublet → doublet transitions occurring near 10 eV energy are also reported.

---

a) This work was supported in part by a contract (No. EY-76-S-03-767) from the Department of Energy. Report Code: CALT-767P4-153.

b) Work done in partial fulfillment of the requirements for the Degree of Doctor of Philosophy in Chemistry.

c) Contribution No. 5705.

I. INTRODUCTION

For over 50 years the electronic spectroscopy of nitric oxide has been intensively studied.[1-5] These investigations have been spurred by the inherent interest of this relatively simple diatomic molecule which possesses a doublet ground state. More recently, nitric oxide has been observed in auroral arcs[6,7] and has been found to play an important role in the atmospheric chemistry of ozone.[8-10] While the doublet excited state spectrum is rather well understood, information on the doublet – quartet transitions is scarce. Prior to the present investigation, no direct doublet – quartet excitations were observed in the nitric oxide spectrum. Indeed, to our knowledge, no direct gas phase doublet – quartet transitions have been previously observed in any molecule.

The objective of our study was to locate doublet – quartet transitions in the electronic spectrum of nitric oxide. The method of low-energy, variable-angle, electron-impact spectroscopy is well suited for the investigation of both spin- and symmetry-forbidden transitions.[11-13] With regard to spin-forbidden excitations, the most important feature of the electron impact technique is the sensitivity of the shape of the differential cross section (DCS) versus scattering angle curve to the change in spin quantum number of the target molecule. Optically-allowed processes have sharply forward-peaked DCS's for impact energies, E_0, 15 eV or more above the excitation threshold. In contrast, singlet – triplet[11,12] and triplet – singlet[13] transitions have a more nearly isotropic DCS over the angular range 10° to 80°. Such transitions occur by the mechanism of electron exchange.[14] For this reason, the ratio of the intensity of a spin-forbidden excitation to that of an optically-allowed one is found to increase by about two orders of magnitude as the scattering angle, θ, increases from 10° to 80°.[11,12] Moreover, this ratio is usually found to be

larger at low impact energies than at high ones.[12] On firm theoretical grounds, this behavior should characterize any transition involving a change of unity in the spin-multiplicity, as would be the case for doublet → quartet excitations, although heretofore no such processes have been observed. In addition, the ratio of intensities of two electric dipole-allowed transitions is nearly independent of angle, usually varying by less than a factor of three over the angular range 10° to 80°.[11-13] Finally, spin-allowed but symmetry-forbidden transitions may display somewhat less forward-peaked DCS's than fully-allowed excitations. Consequently, the ratios of their intensities to those of fully-allowed excitations may increase by factors from three to about eight as the scattering angle increases from 10° to 80°.[12]

II. ELECTRONIC STRUCTURE OF NITRIC OXIDE

The electronic configuration of the $X\ ^2\Pi$ ground state of nitric oxide is[15] $(KK)^4(\sigma_{2s})^2(\sigma_{2s}^*)^2(\sigma_{2p})^2(\pi_{2p})^4(\pi_{2p}^*)^1$. The electronically excited states of nitric oxide consist of two different classes of excitation. Rydberg transitions involve the excitation of an electron into a Rydberg-like orbital. Miescher[4] has assigned the first few excited states as excitations from the π_{2p}^* orbital to the Rydberg orbitals $3s\sigma$ ($X\ ^2\Pi \rightarrow A\ ^2\Sigma^+, \gamma$ bands), $3p\pi$ ($X\ ^2\Pi \rightarrow C\ ^2\Pi, \delta$ bands), $3d\sigma$ ($X\ ^2\Pi \rightarrow D\ ^2\Sigma^+, \epsilon$ bands), and $4s\sigma$ ($X\ ^2\Pi \rightarrow E\ ^2\Sigma^+, \gamma'$ bands). Rydberg excitations involving transitions from the π_{2p}^* orbital can only result in doublet excited states. As would be expected for excitations from an antibonding orbital to a nonbonding orbital, the vibrational spacings for these lower lying Rydberg states are larger ($\sim 2350\ cm^{-1}$) than those of the ground state ($\sim 1900\ cm^{-1}$).[16] Both doublet and quartet Rydberg states may result from excitations from orbitals other than the π_{2p}^*.

The second category of excitations is comprised of transitions to valence excited states. These are of particular interest in the present study because their doublet-quartet splittings are expected to be larger than those for Rydberg excitations, leading to easier resolution of quartet states from doublet states. The valence excited configuration $(KK)^4(\sigma_{2s})^2(\sigma_{2s}^*)^2(\sigma_{2p})^2(\pi_{2p})^3(\pi_{2p}^*)^2$ yields one $^4\Pi$ and several $^2\Pi$ excited states. The $X\ ^2\Pi \rightarrow B\ ^2\Pi$ transitions (β bands) are believed to result from excitation to one of these $^2\Pi$ states.[17] The configuration $(KK)^4(\sigma_{2s})^2(\sigma_{2s}^*)^2(\sigma_{2p})^1(\pi_{2p})^4(\pi_{2p}^*)^2$ yields term symbols $^4\Sigma^-$, $^2\Delta$, $^2\Sigma^-$, and $^2\Sigma^+$. It is believed that the β' bands ($X\ ^2\Pi \rightarrow B'\ ^2\Delta$) result from excitation to this $^2\Delta$ state.[2,18] Excitations to these valence states weaken the internuclear bond, resulting in vibrational frequencies of approximately $1100\ cm^{-1}$.[4]

III. EXPERIMENTAL

The experimental apparatus used in this study was similar to that described by Kuppermann et al.[11] The spectrometer consists basically of a multistage electron gun, a hemispherical electrostatic energy monochromator, a flexible bellows scattering chamber which contains the target gas, an energy-loss analyzer identical to the monochromator, and a Spiraltron electron multiplier. Pulses from the multiplier are amplified and shaped, and then counted with a 1024 channel scaler. In a typical experiment, the incident electron energy and scattering angle of detection are both fixed, and the energy-loss spectrum is scanned repeatedly, usually for a period of four to eight hours, corresponding to an accumulation time per channel of approximately 20 sec to 30 sec. However, in these studies, in order to obtain the desired signal-to-noise ratios, accumulation times per channel were increased to 150-900 sec.

In the present experiments, the electron-impact spectrum of nitric oxide in the energy-loss region 4 to 10 eV was studied at impact energies of 25, 35, and 50 eV, over scattering angles from 5° to 80°. Sample pressures in the scattering chamber were typically 1.8 mTorr as indicated by an uncalibrated Schulz-Phelps ionization gauge, while the incident electron beam current was approximately 70 nA. The energy resolution, as measured by the full width at half maximum (FWHM) of the elastic peak was set electron-optically at about 0.085 eV. The nitric oxide sample was obtained from Matheson Gas Products with a stated minimum purity of 99.0%. Our samples were further purified by trap-to-trap distillation at liquid nitrogen temperature. No indication of impurity was observed in any spectrum.

IV. RESULTS AND DISCUSSION

A. Doublet excited states

Figures 1 and 2a show the spectrum of nitric oxide at low scattering angles. These spectra result from predominantly doublet–doublet excitations. The transition energies are in good agreement with previous optical studies and are summarized in Table I. The doublet – doublet spectrum in the energy region studied has been well characterized by previous optical studies.[1-5] In our spectra we have detected several spin-allowed transitions near 10 eV that do not appear to have been previously observed. Their excitation energies are listed in Table I. Considering our relatively limited resolution, further discussion of doublet – doublet transitions in this energy-loss region is not warranted.

B. Subtraction techniques

As discussed in the Introduction, the ratio of the intensities of spin-forbidden to spin-allowed transitions increases significantly as the scattering angle is increased. We may make use of this fact to nearly eliminate the contribution of spin-allowed transitions to the high angle spectra by subtracting from the latter, after appropriate scaling, the low-angle spectra. The resulting difference spectrum is believed to be primarily due to spin-forbidden transitions. This technique has been used previously.[12a, 19] Its validity rests upon the assumptions that (a) relative intensities of different vibronic elements of the same electronic transition remain constant with varying scattering angle (i. e., Franck-Condon factors are independent of scattering angle) and (b) relative intensity changes as a function of scattering angle between spin-allowed transitions resulting from excitations to different electronically excited states will be much smaller than the corresponding relative intensity changes between spin-allowed and spin-forbidden excitations over the

same angular regions. Experimental observations indicate that these assumptions are well-founded.[11, 20]

Spectra taken at 20° are used as low-angle standards in all subtractions reported for reasons discussed below. In this subtraction technique it is desirable to use as a low-angle standard spectrum one that has minimal contribution from spin-forbidden transitions while simultaneously possessing spin-allowed structure for which relative intensities among different doublet–doublet electronic excitations change as little as possible in going from the selected low scattering angle to high scattering angles. Relatively large spin-allowed transition intensity variations among such electronic states are frequently observed between high-angle spectra and spectra obtained at angles of 5° or 10° when compared with the differences between 20° spectra and high-angle spectra. In addition, the relative contribution of spin-forbidden transitions to the spectrum increases rapidly as the scattering angle is increased beyond 20°.

In preparation for subtraction, both the high- and low-angle spectra are corrected for background noise contributions. Intensity scaling is accomplished by multiplying the low-angle spectrum by a factor that makes the intensity of a selected spin-allowed vibronic peak (hereafter called the scaling peak) equal to the intensity of the corresponding peak in the high-angle spectrum. It is important that the peaks used for scaling have minimal underlying spin-forbidden structure. Subtraction is performed channel by channel after appropriate energy scale calibration, and the intensities of the features in the resulting difference spectrum are expressed as fractions of the intensity of the strongest feature in the original high-angle spectrum. This normalization gives a clear representation of the fractional contribution of the spin-forbidden transitions to the high-angle spectra.

We have performed extensive tests to guarantee that the difference spectra obtained in this manner are not simply artifacts of the subtraction technique

Instrumental background is usually affected by the presence of the sample in the apparatus and is determined with sample present using the energy-loss regions between non-overlapping transitions, such as the region below 5 eV in nitric oxide. Above 7 eV, such a region does not exist in NO, preventing an accurate determination of the noise background. We assumed that it was the same as below 5 eV but varied it significantly (± 50%); we found that the difference spectra were essentially unchanged. An examination of the widths of the elastic peaks indicates that the difference in resolution between our high- and low-angle spectra is no larger than 5 meV. In order to test the effects of this possible resolution variation on the structure of the difference spectra, we convoluted gaussian peaks of FWHM varying between 10 meV and 40 meV into a low-angle spectrum yielding resolutions as much as 10 meV worse than in the unconvoluted spectrum. After subtracting the unconvoluted spectrum from the convoluted ones, the resulting difference spectra were found to have residual structural features with a maximum relative intensity no greater than 6% of the strongest feature of the convoluted spectra for a 10 meV resolution deterioration and 3% for a 5 meV resolution worsening. This is a small effect compared with most of our observed difference spectra. These spectra, resulting from experimental data, also meet the following criteria. The general features are unchanged upon changing the angle of the high-angle spectrum used in the subtraction and the impact energy used for both the high- and low-angle spectra. In addition, intensities of the peaks in the difference spectrum relative to the spin-allowed contributions at the same angle increased as the high-angle spectrum angle was increased. This behavior is consistent with that expected for a spin-forbidden transition.

C. Doublet → quartet transitions

Figure 2 shows the energy-loss spectrum of nitric oxide at 20° and 80° scattering angles over the energy-loss region 5 eV to 10 eV. Significant

changes between the high- and low-angle spectra are observed. The new vibronic peaks at 5.86 and 6.14 eV, never previously observed, are seen in the high angle spectrum. In addition, the relative intensities of the other peaks are very different in the two spectra, and close inspection reveals small shifts in energy of the intensity maxima of several vibronic peaks. This change is due to the increase in the relative intensity of doublet → quartet transitions (with respect to doublet → doublet excitations) in going from 20° to 80°. To facilitate discussion of the spectra, we will consider various energy-loss regions separately.

1. $X\,^2\Pi \rightarrow a\,^4\Pi$ excitations (5.0 to 5.7 eV)

The lowest energy spin-forbidden transition in nitric oxide is predicted by a semi-empirical calculation to be the $X\,^2\Pi \rightarrow a\,^4\Pi$ excitation.[18] Broida and Peyron[21] and Frosch and Robinson[22] have observed emission bands from NO in rare gas matrices which they assign as the $a\,^4\Pi\ v' = 0 \rightarrow X\,^2\Pi\ v'' = n$ transitions (M bands). Ogawa[23] and Brook and Kaplan[24] have observed emission bands in the infrared which Ogawa suggested were the result of $^4\Sigma^- \rightarrow {}^4\Pi$ fluorescence. Frosch and Robinson, using vibrational data derived from these results and their own estimation of the gas phase $X\,^2\Pi\ v'' = 0 \rightarrow a\,^4\Pi\ v' = 0$ transition energy, predicted the positions of the vibronic elements of this transition as shown in Table II. There has been no previous direct observation of the $X\,^2\Pi \rightarrow a\,^4\Pi$ excitations in spite of attempts by Bernstein and Herzberg[25] using a 28 m atm path.

In Fig. 3b and the low energy-loss region of Fig. 4d we observe very weak structure at 5.22, 5.31, 5.41, and 5.60 eV. The intensities of these peaks relative to that of the γ (0-0) at 5.47 eV increase by more than one order of magnitude as the scattering angle increases from 20° to 80°. This behavior is indicative of a spin-forbidden transition. Using this angular

behavior and the predictions of Frosch and Robinson[22] we assign these excitations to the $X\ ^2\Pi\ v'' = 0 \rightarrow a\ ^4\Pi\ v' = 4, 5, 6,$ and 8 transitions. The 5.41 eV feature is only distinguishable in the difference spectra (using the γ (0, 0) feature at 5.47 eV as the scaling peak) shown in Figs. 3c, 4e, f, and g: however, a noticeable broadening of the $\gamma(0, 0)$ transition is observed at the high-angles. The peak occurring at 5.55 eV in the difference spectra is most likely the $v' = 7$ member of the $X\ ^2\Pi \rightarrow a\ ^4\Pi$ vibrational series. However, the exact location of the transition corresponding to the 5.55 eV feature in the difference spectrum is uncertain because of its closeness to the scaling peak. Although the peak observed at 5.70 eV corresponds exactly to the predicted location of the $v' = 9$ transition, its significantly increased intensity relative to the other vibrational members of this transition contradicts the Franck-Condon factors predicted by Frosch and Robinson.[22] For this reason it seems more reasonable to attribute this 5.70 eV feature predominantly to another doublet – quartet transition.

2. $X\ ^2\Pi \rightarrow b\ ^4\Sigma^-$ excitations (5.7 to 7.3 eV)

Figure 4 shows the 5 eV to 7.4 eV region in great detail. Spectra taken at 20°, 40°, 60°, and 80° and the results of subtracting the 20° spectrum from the other three spectra are shown in this figure. In addition to the peaks previously discussed, a new series of vibronic bands is observed beginning with the feature at 5.70 eV in the difference spectra (Fig. 4e, f, and g). The new transitions at 5.86 and 6.14 eV, clearly distinguishable, even in the high angle original spectra, increase in intensity by nearly two orders of magnitude relative to the $\gamma(0, 0)$ intensity as the scattering angle increases from 20° to 80°. The other peaks observed in the difference spectra maintain a nearly constant intensity relative to the transitions at 5.86 eV and 6.14 eV.

This constancy indicates that the transitions which are distinguishable only in the difference spectra undergo an increase in intensity relative to doublet – doublet transitions similar to that of the 5.86 and 6.14 eV transitions, allowing us to assign these transitions as doublet – quartet in nature.

Semi-empirical calculations[18] suggest that the second quartet excited state should be the $b\ ^4\Sigma^-$ resulting from an excitation of a σ_{2p} electron to the π^*_{2p} orbital. Using the infrared emission results of Ogawa[23] and Brook and Kaplan,[24] which were suggested to be due to $b\ ^4\Sigma^- - a\ ^4\Pi$ transitions, and the $X\ ^2\Pi\ v'' = 0 - a\ ^4\Pi\ v' = 0$ excitation energy of Frosch and Robinson,[22] the following excitation energies for vibronic members of the $X\ ^2\Pi - b\ ^4\Sigma^-$ transition may be predicted: 5.99, 6.15, 6.28, and 6.43 eV. In our difference spectra the corresponding transitions are observed at 6.00, 6.14, 6.29, and 6.43 eV. This agreement allows definite assignment of the infrared transitions[23] to a $b\ ^4\Sigma^- - a\ ^4\Pi$ emission. However, the presence of peaks in our spectrum at 5.70 and 5.86 eV, which we tentatively assign to the $X\ ^2\Pi\ v'' = 0 - b\ ^4\Sigma^-\ v' = 0, 1$ transitions, indicates that previous vibrational assignments of the emission spectrum were incorrect due apparently to the lack of observation of emission from $b\ ^4\Sigma^-\ v' = 0, 1$. We assign the transitions in the difference spectra from 5.70 eV to 7.24 eV to the $X\ ^2\Pi\ v'' = 0 - b\ ^4\Sigma^-\ v' = 0 - 11$ transitions. Our specific assignment of the vibration quantum numbers for elements of $b\ ^4\Sigma^-$ is not however definitive, since experimental resolution precludes rotational analysis. The possibility exists that the true $v' = 0$ lies at a lower excitation energy than 5.70 eV. This preliminary assignment is based on the inability to detect transitions below 5.70 eV which have intensity sufficient, in our opinion, to belong to the $b\ ^4\Sigma^-$ progression. We do feel that if our assignment of vibronic quantum number, v', is in error, this would shift our assignments by no more than unity, in which case the 5.70 eV feature would correspond to $v' = 1$. The transition energies are summarized in Table II. Peaks

at 6.70 eV and 6.97 eV have intensities which are greater than would be expected for consistency with the remainder of the Franck-Condon envelope. This behavior may result from the presence of an additional underlying doublet – quartet transition or to a vibrational perturbation[26] resulting from an avoided potential crossing with another electronic state.[26-29]

3. Higher energy quartet transitions (7.3 to 10.0 eV)

Figure 5 shows the nitric oxide spectrum at 20° and 80° between 6.5 and 9.0 eV and the resulting difference spectrum. The low-angle spectrum was normalized to the 8.36 eV feature of the high-angle spectrum. While relative peak intensities in the difference spectrum vary somewhat depending on the peak used for such scaling, peak locations are independent of the choice of scaling peak. The ratios of the intensities of the difference peaks observed above 7 eV to those between 5.0 and 7.0 eV, which we previously assigned as doublet – quartet transitions, remain relatively constant over the angular region we have studied. This behavior suggests a doublet – quartet assignment for these bands. However, the presence of over 20 previously identified doublet excited states in this energy-loss region[2] might result in a significant contribution to the difference spectrum from relative doublet – doublet transition intensity variations with angle. We do not believe this to be the case, though, for the following reasons. (a) Essentially the same spectrum is observed regardless of the peak chosen for scaling. Since each of the scaling peaks corresponds to a different doublet excited state, changes in the relative intensities in resulting difference spectra would be expected to appear if relative changes in doublet – doublet transition intensities with angle were significant. (b) We are unable to correlate any more than two or three difference features out of the 17 observed to known vibronic elements of any given doublet – doublet transition. Since vibronic envelopes are independent of scattering angle, if one element of the

envelope is observed, then the remaining elements of comparable intensity should also be observed. (c) Finally, the angular behavior of the intensities of the features observed in the difference spectrum appears to be consistent with their assignment as doublet → quartet transitions.

The appearance of the difference spectrum above 7 V suggests the overlapping of several different quartet states. At the present time we are unable to assign these features to specific transitions. Excitation of a σ_{2s}^* electron to a π_{2p}^* orbital will result in a higher lying $^4\Sigma^-$ state. Also, excitation from orbitals lying below the π_{2p}^* to Rydberg orbitals will lead to quartet excited states. In light of our present experimental results, we feel that further theoretical investigations are warranted.

V. SUMMARY AND CONCLUSIONS

In summary, using the technique of low-energy, variable-angle, electron-impact spectroscopy, we have studied the 4 to 10 eV region of the nitric oxide electronic spectrum in detail and have observed the first doublet – quartet transitions in the gas phase. We have located and assigned two doublet – quartet transitions, $X\ ^2\Pi - a\ ^4\Pi$ and $X\ ^2\Pi - b\ ^4\Sigma^-$. These assignments allow reinterpretation of previously observed infrared emission bands of nitric oxide. In addition, transitions above 7 eV energy-loss have been tentatively assigned as doublet–quartet in nature, though specific electronic state assignments were not possible. Finally, we have observed several doublet – doublet transitions near 10 eV energy which have not been previously reported.

ACKNOWLEDGEMENT

The authors would like to thank Dr. R. H. Reiner for helpful suggestions.

TABLE I. Observed features in the nitric oxide spectrum in the 5-10 eV region attributable to doublet→doublet excitations.

Present Results (eV ± 0.02 eV)	Leifson[a] (eV ± 0.001 eV)	Present Results (eV ± 0.02 eV)	Leifson[a] (eV ± 0.001 eV)
5.47	5.475		7.752
5.75	5.765		7.780
	5.873	7.84	7.842
	5.998	7.97	7.965
6.04	6.052		7.989
	6.119	8.10	8.116
	6.241	8.24	8.254
6.33	6.335		8.282
	6.357	8.36	8.309
6.48	6.490		8.440
6.59	6.605	8.51	8.536
	6.712	8.56	8.563
6.76	6.779	8.67	8.590
6.88	6.890		8.713
	6.929	8.78	8.808
7.04	7.029	8.88	8.915
	7.072	8.98	9.007
7.14	7.126	9.08	9.098
	7.168	9.26[b]	
	7.254	9.54	9.564
7.33	7.336	9.62[b]	
7.41	7.391	9.72[b]	
	7.440	9.84[b]	
7.56	7.550		
	7.649		
7.70	7.699		
	7.723		

[a] Reference 1.

[b] Previously unreported.

TABLE II. $X\ ^2\Pi\ v'' = 0 \rightarrow$ quartet excitation energies in the 5 to 10 eV region.

Excitation Energy (eV)		Present quartet assignment	Excitation Energy (eV)		Present quartet assignment
Present observations (± 0.02 eV)	Estimations from optical data		Present observations (± 0.02 eV)	Estimations from optical data	
5.22	5.19[a]	a $^4\Pi$ v' = 4	7.24		b $^4\Sigma^-$ v' = 11[e]
5.31	5.30[a]	5	7.36		
5.41	5.41[a]	6	7.48		
5.55[b]	5.51[a]	7	7.64		
5.60	5.60[a]	8	7.77		
5.70	5.70	b $^4\Sigma^-$ v' = 0[c]	7.91		
5.86		1	8.05		
6.00	5.99[d]	2	8.17		
6.14	6.15[d]	3	8.31		
6.29	6.28[d]	4	8.43		
6.43	6.43[d]	5	8.53		
6.57		6	8.63		
6.70		7	8.74		
6.83		8	8.85		
6.97		9	8.95		
7.12		10[e]	9.05		

[a] Estimated transition energies based on rare gas matrix optical emission data; Ref. 22.

[b] Energy uncertainty ± 0.05 eV; see text.

[c] The upper state is predominantly b $^4\Sigma^-$ v' = 0 with a small a $^4\Pi$ v' = 9 contribution. The latter is also estimated in Ref. 22 to occur at 5.70 eV.

[d] Present paper's transition energy estimates using data in Refs. 22 and 23; see text.

[e] Assignment uncertain.

REFERENCES

1. S. Leifson, Astrophys. J. 63, 73 (1926).
2. L. Wallace, Astrophys. J. Suppl. Ser. 7, 165 (1962).
3. H. W. Thompson and B. A. Green, Spectrochim. Acta 8, 129 (1956).
4. E. Miescher, J. Quant. Spectrosc. Radiat. Transfer 2, 421 (1962).
5. K. P. Huber and E. Miescher, Helv. Phys. Acta 36, 257 (1963).
6. T. M. Donahue, E. C. Zipf, Jr., and T. D. Parkinson, Planet. Space Sci. 18, 171 (1970).
7. E. C. Zipf, W. L. Borst, and T. M. Donahue, J. Geophys. Res. 75, 6371 (1970).
8. H. S. Johnston, Acta Astronautica 1, 135 (1974).
9. J. London and J. H. Park, Can. J. Chem. 52, 1599 (1974).
10. H. Levy II, Adv. Photochem. 9, 369 (1973).
11. (a) A. Kuppermann, J. K. Rice, and S. Trajmar, J. Phys. Chem. 72, 3894 (1968); (b) S. Trajmar, J. K. Rice, and A. Kuppermann, Adv. Chem. Phys. 18, 15 (1970).
12. (a) O. A. Mosher, W. M. Flicker, and A. Kuppermann, J. Chem. Phys. 59, 6502 (1973); (b) idem, ibid. 62, 2600 (1975).
13. S. Trajmar, W. Williams, and A. Kuppermann, J. Chem. Phys. 56, 3759 (1972).
14. J. R. Oppenheimer, Phys. Rev. 29, 433 (1927).
15. G. Herzberg, Spectra of Diatomic Molecules (D. Van Nostrand and Reinhold, New York, 1950), p. 343.
16. Ref. 15, p. 558.
17. L. H. Suttcliffe and A. D. Walsh, Proc. Phys. Soc. Lond. A 66, 209 (1953).

18. P. Carsky, J. Kuh, and R. Sahradnik, J. Mol. Spectrosc. 55, 131 (1975).

19. K. E. Johnson and S. Lipsky, J. Chem. Phys. 66, 4719 (1977).

20. E. N. Lassettre, A. Skerbele, M. A. Dillon, and K. J. Ross, J. Chem. Phys. 48, 5066 (1968).

21. H. P. Broida and M. Peyron, J. Chem. Phys. 32, 1068 (1960).

22. R. P. Frosch and G. W. Robinson, J. Chem. Phys. 41, 367 (1964).

23. M. Ogawa, Science of Light 3, 39 (1954).

24. M. Brook and J. Kaplan, Phys. Rev. 96, 1540 (1954).

25. H. J. Bernstein and G. Herzberg, J. Chem. Phys. 15, 77 (1947).

26. Ref. 15, pp. 280-295.

27. (a) I. Kovacs, Can. J. Phys. 36, 309 (1958);

(b) idem, ibid., 329 (1958).

28. R. W. Field, J. Chem. Phys. 60, 2400 (1974).

29. R. W. Field, C. R. Jones, and H. P. Broida, J. Chem. Phys. 60, 4377 (1974).

FIGURE CAPTIONS

FIG. 1. Electron energy-loss spectrum of nitric oxide at a scattering angle of 10° and impact energy of 35 eV; channel width 10 meV; accumulation time per channel 16 sec.

FIG. 2. Electron energy-loss spectrum of nitric oxide at a scattering angle of (a) 20° and (b) 80°; 25 eV incident electron energy; channel width 10 meV; accumulation time per channel (a) 12 sec and (b) 45 sec.

FIG. 3. Electron energy-loss spectrum of nitric oxide at scattering angles (a) 20° and (b) 60°, at an impact energy of 25 eV and channel width of 5 meV. (c) shows the resulting difference spectrum of (b) minus (a) as a fraction of the most intense feature of (b); accumulation time per channel (a) 329 sec and (b) 990 sec. See Section IV.B for details of calculation of difference spectrum. In panel (a), the bands designated γ belong to the $X\ ^2\Pi \rightarrow A\ ^2\Sigma^+$ transition and the two numbers in parentheses designate final and initial vibrational states, in that order.

FIG. 4. Electron energy-loss spectra of nitric oxide at scattering angles of (a) 20°, (b) 40°, (c) 60°, and (d) 80° at an impact energy of 25 eV and channel width of 10 meV. The energy resolution is 0.085 (fwhm). (e) to (g) are difference spectra resulting, respectively, from (b) minus (a), (c) minus (a), and (d) minus (a), each expressed as a fraction of the most intense feature of the corresponding higher-angle spectrum; average accumulation time per channel 150 sec. See Section IVB for details of calculation of difference spectra. In panel (a), the bands designated γ, δ, and ϵ belong to transitions $X\ ^2\Pi \rightarrow A\ ^2\Sigma^+$, $C\ ^2\Pi$, and $D\ ^2\Sigma^+$, respectively, and the two numbers in parentheses designate the final and initial vibrational states, in that order. The assignment of the vibrational levels of the $b\ ^4\Sigma^-$ state indicated in panel (g) are those proposed in the present work (see Section IV. C. 2).

FIG. 5. Electron energy-loss spectrum of nitric oxide at scattering angles of (a) 20° and (b) 80° at an impact energy of 25 eV and channel width of 10 meV. (c) shows the resulting difference spectrum (b) minus (a) expressed as a fraction of the most intense feature of (b); accumulation time per channel (a) 64 sec and (b) 360 sec. See Section IV. B for details of calculation of difference spectrum.

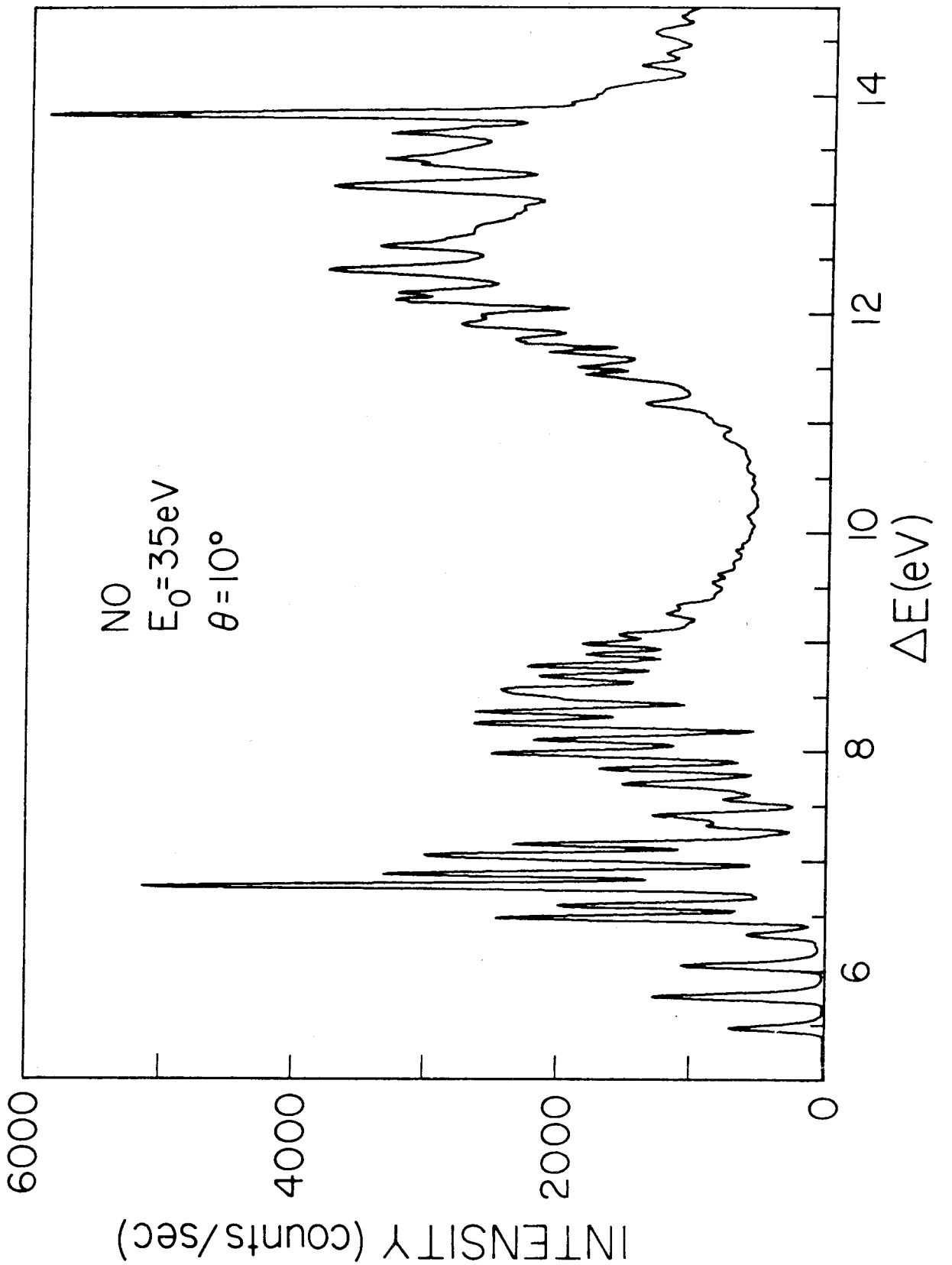
NO
E_0=35eV
θ=10°
INTENSITY (counts/sec)
6000
4000
2000
0
6
8
10
12
14
ΔE(eV)

Figure 1

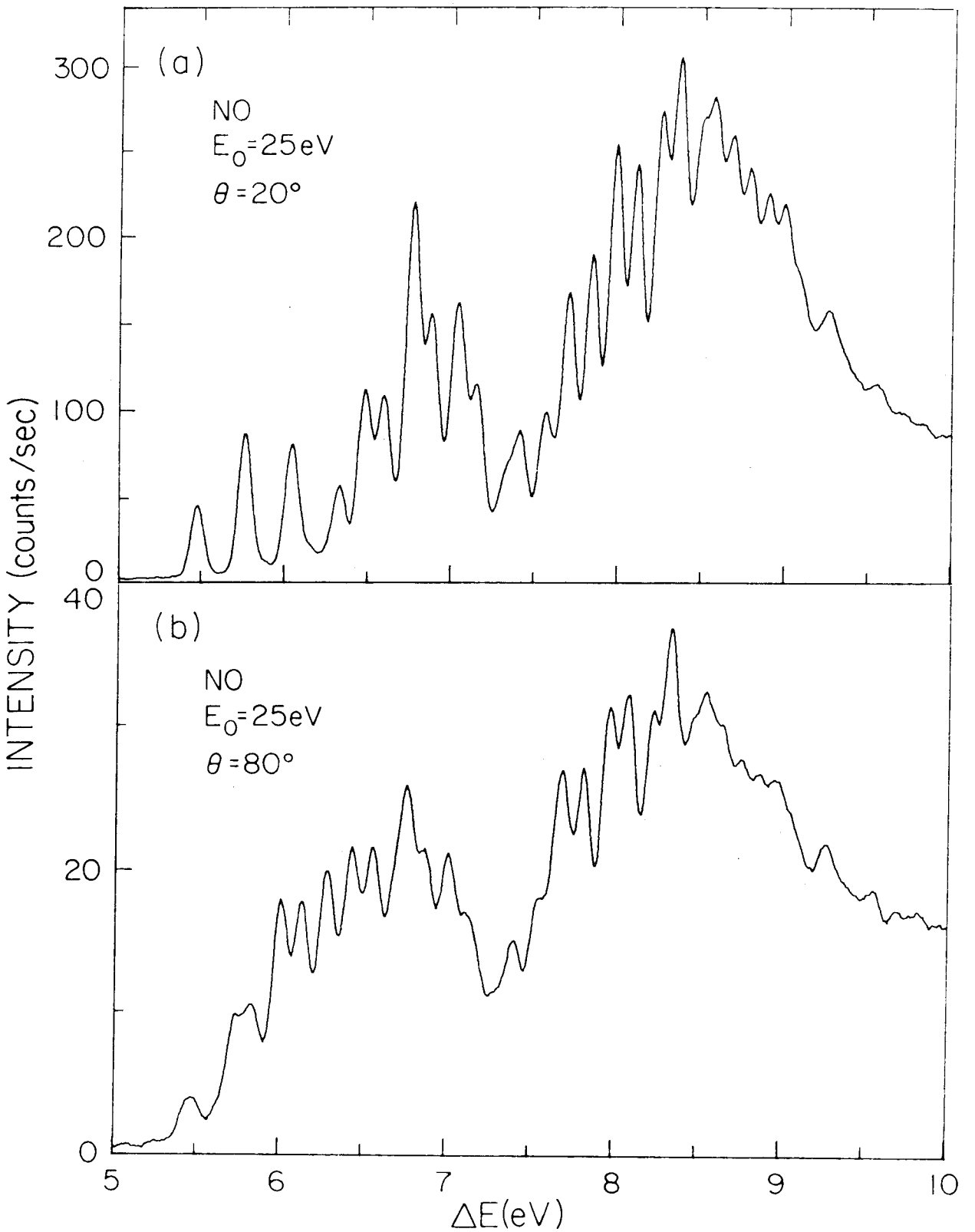
(a)
NO
E_0=25eV
θ=20°
(b)
NO
E_0=25eV
θ=80°
INTENSITY (counts/sec)
300
200
100
0
40
20
0
5
6
7
8
9
10
ΔE(eV)

Figure 2

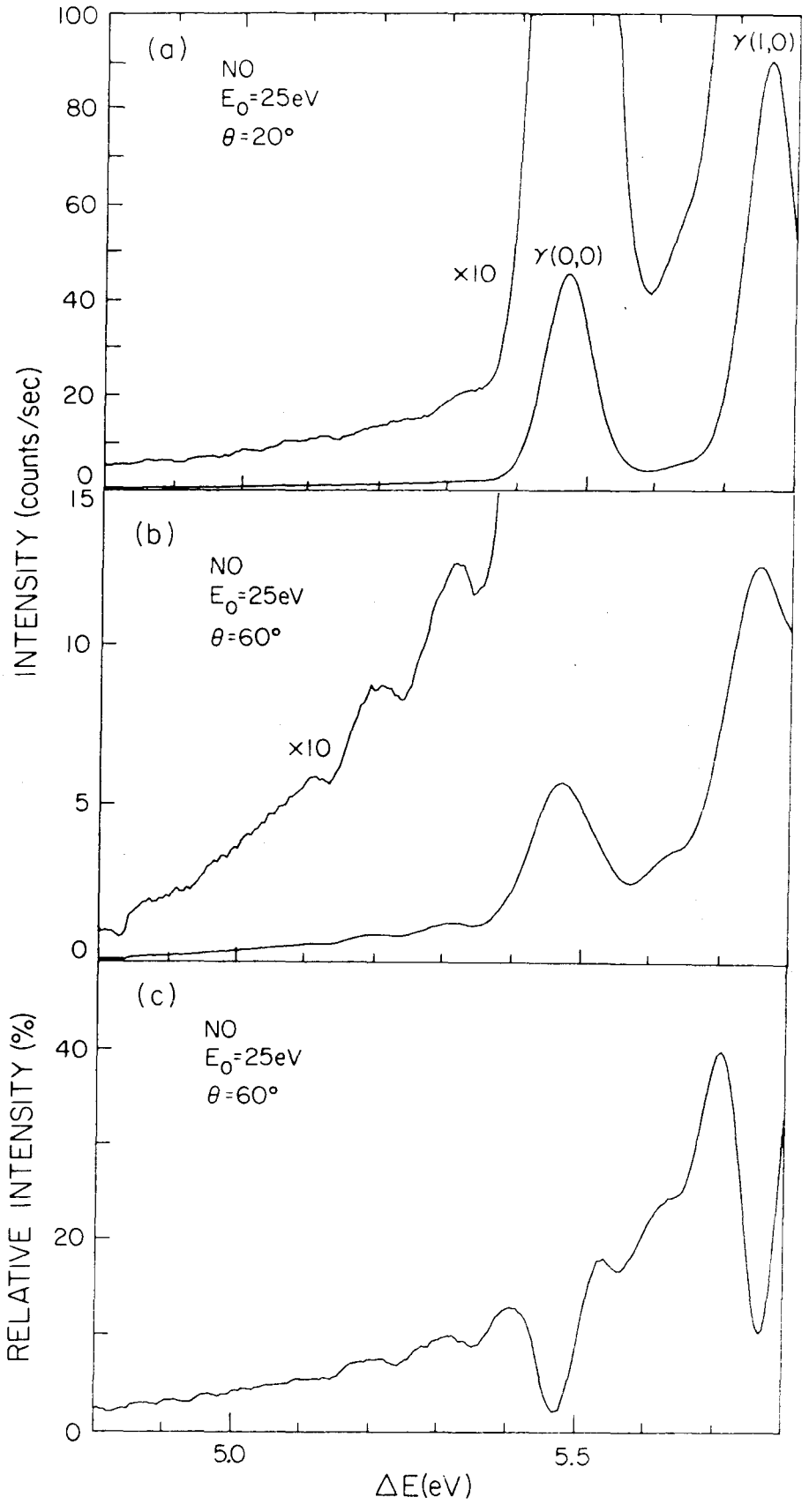
(a)
NO
E_0=25eV
θ=20°
×10
γ(0,0)
γ(1,0)
(b)
NO
E_0=25eV
θ=60°
×10
(c)
NO
E_0=25eV
θ=60°
INTENSITY (counts/sec)
RELATIVE INTENSITY (%)
ΔE(eV)
100
80
60
40
20
0
15
10
5
0
40
20
0
5.0
5.5

Figure 3

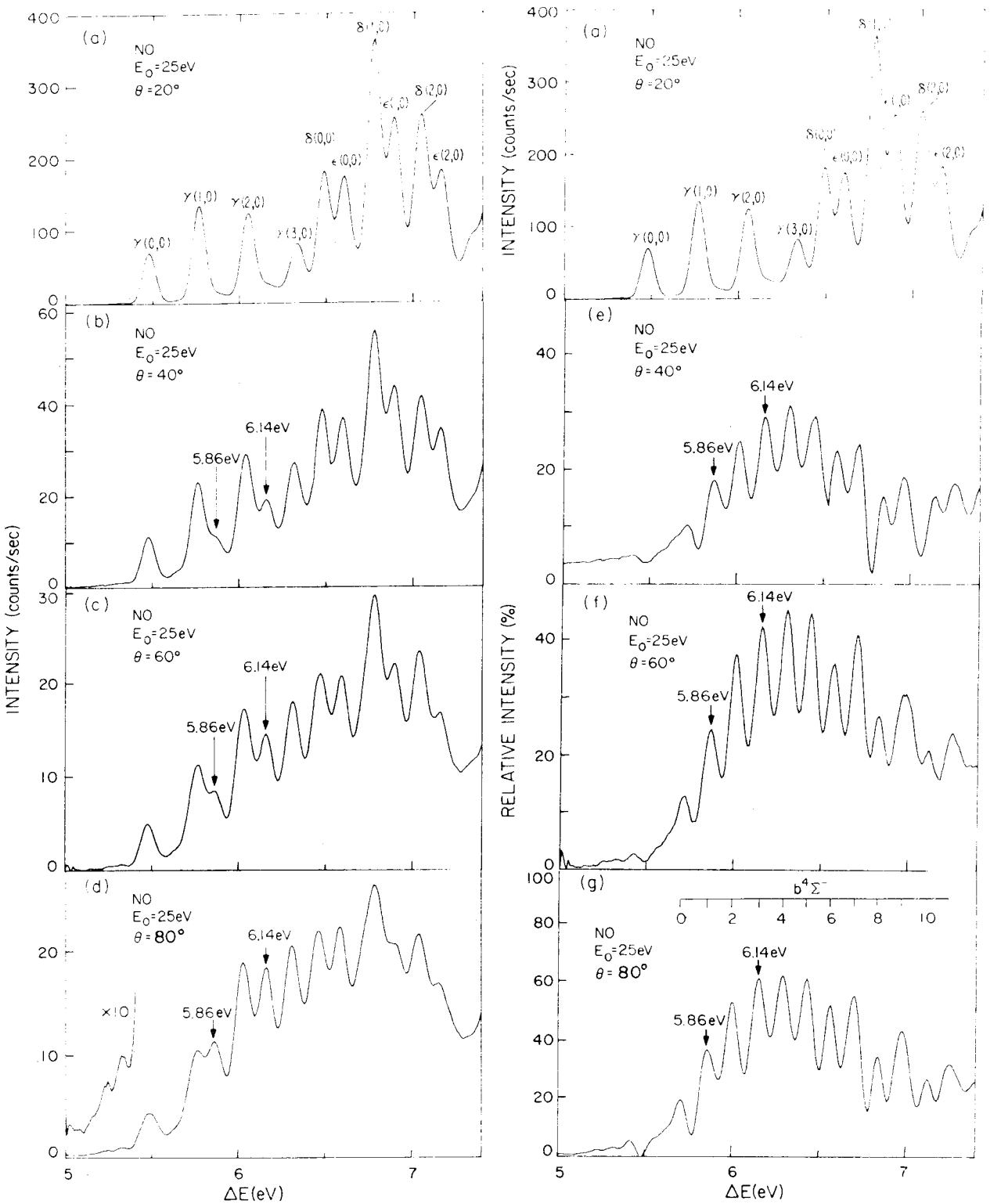
(a)
NO
E0=25eV
θ=20°
γ(0,0)
γ(1,0)
γ(2,0)
γ(3,0)
δ(0,0)
ε(0,0)
δ(1,0)
ε(1,0)
δ(2,0)
ε(2,0)
(b)
NO
E0=25eV
θ=40°
5.86eV
6.14eV
(c)
NO
E0=25eV
θ=60°
5.86eV
6.14eV
(d)
NO
E0=25eV
θ=80°
×10
5.86eV
6.14eV
INTENSITY (counts/sec)
ΔE(eV)
(e)
NO
E0=25eV
θ=40°
5.86eV
6.14eV
(f)
NO
E0=25eV
θ=60°
5.86eV
6.14eV
(g)
b4Σ-
NO
E0=25eV
θ=80°
5.86eV
6.14eV
RELATIVE INTENSITY (%)
ΔE(eV)

Figure 4

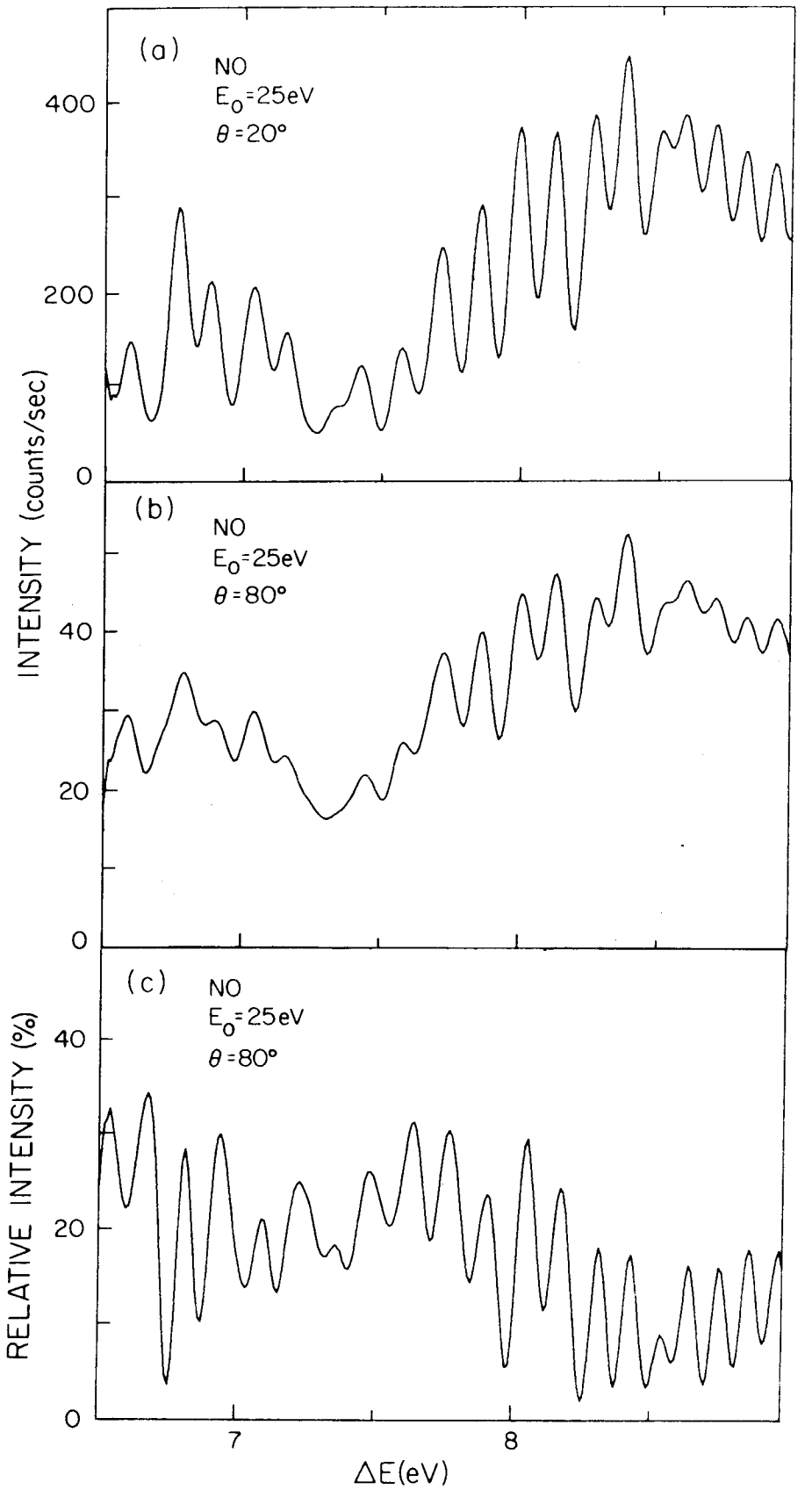
(a)
NO
E_0=25eV
θ=20°
400
200
0
(b)
NO
E_0=25eV
θ=80°
40
20
0
INTENSITY (counts/sec)
(c)
NO
E_0=25eV
θ=80°
40
20
0
RELATIVE INTENSITY (%)
7
8
ΔE(eV)

Figure 5

Appendix II: Electronic Spectroscopy of UF_6 and WF_6 by Electron Impact

Electronic spectroscopy of UF_6 and WF_6 by electron impact[a)]

Ronald Rianda,[b)] Robert P. Frueholz, and Aron Kuppermann

Arthur Amos Noyes Laboratory of Chemical Physics,[c)]
California Institute of Technology, Pasadena, California 91125

(Received)

The electron-impact excitation spectra of uranium hexafluoride (UF_6) and tungsten hexafluoride (WF_6) have been studied experimentally at impact energies of 30, 50, and 75 eV and at scattering angles from 5° to 80°. Eleven transitions in UF_6 are observed with apparent maxima at 3.26, 4.2, ~4.7, 5.8, 7.0, 7.86, 9.26, 11.01, 11.75, 12.5, and 13.2 eV. Four transitions in WF_6 are observed with maximum intensity at 7.25, 7.9, 8.5, and 9.85, in good agreement with optical work. In addition three previously unobserved transitions in WF_6 at 11.75, 12.6, and 13.5 eV are reported. Similarity between the spectra of UF_6 and WF_6 suggests that the primary contribution to the absorption intensity in UF_6 above 5.8 eV and in WF_6 results from charge transfer transitions from fluorine p orbitals to metal d orbitals. Tentative assignments based in part on recent theoretical studies are made.

---

a) This work was supported by the Department of Energy (Contract No. EY-76-S-02-767). Report Code: CALT-767P4-162.

b) Work completed in partial fulfillment of the requirements for the PhD in chemistry at the California Institute of Technology.

c) Contribution No. 5753.

I. INTRODUCTION

A potential uranium isotope separation scheme involves isotopically specific vibrational excitation of the ν_3 mode of $^{235}UF_6$ followed by the electronic excitation of the vibrationally excited species by one or two ultraviolet photons to a dissociative or predissociative state. In order to determine the positions and nature of the electronically excited states which might prove important to such a scheme the electron-impact spectrum of UF_6 has been studied. As an aid to assignment of the spectrum of UF_6 the electron impact spectrum of WF_6 has also been determined.

In previous studies the technique of low-energy variable-angle electron-impact spectroscopy has been primarily applied to molecules composed of light nuclei (first and second row elements) with principal emphasis on the detection of spin-forbidden transitions.[1-4] In these systems the differential cross section (DCS) as a function of angle is a sensitive probe of the spin-forbiddenness or allowedness of a transition. Typically, the DCS for an optically allowed transition decreases by approximately two orders of magnitude as the scattering angle is increased from 10° to 80°. In contrast the DCS for a spin-forbidden excitation (one in which the spin quantum number changes by unity) remains relatively constant, within a factor of 2 or 3, over a similar angular range. Electron impact spectroscopy is also suitable for studying molecules containing heavy nuclei[5-7] such as UF_6 and WF_6, but in these systems spin-orbit coupling may be significant. The

resultant mixing of states of different spin multiplicities causes the correlation between the angular behavior of the DCS and the spin nature of the transition to become less clear.[5]

Both UF_6 and WF_6 posess O_h symmetry.[8] From the viewpoint of ligand field theory the valence electrons of the central metal atom (the 5f, 6d, and 7s electrons of uranium and the 5d and 6s electrons of tungsten) are assumed to be transferred to the fluorine atoms yielding a complex of the form $M^{6+} F_6^{6-}$. This is a crude approximation which nevertheless is helpful in explaining the observed spectra. In this model,transitions correspond to charge transfer from ligand fluorine atom orbitals to the 5f, 6d, and 7s orbitals of uranium and the 5d and 6s orbitals of tungsten.

Previous theoretical studies on UF_6 have considered only transitions from ligand orbitals to uranium 5f orbitals and therefore assignment of only the low energy portion of the spectrum was attempted.[9-11] The most reliable calculation to date is that of Koelling, Ellis, and Bartlett[11] using the relativistic,self-consistent, Dirac-Slater model. They have obtained one-electron energy levels, charge distributions, ligand-to-uranium 5f orbital transitions energies, and ionization potentials which agree well with experiment. Figure 1 shows the orbital energy diagram obtained for UF_6 based in part on their calculations. There have been no theoretical studies of the electronic structure of WF_6 to date.

Prior to our investigation numerous optical absorption studies of UF_6 in the region below 6 eV have been performed.[12-16] Agreement

between these previous experimental results and the theoretical calculations is fair. However, considering the density of predicted transitions, any apparent agreement may be fortuitous. McDiarmid has performed the only optical studies of UF_6 and WF_6 above 6 eV.[17,18] In addition to the optical work, previous electron-impact studies of UF_6 have been performed by Chutjian et al.[6] and Srivastava et al.[7] from which photoabsorption cross sections were obtained. Attempts at interpreting the observed spectra were limited.

II. EXPERIMENTAL

The electron-impact spectrometer used in this study was that reported by Kuppermann et al.[1] with the surfaces of all electron optical elements having been goldplated. With unplated surfaces (oxygen-free, high-purity copper lenses and hemispherical analyzers and molybdenum apertures) operation of the instrument was limited to periods of one to two hours before complete disassembly and cleaning of the electron optics was required, due to the reactivity of the hexafluorides. After goldplating continuous operation for periods up to one week was possible.

Spectra of UF_6 and WF_6 in the energy-loss region 0-18 eV were taken at impact energies of 30, 50, and 75 eV at scattering angles from 5° to 80°. The sample chamber pressure was typically 2 mTorr as indicated by an uncalibrated Schulz-Phelps ionization gauge, while the incident electron beam current was approximately 40 nA. Instrumental resolution was electron-optically set at approximately 0.18 eV. Accumulation times for typical spectra ranged from 3 hours for a 10° spectrum to about 12 hours for an 80° spectrum. This corresponds to a 10 meV channel width accumulation time of between 10 sec and 40 sec. Spectra presented in Figs. 2 through 5 were digitally smoothed using an 11 to 19 channel least-squares cubic polynomial convolution. Before smoothing, typical signal-to-noise ranged from about 3 : 1 on weak features in high-angle spectra to approximately 100 : 1 for strong features in low-angle spectra.

The UF_6 was supplied by Varlacoid Chemical Co.[19] with a stated purity of 99.9%. The WF_6 was obtained from PCR Inc.[20] with a stated purity of 99%. Both samples were used without further purification.

III. RESULTS

Figures 2 and 3 show the electron-impact spectrum of UF_6 and WF_6 at an impact energy of 50 eV and scattering angles of 10° and 70°. The higher energy-loss regions of both UF_6 and WF_6 are shown in greater detail at 75 eV impact energy in Figs. 4 and 5. The ratios of DCS's of several features in the spectrum of UF_6 at 50 eV to the DCS of the 5.8 eV feature are shown in Fig. 6. Similarly, for WF_6 DCS ratios with respect to the 8.5 eV feature are shown in Fig. 7.

The most significant changes with angle in the spectra of UF_6 occur in the 3-5 eV region and at the 11.01 eV feature. At an impact energy of 50 eV the integrated intensity under the 3.26 eV feature increases by about an order of magnitude relative to that under the feature at 5.8 eV as the scattering angle is increased from 10° to 80°. For molecules with light nuclei such behavior would be consistent with three possible interpretations: a) this feature is due to a spin-forbidden transition; b) it is due to a spin-allowed but symmetry-forbidden transition; and c) it results from a spin-allowed transition with an underlying spin-forbidden transition, a possibility which would have been considered to be the most likely.

However, the relationship of the variation of the DCS with scattering angle and the spin-allowedness of a transition is ambiguous for molecules such as UF_6 and WF_6 which contain heavy nuclei. In these systems the "goodness" of the orbital and spin angular momentum quantum numbers L and S is questionable. Both theoretical and experimental information regarding the spin-orbit interaction as applied to

the spin nature of the wavefunction is lacking. Similarly, attempts at correlating the electron impact DCS with the magnitude of the spin-orbit interaction have been limited to a study of Xe by Williams, Trajmar, and Kuppermann.[5] The results of this study indicate that for atoms with significant spin-orbit interactions DCS variations with angle may no longer be used with reliability to assign the spin nature of a transition. In molecular systems containing a heavy central atom in a strong ligand field provided by surrounding atoms, the influence of that field on the central atom orbitals may predominate over the spin-orbit interaction.[21-23] However, the implication of this regarding DCS variations is unknown.

In the 4 to 5 eV region the low-angle spectrum shows an unresolved feature with an apparent (deconvoluted) intensity maximum at approximately 4.7 eV, while the high-angle spectrum shows a feature with a distinct maximum at 4.2 eV. This observed shift in position indicates the overlap of at least two electronic transitions. Optically, a feature is observed at 4.8 eV as well as two much weaker transitions at 4.2 and 4.0 eV.[11] The intensity under the 11.01 eV feature increases by a factor of 5 relative to that under the 5.8 eV one as the scattering angle increases from 10° to 80°. This increase is significant and will be used in discussing the assignments of this 11.01 eV transition in Section IV.

In the spectrum of WF_6 there is no detectable absorption below 5.5 eV. The only significant change with angle in the spectrum of this molecule occurs at 11.75 eV. The integrated intensity under this feature increases by a factor of about 7 relative to that under the 8.5 eV

one as the scattering angle is increased from 10° to 80°.

The similarities between the spectra of UF_6 and WF_6 are quite apparent from comparison of Figs. 2-5. In addition to the absence of the low-lying absorptions in WF_6, the principal difference is that the WF_6 spectrum is shifted to higher energy by about 1 eV with respect to the UF_6 spectrum. Table I summarizes our results for UF_6 and WF_6, respectively.

V. DISCUSSION

In order to assign the bands in the UF_6 spectrum it is worthwhile to make use of the similarities between it and the WF_6 spectrum. Since WF_6 does not possess low-lying unoccupied f valence orbitals we believe all transitions observed below 14 eV in this molecule correspond to a valence charge transfer from fluorine ligand σ and π orbitals to tungsten 5d orbitals. The possibility exists that features observed in the region of the spectrum above approximately 10 eV are due to Rydberg excitations. We do not think this to be a correct assignment for the features below 14 eV for the following reasons. The intensities of the transitions at 12.6 and 13.5 eV are significantly greater than would be expected for Rydberg excitations. The oscillator strength for the transition at 13.5 eV in WF_6 may be estimated in the following manner. The generalized electron impact oscillator strength,[25] f_{ei}, is given by

$$f_{ei} = \frac{W}{2} \frac{k_0}{k_n} K^2 \sigma \quad ,$$

where W is the excitation energy, k_0 and k_n are the incident and scattered electron momenta, respectively, K is the change in momentum suffered by the electron as a result of the collision, and σ is the differential cross section for the transition being considered. Since we have not obtained absolute DCS's we are only able to estimate ratios of f_{ei}. Lassettre et al.[25] have shown that as K^2 approaches zero, f_{ei} approaches the optical oscillator strength f_{opt}. From the optical data of R. McDiarmid[17] we estimate f_{opt} of the 8.5 eV feature to be 0.3.[26]

Using our 50 eV incident energy spectra, and extrapolating the f_{ei} versus K^2 curve monotonically to $K^2 = 0$, we obtained an unnormalized f_{opt} for the 8.5 eV transition. Since this must correspond to the value of f_{opt} (absolute) obtained from the data of ref. 17, we are able to calculate the normalization factor which makes our measurements absolute. This factor is independent of the transition being considered and is, hence, the same for the 13.5 eV feature. The resulting absolute value of f_{opt} for this transition is 0.8 which is roughly three times greater than the maximum oscillator strength expected for a Rydberg excitation.[27] The transition at 11.75 eV in WF_6 is weaker than that at 13.5 eV, rekindling the possibility that it may be due to a Rydberg state. However, the angular behavior of its differential cross section suggests, as indicated below, that this is not the case.

The similarity of the UF_6 spectrum above 5 eV energy loss to that of WF_6 suggests that the primary contribution to the spectrum in this region is also due to transitions from fluorine ligand σ and π orbitals to uranium 6d orbitals, although the apparently increased intensity of the features at 5.8 and 7.86 eV in UF_6 relative to the corresponding features in WF_6 may indicate an additional contribution in UF_6 from ligand to 5f orbital excitations.

Use of the orbital energy ordering for UF_6 as well as excitation energies calculated by Koelling et al.[11] (orbital energy diagram shown in Fig. 1) allows a more specific assignment of some of the transitions. Orbital designations are those appropriate for the O_h' double group[24] re-

quired by the spin-orbit interactions in these systems. Since no electronic structure calculations have been reported for WF_6, we assume in our analysis that the orbital ordering in that molecule is the same as for the corresponding orbitals in UF_6. Transitions below 5.8 eV in UF_6 have been assigned by Koelling et al. as ligand to 5f orbital excitations.[11] These assignments are consistent with our results and are summarized in Table 1. The 5.8 eV feature in UF_6 has been assigned as a ligand to 5f transition for which the calculated excitation energy is 6.31 eV. However, comparison with our WF_6 results indicates that a significant fraction of the intensity of this feature is due to excitation to the uranium 6d ($4\gamma_{8g}$, $2\gamma_{7g}$) orbitals (see Fig. 1). Therefore, the most reasonable explanation would be that this UF_6 feature results from a superposition of at least the $3\gamma_{8g} \rightarrow 5\gamma_{8u}$ and $3\gamma_{8u} \rightarrow 4\gamma_{8g}$, $2\gamma_{7g}$ one-electron excitations. Analogously, the 7.25 eV feature in WF_6 is assigned to the $3\gamma_{8u} \rightarrow 4\gamma_{8g}$, $2\gamma_{7g}$ transitions. The next two excitations in UF_6 at 7.0 and 7.86 and in WF_6 at 7.9 and 8.5 eV are assigned as the $2\gamma_{6u} \rightarrow 4\gamma_{8g}$, $2\gamma_{7g}$ and $2\gamma_{8u}$, $1\gamma_{7u} \rightarrow 4\gamma_{8g}$, $2\gamma_{7g}$ one-electron transitions, respectively. In the ligand field theory approach, using O_h symmetry, among the most intense transitions is expected to be the transition from the fluorine $p\sigma$ (t_{2u}) orbital to the metal e_g-orbital (from spatial overlap considerations). Therefore we assign the intense features at 13.5 eV in WF_6 and 13.2 eV in UF_6 as the $1\gamma_{6u}$, $1\gamma_{8u} \rightarrow 5\gamma_{8g}$ transitions. In UF_6 the nearly degenerate $1\gamma_{7u}$ and $2\gamma_{8u}$ orbitals are calculated to lie approximately 0.6 eV higher in energy than the $1\gamma_{6u}$ and $1\gamma_{8u}$ orbitals. Excitation from these orbitals is allowed and

is expected to be about 0.6 eV below the $1\gamma_{6u}$, $1\gamma_{8u} \rightarrow 5\gamma_{8g}$ transition. Therefore we tentatively assign the 12.5 eV feature in UF_6 and the 12.6 eV feature in WF_6 to the $1\gamma_{7u}$, $2\gamma_{8u} \rightarrow 5\gamma_{8g}$ excitations. The angular behavior of the features at 3.26 and 11.01 eV in UF_6 and at 11.75 eV in WF_6 is distinctly different from that of the other features in the spectra. Figure 6 displays the ratios of integrated intensities of some bands of UF_6 relative to the 5.8 eV feature. Figure 7 shows the corresponding ratios for features of WF_6 relative to the integrated intensity of the 8.5 eV band. The ratios demonstrate that the features at 3.26 and 11.01 in UF_6 and at 11.75 eV in WF_6 display a significant increase in relative intensity as the scattering angle is increased. While the concept of singlet and triplet states is not well defined for these molecules (see Section I), this angular behavior is very similar to that displayed by transitions which have been definitively assigned as singlet → triplet in systems containing only light nuclei.[1-4] A possible explanation for the angular behavior of the 11.01 eV feature in UF_6 and the 11.75 eV feature in WF_6 is that these transitions contain significant singlet → triplet contributions. Since we believe them to be ligand-to-metal d-orbital excitations, it is possible that the ligand field interaction is sufficiently strong to predominate over the spin-orbit interaction yielding states which are either primarily singlet or primarily triplet in nature.[21-23] In addition to the feature at 11.01 eV in UF_6 there is also a transition at 11.75 eV which appears to display similar angular behavior, suggesting that it too may be due to a singlet → triplet transition. Unfortunately, this transition is heavily overlapped with the 12.5 eV feature and reliable integrated intensity ratios were not obtainable.

The feature at 3.26 eV in UF_6 has been previously assigned to overlapping singlet → singlet and singlet → triplet transitions.[16] This transition is presumably due exclusively to a ligand to uranium 5f orbital excitation, and consequently care must be taken when attempting to assign it using an LS coupling scheme. This is due to the fact that the ligand field interaction for the 5f orbitals is significantly weaker than that for the 6d orbitals and is expected to be of the same order as the spin orbit interaction, weakening the argument in behalf of an LS coupling scheme.[21-23]

Three additional optically allowed excitations, $1\gamma_{6u}$, $1\gamma_{8u} \rightarrow 4\gamma_{8g}$, $2\gamma_{7g}$, $3\gamma_{8u} \rightarrow 5\gamma_{8g}$ and $2\gamma_{6u} \rightarrow 5\gamma_{8g}$ are predicted by the ordering scheme of Fig. 1. They may lie in the 8-11 eV region where only one feature is apparent in our spectra: the 9.26 eV feature in UF_6 and the 9.85 feature in WF_6. Several higher lying transitions are also observed in both WF_6 and UF_6 above 14 eV which we tentatively assign to Rydberg excitations.

VI. CONCLUSIONS AND SUMMARY

We have obtained electron impact spectra of UF_6 and WF_6 at several different impact energies and scattering angles from 5° to 80°. Our measurements for UF_6 are in good agreement with previous ones. For WF_6 the results of our experiments are also in good agreement with previous limited optical studies. We have reported several previously unobserved transitions at higher energy losses. Assignments of the spectra of both UF_6 and WF_6 are proposed using the theoretical results of Koelling et al.[11] and relying heavily upon similarities in the UF_6 and WF_6 spectra. Below 14 eV we assign all transitions in WF_6 as ligand to tungsten 5d orbital charge transfer excitations. The spectrum of UF_6 between 5 eV and 14 eV is very similar to that of WF_6 and the primary contribution to this region is similarly assigned to ligand to uranium 6d orbital excitations. Correspondingly, transitions in UF_6 below 5 eV are assigned exclusively to ligand to 5f excitations.

ACKNOWLEDGMENT

The authors express their appreciation to Professor H. B. Gray for useful discussions.

TABLE I. Energy-loss features in UF_6 and WF_6.[1,b]

Transition	UF_6	WF_6
$3\gamma_{8u} \rightarrow 2\gamma_{7u}$, $4\gamma_{8u}$, $3\gamma_{7u}$	3.26	
$3\gamma_{8g} \rightarrow 2\gamma_{7u}$	4.2	
$3\gamma_{8g} \rightarrow 4\gamma_{8u}$	~4.7	
$3\gamma_{8u} \rightarrow 4\gamma_{8g}$, $2\gamma_{7g}$	5.8[c]	7.25
$2\gamma_{6u} \rightarrow 4\gamma_{8g}$, $2\gamma_{7g}$	7.0[c]	7.9
$2\gamma_{8u}$, $1\gamma_{7u} \rightarrow 4\gamma_{8g}$, $2\gamma_{7g}$	7.86[c]	8.5
	9.26	9.85
	11.01	
	11.75	11.75
$2\gamma_{8u}$, $1\gamma_{7u} \rightarrow 5\gamma_{8g}$	12.5	12.6
$1\gamma_{6u}$, $1\gamma_{8u} \rightarrow 5\gamma_{8g}$	13.2	13.5

[a]The energy losses are in eV and have an accuracy of ± 0.05 eV.

[b]The assignments in this table are based in part on the calculations of ref. 11; the energy losses are those of the present experiments.

[c]There may also be contribution to these features from ligand-to-5f transitions.

References

[1](a) A. Kuppermann, J. K. Rice and S. Trajmar, J. Phys. Chem. 72, 3894 (1965); (b) J. K. Rice, Ph.D. Thesis, California Institute of Technology, Pasadena, California (1969).

[2]S. Trajmar, J. K. Rice and A. Kuppermann, Advan. Chem. Phys. 78, 15 (1970).

[3](a) O. A. Mosher, W. M. Flicker and A. Kuppermann, J. Chem. Phys. 59, 6502 (1973); (b) O. A. Mosher, W. M. Flicker and A. Kuppermann, J. Chem. Phys. 62, 2600 (1975).

[4]R. P. Frueholz, W. M. Flicker, O. A. Mosher and A. Kuppermann, Chem. Phys. Lett. 52, 86 (1977).

[5]W. Williams, S. Trajmar and A. Kuppermann, J. Chem. Phys. 62, 3031 (1975).

[6]A. Chutjian, S. K. Srivastava, S. Trajmar, W. Williams and D. C. Cartwright, J. Chem. Phys. 64, 4791 (1976).

[7]S. K. Srivastava, D. C. Cartwright, S. Trajmar, A. Chutjian and W. X. Williams, J. Chem. Phys. 65, 208 (1976).

[8]R. S. McDowell, L. B. Asprey and R. T. Paine, J. Chem. Phys. 61, 3571 (1974).

[9]D. H. Maylotte, R. L. St. Peters and R. P. Messmer, Chem. Phys. Lett. 38, 181 (1976).

[10]M. Boring and J. W. Moskowitz, Chem. Phys. Lett. 38, 185 (1976).

[11]D. D. Koelling, D. E. Ellis, R. J. Bartlett, J. Chem. Phys. 65, 3331 (1976).

[12]G. H. Dieke and A. B. F. Duncan, Spectroscopic Properties of Uranium Compounds, (McGraw-Hill, Inc., New York, 1949).

[13]G. P. Sheretmet'ev, Optika i Spektroskopiya 1, 181 (1956).

[14]H. J. Hurst and P. W. Wilson, Spectr. Lett. 5, 275 (1972).

[15]G. L. De Poorter and C. K. Rofer-De Poorter, Spectr. Lett. 8, 521 (1975).

[16]W. B. Lewis, L. B. Asprey, L. H. Jones, R. S. McDowell, S. W. Rabideau, A. H. Zeltmann and R. T. Paine, J. Chem. Phys. 65, 2707 (1976).

[17]R. McDiarmid, J. Chem. Phys. 65, 168 (1976).

[18]R. McDiarmid, J. Chem. Phys. 6, 3333 (1977).

[19]Varlacoid Chemical Co., 666 S. Front St., Elizabeth, NJ 07202.

[20]PCR Inc., Research Chemicals Division, P.O. Box 1466, Gainesville, FA 32602.

[21]W. Moffitt, G. L. Goodman, M. Fred and B. Weinstock, Mol. Phys. 2, 109 (1959).

[22]N. J. Reisfeld and G. A. Crosby, Inorg. Chem. 4, 65 (1965).

[23]G. C. Allen and K. D. Warren, Coord. Chem. Rev. 16, 227 (1975).

[24]N. Tinkham, Group Theory and Quantum Mechanics, (McGraw-Hill, Inc., New York, 1964) pp. 75-80.

[25]E. N. Lassettre, A. Skerbele and N. A. Dillon, J. Chem. Phys. 50, 1829 (1969).

[26]Value of f_{opt} obtained using data of ref. 17 and a path length of 10 cm (personal communication, R. McDiarmid).

[27]M. B. Robin, Higher Excited States of Polyatomic Molecules, Vol. I, (Academic Press, New York, 1974) p. 30.

Figure Captions

Figure 1. Valence orbital energy ordering for UF_6. Symmetry designations listed under O_h are those appropriate for the octahedral point group, while those beneath O_h' are appropriate for the octahedral double point group. The $5\gamma_{8g}$ is about 13.2 eV above the $1\gamma_{8u}$. The location of the others is approximate. The levels $3\gamma_{8u}$ and below represent fully occupied valence orbitals involved in the U–F bonding.

Figure 2. Electron energy loss spectrum of UF_6 at (1) 10° and (b) 70°; 50 eV incident electron energy; 4×10^{-8} A incident beam current; 2 mTorr sample pressure reading from an uncalibrated Schulz-Phelps gauge; resolution approximately 0.18 eV (fwhm).

Figure 3. Electron energy loss spectrum of WF_6 at (a) 10° and (b) 70°; 50 eV incident electron energy; 7×10^{-8} A incident beam current; 1 mTorr sample pressure reading from an uncalibrated Schulz-Phelps gauge; resolution approximately 0.18 eV (fwhm). No absorption is observed for ΔE below 5.5 eV.

Figure 4. Electron energy loss spectrum of UF_6 at 5°; 75 eV incident electron energy; other experimental parameters are similar to those in Fig. 2.

Figure 5. Electron energy loss spectrum of WF_6 at 5°; 75 eV incident electron energy; other experimental parameters are similar to those in Fig. 3.

Figure 6. Integrated intensities of several electronic transitions in UF_6 divided by the integrated intensity of the 5.8 eV feature as a function of scattering angle θ at an incident electron-energy of 50 eV; the transition energies for each of the curves are indicated. The scale factors in parentheses indicate the coefficients by which the intensity ratios were multiplied before being plotted.

Figure 7. Integrated intensities of several electronic transitions in WF_6 divided by the integrated intensity of the 8.5 eV feature as a function of θ at an incident electron energy of 50 eV; the transition energies for each of the curves are indicated. The intensity ratio for the 11.01 eV transition was multiplied by 0.01 before plotting.

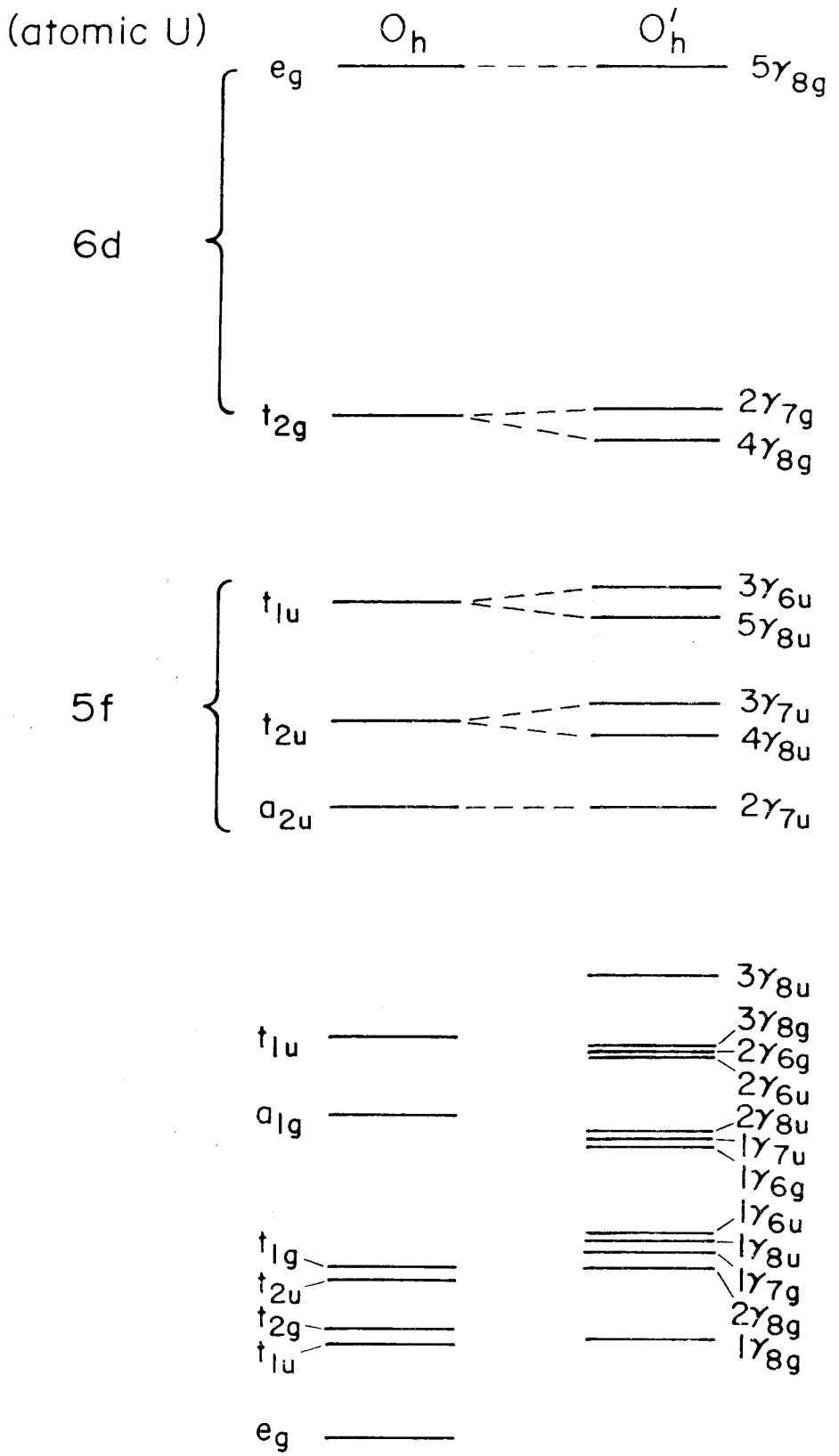
(atomic U)
O_h
O_h'
e_g
$5\gamma_{8g}$
6d
t_{2g}
$2\gamma_{7g}$
$4\gamma_{8g}$
t_{1u}
$3\gamma_{6u}$
$5\gamma_{8u}$
5f
t_{2u}
$3\gamma_{7u}$
$4\gamma_{8u}$
a_{2u}
$2\gamma_{7u}$
$3\gamma_{8u}$
t_{1u}
$3\gamma_{8g}$
$2\gamma_{6g}$
$2\gamma_{6u}$
a_{1g}
$2\gamma_{8u}$
$1\gamma_{7u}$
$1\gamma_{6g}$
t_{1g}
$1\gamma_{6u}$
t_{2u}
$1\gamma_{8u}$
t_{2g}
$1\gamma_{7g}$
t_{1u}
$2\gamma_{8g}$
$1\gamma_{8g}$
e_g

Figure 1

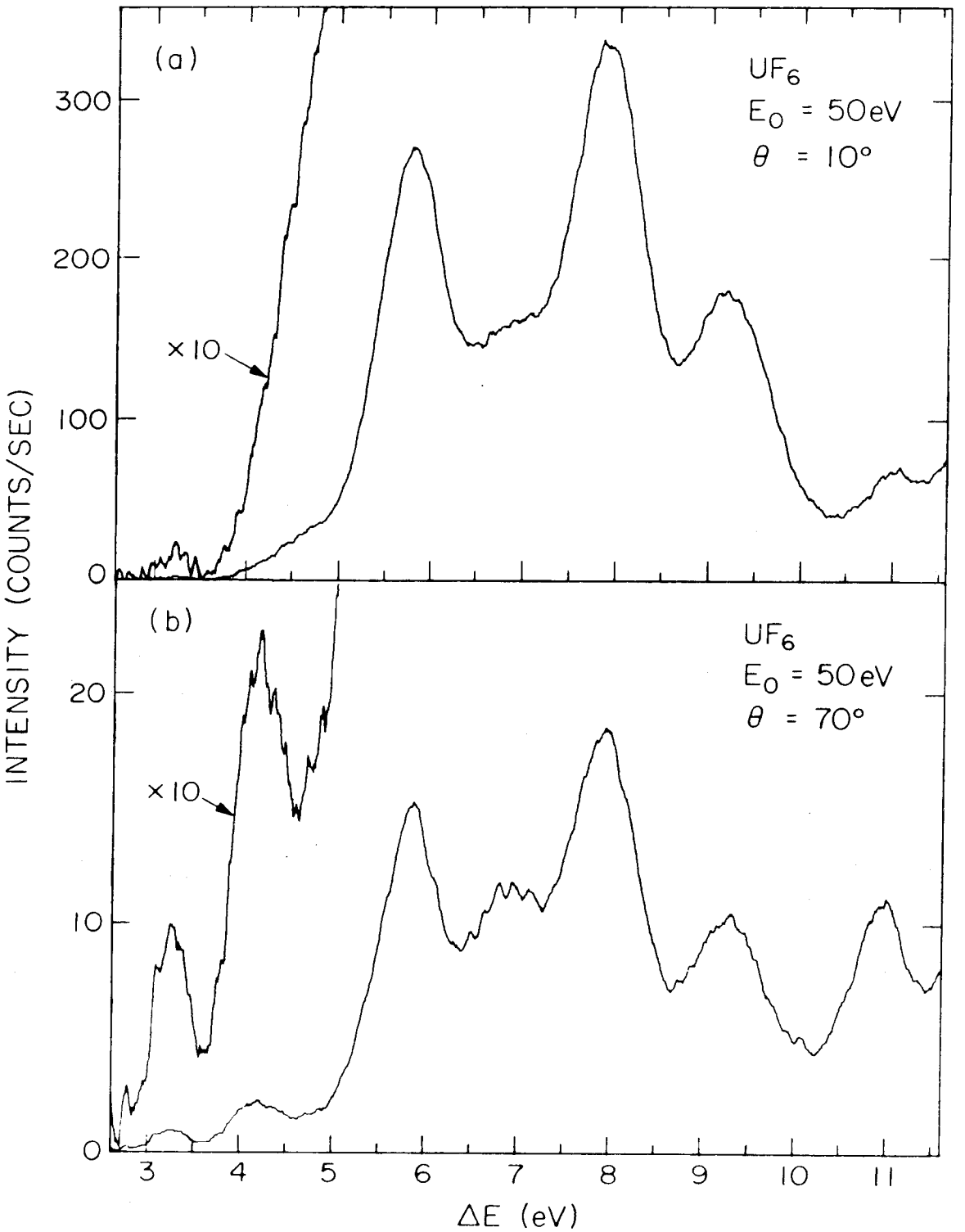
(a)
UF6
E0 = 50eV
θ = 10°
×10
300
200
100
0
(b)
UF6
E0 = 50eV
θ = 70°
×10
20
10
0
INTENSITY (COUNTS/SEC)
3
4
5
6
7
8
9
10
11
ΔE (eV)

Figure 2

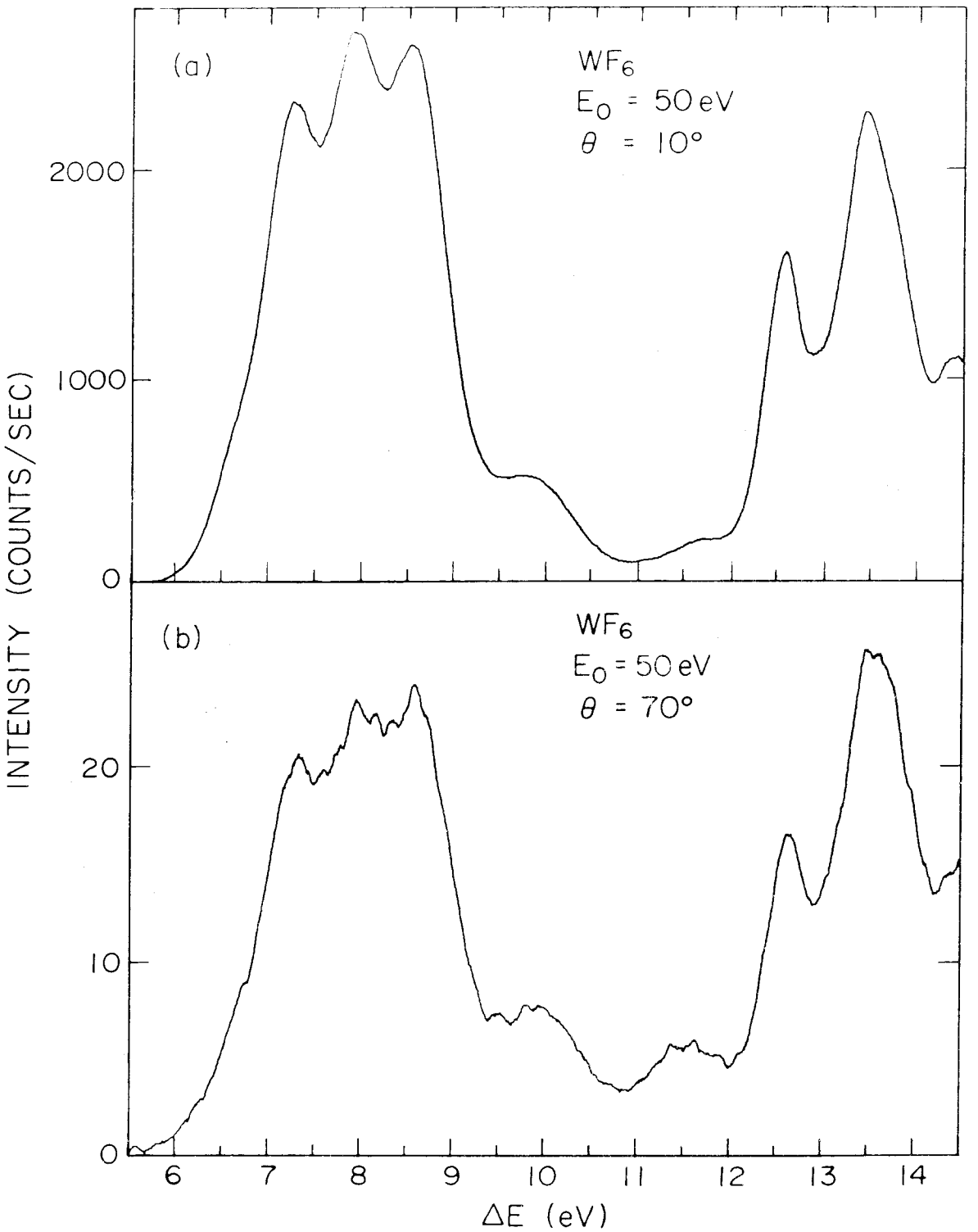
(a)
WF6
E0 = 50 eV
θ = 10°
2000
1000
0
(b)
WF6
E0 = 50 eV
θ = 70°
20
10
0
INTENSITY (COUNTS/SEC)
6
7
8
9
10
11
12
13
14
ΔE (eV)

Figure 3

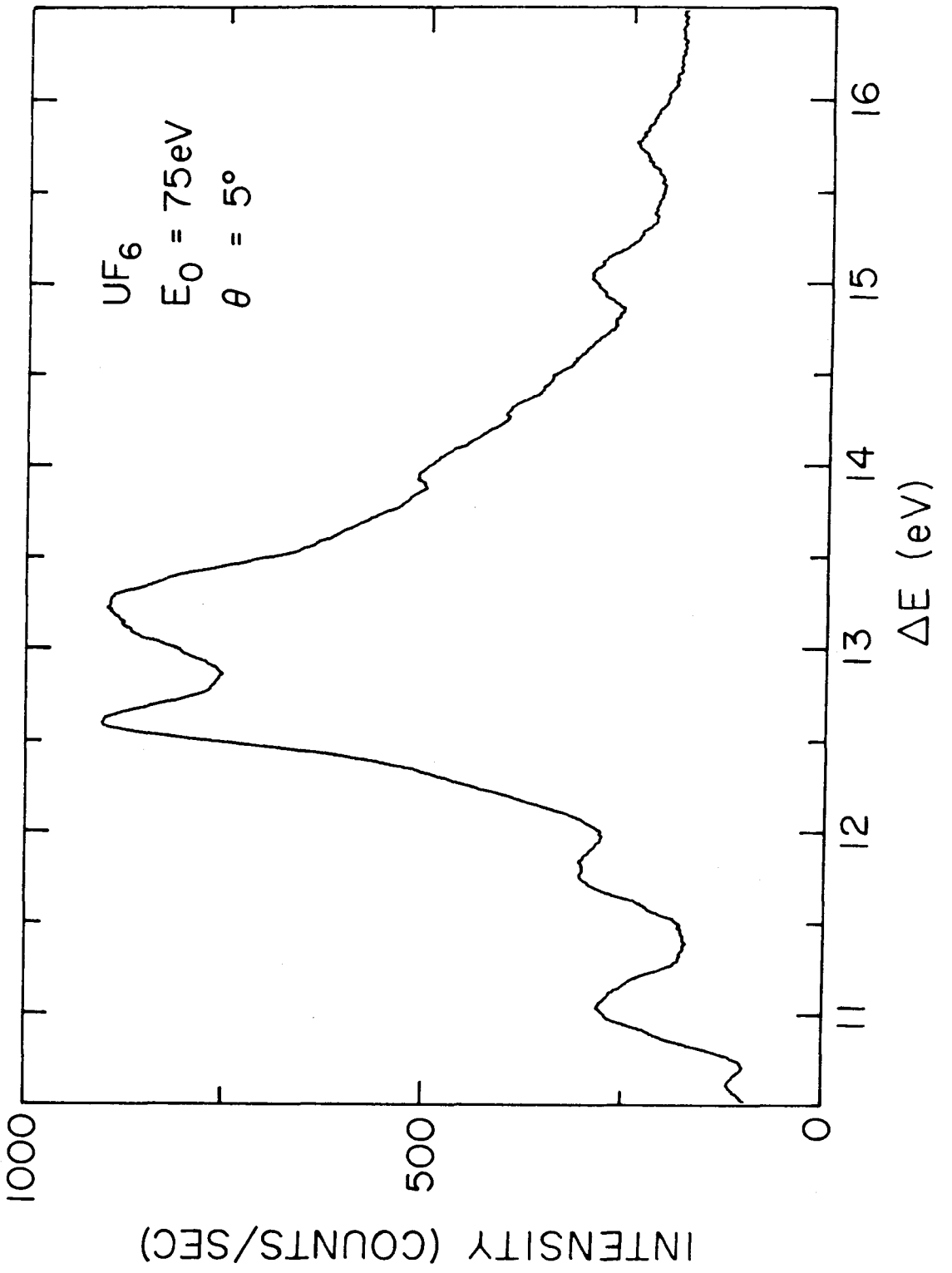
UF6
E0 = 75eV
θ = 5°
INTENSITY (COUNTS/SEC)
1000
500
0
11
12
13
14
15
16
ΔE (eV)

Figure 4

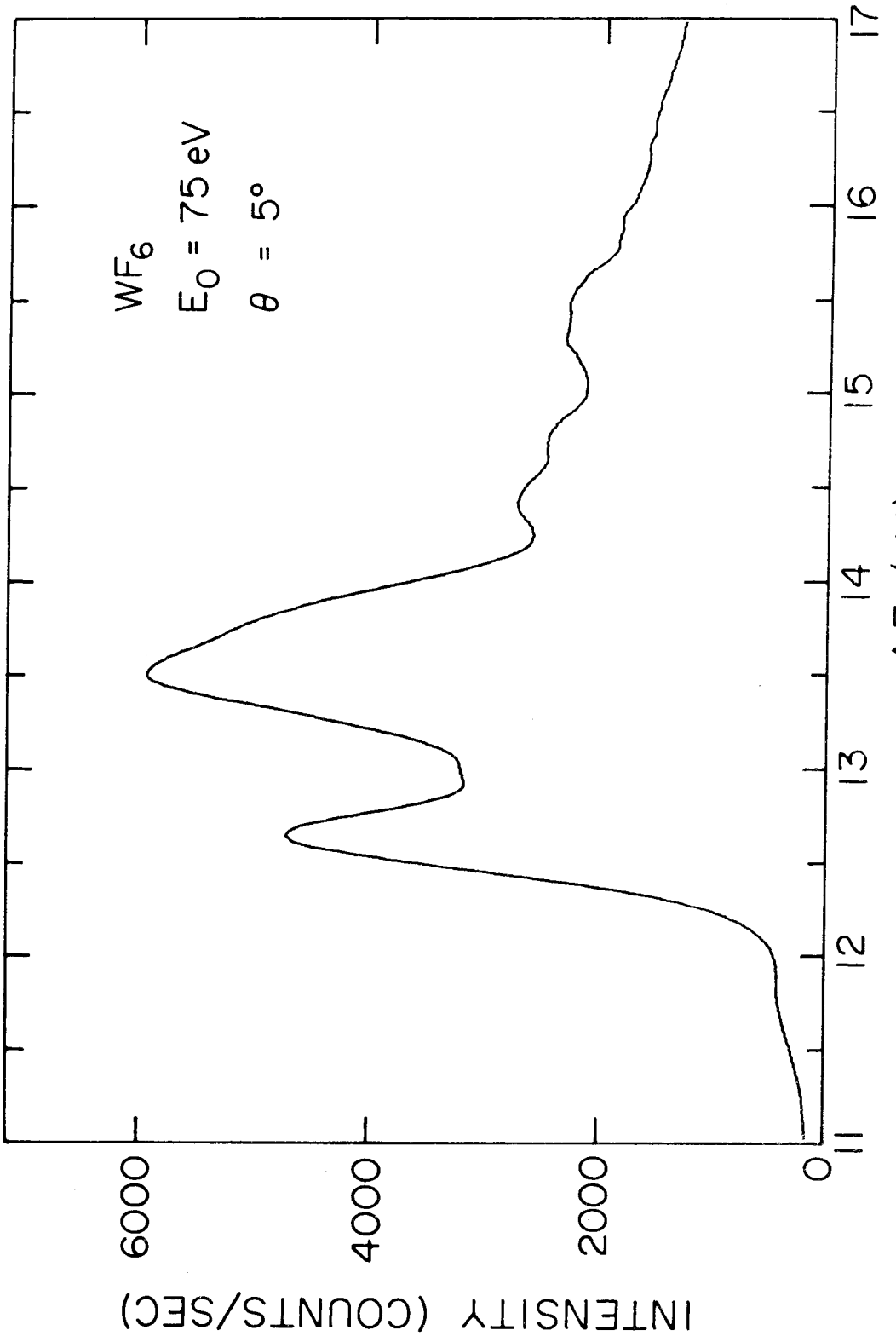
WF6
E0 = 75 eV
θ = 5°
INTENSITY (COUNTS/SEC)
0
2000
4000
6000
11
12
13
14
15
16
17
ΔE (eV)

Figure 5

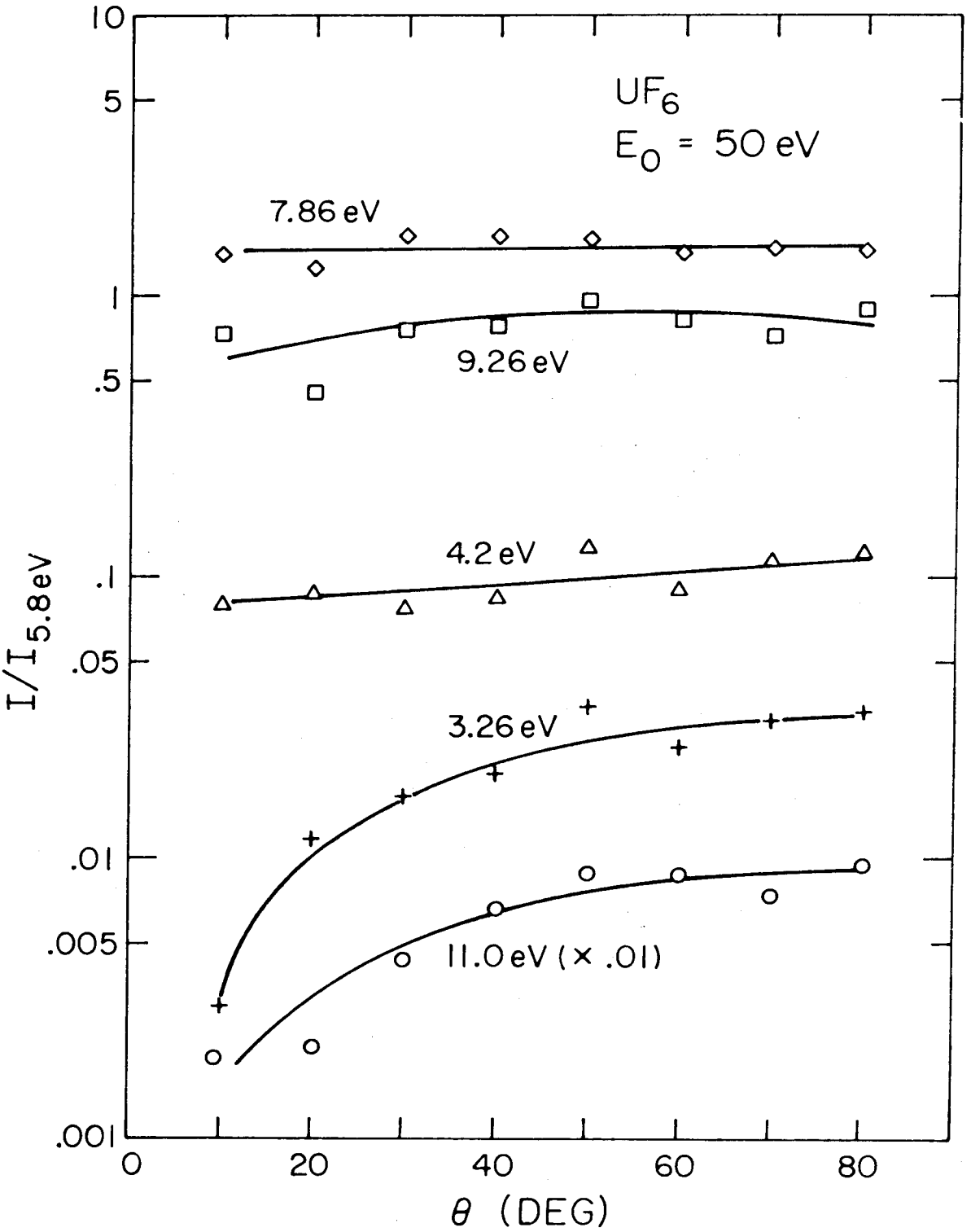
UF6
E0 = 50 eV
7.86 eV
9.26 eV
4.2 eV
3.26 eV
11.0 eV (× .01)
I/I5.8eV
θ (DEG)
10
5
1
.5
.1
.05
.01
.005
.001
0
20
40
60
80

Figure 6

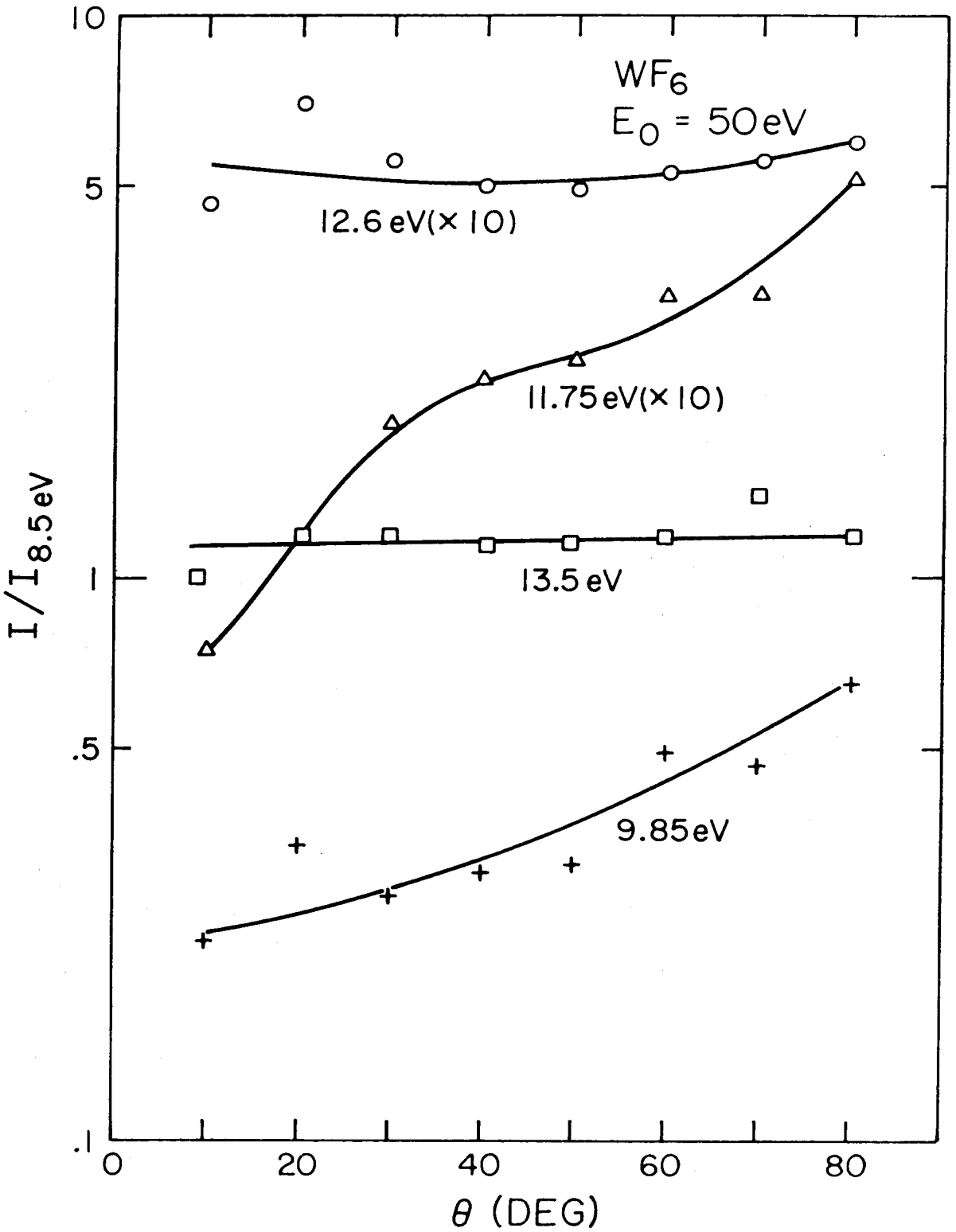
WF6
E0 = 50eV
12.6 eV(× 10)
11.75eV(× 10)
13.5 eV
9.85eV
I/I8.5eV
θ (DEG)
10
5
1
.5
.1
0
20
40
60
80

Figure 7

PROPOSITIONS

Proposition I

It is proposed that the electron momentum distribution for the 3d electrons of atomic copper be determined. This is to be accomplished through the use of electron impact ionization coincidence studies.

The problem of measuring electron momentum distributions in atoms, molecules and crystals is a long-standing one.[1] Various techniques have been used to obtain these momentum distributions. These include quasi free electron scattering at large angles,[2] Compton scattering of X-rays,[3] and positron annihilation.[4] Using these techniques it has been impossible to separate the electron momentum distribution due to electrons belonging to different bound states. This was due to the fact that only one of the reaction products was detected.[4] In Compton scattering when the scattered X-ray is detected in coincidence with a fluorescence photon, the initial state of the bound electron is defined.[4] The Compton profile still does not give direct information on the electron momentum distribution because it is determined by an integral of this function.

Electron impact ionization coincidence studies provide an alternative to the methods previously mentioned.[5-7] Previous experimental studies have determined momentum distributions for s and p type atomic electrons[4-8] and electrons in molecules such as ammonia,[9] methane,[10] H_2O,[11] and phosphine.[12] In addition, the experimental momentum distributions may be compared with theoretical distributions obtained from various calculated molecular wavefunctions. These comparisons provide a test for the validity of the different forms of calculated wavefunctions.[8,11,12] In the

previous experiments almost no information has been obtained on d electron momentum distribution. Consequently comparison of experimental results with various calculated results is completely lacking. Copper is suggested as a suitable target atom because of its electronic structure, $3d^{10}\ 4s^{1}$.[13] The d electrons in copper will not be effected by 4p electrons as would be the case for other possible target atoms, e.g., krypton. Also, Williams and Trajmar[14,15] have recently performed an electron impact study of atomic copper indicating the feasibility of copper as the target atom.

Figure 1 shows the experimental reaction dynamics. $\underset{\sim}{K}_0$ and E_0 represent the momentum and energy of the incident electron. $\underset{\sim}{K}_A$ and $\underset{\sim}{K}_B$ are the momenta of the two outgoing electrons while E_A and E_B are their energies. Experimentally, the incident beam of electrons with both a narrow energy spread and a small angular divergence is obtained from an electron gun. The incident energy, E_o, may be precisely set and the narrow energy spread may be obtained by the use of a hemispherical electrostatic analyzer. The outgoing electrons are detected using two independent sets of electron optics, each having a hemispherical analyzer to accurately determine E_A and E_B. One set of optics is rotatable only in-plane determining Θ_A, while the other is rotatable both in- and out- of plane determining Θ_B. The electrons, which are analyzed with respect to their energies and scattering angles, are detected in coincidence.

The results of angular correlation studies on helium and argon by Ehrhardt et al.,[5,16-18] have established the existence of two distinct peaks corresponding to two different scattering processes.

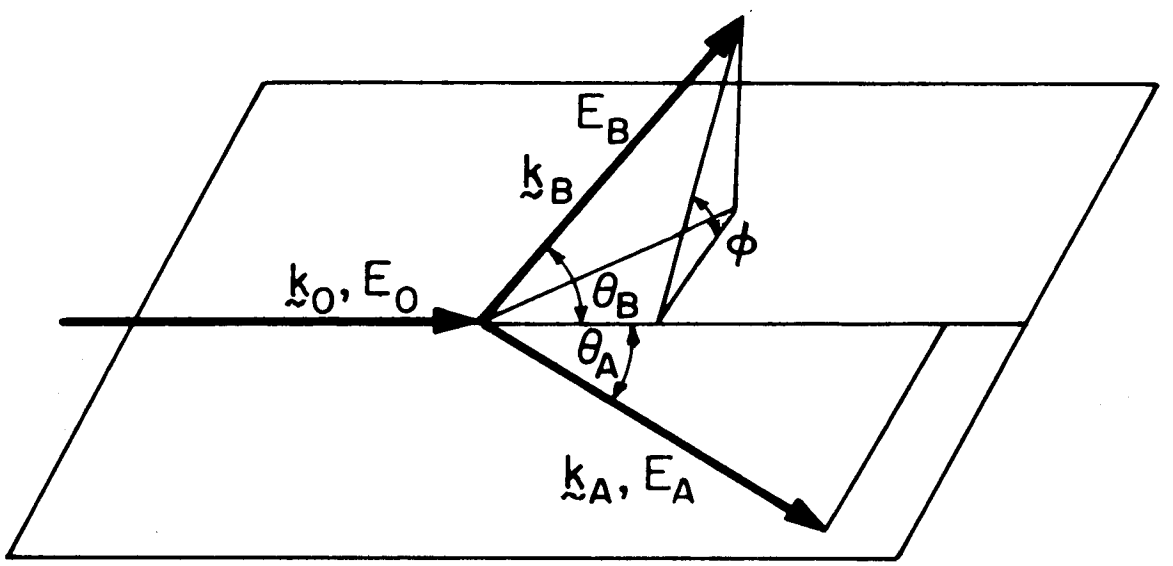

Fig. 1 Experimental arrangement for the (e, 2e) process.

Recoil collisions are characterized by large momentum transfer to the ion and appear as a backward peak of the coincidence rate plotted as a function of the detecting angle of the ejected electron, keeping all other scattering parameters fixed. The other scattering process is a more obvious one in which there is a very small momentum transfer to the ion. This appears as a forward peak, the "binary encounter peak", on a coincidence rate plot.[18]

The origin of the recoil peak is not well understood. Vriens[19] has suggested that the atomic electron, after interacting with the exciting electron, moves with positive energy in a potential well. The electron traveling in a varying potential field may be reflected by it and thus may be ejected in a direction more or less opposite to that in which it was originally moving.

The proposed experimental study requires negligible momentum transfer to the ion. Thus, we are interested in the "binary encounter" so named because the collision may be described with some success as a binary encounter between an incident and a free target electron.[20] This form of interaction becomes predominant as impact energies and the corresponding momentum transferred to the atomic electron increase.[19] This requires that experimental impact energies be of the order of .5 KeV.[6]

For the process of electron impact ejection both energy and momentum are conserved. Energy conservation is given by the equation

$$E_0 = E_A + E_B + E_I \ , \qquad (1)$$

where E_I is the binding energy of the ejected electron. Eq. 1 neglects the very small energy[19] of the recoiling ion. Eq. 2 expresses

the conservation of momentum

$$\underset{\sim}{q} = \underset{\approx}{K}_0 - (\underset{\approx}{K}_A + \underset{\approx}{K}_B) \quad , \tag{2}$$

where $\underset{\sim}{q}$ is the recoil momentum of the ion after the collision. Within both the classical and quantum mechanical description of the binary encounter model, $-\underset{\sim}{q}$ is equal to the momentum of the ejected electron in its orbital prior to the collision.[19] The momentum, q, may be related to the experimental parameters given in Fig. 1 by the expression

$$q = [(2K_A \cos\Theta_A - K_0)^2 + 4K_A^2 \sin^2\Theta_A \sin^2\phi/2]^{\frac{1}{2}} . \tag{3}$$

Within the plane wave impulse approximation for the ionization process, the differential cross section for a final state γ is given[20-22] by

$$\frac{d^5\sigma(E_0, E_A, E_B, \Theta_A, \Theta_B, \phi)}{dE_A d\Omega_A d\Omega_B} = C \frac{d\sigma_m(\underset{\approx}{K}_0, \underset{\approx}{K}_A, \underset{\approx}{K}_B)}{d\Omega_A} |F_\gamma(q)|^2 . \tag{4}$$

C represents kinematic factors which may be ignored.[20] σ_m is the Mott cross section for electron-electron scattering and is essentially independent of ϕ for the scattering geometry, $\Theta_A = \Theta_B = 45^o$ and $E_A = E_B$. $F_\gamma(q)$ is a form factor which for atoms is proportional to Fourier transform of the one-electron overlap function $\langle \psi(Z) | \psi'_\gamma (Z-1) \rangle$, where the integration is carried out over the coordinates of the Z-1 electrons common to the atom and ion.[20] Averaging over initial and summing over final magnetic sublevels eliminates dependence on the direction of $\underset{\sim}{q}$. Finally, if one assumes a Hartree-Fock description of the target atom with frozen orbitals,

then the form factor is given by the radial part of the Fourier transform of the wave function of the ionized orbital, i.e., the ionized electron's momentum distribution prior to the collision.

With $\theta_A = \theta_B$ and the energy analyzers adjusted so that $E_A = E_B$ ionization potentials E_I may be obtained by scanning E_0 . However, the second ionization potential of copper, corresponding to the ionization of a d electron, has been experimentally found to be 10.9 eV.[23] Using the value and adjusting the energy parameters to satisfy Eq. 1, the momentum distribution of the d electrons may be obtained by varying ϕ and determining the rate of coincidences.

One experimental difference between the proposed copper experiment and previously successful coincidence studies of electron momentum distributions is in the method of sample preparation. In order to study atomic copper it is necessary to have some type of copper atom beam. Williams and Trajmar[14] described such a beam which was used in the electron impact study of copper. Their atomic copper beam was generated by the heating of a tantalum crucible, containing copper, by electron bombardment to approximately 1250°C. The copper vapor diffused through a 0.1 cm diameter, 0.5 cm long channel to form the target beam. This method should perform quite well in the proposed experiment.

Studies of this type would provide the first experimental determination of d electron momentum distributions and would supply information concerning the appropriateness of various theoretical descriptions of the d electron wavefunctions.

References

1. R. Camilloni, A. Giardini-Guidoni, R. Tiribelli, and G. Stefani, Phys. Rev. Lett. 29, 618 (1972).
2. A. L. Hughes and M. M. Mann, Phys. Rev. 55, 50 (1937).
3. M. Cooper, Advan. Phys. 20, 453 (1971).
4. P. E. Mijnarends, Phys. Rev. 160, 512 (1967).
5. H. Ehrhardt, M. Schulz, T. Tekaat, and K. Willmann, Phys. Rev. Lett. 22, 89 (1969).
6. E. Weigold, S. T. Hood, and P. J. O. Teubner, Phys. Rev. Lett. 30, 475 (1973).
7. I. E. McCarthy, A. Ugbabe, E. Weigold, and P. J. O. Teubner, Phys. Rev. Lett. 33, 459 (1974).
8. E. Weigold, S. T. Hood, and I. E. McCarthy, Phys. Rev. A11, 566 (1975).
9. R. Camilloni, G. Stefani, A. Giardini-Guidoni, R. Tiribelli, and D. Vinciguerra, Chem. Phys. Lett. 41, 17 (1976).
10. E. Weigold, S. Dey, A. J. Dixon, I. E. McCarthy, and P. J. O. Teubner, Chem. Phys. Lett. 41, 21 (1976).
11. A. J. Dixon, S. Dey, I. E. McCarthy, E. Weigold, and G. R. J. Williams, Chem. Phys. 21, 81 (1977).
12. A. Hamnett, S. T. Hood, and C. E. Brion, J. Electron Spectrosc. Relat. Phenom. 11, 263 (1977).
13. F. A. Cotton and G. Wilkinson, Advanced Inorganic Chemistry, 3rd Ed. (Interscience Publishers, New York, 1972), p. 903.
14. W. Williams and S. Trajmar, Phys. Rev. Lett. 33, 187 (1974).

15. S. Trajmar, W. Williams, and S. K. Srivastava, J. Phys. B:Atom. Molec. Phys. 10, 3323 (1977).

16. H. Ehrhardt, K. H. Hesselbacher, K. Jung, and K. Willmann, J. Phys. B:Atom. Molec. Phys. 5, 1559 (1972).

17. H. Ehrhardt, K. H. Hesselbacher, K. Jung, M. Schulz, and K. Willmann, J. Phys. B:Atom. Molec. Phys. 5, 2107 (1972).

18. H. Ehrhardt, K. H. Hesselbacher, K. Jung, E. Schubert, and K. Willmann, J. Phys. B:Atom. Molec. Phys. 7 (1), 69 (1974).

19. L. Vriens, Physica 45, 400 (1969).

20. L. Vriens, Physica 47, 267 (1970).

21. S. T. Hood, A. Hamnett, and C. E. Brion, J. Electron Spectrosc. Relat. Phenom. 11, 205 (1977).

22. S. T. Hood, I. E. McCarthy, P. J. O. Teubner, and E. Weigold, Phys. Rev. A. 8, 2494 (1973).

23. Derived from optical spectral data in C. E. Moore, Atomic Energy Levels (U. S. Department of Commerce, National Bureau of Standards, Washington, D. C., 1952), NBS No. 467, Vol. II, pp. 111-114.

Proposition II

It is proposed that for a nematic liquid crystal the elastic constants corresponding to the restoring forces opposing splays (K_1) and bends (K_3) be determined by an entirely experimental method described below. It is also suggested that this method be applied initially to the nematic liquid crystalline material, MBBA, (methoxybenzilidene-butyloniline) because the two elastic constants have been previously obtained using different techniques based on combinations of experimental results and theoretical predictions.

In 1888, Friedrich Reinitzer[1] prepared a number of esters of cholesterol in which he observed a new and peculiar melting phenomenon. In the case of cholesteryl benzoate, the crystals melted sharply at 145.5°C but the melt was definitely opaque. Not until the temperature was increased to 178.5°C did opacity disappear suddenly, giving the true isotropic liquid. Reinitzer is generally regarded as the first to have observed such behavior.

When many organic substances are melted, liquid crystals or crystalline liquids are obtained. They are formed at the state of melting when insufficient heat has been supplied to bring about the transition into the normal isotropic liquid.[2] They are phases that are strongly anisotropic in some of their properties. Though this anisotropy is generally considered to be a property of crystals, the phases themselves may be quite mobile. Compounds which exhibit this thermal dependence are thermotropic liquid crystals. The thermotropic phases are separated from the normal liquid and from the crystal by first-order transitions.[2] A given liquid crystalline substance may have several mesomorphous phases, which, so far as can be observed,

are then separated from one another by first-order transitions.

A second type of crystalline liquids results from the mixture of two or more components, one of which is generally rather polar, e.g., water. The other component(s) may be an organic or inorganic compound.[3] These "lyotropic" liquid crystals will not be dealt with.

The anisotropy of liquid crystals is generally exhibited in the form of birefringence.[4] When a beam of light strikes the surface of a liquid crystal, it is split into two polarized components vibrating at right angles to each other. The two components travel at different velocities through the material and are refracted at different angles. They emerge as parallel beams of mutually perpendicular polarized light.

Molecules which exhibit liquid crystalline behavior often possess the following characteristics.[3]

(1) The molecules will be elongated and rectilinear, e.g., p-azoxyanisole, 4, 4'-dimethoxy-stilbene, and 2, 7-di-(benylidene-amino)fluorene.

(2) The molecules will be rigid along their long axis, with a double bond common along this axis.

(3) There is usually a simultaneous occurrence of strong dipoles and easily polarizable groups.

The basic types of mesophases shown by thermotropic liquid crystals are:[3]

A. The smectic mesophase - a turbid viscous state. The structure is stratified with the molecules arranged in layers, their long axes parallel to each other in layers and approximately normal to the

plane of the layer. The molecules can move in two directions in the plane and may rotate about one axis.

B. The nematic mesophase - a turbid but mobile state. Thread-like lines are seen under a microscope. The molecules maintain a parallel or nearly parallel arrangement to each other. They are mobile in three directions and again may rotate about one axis.

C. The cholesteric mesophase - also termed the twisted nematic structure. This mesophase exhibits some unique optical properties quite different from those of the nematic and smectic mesophases. The majority of compounds exhibiting this type of behavior are derived from cholesterol or other sterol systems.

Basic structural information about these mesophases has been gained through microscope and X-ray studies.[5]

Two descriptions of molecular ordering in liquid crystal mesophases are under consideration at the present time. The first is the "swarm theory" which applies only to the nematic mesophase. The swarm theory as its name implies states that molecules in a nematic liquid crystal form aggregates in swarms containing on the average 10^5 molecules. The molecules in a swarm have their long axes parallel and the entire swarm is bounded by isotropic liquid. The orientation of the swarms to one another is random.[5]

The second description is the "continuum theory." This description is based on the assumption that at every point in an undisturbed crystalline liquid, there is a definite preferred direction for orientation of the longitudinal axes. This preferential orientation is assumed to vary continuously with position except at a few special surfaces

or lines.[2]

Liquid crystals possessing a nematic mesophase have had their properties studied more intensely than either those displaying smectic or cholesteric liquid crystalline phases. The strong interest in the nematic mesophase is due, in great part, to the use of these liquid crystals for alphanumeric displays.[6-9] For nematic liquid crystals, it has been found that AC voltages ($\sim$8 to 20 Vrms)[8] with frequencies below some critical value ($\sim$50Hz to several hundred Hz)[10] induce a "dynamic scattering" phenomenon in which the percentage of light transmitted through a thin liquid crystal sample drops while scattering increases significantly.[6-10]

The bulk elastic properties of nematic liquid crystals are determined by three constants (Oseen-Frank constants) corresponding to the restoring forces opposing splays (K_1), twists (K_2), and bends (K_3) (see Fig. 1).[11-13] For a nematic liquid crystal, the free energy density, G_d, due to distortion and electromagnetic effects is given by[13]

$$G_d = 1/2 \left[K_1(\underset{\sim}{\nabla}\cdot\underset{\sim}{d})^2 + K_2(\underset{\sim}{d}\cdot\underset{\sim}{\nabla}\times\underset{\sim}{d})^2 + K_3(\underset{\sim}{d}\cdot\underset{\sim}{\nabla}\underset{\sim}{d})^2 - \underset{\sim}{D}\cdot\underset{\sim}{E} - \underset{\sim}{B}\cdot\underset{\sim}{H}\right] . \quad (1)$$

$\underset{\sim}{d}$ is the direction of the long axis of the liquid crystal and may be a function of position in a nematic sample. $\underset{\sim}{E}$ is the electric field and $\underset{\sim}{B}$ is the magnetic flux density while $\underset{\sim}{D}$ and $\underset{\sim}{H}$ are the electric displacement and magnetic field. These electromagnetic quantities are related by the expressions

$$D_i = \epsilon_{ij}E_j \text{ and } B_i = u_{ij}H_j \ (i, j = x, y, z) \ . \quad (2)$$

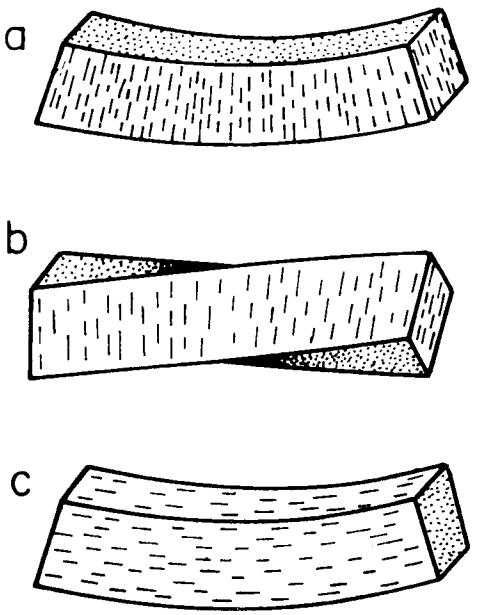

Fig. 1 The three distinct curvature strains of a liquid crystal: (a) splay, (b) twist, and (c) bend.

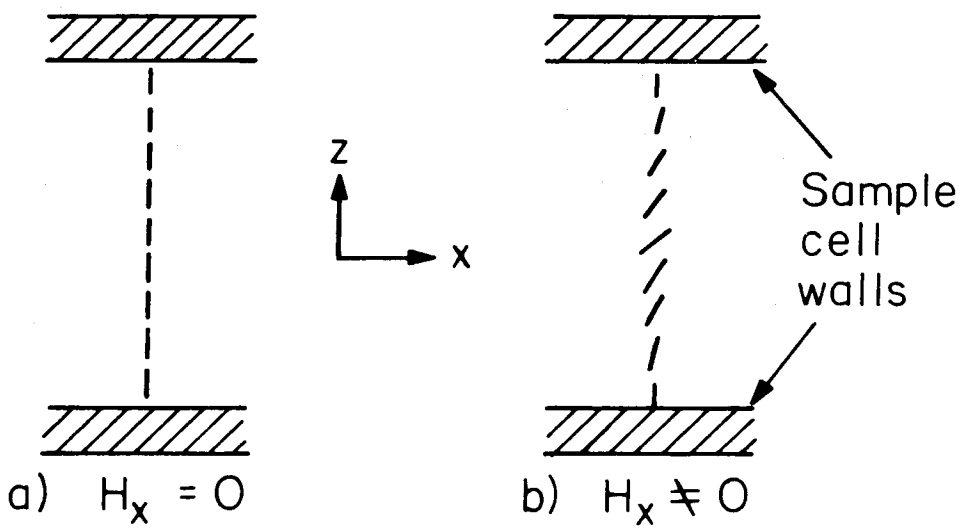

Fig. 2 Nematic liquid crystal (a) initially aligned by cell walls, (b) distorted by magnetic field.

ϵ refers to the dielectric constant of the liquid crystal and u its magnetic permeability; $\epsilon_{ij} = \epsilon_{\perp}\,\delta_{ij} + \epsilon_a\, d_i d_j$, $\epsilon_a = \epsilon_{\parallel} - \epsilon_{\perp}$ and $u_{ij} = u_{\perp}\delta_{ij} + u_a\, d_i d_j$, $u_a = u_{\parallel} - u_{\perp}$. Here $\parallel$ denotes parallel and $\perp$ perpendicular to the molecular axis.

The alignment of the molecules in the liquid crystalline phase may be significantly affected by the application of external effects e.g., electric and magnetic fields.[11] The elastic constants appear in nearly all descriptions of these phenomena.[12] As was indicated previously, the goal of the proposed studies is the development of a new technique to determine K_1 and K_3. In addition, during the course of the experiments, data will be obtained which could be used to determine the order parameter, S, for a variety of magnetic fields. The order parameter is defined as[7]

$$S = 1/2\ \langle 3\cos^2\theta - 1\rangle\ , \qquad (3)$$

where $\langle\ \ \rangle$ implies averaging over a small but macroscopic sample and θ is the angle between the long axis of the molecule and the optic axis of the medium (in the proposed study an axis perpendicular to the sample cell walls).

The elastic constants of nematic liquid crystals have been studied previously, although not extensively.[8, 11-17] Typically the experimental apparatus consists of a nematic sample held at a constant temperature within a thin cell. The molecules are oriented such that the long axes are all perpendicular to the cell wall. Magnetic fields of varying intensities are applied perpendicular to the molecular axis causing the molecules to attempt to rotate to an orientation parallel to

the applied field. This experimental configuration is shown schematically in Fig. 2. The cell walls are in the xy plane while each molecule lies in a plane parallel to the zy plane. The molecular orientation can be described by θ, the angle between the z axis and $\underset{\sim}{d}$, the direction of the molecular axis. The average amount of distortion for the entire sample can be related to $\bar{\delta}$, the difference between the refractive index of the extraordinary wave and unpolarized light.[11,18]

Within the experimental constraints Eq. 1 reduces to

$$G_d = 1/2\left\{K_1 \sin^2\theta\left|\frac{\partial\theta}{\partial z}\right|^2 + K_3\left(\cos^4\theta\left|\frac{\partial\theta}{\partial z}\right|^2 + \cos^2\theta\sin^2\theta\left|\frac{\partial\theta}{\partial z}\right|^2\right) - \underset{\sim}{B}\cdot\underset{\sim}{H}\right\} . \qquad (4)$$

By minimizing the free energy density given by Eq. 4 a theoretical relation between the angle θ and a molecule's z coordinate is obtained.[11,18] Using this result an expression for $\bar{\delta}$ as a function of $\underset{\sim}{H}(=H_z\,\hat{z})$ is obtained with K_1 and K_3 as parameters. Varying the elastic constants allows theoretical curves of $\bar{\delta}$ vs H to be compared with the experimentally determined $\bar{\delta}$ vs H curve. This matching permits determination of K_1 and K_3 within the uniqueness of the fit.

The proposed method, which eliminates the need to match experiment with theoretical predictions, is more complicated experimentally to perform and will be discussed in terms of several sequential steps. The basic idea involves a straightforward use of Eq. 4. First the initial alignment of all molecules along the z axis will be insured by applying a weak magnetic field, approximately 500 Gauss, in the $\hat{z}$ direction. For this initial configuration, since $\theta(z) = 0$, G_d° will equal $-1/2(B_z^\circ H_z^\circ)$. Integration of G_d° over the sample volume yields the initial free energy,

G°, due to electromagnetic and stress contributions. Of course, only magnetic effects contribute to G°.

After determining G°, a more intense magnetic field (>5 K Gauss) will be applied in the $\hat{x}$ direction causing the molecule to turn in that direction. The cell surfaces can be prepared such that molecules near them will always remain perpendicular to these surfaces while molecules farther away will exhibit larger θ's. The largest θ, θ_m, will occur for molecules at the center of the cell. Using an optical technique, to be described, θ as a function of z, $\theta(z)$, will be experimentally determined. This allows calculation of the coefficients of K_1 and K_3, $C_1(H_x, z)$ and $C_3(H_x, z)$ on the right hand side of Eq. 4. The free energy of the sample, $G(H_x)$ will be given by

$$G(H_x) = 1/2 \int [K_1 C_1(H_x, z) + K_3 C_3(H_x, z) - (B_x H_x + B_z^\circ H_z^\circ)] d\tau, \quad (5)$$

while the charge in free energy is given by $\Delta G(H_x) = G(H_x) - G^\circ$, which may be determined calorimetrically. Obtaining Eq. 5 for several values of H_x will allow determination of K_1 and K_3 via a least squares fit. In the following paragraphs the experiment steps will be described in greater detail.

To insure $C_1(H_x, z)$ and $C_2(H_x, z)$ are not zero, $\theta(z)$ must not equal a constant. This is accomplished by forcing molecules near cell walls to remain perpendicular to the walls. The desired alignment of molecules near the cell walls may be obtained by cleaning or etching the glass walls or by the use of surfactants.[19, 20] However for a sample approximately 1.5 mm thick this surface effect will probably not initially orient the entire sample.[21] Therefore, the weak magnetic field

along the $\hat{z}$ axis will be applied. It is also necessary to obtain the magnetic susceptibility of the nematic liquid crystal oriented both parallel and perpendicular to the applied field. This may be done by applying standard techniques[22] to the solid material and correcting for any density changes upon warming to the liquid crystalline phase.

Obtaining the angle θ as a function of z for each applied H_x is necessary. This may be obtained using an optical technique which relates θ to the index of refraction, n, as shown by Eq. 6,[11]

$$n = \frac{n_e n_o}{(n_e^2 \sin^2\theta + n_o^2 \cos^2\theta)^{\frac{1}{2}}} \quad , \tag{6}$$

where n_e and n_o are respectively the refractive indices of the extraordinary and ordinary waves. To probe the refractive index as a function of z a He-Ne laser will be focused using a long focal length lens (850 mm). The effective spot size for a "best form" lens of this focal length optimized for the 632.8 nm laser line is about 40 microns in diameter.[23] This allows determining the average θ for a 40 micron region. Of course, for each 40 micron region n, n_e, and n_o must each be determined. For the 1.5 mm sample thickness $\theta(z)$ will be given in terms of 37 values which via various interpolating formulas can yield the values of $\theta(z)$ to be differentiated and integrated for the evaluation of Eqs. 4 and 5. This experimental determination of $\theta(z)$ as a function of applied H_z is quite interesting in itself, allowing determination of the order parameter for comparison with order parameter results from other techniques.[15]

Finally the change in free energy between the initially ordered sample under only the influence of H_x and the sample when H_z is

applied must be determined. The free energy change is designated $\Delta G(H_x)$. At constant temperature $\Delta G(H_x)$ is related to $\Delta H(H_x)$, the enthalpy change, and $\Delta S(H_x)$, the entropy change by Eq. 7.[24]

$$\Delta G(H_x) = \Delta H(H_x) - T\Delta S(H_x) \tag{7}$$

Differential scanning calorimetry (DSC) will allow determination of the heat given off or absorbed by the nematic sample as the magnetic field is turned on. At constant pressure this Δq is equal to $\Delta H(H_x)$. Obtaining $\Delta S(H_x)$ may also be accomplished using the DSC technique. For a change of state from A to B ΔS is given by

$$\Delta S = \int_A^B \frac{dq}{T} \quad , \tag{8}$$

where dq is the incremental quantity of heat and T is the system temperature. The direct method of determining the difference in S with H_x off and on is to perform the integrals

$$S_0 = \int_{A:T=0}^{B:T=T_{nematic}} \frac{dq}{T} \quad (H_x \text{ off}) \tag{9}$$

$$S(H_x) = \int_{A:T=0}^{B:T=T_{nematic}} \frac{dq}{T} \quad (H_x \text{ on}) \tag{10}$$

with $\Delta S(H_x)$ defined by Eq. 11.

$$\Delta S(H_x) \equiv S(H_x) - S_0 \tag{11}$$

However the effect of H_x on S for the liquid crystalline material when it is in its solid phase should be negligible. H_x will significantly affect S only during the melting and heating of the sample to the

desired temperature, $T_{nematic}$. Now using the DSC apparatus, the q vs T curve may be obtained with H_x both on and off, allowing calculation of $\Delta S(H_x)$. Combining $\Delta H(H_x)$ and $\Delta S(H_x)$ will yield $\Delta G(H_x)$. One experimental difficulty is construction of a DSC apparatus allowing application of magnetic fields along both $\hat{x}$ and $\hat{z}$ axes.

With the determination of the experimental quantities at several values of H_x, K_1 and K_3 may be calculated. These values will be the first constant results based essentially on experimental data. Use of the nematic liquid crystalline substance MBBA (methoxy-benzilidene-butylaniline), will allow comparison of the present results with those of previous studies.[25]

References

1. F. Reinitzer, Monatsh 9, 421 (1888).
2. A. Saupe, Angew. Chem. Int. Ed. Engl. 7, 97 (1968).
3. G. H. Brown, Amer. Scientist 60, 64 (1972).
4. D. Chapman, Science Journal 1, 32 (1965).
5. G. W. Gray, Molecular Structure and the Property of Liquid Crystals, Academic Press Inc., London 1962.
6. P. A. Penz and G. W. Ford, Appl. Phys. Lett. 20, 415 (1972).
7. R. Chang, Mol. Cryst. Liq. Cryst. 30, 155 (1975).
8. M. J. Little, H. S. Lim, and J. D. Margerum, Mol. Cryst. Liq. Cryst. 38, 207 (1977).
9. D. P. McLemore and E. F. Carr, J. Chem. Phys. 57, 3245 (1972).
10. N. V. S. Rao, P. R. Kishore, T. F. S. Raj, M. N. Avadhanlu, and C. R. K. Murty, Mol. Cryst. Liq. Cryst. 36, 65 (1976).
11. M. J. Stephen and J. P. Straley, Rev. Mod. Phys. 46, 617 (1974).
12. W. H. de Jeu and W. A. P. Claassen, J. Chem. Phys. 67, 3705 (1977).
13. S. Holmstrom and S. T. Lagerwall, Mol. Cryst. Liq. Cryst. 38, 141 (1977).
14. C. Williams and P. E. Cladis, Solid State Commun. 10, 357 (1972).
15. P. E. Cladis, Phys. Rev. Lett. 28, 1629 (1972).
16. D. Meyerhofer, J. Appl. Phys. 46, 5084 (1975).
17. C. Maze and D. Johnson, Mol. Cryst. Liq. Cryst. 33, 213 (1976).

18. H. J. Deuling, Mol. Cryst. Liq. Cryst. 19, 123 (1972).

19. W. Helfrich, Mol. Cryst. Liq. Cryst. 21, 187 (1973).

20. H. Tsuchiya and K. Nakamura, Mol. Cryst. Liq. Cryst. 29, 89 (1974).

21. E. A. Kosterin and I. G. Chistyakov, Sov. Phys. – Crystallogr. 13, 229 (1968).

22. D. P. Shoemaker and C. W. Garland, Experiments in Physical Chemistry (McGraw-Hill Book Co. Inc., New York, 1967), pp. 309-317.

23. Melles Griot Optics Guide (Melles Griot, Irvine, CA, 1975), p. 56.

24. J. G. Kirkwood and I. Oppenheim, Chemical Thermodynamics (McGraw-Hill Book Co., Inc., New York, 1961), pp. 231-241.

25. C. E. Williams, P. E. Cladis, M. Kleman, Mol. Cryst. Liq. Cryst. 21, 355 (1973).

Proposition III

It is proposed that the electronic spectroscopy of the van der Waals molecules Ne_2, Ar_2, Kr_2, and Xe_2 be investigated using the technique of low-energy, variable-angle electron scattering. Completion of the proposed study will provide information over the entire range of electronic excitation energies of these weakly bound molecules and represent, as such, their first complete spectroscopic absorption study. In addition, valuable information may be obtained concerning the angular behavior of the differential cross sections of singlet and triplet excited states as the molecular nuclei become increasingly more massive.

In their ground states, rare gas atoms repel each other except for van der Waals attractions which lead to weakly bound ground states for those more massive than helium.[1] In contrast, numerous stable excited states exist for these molecules including He_2.[2-5] Also, ionic states of these molecules are bound.[1,6] Great current interest exists in rare gas dimers due to their possible use in tunable laser systems. When subjected to high voltage electric discharges, krypton and xenon have been made to lase at the vacuum ultraviolet frequencies of 145.7nm and 172.1nm respectively.[7-9] This lasing action is believed to be the result of the transition from the bound $^{1,3}\Sigma_u^+$ states of the dimer to an unbound or continuum region of the ground state, $^1\Sigma_g^+$, potential energy surface.[1,10]

The electric discharge forms excited diatomic molecules, Kr_2^* and Xe_2^*. The most important processes in this formation include (i) electronic excitation of a ground-state atom followed by associative combination with a ground-state atom yielding the excited dimer,

(ii) ionization followed by electronic recombination and associative combination, (iii) ionization followed by formation of diatomic ions and electronic recombination to form the excited dimer, and (iv) direct excitation of van der Waals molecules by electron impact.[8] No experimental study of, for example, a high pressure xenon plasma has satisfactorily determined the relative importance of these production reactions.[8] Because, after emission, the dimer dissociates, a population inversion between its ground and excited states exists during the electric discharge. This population inversion allows the lasing action.

Numerous optical studies of the electronic spectroscopy of Ne_2, Ar_2, Kr_2, and Xe_2 have been previously performed. However, their results are not complete and in some cases are inconsistent. Tanaka, Yoshino, and Freeman[3-5] have studied the vacuum ultraviolet absorption spectra of these dimers. Information was gained about the ground states of these molecules (Ne_2:D_e = 30.2cm^{-1} supporting 2 vibrational levels; Ar_2:D_e = 91.6cm^{-1} supporting 6 vibrational levels; Kr_2:D_e = 150.0cm^{-1} supporting 16 vibrational levels; and Xe_2:D_e = 205.9cm^{-1} supporting 25 vibrational levels)[3-5] and some of the higher excited states. The lowest two excited states, $^{1,3}\Sigma_u^+$, from which lasing occurs, were not studied.

Jortner and coworkers[11-13] investigated portions of the emission spectra of the rare gas dimers in both the solid and gas phases. Broad emission continua were observed for Ar_2 (maximum intensity ~130nm), Kr_2 (maximum intensity ~148nm) and Xe_2 (maximum intensity ~172nm). These emission spectra were unstructed reflecting the bound to continuum nature of the transitions. Their studies were not

completely consistent with the optical solid phase investigations of Belov et al.[14] who observed additional emission bands in the 200nm to 230nm region and somewhat different features in the 100nm to 200nm region of the dimer spectra. Several studies of rare gas emission from electric discharges have been performed. These experiments yielded very little information concerning dimer spectroscopy, predominantly indicating its lack of importance in these emission spectra. Finally, Wilkinson[17] determined the microwave excited emission spectra of rare gases. These spectra showed broad structureless features due to dimer emission. Again, the lack of structure is the result of the bound to continuum emission.

The question arises as to what additional information an electron impact study of these dimers will provide. Several answers are possible. First, this study will allow investigation of the dimer absorption spectra over its entire excitation energy range using a single experimental technique. At the present time no absorption experiments have been performed on lowest lying bands of the dimer spectra. Emission spectra, due to their inherent lack of resolution, provide limited information about the binding strengths of these lowest lying excited states. In addition to increasing observable structure, gas phase absorption studies may supply information which will aid in resolving the discrepancies between the various solid phase emission studies.

For Ne_2 and Ar_2 it may be possible to locate transitions which are best described as singlet $\rightarrow$ triplet. As the weight of the nuclei increases, the validity of the spin quantum, S, is expected to decrease[18] (i.e., S no longer commutes with the Hamiltonian). Very little study of the

effects of the spin-orbit interaction on electron scattering differential cross sections has been performed. Xenon represents the only heavy nuclei atom for which differential cross sections have been obtained and analyzed with regard to spin-orbit effects.[19] These results are not conclusive. It is hoped that a systematic study of molecules, with increasing nuclear weights, will provide more concrete information on the relation between spin-orbit effects, the angular behavior of differential cross sections, and, perhaps, the mixing of states of different spin multiplicities.

Several experimental points should still be considered. The most effective means of obtaining concentrations of Ne_2, Ar_2, Kr_2, and Xe_2 suitable for spectroscopic study appears to be that of a supersonic expansion.[20] Several examples of van der Waals molecules being produced and studied under supersonic molecular beam conditions exist in the literature.[21-23] Recently, the photoelectron spectrum of Xe_2 was obtained with Xe_2 produced in a supersonic expansion.[24] Even using a supersonic molecular beam, the electron impact spectra obtained will be the superposition of the intense monomer spectrum and a much weaker dimer spectrum. For effective study of the dimer spectra the monomer contribution must be removed. This may be most easily accomplished in the following manner. First, the electron impact spectra of the monomer may be obtained by replacing the supersonic expansion by either a simple effusive molecular beam or a scattering chamber. Once monomer spectra are obtained and if monomer peaks not overlapped by dimer structure can be found in the superposition spectrum, the monomer contribution may be subtracted out. The

resulting spectrum should be essentially the result of dimer absorption. A similar application of this subtraction technique has been described by Frueholz, Rianda, and Kuppermann.[25,26]

For the reasons discussed previously, the study of the absorption spectra of Ne_2, Ar_2, Kr_2, and Xe_2 would be a useful undertaking. Through the use of a supersonic expansion and spectral enhancement via a simple subtraction technique it also appears experimentally feasible.

References

1. R. S. Mulliken, J. Chem. Phys. 52, 5170 (1970).
2. M. L. Ginter, (a) J. Chem. Phys. 45, 248 (1966); (b) J. Mol. Spectrosc. 17, 224 (1965).
3. Y. Tanaka and K. Yoshino, (a) J. Chem. Phys. 53, 2012 (1970); J. Chem. Phys. 57, 2964 (1972).
4. Y. Tanaka, K. Yoshino, and D. E. Freeman, J. Chem. Phys. 59, 5160 (1973).
5. D. E. Freeman, K. Yoshino, and Y. Tanaka, J. Chem. Phys. 61, 4880 (1974).
6. P. M. Dehmer and J. L. Dehmer, J. Chem. Phys. 67, 1774 (1977).
7. P. W. Hoff, J. C. Swingle, and C. K. Rhodes, Appl. Phys. Lett. 23, 245 (1973).
8. J. B. Gerardo and A. W. Johnson, J. Appl. Phys. 44, 4120 (1973).
9. A. W. Johnson and J. B. Gerardo, J. Appl. Phys. 45, 867 (1974).
10. J. K. Rice and A. W. Johnson, J. Chem. Phys. 63, 5235 (1975).
11. A. Gedanken, J. Jortner, B. Raz, and A. Szöke, J. Chem. Phys. 57, 3456 (1972).
12. O. Cheshnovsky, B. Raz, and J. Jortner, (a) J. Chem. Phys. 57, 4628 (1972); J. Chem. Phys. 59, 3301 (1973).
13. A. Gedanken, B. Raz, and J. Jortner, J. Chem. Phys. 59, 5471 (1973).
14. A. G. Belov, I. Ya. Fugol, and E. V. Savchenko, Solid State Commun 12, 1 (1973).
15. J. F. Prince and W. W. Robertson, (a) J. Chem. Phys. 45, 2577

(1966); (b) J. Chem. Phys. 46, 3309 (1967).

16. R. Turner and H. D. Riccius, J. Chem. Phys. 48, 4351 (1968).

17. P. G. Wilkinson, Can. J. Phys. 45, 1716 (1967).

18. E. U. Condon and G. H. Shortley, The Theory of Atomic Spectra (Cambridge University Press, London, 1970) p. 257.

19. W. Williams, S. Trajmar, and A. Kuppermann, J. Chem. Phys. 62, 3031 (1975).

20. M. A. D. Fluendy and K. P. Lawley, Chemical Applications of Molecular Beam Scattering (Chapman and Hall Ltd., London, 1973) p. 72.

21. E. T. Verkhoutseva, A. E. Ovechkin, and Ya. M. Fogel, Chem. Phys. Lett. 30, 120 (1975).

22. C. Y. Ng, P. W. Tiedemann, B. H. Mahan, and Y. T. Lee, J. Chem. Phys. 66, 5737 (1977).

23. R. E. Smalley, D. H. Levy, and L. Wharton, J. Chem. Phys. 64, 3266 (1976).

24. P. M. Dehmer and J. L. Dehmer, J. Chem. Phys. 67, 1774 (1977).

25. R. P. Frueholz, R. Rianda, and A. Kuppermann, (a) J. Chem. Phys. 68, 775 (1978); (b) Chem. Phys., in press.

Proposition IV

It is proposed that semi-classical transition probabilities induced by an intense monochromatic electromagnetic field be investigated using a close coupling expansion. These calculations will also investigate the effects on the transition probabilities of including and deleting the $\underset{\sim}{A}^2$ term in the time dependent Hamiltonian. It is suggested that calculations be performed initially on the atomic hydrogen system.

Typically the interaction of radiation with matter is studied within a semi-classical approximation.[1] At this level the electromagnetic field is treated classically while the atomic or molecular systems and their interactions with the field are treated quantum mechanically. The semi-classical treatment is generally more tractable for problems of chemical interest than a quantum electrodynamical approach.[2] The Hamiltonian, H, for the interaction of radiation with a hydrogen atom, within this semiclassical framework, may be written as[3]

$$H = \frac{1}{2m}\left(\underset{\sim}{p} - \frac{e\underset{\sim}{A}}{c}\right)^2 + e\phi - \frac{e^2}{r} \quad . \tag{1}$$

$\underset{\sim}{A}$ is the classical vector potential of the field while ϕ is the scalar potential. $\underset{\sim}{p}$ is the electron's momentum, m its mass, e its charge, and r the magnitude of the electron's position vector, $\underset{\sim}{r}$. The speed of light is represented by c. With minor manipulations the Hamiltonian becomes

$$H = \frac{\underset{\sim}{p}^2}{2m} - \frac{e}{mc}\,\underset{\sim}{A}\cdot\underset{\sim}{p} + \frac{ie\hbar}{2mc}\,\underset{\sim}{\nabla}\cdot\underset{\sim}{A} + \frac{e^2}{2mc^2}\,\underset{\sim}{A}^2 + e\phi - \frac{e^2}{r} \quad . \tag{2}$$

With the appropriate choice of gauge,[4] in empty space $\underset{\sim}{\nabla}\cdot\underset{\sim}{A} = 0$ and $\phi = 0$ yielding,

$$H = \frac{\underset{\sim}{p}^2}{2m} - \frac{e}{mc}\,\underset{\sim}{A}\cdot\underset{\sim}{p} + \frac{e^2}{2mc^2}\,\underset{\sim}{A}^2 - \frac{e^2}{r} \quad . \tag{3}$$

For monochromatic radiation in the form of a plane wave with wave vector $\underset{\sim}{k}$, frequency ω, and polarization $\underset{\sim}{u}$, the vector potential may be written as,[1]

$$\underset{\sim}{A} = A_0\,\underset{\sim}{u}\cos[(\underset{\sim}{k}\cdot\underset{\sim}{r}) - \omega t] \quad . \tag{4}$$

The amplitude of the vector potential then assumes the form

$$A_0 = 2c\sqrt{\frac{2\pi\hbar N}{\omega V}}\,, \tag{5}$$

where $2\pi\hbar$ is Planck's constant and N/v is the number of photons per unit volume. In Eq. 3 the ratios of the second term to the first term and the third term to the second term are of the order eA/2cp. Incoherent light sources, for example a 2500 watt xenon mercury arc lamp at 3400Å (band pass 8Å) radiate approximately 10^{15} photons per second.[5] If it is assumed that all of this light may be focussed to a spot size of a square millimeter the density of photons per cubic centimeter is 10^7. For a hydrogen atom in its ground state eA/2cp is of the order of 10^{-8}. Clearly for these intensities the second term in Eq. 3 may be considered as a perturbation while the third term may be neglected entirely.

For coherent light sources, lasers in particular, obtainable photon densities are many orders of magnitude higher. For intense focussed laser beams intensities of 10^{14} to 10^{16} W/cm^2 may be achieved.[6] For these intensities eA/2cp is of the order of 1. It is no longer valid to treat the second term in Eq. 3 as a perturbation or neglect the third term entirely. For these high intensities it seems necessary to solve

the entire time dependent Schrodinger equation,

$$i\hbar \frac{d\psi(\underset{\sim}{r},t)}{dt} = \left[\frac{\underset{\sim}{p}^2}{2m} - \frac{e^2}{r} - \frac{e}{mc} \underset{\sim}{A}\cdot\underset{\sim}{p} + \frac{e^2}{2mc^2} \underset{\sim}{A}^2 \right] \psi(\underset{\sim}{r},t) \quad . \tag{6}$$

The solution of Eq. 6, $\psi(\underset{\sim}{r},t)$, may be expanded in the series:

$$\psi(\underset{\sim}{r},t) = \sum_n a_n(t)\, \phi_n(\underset{\sim}{r})\, e^{-iE_n t/\hbar} , \tag{7}$$

where E_n and ϕ_n are respectively the eigenfunctions and eigenvalues of the isolated hydrogen atom. For the sake of completeness, the sum in Eq. 7 must be over both bound and continuum states. Substitution of Eq. 7 into Eq. 6, multiplication by ϕ_n^*, and integration over $\underset{\sim}{r}$ yields,

$$i\hbar \frac{da_n(t)}{dt} = \sum_{\substack{\ell \\ \ell \neq n}} \langle n \,|\, w(t) \,|\, \ell \rangle e^{i\omega_{n\ell}} a_\ell(t) , \tag{8}$$

where

$$w(t) = - \frac{e}{mc} \underset{\sim}{A}\cdot\underset{\sim}{p} + \frac{e^2}{2mc^2} \underset{\sim}{A}^2 \tag{9}$$

and

$$\hbar\omega_{n\ell} = E_n - E_\ell \quad . \tag{9a}$$

Eq. 8 is subject to the initial condition at $t = 0$, $a_n(0) = \delta_{nm}$, that is the H atom is initially in its ground eigenstate.

The normal first order approximation used to solve the system of equations represented by Eq. 8 is to assume that the $a_n(t)$ remain very close to the $a_n(0)$ and substitute these initial conditions into Eq. 8 yielding,

$$i\hbar \frac{d\, a_n}{dt} = \langle n \mid w(t) \mid 0 \rangle\, e^{i\omega_{no} t} , \tag{10}$$

which may be solved by direct integration.

The method suggested in this proposal is to truncate the expansion of Eq. 7 after a finite number, g, of terms, and solve the resulting system of equations numerically. Within the dipole approximation[1] for monochromatic radiation in the form of plane wave, Eq. 8 may be separated into its real and imaginary parts. Further algebraic manipulation results in Eqs. 11a, b and 12a, b, c, which form a system of 2g coupled first order differential equations.

$$-\hbar \frac{d\, d_n}{dt} = \sum_{\ell=1}^{g} (2C \cos(\omega t) \underset{\sim}{u} \cdot \langle n \mid \underset{\sim}{r} \mid \ell \rangle [c_\ell \cos(\omega_{n\ell} t)$$

$$- d_\ell \sin(\omega_{n\ell} t)]) - D[1 + \cos(2\omega t)]\, d_n \tag{11a}$$

$$-\hbar \frac{d\, d_n}{dt} = \sum_{\ell=1}^{g} (2C \cos(\omega t) \underset{\sim}{u} \cdot \langle n \mid \underset{\sim}{r} \mid \ell \rangle [d_\ell \cos(\omega_{n\ell} t)$$

$$+ c_\ell \sin(\omega_{n\ell} t)] + D[1 + \cos(2\omega t)]\, c_n \tag{11b}$$

$$C = e\omega_{n\ell} A_0 \tag{12a}$$

$$D = \frac{e^2}{4mc^2} A_0^2 \tag{12b}$$

$$a_n = c_n + i d_n \tag{12c}$$

Within the semi-classical framework, other approaches have been used to study the interaction of atomic and molecular systems with intense electromagnetic fields. Reiss[7, 8] has studied bound to bound transitions for hydrogen like atoms. His technique is based on

transforming the time dependent Schrodinger equation into a more tractable form using a unitary transformation. However approximations were required when solving for transition probabilities. DeWitt[6] and Mohan and R. K. Thareja[9] have employed the Reiss method to study multiphoton ionization of atomic hydrogen. For the case of a two level laser system, Bambini[10] has investigated its interaction with a multimode electromagnetic field using a density matrix approach. Finally, Hodgkinson and Briggs[11] considered the excitation of polyatomic molecules by an intense radiation field. However no attempt to include the effects of the $\underset{\sim}{A}^2$ term was made. To my knowledge no one has used direct numerical solution of the truncated system of equations.

In electron scattering calculations the truncation of an infinite expansion is termed a close coupling approximation.[12-16] The principal computational difference is that resulting electron scattering equations are coupled second order integro-differential equations containing non-local coulomb and exchange operators. Due to the time consuming nature of their calculation, accurate electron scattering close coupling calculations have been limited. However when solving Eqs. 11a, b this is no longer the case. The integrals are effectively constants which need only be evaluated once. This should allow the use of fairly large expansions. In addition, calculation of the $a_n(t)$ yields transition probabilities immediately since this probability is just $|a_n(t)|^2$.[17]

Atomic hydrogen is suggested as the initial system to be studied because all integrals may be evaluated exactly. Results may readily be compared to perturbation theory results and those of earlier calculations.[6,8,9] The validity of perturbation theory as the electromagnetic

field strength is increased may also be tested. Finally, in ascertaining the effect of varying the number of terms in the expansion, a simple system such as hydrogen is probably best. To study the effect of the $\underset{\sim}{A}^2$ term on transition probabilities, the last term in both Eq. 11a and 11b may be deleted. These terms result from the $\underset{\sim}{A}^2$ term in the Hamiltonian.

In summary, a non-perturbative scheme for study of the interaction between atomic and possibly molecular systems and electromagnetic radiation has been suggested. This technique is based on a close coupling approximation and numerical solution of the resulting system of equations. These calculations should provide information about the validity of the typical perturbative approach.

References

1. A. S. Davydov, Quantum Mechanics, 1st ed. (Addison-Wesley Publishing Co., Reading, Mass., 1965), pp. 285-315.
2. S. Stenholm, Phys. Rep. 6, 1 (1973).
3. L. I. Schiff, Quantum Mechanics, 3rd ed. (McGraw-Hill Book Co., New York, 1968), pp. 177-180, 397-424.
4. J. D. Jackson, Classical Electrodynamics, 1st ed. (John Wiley and Sons, Inc., New York, 1962), p. 181.
5. J. A. Betts, Ph.D. Thesis, California Institute of Technology, Pasadena, California, p. 213 (1970).
6. R. N. DeWitt, J. Phys. B:Atom. Molec. Phys. 6, 803 (1973).
7. H. R. Reiss, Phys. Rev. Lett. 17, 1149 (1970).
8. H. R. Reiss, Phys. Rev. A. 1, 803 (1970).
9. M. Mohan and R. K. Thareja, J. Phys. B:Atom. Molec. Phys. 5, L134 (1972).
10. A. Bambini, Phys. Rev. A 14, 1479 (1976).
11. D. P. Hodgkinson and J. S. Briggs, J. Phys. B:Atom. Molec. Phys. 10, 2583 (1977).
12. J. E. Purcell, R. A. Berg, and A. E. S. Green, Phys. Rev. A 2, 107 (1970).
13. J. Callaway, R. W. LaBahn, R. T. Pu, and W. Duxler, Phys. Rev. 168, 12 (1968).
14. D. L. Walker, J. Phys. B:Atom. Molec. Phys., Ser. 2, 2, 356 (1969).
15. R. W. LaBahn and J. Callaway, Phys. Rev. A. 2, 366 (1970).

16. D. Andrick and A. Bitsch, J. Phys. B:Atom. Molec. Phys. 8, 393 (1975).

17. A. Messiah, Quantum Mechanics (John Wiley and Sons, Inc., New York, 1958), pp. 722-728.

Proposition V

It is proposed that the 5.0 eV (~40,000 cm^{-1}) to 5.8 eV (~45,000 cm^{-1}) region of the absorption spectrum of hexafluorobenzene (C_6F_6) be investigated using the techniques of gas phase multiphoton ionization and single photon absorption in rare gas matrices. The C band[1] of hexafluorobenzene is observed in this energy region and it is hoped that these experimental studies will help clarify its origin.

The electronic spectroscopy of benzene has been extensively studied both theoretically and experimentally.[2] Benzene represents the first clear cut example of the use of vibronic selection rules to interpret an electronic transition.[2] Similarly the fluorinated derivatives of benzene have also been extensively investigated.[1,3-6] Study of their spectra is inherently interesting because addition of fluorine to the benzene system should perturb both σ and π orbitals.[3,7] The spectra of the fluorobenzenes are in many respects quite similar to that of benzene.[1,2,6,8] At excitation energies below 8 eV the spectra of the fluorobenzenes display three singlet → singlet transitions apparently analogous to the $\tilde{X}\,^1A_{1g} \rightarrow 1\,^1B_{2u}$, $\tilde{X}\,^1A_{1g} \rightarrow 1\,^1B_{1u}$, and $\tilde{X}\,^1A_{1g} \rightarrow {}^1E_{1u}$ transitions observed in benzene's spectrum.[1,6] These excitations are found in the fluorobenzenes' spectra at approximately 4.8, 6.2 to 6.4, and 7.0 to 7.2 eV, respectively.

In their electron impact study of the fluorinated benzenes, Frueholz and coworkers[1] have detected an additional singlet → singlet transition in the spectra of the tetrafluoro-, pentafluoro-, and hexafluoro- compounds. This excitation was designated the C band to avoid confusion with the A, B, and E type irreducible representations of D_{6h} symmetry. In the tetrafluoro- and pentafluoro- com-

pounds this feature overlaps heavily with the 6.2 eV transition; however, in hexafluorobenzene it is clearly observed with intensity maxima occurring at 5.32 eV.[1] The excitation energies of these C bands display an interesting dependence on the degree of fluorine substitution. In the tetra- compounds the C bands occur above 6 eV, while in pentafluorobenzene the feature occurs at 5.85 eV and in hexafluorobenzene at 5.32 eV.[1]

At present the nature of the C bands is unknown. Frueholz et al.[1] suggested it might be due to either a fluorine p_π to carbon $p_{\pi*}$ charge transfer excitation or a fluorine p_π to carbon-fluorine $\sigma*$ transition. The goal of this proposition is to use high resolution optical techniques to gain information about the vibronic structure of this feature and thereby obtain information about the symmetry of the excited state and the origin of this excitation. Hexafluorobenzene is suggested as the molecule for study because it rigorously possesses D_{6h} symmetry and the transition is most clearly observed in this molecule's spectrum. Previously obtained information about this feature is extremely limited. In addition to the electron impact study which inherently had limited resolution, a single optical study of hexafluorobenzene, showing the C band, has been performed.[9] Unfortunately, this study was conducted at high temperatures and vibronic structure was almost entirely smeared out.

The first phase of the proposed study consists of investigating the single photon absorption spectrum of C_6F_6 between 5.0 eV to 5.8 eV in rare gas matrices of low temperature. These spectra will provide several pieces of information. First, the question whether the C

band is valence or Rydberg in nature will be answered. If the C band's intensity relative to the other valence transitions in the spectrum is significantly weaker in the rare gas matrix as compared to its gas phase relative intensity, it may be assigned as a Rydberg excitation. If its relative intensity is unaffected by the matrix environment, a valence assignment would be most reasonable. The low temperature environment should also minimize any hot band contributions[8] and allow optimum single photon vibronic structure to be observed.

Multiphoton absorption spectroscopy should also be applied to study the C band. While the single photon spectrum is subject to dipole selection rules,[2] two-photon absorption obeys different selection rules.[10,11] The two-photon transition probability is proportional to the modulus squared of a sum, S_{if}, over all molecular states,[10,11]

$$S_{if} = \sum_n \left(\frac{(\underset{\sim}{\lambda} \cdot \underset{\sim}{p}_{in})(\underset{\sim}{p}_{nf} \cdot \underset{\sim}{u})}{E_{nf} - E_{\underset{\sim}{\lambda}}} + \frac{(\underset{\sim}{u} \cdot \underset{\sim}{p}_{in})(\underset{\sim}{p}_{nf} \cdot \underset{\sim}{\lambda})}{E_{nf} - E_{\underset{\sim}{u}}} \right) , \qquad (1)$$

where $\underset{\sim}{\lambda}$ and $\underset{\sim}{u}$ are the polarization vectors of the two photons in the lab coordinates, $\underset{\sim}{p}_{in}$ and $\underset{\sim}{p}_{nf}$ are the dipole transition moments between the initial state, i, and the intermediate state, n, and the intermediate state and the final state, f, written in terms of the molecular coordinates. $E_{\underset{\sim}{\lambda}}$ and $E_{\underset{\sim}{u}}$ are the energies of the two photons and E_{nf} is the energy difference between the final state and the intermediate state.

For a molecular system possessing D_{6h} symmetry with ground state vibronic symmetry (vibronic symmetry will be defined as symmetry resulting from the direct product of the electronic and vibrational symmetries) A_{1g}, dipole selection rules allow transitions

to states of the same spin multiplicity with vibronic symmetries A_{2u} and E_{1u}.[2] The two-photon selection rules will allow excitations to states possessing vibronic symmetries A_{1g}, A_{2g}, E_{1g}, and E_{2g}.[12] For excitations to the same electronic state, one- and two-photon absorptions will excite different vibrational modes. This statement has been born out experimentally in two-photon studies of the $^1B_{2u}$ state of benzene.[13-15] Study of the different vibrations excited in the one- and two-photon spectra of the C-band in C_6F_6 should aid in its identification.

Typically two-photon absorption is determined by measuring single photon fluorescence from the excited state.[13-15] However, often molecules relax via nonradiative pathways rather than fluorescencing. This is the case for benzene excited above 42,440 cm^{-1} (5.26 eV).[13] Also, while fluorescence from the $^1B_{2u}$ state of benzene does occur if the molecule is excited below 42,440 cm^{-1}, it has been found that fluorescence quantum yields decrease as fluorine substitution increases.[16] In light of this information a traditional two-photon absorption/one-photon fluorescence experiment applied to the C band of hexafluorobenzene will probably be unsuccessful.

To overcome the probable lack of fluorescence from the C band of C_6F_6, the technique of multiphoton ionization[17-21] should be applied. In this technique multiphoton absorption results in the ionization of the target. The resulting ionization current is collected. Fluctuations in the ionization current represent resonances in the lower order photon absorptions. C_6F_6 has an adiabatic ionization potential of about 9.95 eV.[22] The two-photon study of the 5.0 eV to 5.8 eV region

of the C_6F_6 spectrum will necessitate four-photon ionization. Structure in the ionization current as a function of laser wavelength will be due to two-photon structure (5.0 eV to 5.8 eV excitation energy region) and three-photon structure (7.5 eV to 8.7 eV excitation energy range). The single-photon energy range to be scanned will consequently be 2.5 eV (495 nm) to 2.9 eV (427 nm). These wavelengths are readily obtainable using commercially available dye lasers.

Separation of structure due to two- and three-photon resonances is important. The structure due to two-photon resonances is effectively the two-photon absorption spectrum. Johnson[19a] has performed four-photon ionization studies on benzene. Several interesting features were found. First, above 42,440 cm^{-1} (two-photon total energy) where fluorescence is not observed, structure due to two-photon absorption was still detected. Also, three-photon structure was found to correspond almost entirely to the vacuum UV spectrum of benzene. The remaining structure was assigned as resonances in the two-photon absorption. These results indicate that lack of fluorescence will not affect the multiphoton ionization technique and that three-photon structure can be successfully separated from two-photon structure. The vacuum UV spectrum of C_6F_6, which was obtained by Smith and Raymonda,[22] should allow a similar separation of two- and three-photon structure in the multiphoton ionization spectrum of C_6F_6.

In summary, it is suggested that the one-photon absorption spectrum of C_6F_6 in a rare gas matrix environment along with its multiphoton ionization spectrum be obtained. These techniques, which yield complementary information, should aid in assigning the C band

excitation observed in the 5.0 eV to 5.8 eV region of hexafluorobenzene's spectrum.

References

1. a) R. P. Frueholz, W. M. Flicker, O. A. Mosher, and A. Kuppermann, Chem. Phys. Lett. 52, 86 (1977); b) J. Chem. Phys. Manuscript in preparation.
2. G. Herzberg, Molecular Spectra and Molecular Structure III. Electronic Spectra and Electronic Structure of Polyatomic Molecules (Van Nostrand Reinhold Co., New York, 1966), pp. 128-141, 555-561.
3. H. Sponer, J. Chem. Phys. 22, 234 (1954).
4. C. D. Cooper, J. Chem. Phys. 22, 503 (1954).
5. P. D. Singh and A. N. Pathak, Indian J. Pure Appl. Phys. 7, 39 (1969).
6. R. Gilbert, P. Sauvageau and C. Sandorfy, Can. J. Chem. 50, 543 (1972).
7. C. Brundle, M. B. Robin, and N. A. Kuebler, J. Am. Chem. Soc. 94, 1466 (1972).
8. B. Katz, M. Brith, B. Sharf and J. Jortner, J. Chem. Phys. 52, 88 (1970).
9. S. H. Bauer and C. F. Aten, J. Chem. Phys. 39, 1253 (1963).
10. W. L. Peticolas, Ann. Rev. Phys. Chem. 18, 233 (1967).
11. P. R. Monson and W. M. McClain, J. Chem. Phys. 53, 29 (1970).
12. W. M. McClain, J. Chem. Phys. 55, 2789 (1971).
13. D. M. Friedrich and W. M. McClain, Chem. Phys. Lett. 32, 541 (1975).
14. J. R. Lombardi, R. Wallenstein, T. W. Hänsch, and D. M.

Friedrich, J. Chem. Phys. 65, 2357 (1976).

15. L. Wunsch, F. Metz, H. J. Neusser, and E. W. Schlag, J. Chem. Phys. 66, 386 (1977).
16. G. L. Loper and E. K. C. Lee, Chem. Phys. Lett. 13, 140 (1972).
17. P. Agostini, G. Barjot, G. Mainfray, C. Manus, and J. Thebault, IEEE J. Quant. Electron. QE-6, 782 (1970).
18. P. M. Johnson, M. R. Berman, and D. Zakheim, J. Chem. Phys. 62, 2500 (1975).
19. a) P. M. Johnson, J. Chem. Phys. 64, 4143 (1976); b) 64, 4638 (1976).
20. D. H. Parker, S. J. Sheng, and M. A. El-Sayed, 65 5534 (1976).
21. K. Aron and P. M. Johnson, J. Chem. Phys. 67, 5099 (1977).
22. D. R. Smith and J. Raymonda, Chem. Phys. Lett. 12, 269 (1971).